Exploring High-Resolution Carbon Isotopes in Archaeological Charcoal as a Rainfall Seasonality Proxy

by

GEMMA DIMITRA PORETTI

Dissertation submitted in fulfilment of the
requirements for the degree of

MASTER OF PHILOSOPHY

in the subject

ARCHAEOLOGY

at the

UNIVERSITY OF CAPE TOWN

SUPERVISOR: Vincent Hare

November 2024

DECLARATION

I declare that this dissertation entitled 'Exploring High-Resolution Carbon Isotopes in Archaeological Charcoal as a Rainfall Seasonality Proxy' is my own work which I am presenting in full fulfilment of the requirements for my degree.

No part of this work has been previously submitted for the award of any degree at the University of Cape Town or any other university.

Each source that has contributed to or been quoted in this dissertation has been acknowledged, cited, and referenced.

I declare that I have submitted this dissertation to plagiarism detection software and confirm that it adheres to the necessary standards of originality.

25 November 2024

Signed by candidate

Gemma Dimitra Poretti

ABSTRACT

Rainfall in present-day South Africa is distinctly seasonal, with a Summer Rainfall Zone (SRZ) in the east, a Winter Rainfall Zone (WRZ) in the west, and a Year-Round Rainfall Zone (YRZ) along the south coast and interior between them. Understanding shifts in these zones during Late Pleistocene glacial-interglacial cycles is crucial for both regional climate reconstructions and interpreting behavioural variability in the South African Later Stone Age (LSA) archaeological record. However, several key palaeoarchives employed to reconstruct rainfall seasonality during the Late Pleistocene are hindered by low temporal resolution, reliance on inference and untenable ecological relationships, and their spatial and temporal distance from archaeological evidence. This research tests whether a proven seasonal precipitation proxy (SPP) based on high-resolution carbon isotope profiles — successfully applied to evergreen wood in the Northern Hemisphere — can be used to reconstruct rainfall seasonality from South African archaeological Proteaceae (angiosperm) and Podocarpaceae (gymnosperm) charcoal. Modern *Protea* and *Podocarpus* wood and charcoal samples from all three rainfall zones are tested to assess the SPP's applicability in South Africa and its ability to extract seasonal climate data from different materials. Results show that seasonal amplitudes ($\Delta\delta^{13}C_{meas}$), changes in precipitation (ΔP), and ratios of summer to winter rainfall (P_S/P_W) align with local rainfall data. Slight discrepancies between wood and charcoal seasonal amplitudes and therefore values for ΔP and P_S/P_W are attributed to carbonisation effects, including ^{13}C depletion and volume shrinkage leading to reduced sampling resolution, which lead to a repeated but quantifiable overestimation of summer rainfall in charcoal. In the WRZ, seasonal amplitudes are dulled relative to local rainfall data due to intermittent growth cessation during seasonal dry periods, but these effects could in some cases be corrected for. Analysis of Podocarpaceae charcoals from Waterfall Bluff showed an increase in summer rainfall during the Last Glacial-Interglacial Transition (LGIT), while Proteaceae charcoals from Boomplaas Cave showed an increase in winter rainfall during the Last Glacial Maximum (LGM). These results support existing models of Southern Hemisphere (SH) westerly shifts. The SPP offers a quantitative, high-resolution, on-site proxy for seasonality in archaeological contexts, with potential applicability to global archaeological sites from which evergreen charcoals have been retrieved.

Key words: carbon isotopes; archaeological charcoal; rainfall seasonality; dendroclimatology; *Protea*; *Podocarpus*

ACKNOWLEDGEMENTS

This project would not have been possible without the exceptional, caring, and formative guidance of my supervisor, Vincent Hare. Thank you for your assistance in the field, your impeccable email responsiveness, and, above all, for believing in this project and my ability to see it through.

I appreciate Justin Pargeter for granting access to the Boomplaas and Waterfall Bluff charcoals, and Alisoun House for her botanical expertise and taxon identifications. Special thanks to Brian Schubert for his time and for helping navigate some analytical hurdles. I am grateful to Judith Sealy for her invaluable insight during the fledgling stages of this research and for teaching me to trust my own judgement. For careful questions and advice that helped steer my analysis, I thank Brian Chase, Grant Hall, Stephan Woodborne, and Jean Baverstock. The completion of this project was made possible through the generous funding provided by my supervisor on behalf of the National Research Foundation (NRF), and the Biogeochemistry Research Infrastructure Platform (BIOGRIP) in collaboration with the Stable Light Isotope Laboratory at the University of Cape Town.

Dendro-fieldwork is not a solo endeavour. I am grateful to Uncle Vince and Bianca Potgieter for taking me up and down the Ukhahlamba-Drakensberg in the Hilux, and to Poppy and Ennia Poretti for doing it all over again just a few months later. I deeply appreciate the help of John Harrison and the Geology workshop, as well as David Sikosana, who were able to free the jammed increment corer of would-be samples. I am thankful to CapeNature and KZN Ezemvelo Wildlife for granting necessary permits to collect these samples in the first place.

For laboratory support, I owe much to Louisa Hutten for access to the Faunal Lab and DinoLite equipment, Bedone Mugabe for the microscope and insightful conversations on embedding, resins, and moulds, and to Hope Chakanetsa for her assistance with weighing. I am especially indebted to Patricia Groenewald for her patience, thorough teaching, attentive nose each time I placed a wood sample in the furnace, and for allowing me unobstructed access to her time and mind.

My deepest gratitude extends to the Department of Archaeology at UCT. Thank you to Dawn Green for her probing questions and her reminder that Science is always theoretical. To my fellow Masters students who have been my colleagues in the lab, my grounding rocks in the Tea Room, and my supportive friends all the time and everywhere: Jenna Larangeira, Juliette Rabie, and Zarah Abrahams – thank you. And I cannot forget Amber Wilson; for the home, the meals, the lifts, the unspeakable generosity – thank you ten times over.

Beyond the academy, I am supported by a family who has shared this sometimes challenging but always worthwhile journey: Dimitra, Evi, Pany, and Hali; Zetta, Xenia, and Soula. My mother, Poppy. My sister, Ennia. It is for you and with you that I celebrate this project.

Finally, to Giulio and Cecco, who never got to see this project but would have been its most engaged readers – thank you for the tree books.

TABLE OF CONTENTS

LIST OF FIGURES

LIST OF TABLES

LIST OF VARIABLES

The following variables are included in the Seasonal Precipitation Proxy (Schubert & Jahren 2011: 7299):

$\delta^{13}C$	The ratio of the heavy carbon isotope (^{13}C) to the lighter carbon isotope (^{12}C) in a sample relative to the internationally recognised standard Vienna Pee Dee Belemnite (VPDB), expressed in parts per thousand (‰).
$\Delta\delta^{13}C_{CO2}$	Seasonal changes in the carbon isotope composition of atmospheric CO_2.
$\Delta\delta^{13}C_{meas}$	Average seasonal change in $\delta^{13}C$ measured over successive growth increments; the measured seasonal amplitude.
$\Delta\delta^{13}C_{model}$	Average seasonal change in $\delta^{13}C$ modelled using climate data.
$\delta^{13}C_{max}$	Maximum $\delta^{13}C$ value in a given growth increment.
$\delta^{13}C_{min}$	Minimum $\delta^{13}C$ value in a given growth increment, preceding $\delta^{13}C_{max}$.
$\Delta\delta^{13}C_{max}$	Maximum possible $\Delta\delta^{13}C_{meas}$ for a series of growth intervals.
ΔP	The ln-transformed difference between summer and winter rainfall. Positive values indicate summer rainfall dominance and negative values winter rainfall dominance.
P_S	Six month summer period (November-April in the Southern Hemisphere).
P_W	Six month winter period (May-October in the Southern Hemisphere).
P_S/P_W	The ratio of six-month summer to six-month winter rainfall amount.
ΔY	Post-photosynthetic physiological process leading to carbon isotope fractionation and contributing to the value for $\Delta\delta^{13}C_{meas.}$

CHAPTER 1

Introduction

1.1. Proposing a new proxy for rainfall seasonality

Changes in rainfall seasonality has influenced South Africa's human past and will continue to influence its future. An understanding of past rainfall seasonality is critical to contextualising contemporary climate change. Several climate analysts have thus turned to the country's historical records to offer perspective on emergent changes (e.g. Botai *et al.* 2017; Wolski 2018; Sousa *et al.* 2018; Burls *et al.* 2019 for the Cape Town Drought of 2015-2020). Yet many of these studies are often encumbered by observed records that are constrained by gaps, discrepancies, or systemic errors (Wolski 2018; Otto *et al.* 2018), and which lack long-term temporal coverage, rendering them less likely to capture significant trends in seasonal rainfall variability (Kruger 2006; Wolski 2018; Pascale *et al.* 2020; Ndebele *et al.* 2020; Roffe *et al.* 2021a, 2022).

An understanding of rainfall seasonality over glacial-interglacial cycles, particularly the movements of the Southern Hemisphere (SH) westerlies (Van Zinderen Bakker 1967, 1976; Chase & Meadows 2007; Stone 2014; Fitchett & Bamford 2017; Engelbrecht *et al.* 2019), is of interest to archaeologists hoping to contextualise the cultural adaptations and variability of Later Stone Age (LSA, beginning *ca*. 43 ka BP) hunter-gatherers in the region (Marean *et al.* 2014; Sealy *et al.* 2016; Pargeter *et al.* 2018). For these archaeological episodes, of course, there are naturally no instrumental records, no ways to directly measure and map past climate. Consequently, evidence for the movement of rain-bearing systems over the Late Pleistocene are sought in proxies that record climate conditions during specific time intervals (Fitchett 2019; Knight & Fitchett 2019), and it is from these that past variables like rainfall are often inferred. Still, isolating rainfall changes to a seasonal resolution is difficult using many of these proxies which tend to record long-term, millennial-scale climatic shifts (Chase & Meadows 2007; Stone 2014; Fitchett & Bamford 2017; Engelbrecht *et al.* 2019; Lukich & Ecker 2022). Moreover, integrating these climatological seasonality reconstructions with archaeological investigations is limited by the prevalence of off-site archives that are temporally mismatched and spatially distant from the archaeological units they aim to interpret (see Roberts *et al.* 2016; Patalano & Roberts 2021).

Contemporary climate scientists working in southern Africa require long-term, highly resolved records to make more accurate predictions about the future, and archaeologists and palaeoscientists require long-term, highly resolved records to make improved interpretations and knowledge claims about the

past. The rarity of such records has resulted in an increasing urge to identify alternative palaeoclimate proxies that preserve rainfall information at a resolution fine enough for seasonality reconstruction (Chase & Meadow 2007; Stone 2014; Thackeray & Fitchett 2016; Fitchett & Bamford 2017; Knight & Fitchett 2019; Faith *et al.* 2019), and which can be integrated into archaeological studies (Prendergast *et al.* 2018; Kweicien *et al.* 2022). This study therefore aims to investigate whether such a proxy might be found in an abundant but arguably underutilised material: archaeological charcoal.

1.2. Schubert and Jahren's (2011) Seasonal Precipitation Proxy

The demand for highly resolved on-site palaeoclimate records sets the stage for the present study. The primary aim is to test whether a seasonal precipitation proxy (SPP) developed by Brian Schubert and Hope Jahren (2011), and which has been established to work on Northern Hemisphere evergreen trees, may similarly be applied to archaeological charcoal from South Africa. In addition to its ability to identify seasonal rainfall signals in modern evergreen wood, the SPP has also shown success in its ability to extract seasonally resolved palaeoclimate information from fossilised evergreen wood. It identified a summer rainfall dominated climate in the Arctic forests during the Eocene (Schubert *et al.* 2012), a more variable winter rainfall dominated transitional climate in the Arctic during the Miocene (Schubert *et al.* 2017), and a relatively aseasonal Eocene rainfall regime in the Antarctic Peninsula (Judd *et al.* 2019). More recently, the SPP was used to determine that the Late Oligocene Nanning Basin received four times more precipitation in summer than in winter, making it almost indistinguishable from southern China's present-day monsoon climate (Vornlocher *et al.* 2021). However, its applicability to South African evergreen taxa, carbonised evergreen wood (charcoal), and to the Pleistocene, is yet to be studied and established.

In their 2011 paper, Schubert and Jahren (2011) explored the cyclical rise and fall pattern in $\delta^{13}C$ values that appears when multiple sequential measurements are taken from each growth increment along the radial axis of evergreen wood (Figure 1). While these scholars were not the first to identify such a pattern (see for example Leavitt & Long 1986, 1991; Barbour *et al.* 2002; Helle & Schleser 2004; Fonti *et al.* 2018), they were the first to systematically identify its primary climatic drivers – which explain $\delta^{13}C$ variability across all evergreens – using a dataset of 33 evergreen taxa representing 10 genera and 15 global sites. Their findings showed that across various latitudes, temperatures, and rainfall conditions, the average measured change in $\delta^{13}C$ across a series of growth bands ($\Delta\delta^{13}C_{meas}$) is a function of seasonal changes in the isotopic composition of atmospheric CO_2 ($\Delta\delta^{13}C_{CO2}$), and seasonal changes in precipitation (ΔP)(Figure 2). Other factors, such as seasonal temperature, atmospheric CO_2 concentration (pCO_2), and light availability were found to have no significant impact on $\Delta\delta^{13}C_{meas}$. By

comparing the average carbon isotope change measured (Figure 2) to what was modelled using instrumental rainfall records ($\Delta\delta^{13}C_{model}$), they found a significant correlation for all 15 sites ($R^2 = 0.96$). Consequently, they proposed a proxy which is able to quantify rainfall seasonality by considering $\Delta\delta^{13}C_{meas}$ as the amplitude of seasonality (Figure 1). From the value for $\Delta\delta^{13}C_{meas}$, one obtains not just an amplitude of seasonality, but one can also quantify the seasonal change in rainfall (ΔP) and the ratio of summer to winter rainfall (P_S/P_W) (Schubert & Jahren 2011; Schubert & Timmermann 2015). Higher values for ΔP and P_S/P_W indicate a dominance of summer rainfall and therefore a summer rainfall regime, while comparatively lower values indicate a dominance of winter rainfall and a winter rainfall regime.

The SPP makes sense in light of both the wood anatomy and growth, as well as carbon isotope theory. Both indicate that the appearance of the radial surface (i.e. banded growth increments) and the $\delta^{13}C$ values of wood fluctuate in response to whether growing conditions are optimal or suboptimal (Fritts 1976; Schweingruber 1988; Speer 2010; McCarroll & Loader 2004; Diefendorf *et al.* 2010; Kohn 2010). These climate shifts occur over longer timescales (i.e. decadal or centennial), but also over short timescales according to a predictable seasonal pattern. It appears that as evergreen wood grows over the year, forming a growth increment, the wet season (i.e. more negative $\delta^{13}C$ values), dry season (i.e. more positive $\delta^{13}C$ values), and the gradual transition between them are preserved in wood tissues in the form of a rise and fall isotope pattern – a seasonal signal (Figure 1).

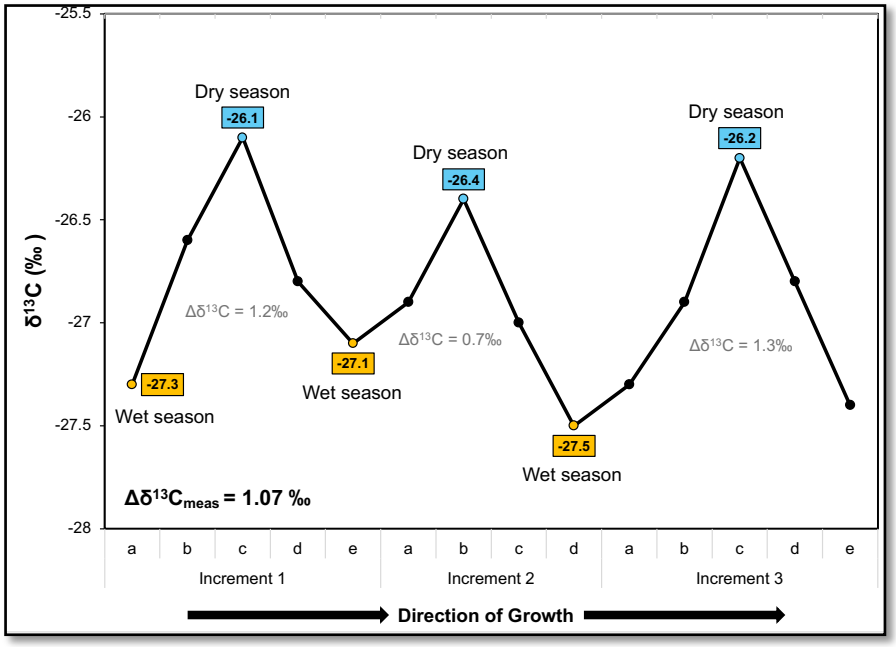

Figure 1. A hypothetical pattern of serial $\delta^{13}C$ measurements taken across three successive evergreen growth increments. The $\Delta\delta^{13}C$ for each increment, as defined by the seasonal precipitation proxy (SPP), is calculated as the difference between the maximum value ($\delta^{13}C_{max}$; blue) and the preceding minimum value to the left ($\delta^{13}C_{min}$; orange). These differences are averaged to calculate the average measured carbon isotope change, the seasonal amplitude ($\Delta\delta^{13}C_{meas}$), for the three increments. In this example $\Delta\delta^{13}C_{meas}$ = 1.07 ‰. The arrows along the x axis indicate direction of growth.

In evergreens, understanding whether the seasonal $\delta^{13}C$ signal reflects a predominance of winter or summer rainfall depends on an additional variable: seasonal cycling in the $\delta^{13}C$ value of atmospheric CO_2 ($\Delta\delta^{13}C_{CO2}$). The mean $\delta^{13}C$ value of the atmosphere (at the turn of the present century) is ~−8‰ (McCarroll & Loader 2004), but this value experiences seasonal changes in response to periods of increased photosynthesis (summer/spring) versus increased respiration (winter/autumn) (Gessler *et al.* 2014; Keeling & Graven 2021). In summer, the atmosphere is enriched in ^{13}C, leading to less negative $\delta^{13}C_{CO2}$, and in winter the atmosphere is conversely enriched in ^{12}C, leading to more negative $\delta^{13}C_{CO2}$ (Gessler *et al.* 2014; Keeling & Graven 2021). In a region governed by a winter rainfall regime, $\Delta\delta^{13}C_{CO2}$ and carbon isotope discrimination ($\Delta^{13}C$) – the preferential selection for the lighter ^{12}C over the heavier ^{13}C (which is, in turn, a response to changes in precipitation (ΔP)) – are thus in-phase, the signals amplifying one another, and so one would expect a greater amplitude of seasonality or value for $\Delta\delta^{13}C_{meas}$ (Figure 2). In a summer rainfall regime, $\Delta\delta^{13}C_{CO2}$ and $\Delta^{13}C$ are out of phase, the signals effectively cancelling one another out, and so one would expect a reduced or dulled amplitude of seasonality or value for $\Delta\delta^{13}C_{meas}$ (Figure 2).

Schubert and Jahren (2011) suggest that such as signal is only identifiable in evergreen trees due to fundamental differences in the cycling of stored carbon between deciduous and evergreen taxa. Photosynthesis in deciduous trees ceases during winter months. Deciduous trees also incorporate older, remobilised photosynthates from storage reserves into their tissues just as the favourable conditions of the growing season begin (e.g. Kagawa *et al.* 2006). This explains why wood grown later into or at the end of the growing season (the latewood) presents a current-year $\delta^{13}C$ signal as more recent photosynthates are used in tissue formation (Loader *et al.* 1995). Stored carbon is enriched in ^{13}C relative to recent photosynthates, and so the serial subsampling of deciduous growth increments produces a pattern wherein $\delta^{13}C$ values peak and then become more negative as the tree grows, before peaking again when stored carbon is used at the start of the vegetative period (Figure 1a Schubert & Jahren 2011: 7293). The use of stored carbon to form tissues means that $\delta^{13}C$ values do not necessarily reflect seasonal conditions at the time of tissue formation. Conversely, it has been demonstrated that evergreen gymnosperms and angiosperms depend almost entirely on more recently assimilated carbon for their secondary growth (Vincent-Barbaroux *et al.* 2019). Thus, SPP has been validated for use in only modern and fossilised evergreen wood. The subsequent question underpinning this research is whether it can be applied with equal reliability to evergreen archaeological charcoal to address the need for seasonally resolved on-site proxies that are less reliant on the qualitative inference of past climate conditions.

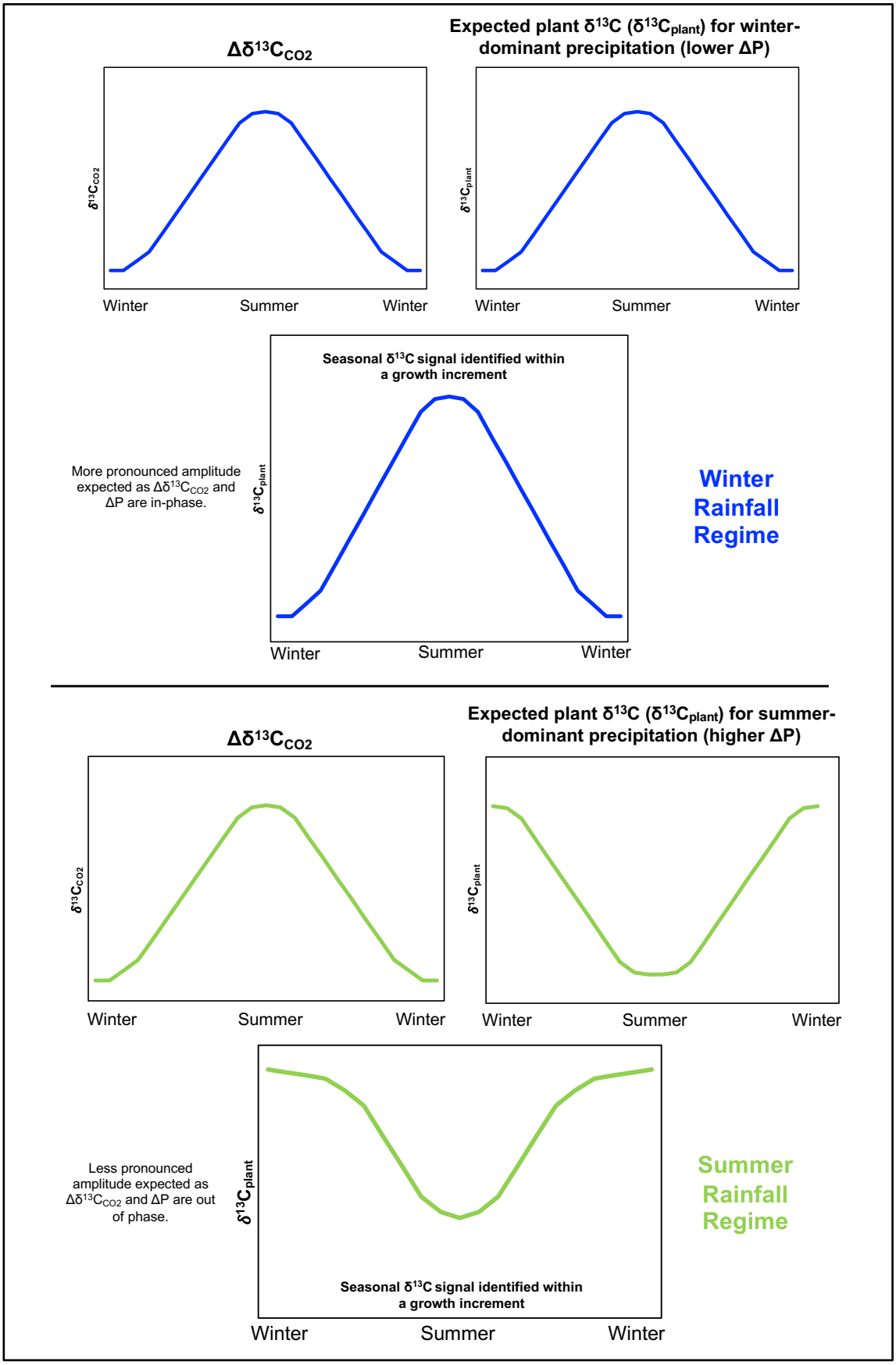

Figure 2. Hypothetical plots demonstrating how the two variables $\Delta\delta^{13}C_{CO2}$ and ΔP, in theory, combine to have a net effect on the seasonal $\delta^{13}C$ amplitude measured from trees in both a winter (top) and summer (bottom) rainfall regime. The variables are in-phase in a winter rainfall regime, leading to more pronounced amplitudes. In a summer rainfall regime, they are out of phase, leading to reduced amplitudes.

1.3. Project Aims & Objectives

Whether the SPP can extract seasonal information from carbonised evergreen wood remains unknown. More importantly for this project, however, whether the SPP is at all able to extract seasonal information from South African evergreen taxa has never before been tested. Of the Schubert and Jahren (2011) global dataset, three *Rhizophora* trees from Kenya were the sole representatives of Africa. Therefore, before the SPP can be applied directly to archaeological charcoal specimens in South Africa, it is essential to validate its effectiveness within the South African climatic context and local evergreen taxa. Once the SPP has been ground-truthed and calibrated, the archaeological application can proceed.

As a result, this study is structured around three sequential aims, presented here as questions:

1. **Does the SPP identify a seasonal signal in the serial $\delta^{13}C$ measurements of modern evergreen wood from South Africa?**

   The SPP is effective across a range of latitudes and environments but utility in the South African context is yet to be seen, and whether the SPP is able to differentiate between different rainfall regimes in close proximity is thus far an equally overlooked question. The evergreen genera *Protea* and *Podocarpus* were selected for analysis. Results obtained from these genera, collected across all three of the country's seasonal rainfall zones, can be compared to assess whether local evergreen angiosperm and gymnosperm wood indeed preserve seasonal signals.

2. **Does the SPP identify a seasonal signal in the serial $\delta^{13}C$ measurements of evergreen charcoal from South Africa?**

   The charcoal counterparts of the *Protea* and *Podocarpus* wood samples analysed as part of Question 1 must be similarly processed and analysed to determine the ability of the SPP to identify a seasonal signal in carbonised wood.

3. **Does the SPP identify a seasonal signal in the serial $\delta^{13}C$ measurements of archaeological charcoal from the Last Glacial Maximum (LGM) and Last Glacial-Interglacial Transition (LGIT) in South Africa?**

   Should utility in modern *Protea* and *Podocarpus* wood and charcoal be established, it follows that the SPP can be applied to archaeological Proteaceae and Podocarpaceae specimens to obtain an amplitude of seasonality but also to quantify ΔP and P_S/P_W. The modern results from all three rainfall zones will aid in assessing the seasonal signals, if any, identified in the LGM

charcoals from Boomplaas Cave (see J. Deacon 2023 for a current review) and LGIT charcoals from Waterfall Bluff (see Esteban *et al.* 2023a for a current review).

The majority of this project therefore comprises a modern calibration of the SPP, and a limited number of archaeological specimens are analysed to provide preliminary insight into the potential the proxy holds for South African archaeology. Greater insight into Late Pleistocene seasonal rainfall variability is needed, particularly for the LGM (Chase & Meadows 2007; Stone 2014; Marean *et al.* 2014; Engelbrecht *et al.* 2019; Faith *et al.* 2024). Locally, the hope is that the knowledge and methods gained here may elsewhere be employed to better understand the technologies, choices, and behaviours of LSA hunter-gatherers. However, should the SPP show promise in archaeological charcoal as a material, there is little reason to suggest that this method cannot be applied to any site globally where evergreen charcoals have been found.

CHAPTER 2

Growth Ring Studies in South Africa

2.1. Introduction

To determine the effectiveness of the SPP when applied to archaeological charcoals, modern wood and charcoal specimens are initially studied for comparative purposes. Since the growth rings of these specimens are analysed for climate reconstruction, this study is broadly situated within the field of dendrochronology and its subfield dendroclimatology, even if the goal is not to apply 'classical' methods (Heinrich & Allen 2013: 181) to test the modern samples for their dendrochronological potential. Still, much of the theory underpinning dendrochronology and dendroclimatology do apply here and therefore must be addressed.

Consequently, this Chapter critically examines the theory and methods of classical dendrochronology and dendroclimatology (hereafter collectively termed 'dendrology' unless otherwise stated) and their applications to South African trees and environments. The aim is to explore the limitations that have hindered the field's development in the region. I propose that isotope methods offer an alternative approach for reconstructing climate patterns, particularly in local trees where classical methods encounter challenges and yield less consistent results. Finally, this Chapter bridges modern dendrology and archaeological science by discussing the potential of stable carbon isotopes in archaeological charcoal as a tool for reconstructing past climates.

This Chapter is therefore organised around the following goals:

- Review foundational knowledge: Define key terms and outline how tree growth, wood anatomy, carbon isotopes, and climate interact.
- Assess the state of growth ring research in South Africa: Review existing studies on gymnosperms and angiosperms in the region, highlighting the challenges that have limited the wider applications of these methods.
- Introduce alternative isotope approaches: Explore carbon isotope dendroclimatology as a promising alternative for reconstructing climate patterns.
- Bridge modern and archaeological applications: Discuss the potential of applying isotope methods to archaeological charcoal to illuminate past climate conditions.

2.2. Trees and climate: Wood growth and anatomy

The trunk of a tree is made up of a protective outer bark combined with an inner bark (secondary phloem) which distributes sugars, nutrients, and hormones throughout the tree. Additionally, the trunk contains wood (secondary xylem), which consists of tube-like structures that transport water from the roots to the leaves (Stokes & Smiley 1968; Suresh 2012; Hirons & Thomas 2018). Situated between the secondary phloem and secondary xylem is the vascular cambium – a thin layer of undifferentiated, meristematic tissue which generates phloem on its outer side and xylem on its inner side (Stokes & Smiley 1968; Schweingruber 1988). As a secondary meristem, the vascular cambium divides and specialises in ways that allow the tree to grow in diameter, a process known as secondary or radial growth. This process is responsible for the formation of growth bands or increments (popularly known as 'tree rings') in woody plants (Schweingruber 1988). The oldest growth increment forms at the core or pith of the trunk, while the newer increments form outward as the central stem increases in diameter (Schweingruber 1988; Groover & Robischon 2006; Suresh 2012). The tissue laid down in each growth increment is made up of several elements including carbon from the atmosphere as well as oxygen and hydrogen from the tree's water source (McCarroll & Loader 2004; Gagen *et al.* 2011).

It is widely accepted that tree growth patterns reflect environmental and climatic conditions under which they are formed (Fritts 1976; Hughes *et al.* 1982; Schweingruber 1988). Temperature, precipitation, atmospheric pressure, wind, humidity, sunshine, competition, nutrient supply, grazing, disease, and disturbances are among some of the parameters that affect or limit physiological processes within trees and their growth responses (Hughes *et al.* 1982). Physiological processes and growth responses are recorded in the structure of the wood almost immediately and are consequently directly measurable (Schweingruber 1988).

In both gymnosperms (softwoods producing exposed seeds) and angiosperms (hardwoods bearing flowers and fruit), growth increment boundaries are indicated by a change in the density, size, and shape of wood cells, including xylem tracheids in gymnosperms, and xylem vessels in angiosperms (Schweingruber 1988; Speer 2010). Such changes tend to follow an annual pattern in response to environmental controls that regulate the activity of the dividing vascular cambium (Groover & Robischon 2006). These changes take the form of earlywood – intensive growth at the start of the growing season in response to the onset of desirable conditions and marked by a lighter hue and less dense cells with thinner cell walls – and latewood – reduced growth at the end of the growing season in response to a decline in favourable conditions, marked by a darker hue and smaller cells with thicker

cell walls (Schweingruber 1988; Hirons & Thomas 2018; Frank *et al.* 2022). What results is a sequence of patterned growth rings containing attributes that can be used to make inferences about growing environments (Schweingruber 1988; Smith & Lewis 2007).

2.3. Definitions, principles, and terminology

Dendrochronology is the science that studies and dates the patterns of growth rings in trees (February 2000; Speer 2010; Frank *et al.* 2022). It has long been regarded as perhaps the most precise and highly resolved method for extending climate records deeper into the past (Jones *et al.* 2009; Speer 2010; Pearl *et al.* 2020). Growth rings can be dated with a great degree of precision and assigned a calendar year given that growth occurs incrementally and often according to an annual periodicity (Fritts 1976; Schweingruber 1988).

A prominent subfield of dendrochronology is dendroclimatology, the study of tree growth rings and the past environmental conditions they reflect (Fritts 1976; Speer 2010; Sheppard 2010). Climate reconstructions harness the inbuilt chronometric feature of growth rings and are thus able to resolve climate variables to decadal, annual, and even subannual timescales (McCarroll & Loader 2004; Pearl *et al.* 2020). In the Northern high latitudes – the birthplace of dendrology – records from living trees are combined with those from dead and fossil trees to construct extensive growth ring-climate chronologies, often reaching back several hundred, and in some cases, over a thousand years (George 2014; Pearl *et al.* 2020).

Here, the term 'classical' dendrology, as defined by Heinrich and Allen (2013), refers to the traditional theory, principles, and methods that have historically dominated and defined growth ring studies, particularly in the Northern Hemisphere. Foundational to this conceptualisation of dendrology are key concepts and principles. While these have been extensively detailed elsewhere (e.g. Stokes & Smiley 1968; Fritts 1976; Speer 2010), I want to highlight four interrelated principles that set the framework for how classical dendrology works in practice. These are limiting factors, sensitivity, the annual ring, and cross-dating. The focus of classical dendrology is ring width measurement.

The biological principle of *limiting factors* proposes that a tree's growth is governed by the environmental condition that most restricts it (Fritts 1976). Additionally, the degree to which tree growth reflects responses to this limiting factor is described as its *sensitivity* (Stokes & Smiley 1968; Fritts 1976; Speer 2010). Trees with high sensitivity show marked variability in ring widths across the transverse surface which closely mirror changes in climate. Theory suggests that wider rings form

under favourable growing conditions while more narrow rings form under conditions of increased stress (Schweingruber 1988; Frank *et al.* 2022). Sensitive trees are preferred in dendrology because the distinct patterns of wide and narrow rings they produce facilitate cross-dating and also confirm the suitability of the tree for climate reconstruction.

The principle of the *annual ring* forms the foundation of dendrology (McNaughton & Tyson 1979; Speer 2010; Gebrekirstos *et al.* 2014; Frank *et al.* 2022). Theory indicates that the activity of the vascular cambium coincides with seasonal shifts in optimal and suboptimal conditions, meaning that the rhythm of the cambium is considered annual (Speer 2010). If each ring is accepted as annual, and the widths of each ring are accepted to reflect the influence of a certain limiting factor, then the ring width patterns from different trees of the same species growing in one locality can be matched to date each growth ring to the calendar year. This practice is called *cross-dating* and is used to validate the age determination of each growth ring (Fritts 1976; Speer 2010). Ultimately, a number of validated overlapping tree ring records for the same species are combined to create a chronology representing tree growth at a specific site (Stokes & Smiley 1968; Fritts 1976; Schweingruber 1988; Speer 2010). Moreover, site chronologies are correlated with local climate records, such as temperature, precipitation, or humidity, to identify the primary climate variable limiting tree growth. It is this analysis that underpins climate reconstruction from tree rings (February & Gagen 2003). It is by virtue of the annual ring that dendroclimatology is able to resolve past climate variables to a decadal, annual or even subannual time scale (McCarroll & Loader 2004).

However, annual rings are not guaranteed in all trees and environments (as discussed in Section 2.5), limiting the applicability of this principle – and arguably classical dendrology in its entirety – in contexts where tree growth follows a more complex or less predictable periodicity. Silva *et al.* (2019) argue that the term ‘tree ring’ carries the assumption of annual growth periodicity. This assumption has led to the concept of ‘false rings’, which refer to growth that does not necessarily align with an annual cycle and are often regarded as a flaw and feature to avoid in dendrology. Instead, they advocate for the use of the term ‘growth ring’ which accommodates a range of periodicities that may not be annual. Therefore, alternative terms like ‘growth ring’ and ‘growth increment’ are preferred over ‘tree ring’ in this study focusing on South Africa trees that indeed demonstrate more complex growth patterns and periodicities (see Sections 2.5 and 2.6).

2.4. Trees and climate: Carbon isotopes in woody plants

In addition to growth ring widths and classical dendrology, stable isotopes – including carbon, oxygen, and hydrogen – are increasingly studied to better understand year-to-year climate variations recorded in growth increment tissues (McCarroll & Loader 2004; Gessler *et al.* 2014; Frank *et al.* 2022), especially in trees growing in less distinctively seasonal environments like the tropics and subtropics (van der Sleen *et al.* 2017; Frank *et al.* 2022). Carbon isotopes are of particular importance here as the $\delta^{13}C$ values of wood capture the relationship between stomatal conductance and the rate of photosynthesis and, by extension, tree response to external climate factors (McCarroll & Loader 2004; Shestakova & Martínez-Sancho 2021).

In growth rings, the ratio of the heavier stable isotope of carbon (^{13}C) to the lighter stable isotope of carbon (^{12}C) – expressed in delta notation ($\delta^{13}C$) relative to an internationally recognised standard such as VPDB – reflects short-term climatic shifts that influence plant physiological processes (McCarroll & Loader 2004; Gessler *et al.* 2014; Shestakova & Martínez-Sancho 2021). These short-term shifts are commonly argued to concern the hydrological cycle and plant water use, given the relationship between stomatal conductance and the rate of photosynthesis (Farquhar & Sharkey 1982; McCarroll & Loader 2004).

Carbon isotopes are taken in by plants through the diffusion of atmospheric CO_2 ($^{12}CO_2$, $^{13}CO_2$) into leaves during photosynthesis. The mean $\delta^{13}C$ value of the atmosphere is about −8‰ while the $\delta^{13}C$ value of leaves and wood is more negative (−20‰ to −30‰) (McCarroll & Loader 2004). This indicates the occurrence of fractionation between the intake of carbon and the assimilation of this carbon in plant tissues (McCarroll & Loader 2004). Carbon isotope discrimination ($\Delta^{13}C$) – the selection for the lighter ^{12}C over the heavier ^{13}C – in trees and other C3 plants is affected by physiological and climate factors and occurs in two stages: first during the diffusion of CO_2 through leaf stomata and second during the fixation of diffused carbon by the photosynthetic RuBisCO enzyme (Farquhar *et al.* 1989; McCarroll & Loader 2004). This discrimination can be expressed as:

$$\Delta^{13}C(‰) = a + (b - a)(c_i/c_a) \quad (1)$$

where a is the (constant) discrimination against $^{13}CO_2$ during diffusion through leaf stomata (–4.4‰), b is the (constant) net discrimination by RuBisCO during carboxylation (–27‰), c_i is the leaf intercellular concentration of CO_2, and c_a the ambient concentration of CO_2 (McCarroll & Loader 2004). The c_i/c_a ratio represents the balance between the influx of CO_2 via diffusion and the rate of

photosynthesis which uses CO_2. In practice, $\Delta^{13}C$ can also be approximated as the difference between δ13C of atmospheric CO_2 and that of plant tissue, i.e. $\Delta^{13}C \approx \delta^{13}C_{air} - \delta^{13}C_{plant}$.

Under optimal growth conditions, leaf stomata are fully open, allowing CO_2 inflow (stomatal conductance) to surpass the photosynthetic rate such that c_i/c_a increases and maximum carboxylation discrimination against ^{13}C occurs, leading to more negative $\delta^{13}C$ values (Farquhar *et al.* 1989; McCarroll & Loader 2004). However, when plants experience water stress and suboptimal growth conditions, stomata close to minimise water loss through transpiration. This reduces stomatal conductance relative to photosynthesis, decreasing the c_i/c_a ratio and carboxylation ^{13}C discrimination, leading to less negative $\delta^{13}C$ values (Farquhar *et al.* 1989; McCarroll & Loader 2004). Thus, the $\delta^{13}C$ values of woody tissue are indicative of plant water use.

Diefendorf *et al.* (2010) investigated global patterns in carbon isotope discrimination in woody plants. They found a strong positive correlation between discrimination in the leaf (Δ_{leaf}) and mean annual precipitation (MAP). In areas with lower precipitation, plants tend to have reduced discrimination (less negative $\delta^{13}C$). In areas of higher precipitation, discrimination is enhanced (more negative $\delta^{13}C$). This demonstrates the theory presented by Farquhar *et al.* (1989) and confirms that water availability is a major control of plant $\delta^{13}C$ values. The finding is further supported by Kohn (2010), whose analysis of a global dataset of $\delta^{13}C$ values of C3 plants revealed a strong, albeit nonlinear, negative correlation between plant $\delta^{13}C$ and MAP. These relationships tend to be clearest in more extreme environments – very wet or very dry – with greater variability in intermediate settings.

Water availability is an external factor affecting plant $\delta^{13}C$ values. A critical internal factor also affecting $\delta^{13}C$ is differences in leaf structure and physiology between gymnosperms and angiosperms. Gymnosperms are generally understood to produce less negative $\delta^{13}C$ values relative to angiosperms (e.g. Leavitt 2002). Several studies have sought to offer explanations for the $\delta^{13}C$ differences between the two plant groups, which are connected fundamentally to differences in carbon isotope discrimination arising from key physiological and morphological distinctions (e.g. Sheldon *et al.* 2020; Hare & Lavergne 2021). Angiosperms, with higher transpiration costs relative to carboxylation, tend to discriminate more against ^{13}C, resulting in more negative $\delta^{13}C$ values (Hare & Lavergne 2021). Conversely, gymnosperms, distinguished by lower ratios of mesophyll to stomatal conductance of CO_2, as well as a reduced release of CO_2 in photorespiration, discriminate less against ^{13}C, resulting in less negative $\delta^{13}C$ values (Hare & Lavergne 2021). Therefore, angiosperms respond more strongly to changes in atmospheric CO_2 levels compared to gymnosperms (Sheldon *et al.* 2020; Hare & Lavergne

2021). These inherent physiological differences, influenced by growing environment factors like atmospheric CO_2 levels, underscore the importance of considering plant type when interpreting $\delta^{13}C$ measurements in ecological and dendroclimatology studies.

2.5. Classical dendrology in South Africa

One of the key challenges to growth ring studies in South Africa is a limited availability of long-lived, climate-sensitive species. Variable growth patterns, complex wood anatomy, and challenges to sampling (Pearl *et al.* 2020), as well as greater species richness, varied habitats, less predictable cambial activity, and reduced amplitudes of seasonality (Silva *et al.* 2019) have all been identified as major obstacles to dendrology in the tropics and subtropics.

An early South African study by Lilly (1977) surveyed over 100 indigenous species for their dendrochronological potential and concluded that a variety of ring anomalies – such as poorly defined, locally absent, or discontinuous rings – commonly found in local trees make traditional dendrology challenging. It has been suggested that the challenges facing dendrochronology in South Africa are greater than in any other region in the SH (February & Stock 1998a&b).

South Africa's latitudinal position in the subtropics has been widely regarded as the cause of various anatomical complexities which preclude the formation of reliably annual rings and, ultimately, precise age determination (Schweingruber 1988; Gourlay 1995b; February 2000; Gebrekirstos *et al.* 2014; Zhao *et al.* 2019). Temperate regions are characterised by a strong amplitude of seasonality, with a distinct growing season and a distinct period of cambial dormancy (Rathgeber *et al.* 2022). These seasonal periods of inactivity in the cambium are what drive the formation of discernible growth increment boundaries — a prerequisite for the creation of growth ring chronologies using classical dendrochronological methods (Section 2.3). In southern Africa, however, it has historically been suggested that less distinct seasonality renders cambial growth less sensitive to climate fluctuations (Zacharias *et al.* 2017). Moreover, whatever growth increments are identified in tropical and subtropical trees, they appear to be influenced by a more ambiguous periodicity, rather than a reliably annual one (Jones *et al.* 2009; Silva *et al.* 2019). Thus, annual growth rings are not a "biological certainty" (February 1994: 100), making classical dendrochronology, which prioritises the width measurements of ageable tree rings, difficult.

Still, Lilly's (1977) survey identified certain species within the genera *Podocarpus* and *Widdringtonia* as having potential for dendrology in South Africa. This came shortly after Hall's (1976) analysis of a

large *Afrocarpus* (formerly *Podocarpus*) *falcatus* trunk cross-section from Karkloof, KwaZulu-Natal, housed at the KwaZulu-Natal (formerly Natal) Museum in Pietermaritzburg. As a result of these early studies, classical dendrology research in South Africa has predominantly focused on gymnosperms, although more recently attention has been directed toward angiosperms.

The present study has selected for analysis both a gymnosperm genus and an angiosperm genus: *Podocarpus* and *Protea*, respectively. Schubert and Jahren (2011) suggest that the SPP can be successfully applied to all evergreen species. However, the variable vascular structures, growth habits, and reproductive strategies of these two main categories of woody C3 plants (Hare & Lavergne 2021) may differentially influence their abilities to capture and reconstruct climate variables, especially at a seasonal resolution. Consequently, Subsections 2.5.1 and 2.5.2 review previous classical dendrology research conducted on South African gymnosperms and angiosperms to assess potential differences and their implications for testing the SPP.

2.5.1. Classical dendrology on gymnosperms in South Africa

Globally, there are 669 gymnosperm species consisting of seventy-two genera divided into six families (Esteban *et al.* 2023b). The two genera containing the greatest number of species are *Pinus* and *Podocarpus*, with 118 and 115 species, respectively (Esteban *et al.* 2023b). The majority of the dendrochronological research conducted in the Northern Hemisphere has focused on coniferous gymnosperms, namely *Pinus* and *Picea* (George 2014; Zhao *et al.* 2019; Pearl *et al.* 2020). This, and Lilly's (1977) survey, has led traditional growth ring width studies in South Africa to focus primarily on indigenous gymnosperms such as *Widdringtonia* (e.g. Dunwiddie & LaMarche 1980; February & Stock 1998a; February & Gagen 2003) or *Podocarpus* (e.g. Curtis *et al.* 1978; McNaughton & Tyson 1979; February & Stock 1998b; Vogel *et al.* 2001; Baverstock 2021). The goal seems to have been to use indigenous gymnosperms to replicate the dendrochronological achievements seen in the Northern Hemisphere, but the outcomes show less reliable success.

Dunwiddie and LaMarche (1980) were able to successfully develop a growth ring chronology for the period 1564-1977 using *Widdringtonia wallichii* (formerly *Widdringtonia cedarbergensis*) sampled from Die Bos in the Cederberg Mountains of the Western Cape. Although the study found no definitive correlation between the growth ring chronology and climate data, it nonetheless proposed a tentative link to spring and early summer moisture availability. However, narrow growth rings typically used to indicate marker years in the Northern Hemisphere were infrequent, and so wide rings and frost rings were instead used to cross-date the specimens. Ring wedging and lobate growth were reported to be

rare in this species, but identifying growth ring boundaries with precision remained challenging due to the gradual transition into the latewood and the presence of 'false' bands within it.

The same growth ring anomalies in *W. wallichii* were identified by February and Stock (1998a) who analysed both increment cores and stem discs from Algeria and Krakadouw, also in the Cederberg Mountains. The results from stem discs, they found, were more precise and therefore more likely to be included in the final chronologies for both locations. Like Dunwiddie and LaMarche (1980), February and Stock (1998a) also found no correlation between ring widths and rainfall records.

Today, the *W. wallichii* growth ring chronology developed by Dunwiddie and LaMarche (1980) remains the only successfully cross-dated growth ring record in South Africa. While classical dendrochronology applied to *W. wallichii* has shown great promise in chronology building, it remains unclear whether the resulting chronologies can be reliably linked to, and therefore able to reconstruct, climate variables. Chronology building has proven to be less reliable in other *Widdringtonia* species, such as *Widdringtonia nodiflora* and *Widdringtonia schwarzii*. These were concluded to be unsuitable for dendrochronology and dendroclimatology due to the presence of 'false' rings and difficulties in identifying latewood termination (February & Gagen 2003).

Similar problems have been noted by studies focused on *Podocarpus*. Hall's (1976) analysis of the Karkloof *A. falcatus* specimen identified 597 variable growth increments and, after comparison with climate records from the nineteenth and twentieth centuries, tentatively argued the ring width variability present in the specimen to be a function of regular, decadal rainfall oscillations. Hall did not cross-date his ring patterns using either an additional radius from the same specimen, nor other *A. falcatus* trees from the same area, and was therefore unable to confirm annual growth rings. Nevertheless, this study represents an early effort to harness growth ring records to understand archaeological patterns: Hall used the growth ring-climate data to make interpretations about the influence of rainfall on Nguni agricultural practices during the Later Iron Age.

Following Lilly's (1977) survey and Hall's (1976) pioneering work on the Karkloof specimen, *A. falcatus* was further examined by Curtis *et al.* (1978) who sampled from Magoebaskloof, Limpopo, and McNaughton and Tyson (1979) from Witelsbos, Eastern Cape. The former study tested a method of tracing each growth increment along the whole circumference of a single cross-section and concluded that despite certain growth increment anomalies and missing rings, the species does ultimately have dendrochronological potential. The latter study had a greater sample size of twelve cross-sections

from which they examined multiple radii. Based on ring counts and an assumption of annual growth increments, they were able to age five cross sections. Based on ring width measurements, they were able to identify certain commonalities between several samples and matched these against historical periods of enhanced and suppressed rainfall. Despite promising results, both studies were fundamentally exploratory in nature. They essentially sought to demonstrate some relationship between *Podocarpus* ring widths and climate but without going further to thoroughly cross-date all samples for a locality and ultimately build ring width chronologies that could be successfully matched against climate records.

In response, February and Stock (1998b) aimed to confirm once and for all whether or not *A. falcatus* and the related *Podocarpus latifolius* could be used to build site-level ring width chronologies in the traditional sense of dendrochronology. Their assessment of eight *A. falcatus* and six *P. latifolius* cross-sections from Harkerville on the south coast of the Western Cape was only able to cross-date one of each species within themselves, and no trees of the same species across the site. The popular cross-dating software COFECHA did not improve their results. While previous studies identified various growth anomalies as complications to be worked around in the dendrochronological analysis of *A. falcatus*, February and Stock viewed them as more fundamental obstacles to the approach. They argue that poorly defined, locally absent, and converging rings make cross-dating *A. falcatus* and *P. latifolius* for the same site "an impossible task" (February & Stock 1998b: 749), meaning that the collective growth of these taxa cannot meaningfully be compared to local climate, rendering them fundamentally unsuitable for both dendrochronology and dendroclimatology.

With *Podocarpus* at an apparent impasse, Vogel *et al.* (2001) tested an alternative approach to revive its dendrochronological potential. They applied Accelerator Mass Spectrometry (AMS) radiocarbon 'wiggle match dating' along two transects of Hall's (1976) Karkloof specimen. They found that, in general, the species does lay down annual rings, but tens of missing rings during slow growth and tens of 'false' or merging rings during rapid growth mean that future age determinations would require corroboration with radiocarbon dating.

Twenty years later, Baverstock (2021) opted instead for a first principles approach and returned to Karkloof to sample increment cores from twenty *A. falcatus* trees to which she applied classical dendrochronological methods to construct a full ring-width chronology for the area. The study found that the growth increments of *A. falcatus* are annual but, once again, 'false' and missing rings were identified as potential complications. Moreover, Baverstock correlated her chronology with local

climate records and the results indicated the primary driver of ring-width variability in *A. falcatus* was likely temperature, not rainfall as others had found (Hall 1976; McNaughton & Tyson 1979; Vogel 2001).

Indigenous gymnosperms, it seems, are characterised by numerous growth ring complexities that preclude the repeatable application of classical dendrology in South Africa. In response, some studies have targeted alien gymnosperms to see if these might produce reliable chronologies and climate correlations just as they do in the Northern Hemisphere. The first dendrochronological assessment of an alien gymnosperm was conducted by Midgley (2002) who was able to produce a growth index chronology from *Pinus radiata* stem discs for Silvermine Nature Reserve in the Western Cape. However, no significant correlations were found between this chronology and annual, winter, or growth season rainfall. Later, Lester (2019) analysed *Pinus pinaster*, *Sequoia sempervirens*, and *Cupressus lusitanica* from the Cape Town Metropolitan Area, and *Eucalyptus cladocalyx from* Wolseley in the Western Cape to determine the possibility of extending rainfall records and constructing climate forecasting models. The results proved unsuccessful, with none of the utilised time series methods producing significant correlations with rainfall records. Both indigenous and alien gymnosperms, then, appear to be poorly suited for climate reconstruction *sensu* classical dendrology.

2.5.2. Classical dendrology on angiosperms in South Africa

Today, angiosperms constitute 90% of all terrestrial plant species (Govaerts *et al.* 2021), with 13,600 genera organised into 416 families (Zuntini *et al.* 2024). Compared to gymnosperms*,* classical dendrology research on angiosperms has been more limited in South Africa. One possible reason for this is that angiosperms are typically viewed as less favourable for dendrology due to their intricate xylem anatomies, with angiosperm wood being structurally more complex and diverse than gymnosperm wood (Silva *et al.* 2019; Frank *et al.* 2022). The arrangement of secondary xylem vessels and therefore growth rings across the transverse surface of angiosperms varies between species (Rathgeber *et al.* 2022), with taxa classified as either ring porous (earlywood vessels are clearly larger in diameter relative to latewood vessels, and ring boundaries are distinct), semi-ring porous (earlywood vessels are only generally larger in diameter relative to latewood vessels), or diffuse porous (vessel diameters hardly differ between earlywood and latewood, rendering growth ring boundaries indistinct) (Esteban *et al.* 2024).

This anatomical complexity, along with regional ‘aseasonality’, has historically led to the neglect of angiosperms in tree ring studies in South Africa. In more recent decades, indigenous angiosperms,

such as *Vachellia* and *Senegalia* (both formerly *Acacia*), have received some attention and have been considered for their dendrochronological potential (e.g. Gourlay 1995a&b; February *et al.* 2006; Steenkamp *et al.* 2008; Bhugeloo 2014; Zacharias *et al.* 2017). In these species, clear growth ring boundaries were identified based on the presence of marginal parenchyma, and not based on changes in the appearance of xylem vessels between the earlywood and latewood (Gourlay 1995a; February *et al.* 2006; Steenkamp *et al.* 2008; Bhugeloo 2014; Zacharias *et al.* 2017). Apart from that of February *et al.* (2006), these *Vachellia* and *Senegalia* studies further showed that growth rings formed annually. Nevertheless, February *et al.* (2006), working with *Vachellia nilotica* and *Senegalia nigrescens* stem discs from Hululuwe-Imfolozi Park in KwaZulu-Natal, concluded that these species could not be cross-dated even with the help of COFECHA. Bhugeloo (2014) reached a similar conclusion for *V. nilotica* from Bonamanzi Game Reserve also in KwaZulu-Natal, finding that despite the construction of a 99-year master chronology, the inconsistent growth patterns between individual trees ultimately weakened confidence in the cross-dating results. Moreover, the lack of significant correlation between the chronology and climate data led to the conclusion that *V. nilotica* has limited dendroclimatological potential.

South African *Protea* species have also been assessed (e.g. February 1990, 1992, 1994, 1996), but these studies focused on examining modern *Protea* wood properties for comparison with archaeological charcoals and will therefore be discussed in greater detail in Section 2.7. Other angiosperm genera so far analysed in South Africa include *Adansonia* (e.g. Robertson *et al.* 2006; Woodborne *et al.* 2015, 2016), *Breonadia* (e.g. Norström *et al.* 2005, 2008), and *Mimusops* (e.g. Hall *et al.* 2009). What sets these studies apart is their alternative analytical approaches that diverge from the expectations of classical dendrology. Width measurements are not the only growth ring property able to produce climate signals and climate-sensitive chronologies (De Mil *et al.* 2021; Frank *et al.* 2022). In recent decades, interest has grown in exploring wood stable isotope measurements for chronology building and potential climate reconstruction, especially in tropical and subtropical regions where classical approaches have faced significant challenge (McCarroll & Loader 2004; Evans & Schrag 2004; Gebrekirstos *et al.* 2014; van der Sleen *et al.* 2017; Frank *et al.* 2022). Most of the tree ring studies on South African angiosperms have thus been isotopic in nature – with a specific focus on carbon isotopes – resulting in an isotope dendroclimatology for the country that shows greater promise.

2.6. Isotope Dendroclimatology in South Africa

In search of alternative means of extracting climate information from growth rings, several studies in South Africa have applied stable isotope methods to local woody plants. A study presented by Norström *et al.* (2005) analysed the carbon isotope composition of two *Breonadia salicina* trees growing approximately 1 km apart near the Murle Brooks River in Limpopo to reconstruct rainfall patterns between 1375 and 1995. Despite the species' lack of reliably visible growth rings, the study was able to identify major wet and dry periods. This meant that the measured $\delta^{13}C$ values were ultimately determined by changing water availability linked to long-term variations in regional rainfall. Later, Norström *et al.* (2008) examined the oxygen isotope compositions of the same two trees. The study initially aimed to assess the potential of using *B. salicina* $\delta^{18}O$ as a climate proxy and observed a co-variation in $\delta^{13}C$ (Norström *et al.* 2005) and $\delta^{18}O$ before 1600 AD, suggesting a common, likely climatic influence on both isotope signals. However, this co-variation weakened after 1600 AD, coinciding with slow growth and reduced growth ring formation, indicating drier conditions. Furthermore, the weak correlation between the $\delta^{18}O$ values of the two trees is interpreted as indicative of the influence of more localised climate on isotope signals. This highlights the potential impact of local-to-regional factors, such as groundwater or differing contributions of river water, on growth ring isotope values.

While growth ring-data hold the potential for seasonal or even subannual resolution, Norström *et al.* (2005, 2008) were unable to achieve this due to *B. salicina's* irregular growth ring formation of approximately 0.5 rings per year (Norstrom *et al.* 2008), but also to relatively low sampling resolution. By sampling once per growth ring and every few millimetres thereafter, these two isotope studies achieved a multi-year resolution effective for identifying only broad climate patterns. Although the 600-year *B. salicina* records provide valuable insights into long-term rainfall trends in South Africa, the methodology underpinning them inevitably masks finer-scale, seasonal fluctuations embedded within tree growth increments.

Mimusops caffra, another angiosperm, was assessed by Hall *et al.* (2009) who sought to investigate the relationship between carbon isotope composition and climate patterns on the north coast of KwaZulu-Natal. High-precision radiocarbon dating was used to confirm the annual nature of ring formation in this species. While sampling resolution in this study was high (average of >1 $\delta^{13}C$ measurement per annual growth ring) relative to that of Norström *et al.* (2005, 2008), intra-ring samples were averaged to generate annualised $\delta^{13}C$ values. These annual values were then compared to annualised climate data, including rainfall, temperature, and humidity. The analysis revealed a

correlation between $\delta^{13}C$ values and rainfall variations, particularly extreme events. Additionally, the study identified two external effects able to distort $\delta^{13}C$ results: the anthropogenic effect and the juvenile effect. The anthropogenic effect refers to the decreasing trend in $\delta^{13}C$ values observed in recent decades, reflective of the global decrease in atmospheric $\delta^{13}C$ due to fossil fuel combustion (see February & Van der Merwe 1992; Schubert & Jahren 2012; Hare *et al.* 2018). The juvenile effect refers to the $\delta^{13}C$ depletion and variability observed in a tree's early growth stages due to a host of possible causes (see Leavitt 2010 and references therein). These patterns were observed in the *M. caffra* $\delta^{13}C$ time series to produce long-term and cyclical patterns not otherwise related to climate. Nevertheless, *M. caffra* is shown to possess great potential to reconstruct historical rainfall patterns using isotope dendroclimatology.

The species so far receiving the greatest isotopic attention is *Adansonia digitata*, the African baobab. It was first studied by Robertson *et al.* (2006), who analysed radial segment taken from a recently fallen individual as well as an increment core obtained from a living individual, both from Kruger National Park, Limpopo. The growth rings along the radial segment were aged using radiocarbon dating, and the results indicated that incremental growth was likely annual. Moreover, the $\delta^{13}C$ data measured from the increment core revealed a significant correlation with January precipitation. This suggests that *A. digitata* may be a valuable source of information on past seasonal rainfall patterns. However, the study acknowledges that such results should be replicated elsewhere to confirm the species' reliability as a high-resolution palaeoclimate archive.

This confirmation was provided when a regional scale $\delta^{13}C$ dendroclimatology was constructed for the northern SRZ using a network of *A. digitata* data from the Pafuri (Woodborne *et al.* 2015) and Mapungubwe (Woodborne *et al.* 2016) regions of South Africa. The aim of these studies was to reconstruct rainfall patterns over the last millennium, given the scarcity of long-term instrumental records in the region. Radiocarbon dating initially indicated annual growth (Woodborne *et al.* 2015). However, previous analysis of the Lebombo Eco Trail baobab demonstrated a complex stop/start growth dynamic wherein growth ceases for prolonged periods (see Patrut *et al.* 2015), and a later analysis of *A. digitata* from Mapungubwe showed that rings were not always annual (Woodborne *et al.* 2016). These studies revealed a significant correlation between baobab $\delta^{13}C$ and rainfall, suggesting that these long-lived trees can reliably provide insight into past rainfall variability. This would ultimately contribute an additional proxy for investigating regional climate change and historic human societies in southern Africa.

In addition to these angiosperm isotope dendroclimatologies, gymnosperms have also formed the focus of several studies in South Africa. February and Stock (1999) investigated the relationship between $\delta^{13}C$ and climate in several Die Bos *W. wallichii* samples collected by Dunwiddie and LaMarche (1980). They found that $\delta^{13}C$ correlates not with rainfall, but rather increasing concentrations of atmospheric CO_2 – the anthropogenic effect similarly identified by Hall *et al.* (2009) in *M. caffra*. This conclusion was later revisited by De Mil *et al.* (2021) who aimed to construct $\delta^{13}C$ and $\delta^{18}O$ chronologies also for the Die Bos samples. The $\delta^{13}C$ chronology was excluded due to low inter-series correlation between the four analysed trees, and the combined $\delta^{18}O$ chronology was found to have no significant correlation with neither temperature nor precipitation. The potential of *A. falcatus* $\delta^{13}C$ as a climate indicator has also been explored in samples from Karkloof, KwaZulu-Natal (Baverstock 2021). Here, temperature rather than rainfall was found to correlate more closely with ring $\delta^{13}C$, just as it had with the Karkloof *A. falcatus* ring width chronology discussed in Subsection 2.5.1. (Baverstock *et al.* 2021).

A review of these studies shows that isotope dendroclimatology research in South Africa is more frequently conducted on angiosperms than gymnosperms, with angiosperms demonstrating stronger connections between their isotope profiles and climate variables, particularly rainfall. In contrast, gymnosperm have shown limited success. This may be due to the smaller number of gymnosperm-focused studies so far conducted in the region, highlighting the need for further research. Despite these differences, isotope dendroclimatology generally proves more effective in yielding climate correlations compared to traditional dendrology based on ring-width measurements.

Additional insights from the reviewed isotope studies highlight several critical factors to consider when testing the SPP on modern gymnosperms and angiosperms in South Africa. Local environmental conditions must be carefully considered during field sampling, as surrounding hydrological features can influence growth ring isotope values (Norström *et al.* 2005; 2008). Non-climatic influences, such as the anthropogenic and juvenile effects, may also complicate the interpretation of $\delta^{13}C$ results and prove difficult to disentangle from climate trends (February & Stock 1999; Hall *et al.* 2009). While many studies rely on annual growth rings to correlate climate variables, this study hypothesises that the SPP's focus on relative as opposed to absolute changes over time may not require strictly annual or dateable growth rings. Furthermore, none of the isotope studies discussed have achieved a high or subannual subsampling resolution and have been limited to examining broader scale tree-climate relationships. The present study's high-resolution $\delta^{13}C$ analysis of *Protea* and *Podocarpus* from all

three rainfall zones will represent a significant contribution to isotope dendroclimatology and the broader field of growth ring studies in South Africa.

Whether the hypothesised benefits of the SPP can extend farther back in time will depend on its applicability to archaeological charcoals. The promise that isotope dendroclimatology holds for modern wood has also been explored in archaeological carbonised wood, and the following Section 2.7. explores the use of archaeological charcoal in palaeoclimate reconstruction.

2.7. Trees and climate: Carbonised wood from archaeological contexts

The term anthracology refers to the application of dendrology methods to the analysis of charcoal (Théry-Parisot et al. 2010; Kabukcu 2018). Charcoal is produced by the pyrolysis of organic material which has been heated in the absence of oxygen; a process termed carbonisation or charcoalification (Scott & Damblon 2010; Bird & Ascough 2012). Here, I use both terms interchangeably. During carbonisation, wood undergoes significant chemical and structural alterations (Braadpaart & Poole 2008; Mouraux *et al.* 2022). Wood charcoal is biochemically inert and consequently slow to degrade (Forbes *et al.* 2006; Bird & Ascough 2012). As a result, carbonisation promotes the preservation of woody plant remains such that it has come to be recognised as one of the most common materials in archaeological assemblages (Kabukcu 2018; Li *et al.* 2022).

Wood charcoal has been used as a paleoenvironmental indicator in archaeology since the 1940s, with the formative studies in charcoal identification and relative taxa abundance of Salisbury and Jane (1940) and Godwin and Tansley (1941). Such studies examined environmental change by using wood microanatomical features — retained after charcoalification (Chikumbirike & Bamford 2021) — to identify archaeological charcoals to the genus or species level and then make inferences about the environmental conditions likely required by these taxa through comparison with extant samples. H. Deacon (1979) and H. Deacon *et al.* (1983) were the first to conduct such a study in South Africa using charcoals identified in the Holocene deposits of Boomplaas Cave in the Cango Valley. Since then, similar studies have been carried out at various archaeological sites across the country, including Elands Bay Cave (Cartwright & Parkington 1997; Cowling *et al.* 1999), Sibudu Cave (Allott 2006; Lennox *et al.* 2019; Bamford & Zwane 2021), and Wonderwerk Cave (Bamford 2015; House *et al.* 2022), among others. This approach often leads to lower-resolution palaeoclimate reconstructions, offering only broad inferences about longer-term climate patterns. However, a recent study by Zwane *et al.* (2023)

analysed the relative abundance of charcoal taxa at Klasies River 1 in terms of observed adaptation to seasonal rainfall regimes to provide a more precise interpretation of seasonal climate at the site.

An additional method focusing on charcoal microanatomy is xylem analysis. Following H. Deacon, Scholtz (1986) analysed the xylem properties of the Boomplaas charcoals to reconstruct past rainfall conditions. This method is largely inspired by Carlquist's (1977a; 1977b) observation that xylem vessel diameters tend to increase and vessel frequencies decrease in response to increased water availability. With this, Scholtz demonstrated that it is possible to detect past climate change by comparing measurements on archaeological charcoal with those on extant samples obtained from areas of known temperature and rainfall. February (1990) applied Scholtz's (1986) method to archaeological charcoals from Elands Bay Cave in an attempt to establish the exact relationship between xylem morphology and climate and to test the method's precision farther back in time. Such xylem analyses indicate a relationship between certain vessel characteristics and mean annual rainfall (February 1994) and consequently illustrate how archaeological charcoal can be used to ascertain generalised patterns of wetter and drier periods and thus rainfall variability over time (February 1992; 1994; 2000).

The success of isotope methods in contemporary dendrology makes them valuable for archaeological investigations into past climate. Archaeological charcoal $\delta^{13}C$ values have been employed as a palaeoclimate proxy, particularly for reconstructing hydroclimate conditions and assessing past water availability (February & Van der Merwe 1992; Ferrio *et al.* 2006; Baton *et al.* 2017), given the established relationship between $\delta^{13}C$ and water use efficiency (see Section 2.4). February (1990) was the first in South Africa to conduct an analysis of archaeological charcoal $\delta^{13}C$. In search of environmental data going beyond historic records, February studied charcoals from various cave sites in Elands Bay to reconstruct climatic fluctuations over the last 4,000 years. Alongside the archaeological analysis, modern *Rhus* and *Diospyrus* wood and charcoal were analysed for comparative purposes. It was found that while archaeological charcoals do seem to carry a climate signal, that signal is complex and it could not be definitively concluded whether it was produced by temperature or rainfall.

One of February's fundamental assumptions was that carbonised wood indeed preserves the $\delta^{13}C$ values set down in plant tissues during growth, and that little to no fractionation occurs during charcoalification. February (1996) later returned to the matter and tested how the process of charcoaling modern *P. roupelliae* and *Combretum apiculatum* grown in different rainfall conditions

affected $\delta^{13}C$ results, and whether these charcoal results correlated with recent climate records. For *P. roupelliae*, the study found no significant correlation between $\delta^{13}C$ values and rainfall in wood or charcoal. This led February to conclude that the species – and likely the genus in its entirety – was unsuitable for climate reconstruction based on $\delta^{13}C$, both recent and archaeological.

Hall *et al.* (2008) later conducted various burning experiments on modern *Podocarpus* wood derived from stems and branches and found that although combustion temperature has a critical effect on whether the $\delta^{13}C$ values of charcoals are depleted or enriched compared to the original wood, the climate signal is ultimately preserved. These modern experiments provided grounds to isotopically assess charcoal from three of Sibudu Cave's Middle Stone Age (MSA) levels to study broad environmental fluctuations during the Middle Stone Age from approximately 60 ka to 40 ka.

Elsewhere, studies have used archaeological charcoal $\delta^{13}C$ to provide insight into rainfall seasonality, moving beyond generalised patterns of moisture availability (e.g. Aguilera *et al.* 2009; Aguilera *et al.* 2012; Baton *et al.* 2017). To date, however, no studies in South Africa have attempted to analyse archaeological charcoal $\delta^{13}C$ at the subannual or "ring-scale" resolution, as described by Baton *et al.* (2017: 51), to enhance the precision of past climate reconstructions. In fact, while these early studies by February (1990, 1996) and Hall *et al.* (2008) highlighted the potential of isotope anthracology for palaeoclimate reconstruction in South Africa, suggesting a need for further research, no subsequent research has explored the approach in greater depth – even for lower-resolution palaeoclimate analysis, let alone resolving seasonal patterns.

Achieving high precision and resolution in palaeoclimate studies on past seasonality is challenging with current proxies. Given the inherent limitation of the types of materials and therefore potential proxy records that are recoverable from archaeological sites, there is a strong impetus to maximise the palaeoclimate information that can be extracted from these materials, particularly plant remains (Pearl *et al.* 2020: 927). The SPP offers an innovative approach to studying a widely available archaeological material – a new way to extract seasonality information from charcoals. Rooted in isotope dendroclimatology, which has proven relatively successful in South Africa, it presents a promising opportunity to address the gap in high-resolution climate proxies for local palaeoscience and archaeology. This forms the focus of the following Chapter.

CHAPTER 3

Seasonality Studies in South Africa

3.1. Introduction

This Chapter explores the concept of rainfall seasonality, focusing on its definition, climatological drivers, spatial organisation, and Late Pleistocene dynamics in South Africa. In service of proposing a new proxy for rainfall seasonality, existing palaeorecords and proxies are reviewed, highlighting their inherent challenges, including limited resolution and a reliance on qualitative inference. This Chapter further differentiates between climatological seasonality (seasonal climatic fluctuations) and human seasonality (seasonal timing of activities) and addresses the challenge of integrating both concepts for archaeological investigations. This review culminates in Section 3.7, which concisely synthesises the themes explored in Chapters 2 and 3 to restate the project's rationale and aims of addressing the need for alternative, high-resolution, on-site seasonality proxies.

3.2. Defining rainfall seasonality

The term 'rainfall seasonality' lacks a formal, standardised definition, and there exists no widely accepted metric or statistical approach to classify seasonal rainfall regimes (Saha *et al.* 2018; Roffe *et al.* 2019). On a tacit level, the term refers to how the climatological year is divided into a wet season and a dry season, often according to certain "components" of rainfall seasonality (Feng *et al.* 2013: 813). Said components include (Feng *et al.* 2013: 813; Roffe *et al.* 2020, 2021a):

- Timing – in which months of the year does rain fall?
- Duration – how long over the year does rain fall?
- Intensity – how strong are rainfall events? (i.e. the rate of rainfall per unit time during an event)
- Magnitude – how much rain falls? (i.e. the total volume or accumulation of rainfall over a given period)

These components produce yearly cycles of wet and dry seasons in a predictable pattern (Saha *et al.* 2018), and this predictability is a key element used to classify rainfall regimes and rainfall zones. Here, rainfall regime is defined as the complete system of rainfall over a climatological year, the net effect

of the aforementioned components of seasonality. Rainfall zone, however, is a specifically spatial term and refers to the rainfall regime that characterises a given location or geographic region.

3.3. Present-day rainfall climatology

Today, South Africa is situated at the intersection of major atmospheric and oceanic circulation systems. The subtropical belt and Indian Ocean in the east, and the temperate system and Atlantic Ocean in the west together affect the region's seasonal rainfall regimes resulting in significant spatial variation (Van Zinderen Bakker 1976; Tyson & Preston-Whyte 2000; Chase & Meadows 2007).

Here, I discuss South Africa's rainfall regimes, focusing on key atmospheric drivers. Rather than offering an exhaustive overview of meteorological knowledge in South Africa, my aim is to illustrate the (seasonal) movement of moisture-bearing systems, and how these movements contribute to spatial-temporal variability in rainfall patterns.

At the subcontinental scale, southern Africa predominantly experiences a subtropical climate due to the semi-permanent high-pressure belt which produces stable and dry (arid to semi-arid) conditions (Tyson & Preston-Whyte 2000; Lennard & Hegerl 2015; Landman *et al.* 2017; Botai *et al.* 2018). However, at the synoptic scale, rainfall in South Africa is characterised by prominent spatial and temporal variability. Tyson and Preston-Whyte (2000: 176) describe this variability as a function of "perturbations" from the "mean" that is the high-pressure system. Moreover, said perturbations are shaped by the South Africa's latitudinal position (22°S – 34°S), topography, and surrounding ocean currents, which interact with synoptic circulation systems to modulate rainfall across the country, thereby producing a distinct west-to-east gradient (Tyson & Preston-Whyte 2000; Stone 2014; Favre *et al.* 2016; Landman *et al*. 2017; Roffe *et al.* 2019, 2020, 2021a).

In the east and to the north, orographic and convective rainfall dominate. Tropical easterly flows convect moisture off the warm Agulhas current of the Indian Ocean, producing a more humid climate (Tyson & Preston-Whyte 2000; Chase & Meadows 2007; Stone 2014; Favre *et al.* 2016; Landman *et al.* 2017). This side of the country is relatively wetter (600 – 1500 mm yr^{-1}), with the MAP recorded along the Indian Ocean coast and the windward side of the Maloti-Drakensberg mountains which constitute the Great Escarpment (Favre *et al.* 2016; Landman *et al.* 2017). Additional tropical perturbations affecting the eastern region are easterly waves and troughs, associated with heavier rain as the Inter-Tropical Convergence Zone (ITCZ) moves southward in austral summer (Tyson & Preston-Whyte 2000). Easterly waves and troughs follow a distinct annual pattern and occur predominantly during summer months between December and February (Tyson & Preston-Whyte 2000). Ridging anticyclones also

bring rain to the east during warm summer months (Tyson & Preston-Whyte 2000). In winter, however, subsidence is enhanced, resulting in cool and dry conditions in the interior (Lennard & Hegerl 2015).

In the west, subtropical subsidence associated with the regional anticyclone has a greater influence on rainfall, whereas convective rainfall off the colder Benguela current of the Atlantic Ocean plays a lesser role (Tyson & Preston-Whyte 2000; Stone 2014; Favre *et al.* 2016; Landman *et al.* 2017; Burls *et al.* 2019). This side of the country receives less rainfall on average (<400 $mm.yr^{-1}$) (Favre *et al.* 2016; Landman *et al.* 2017). However, there is variability in MAP even within the western area. The southwestern Cape, for example, receives relatively more rain due to the influence of mountain ranges when moist frontal air connected to the westerlies is carried inland (Landman *et al.* 2017). Westerly flows, particularly cold fronts associated with mid-latitude cyclones, are the western region's main source of moisture (Tyson & Preston-Whyte 2000; Reason *et al.* 2002; Lennard & Hegerl 2015; Favre *et al.* 2016). These cold fronts originate in the south/southwest and track eastwards, primarily during winter months when westerly disturbances peak in amplitude (Tyson & Preston-Whyte 2000). Periodic lows that cut off equatorward from the main westerly current have also been linked with heavy rains in the west (Reason *et al.* 2002; Lennard & Hegerl 2015). During summer, when ridging anticyclones are associated with increased moisture in the east, the west experiences greater subsidence leading to clear, hot weather (Tyson & Preston-Whyte 2000; Lennard & Hegerl 2015). Such characteristics – cool, wet winters and warm, dry summers – underpin the Mediterranean climate of the west coast and southwestern Cape (Chase & Meadows 2007; Sousa *et al.* 2018; Mahlalela *et al.* 2019; Roffe *et al.* 2022).

3.4. Mapping rainfall seasonality: Present and past

A consensus exists in the literature that contemporary South Africa can be organised into three rainfall zones: a Winter-Rainfall Zone (WRZ) covering the west coast and southwestern Cape, a Summer Rainfall Zone (SRZ) characterising most of the landscape in the east and north, and a Year-Round Rainfall Zone (YRZ) occupying the south coast (Figure 3)(Tyson & Preston-Whyte 2000; Roffe *et al.* 2019).

Yet, the reality of seasonal rainfall in South Africa is more complex. In some cases, the transition seasons of spring or autumn may have a significant bearing on annual rainfall (Mahlalela *et al.* 2019; Ndebele *et al.* 2020), and the wet season may have either an earlier or later start- or end-date even within a single rainfall zone (see Botai *et al.* 2018; Roffe *et al.* 2020, 2021a).

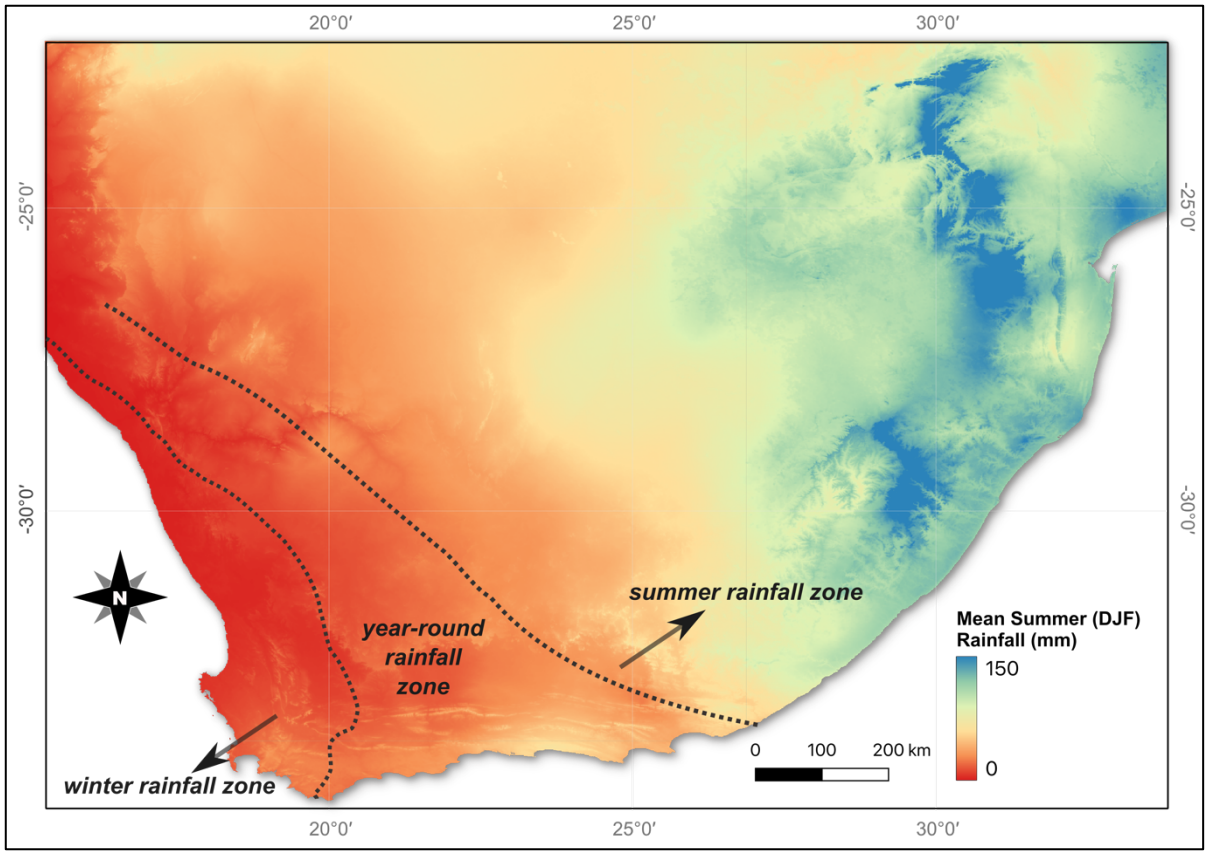

Figure 3. Map showing the mean summer (December, January, February (DJF)) rainfall, seasonal rainfall gradient, and general rainfall zone boundaries of South Africa. Summer Rainfall Zone (SRZ) occupies most of the region to the east and north, Winter Rainfall Zone (WRZ) occupies the west coast, and Year-Round Rainfall Zone occupies the interior and south coast between them. (WorldClim2.1 precipitation data 1970-2000 (Fick & Hijmans 2017))

While the three regional rainfall categories are determined by the timing component of rainfall seasonality, they seemingly neglect rainfall intensity or magnitude, which too can vary within a zone. For example, a map showing the MAP recorded at each weather station included in a country-wide study of the relationship between temperature and rainfall by Roffe *et al.* (Figure 4a 2021b: 2438) reveals that while Mara, Limpopo receives 400-500 mm/yr^{-1}, Paddock, KwaZulu-Natal receives 1000-1100 mm/yr^{-1}, despite both being situated in the SRZ. For both the winter rainfall and summer rainfall sites, then, there is clearly within-zone variability in timing, duration, and magnitude that the spatial categories of WRZ and SRZ alone do not necessarily account for.

Additionally, while the existence of the WRZ, SRZ, and YRZ is widely accepted, there is uncertainty regarding the spatial extent of these zones. Roffe *et al.* (2019) argue that much of this uncertainty stems from practical differences between each study in terms of definitions of seasonality (i.e. the set of components used to classify rainfall regimes), time periods of analysis, resolution of analysis (i.e. monthly or daily rainfall data), assessed weather stations, and sources of data (e.g. South African

Weather Service (SAWS) or Department of Water and Sanitation (DWS)). Inconsistent methods expectedly produce inconsistent results: Roffe *et al.* (2019)'s comparison found that the seasonal rainfall classification of 22% of the landscape is contested by a quarter of authors. Moreover, the region between the WRZ and SRZ is the most notably disputed and ultimately lacks a precise definition (Roffe *et al.* 2019, 2020).

This region is understood to encompass the YRZ (Figure 3). The uncertainty surrounding the rainfall seasonality in this region is not entirely unexpected, given the marked meteorological complexity of this zone, which is influenced by both tropical and temperate systems (Chase & Meadows 2007; Engelbrecht *et al.* 2015). Some authors suggest that the YRZ occupies only the south coast and is constrained by the Cape Fold Belt (e.g. Engelbrecht *et al.* 2015; Roffe *et al.* 2019, 2020) while others argue that it extends to the northwest to cover some of the interior, acting as a buffer or transition between two seasonal extremes (e.g. Carr *et al.* 2006; Chase & Meadows 2007). While rain in this zone appears to fall year-round, there are identifiable rainfall peaks in autumn and spring (Engelbrecht *et al.* 2015). Ultimately, the YRZ is the least understood of South Africa's three rainfall zones (Roffe *et al.* 2019).

What all of this implies is that while the WRZ, SRZ, and YRZ are widely recognised spatial categories, they run the risk of aggregating and simplifying seasonal rainfall over large areas. Additionally, the different ways in which these zones may be theoretically defined and then practically measured and mapped are seldom acknowledged. Still, such broad zonal distinctions remain useful heuristics for thinking about seasonal variability over space, especially if current variability is to be contextualised deeper in time.

Changes in rainfall seasonality during the Late Pleistocene, particularly the dynamics and spatial extent of the WRZ, are thought to be primarily driven by shifts in the position of the SH westerlies over glacial-interglacial cycles (Van Zinderen Bakker 1967, 1976; Chase & Meadows 2007; Stone 2014; Fitchett & Bamford 2017; Engelbrecht *et al.* 2019). The established paradigm is that the expansion of Antarctic sea ice during glacials resulted in the northward displacement of the westerly storm tracks, leading to an increase in the intensity and frequency of winter frontal rains further east (Van Zinderen Bakker 1967, 1976; Chase & Meadows 2007; Engelbrecht *et al.* 2019). Thus, glacials are associated with enhanced winter rainfall, and interglacials with summer rainfall (H. Deacon & Lancaster 1988; Chase & Meadows 2007; Chase *et al.* 2017). The movements of westerlies cannot be directly tracked and mapped over the Late Pleistocene, meaning that contextualising present-day rainfall zones relies on

palaeoclimate records from which past seasonality conditions must be inferred. Yet, existing proxies are not necessarily conducive to such high-resolution reconstructions (Chase & Meadows 2007; Chase *et al.* 2015; Fitchett & Bamford 2017). *Climatological seasonality* is difficult to isolate from these records, but this isolation is critical if archaeologists hope to better understand seasonally-informed human-environment interactions, or *human seasonality*. It is these issues to which I now turn.

3.5. Challenges in identifying climatological seasonality in South Africa

Palaeorecords used to trace the movement of the westerlies and seasonal rainfall history of South Africa include *inter alia* fossil pollen (e.g. Neumann *et al.* 2014; Chevalier & Chase 2015; Fitchett & Bamford 2017; Herbert & Fitchett 2022), micromammals (e.g. Thackeray & Fitchett 2016; Faith et al. 2019), macrofauna (e.g. Faith 2013a&b), speleothems (e.g. Holmgren *et al.* 2003; Braun *et al.* 2019), rock hyrax middens (e.g. Chase *et al.* 2013, 2018, 2023), and bovid tooth enamel (e.g. Lee-Thorp & Beaumont 1995; Sealy *et al.* 2016; Stowe & Sealy 2016). While an exhaustive analysis of each record is beyond the current scope (see reviews by Chase & Meadows 2007; Stone 2014; Marean *et al.* 2014; Stewart & Mitchell 2018), a review of the existing literature reveals two major challenges these records pose to seasonality reconstructions in the region: limitations of proxy inference, and constraints of proxy resolution.

3.5.1. Proxy inference of climatological seasonality

The practice of proxy inference defines palaeoclimate reconstruction in South Africa and elsewhere. Without the ability to directly map the Late Pleistocene westerlies and quantify seasonality, one assumed climate-driven record (e.g. fossil pollen assemblages) must stand in for climate itself (e.g. past rainfall seasonality). However, these ecological relationships are not always guaranteed, introducing uncertainty to seasonality reconstruction.

For example, pollen is among the most widely used palaeorecord for Late Quaternary climate reconstruction (Knight & Fitchett 2019) and serves as a primary focus of most studies investigating shifts in the SH westerlies (Fitchett & Bamford 2017). A common approach to identify a seasonal signal from pollen records links vegetation communities to seasonal rainfall regimes, as they are observed today. Pollen morphotypes are used to infer parent vegetation, and parent vegetation is, in turn, used to infer wetter/drier conditions and/or a stronger/weaker influence of winter/summer rain that may have occurred in the past. This is based on the ecological principle that for each plant species there exist “climate optima” (Figure 7 Quick *et al.* 2022: 105): the climate conditions under which a taxon is

most likely to occur. In practice, however, the relationship between plants, pollen, and seasonality is complex, and it is challenging to determine the precise climatic associations of various pollen morphotypes which may represent multiple plant species (Chevalier *et al.* 2021). These species may, in turn, be associated with a range of climate optima. In the context of seasonality reconstruction, interpretations can thus be unspecific and contradictory.

More recent studies have worked to reduce some of this pollen uncertainty. Chevalier *et al.* (2014, 2021) developed a Climate REconstruction SofTware (CREST) method that uses species-specific probability density functions (*pdfs*) based on the geographic distribution of modern taxa to model the relationship between vegetation and climate. Fitchett and Bamford (2017) also tested the *Asteraceae*:*Poceae* ratio and found it able to statistically differentiate between summer and winter rainfall regimes, rendering it an effective indicator of rainfall seasonality. Such developments may reduce the reliance on inference and assumption in pollen-based seasonality reconstructions. However, while they have received some application (e.g. Chase *et al.* 2015 for CREST and Herbert & Fitchett 2021 for *Asteraceae*:*Poaceae*), these have thus far been limited.

The $\delta^{13}C$ values measured in hyrax middens (e.g. Chase *et al.* 2013, 2018, 2023), speleothems (e.g. Talma & Vogel 1992; Holmgren *et al.* 2003), and bovid tooth enamel (e.g. Lee-Thorp & Beaumont 1995; Sealy *et al.* 2016; Stowe & Sealy 2016) are largely used as indicators of the proportion of vegetation on the landscape with either the C3 or C4 photosynthetic pathway. C3 vegetation is associated with temperate grasses, and C4 with tropical grasses (Green *et al.* 2015). Due to the climate affinities implied by these types of grasses, a stronger/weaker influence of winter/summer rain is often inferred. In contemporary South Africa, the distribution of C3 and C4 grasses are closely controlled by rainfall seasonality (Vogel *et al.* 1978; Chase *et al.* 2012; Scott 2002). Generally, C3 grasses dominate winter rainfall areas, whereas C4 summer rainfall areas and drylands as they are better adapted to effectively take up carbon during warm growing (i.e. wet) seasons (Scott 2002; Ehleringer 2005).

However, distinctions are not absolute, and both C3 and C4 grasses can coexist within the same environment. C3 grasses are associated not only with winter rainfall, but also in zones of transition between winter and summer rainfall, as well as high-altitude areas within the SRZ where cool growing conditions prevail (Lee-Thorp & Beaumont 1995; Scott 2002). The Maloti-Drakensberg region is one such example (Stewart & Mitchell 2018). In these instances, C3/C4 proportions are more temperature- than seasonal rainfall-mediated (Stewart & Mitchell 2018). Thus, seasonal rainfall – both present and

past – is not the only climate variable controlling the relative distributions of C3/C4 grasses, which potentially complicates and undermines rainfall seasonality reconstructions dependent on such an inference.

In sum, qualitative inference, this "chain of assumptions" as Stone (2014: 529) describes it, contributes great uncertainty and contradictory interpretations to palaeoseasonality reconstruction (Chase & Meadows 2007; Chase *et al.* 2012; Faith *et al.* 2019).

3.5.2. Constrained resolution of existing palaeorecords

Resolution is another critical constraint of existing palaeorecords, which rather limits rainfall seasonality reconstructions. Kwiecien *et al.* (2022: 13) draw an essential distinction between 'temporal resolution' and 'sampling resolution'. Temporal resolution refers to inherent capacity of an archive to record a given climate variable, and is determined by the pace at which changes in this variable are translated – via associated environmental and ecological processes – into a preservable signal within the archive. Sampling resolution, by contrast, is a methodological issue that pertains to the extent to which temporal resolution can be captured and represented within a single sample and between samples.

The terms 'high-resolution' and 'low-resolution' further describe an archive's temporal resolution. From the range of palaeoclimate archives in existence, few have the capacity to record seasonal variability (Prendergast *et al.* 2018; Kwiecien *et al.* 2022). Most palaeoarchives are described as low-resolution; they encompass broader timescales, often spanning centuries or millennia, and lack the precision needed to identify seasonal signals. In contrast, high-resolution archives are understood as those able to capture annual or subannual variations in climate parameters like rainfall. Bradley (2011) suggests that for an archive to be considered high-resolution, it must produce proxy data that are comparable with instrumental data, i.e. at an annual resolution. Archives containing such data typically form in growth bands or increments at known or measurable time intervals, such as tree rings, ice cores, corals, or speleothems (Bradley 2011; Kwiecien *et al.* 2022). This point is critical because it ensures that these records are not only largely continuous but also able to be precisely dated, and such chronological control is vital to all palaeoclimate studies (Bradley 2011; Prendergast *et al.* 2018; Patalano & Roberts 2021; Kwiecien *et al.* 2022).

High-resolution and 'seasonal resolution' are often treated as equivalent terms (Prendergast *et al.* 2018; Kwiecien *et al.* 2022) and are used interchangeably here. Many prominent palaeoclimate

archives in South Africa are unable to capture seasonal climate information, due largely to differential rates of accumulation and preservation which lead to gaps and discontinuities, and also to homogenisation and time averaging.

Discontinuous, discrete archives greatly inhibit seasonality reconstructions (Kwiecien *et al.* 2022). A major factor contributing to this issue is South Africa's arid to semi-arid climate which is relatively less favourable for the formation of lakes and wetlands, which elsewhere document long-term environmental changes (Chase & Meadows 2007; Chase *et al.* 2012; Strobel *et al.* 2022). Such a climate also affects the preservation of terrestrial fossil proxies, leading to a paucity of sites with intact and temporally continuous profiles (Chase & Meadows 2007; Stone 2014). This contributes to many existing archives providing only "snapshots" of past climate (Kwiecien *et al.* 2022: 3), where substantial temporal gaps, often stretching for over thousands of years, render even general climate reconstruction impossible. Hyrax middens, for instance, so far are not suitable for investigating climate patterns at a submillennial resolution (Chase *et al.* 2011). Pollen archives are also affected by variable pollen production, dispersal, and preservation over deep-time (Fitchett & Bamford 2017; Scott *et al.* 2022), meaning that data are not equally available for every period of interest, but also that analyses of seasonality are infeasible.

The climate 'snapshots' offered by these archives are further complicated by time averaging and homogenisation (Chase & Meadows 2007; Stone 2014; Lukich & Ecker 2022). The material found in many terrestrial archives accumulates slowly and unpredictably – not every seasonal cycle or even year may be represented. Instead, whatever material is retrieved and then analysed must stand in for an average of climate conditions over much broader timescales. Signals are homogenised, nuance is lost. This "masks" seasonal variability and rather limits the detail that can gleaned from these archives (Chase & Meadows 2007: 166; Lukich & Ecker 2022: 58). Unfortunately, this limitation is inherent to such archives, defining them as low-resolution (Chase & Meadows 2007), and it cannot be overcome by attempts to increase sampling resolution. Ultimately, the limited temporal resolution of existing palaeorecords restricts the precision of the climate reconstructions they enable.

3.6. On-site versus off-site records: Integrating climatological and human seasonality

The seasonality explored in existing palaeorecords can be broadly understood as a *climatological seasonality* – an effort to capture or measure the extent and degree of seasonal climate variables over time. In archaeological studies, this climatological seasonality contrasts with *human seasonality*, which

relates to how the concept of seasons and seasonality time cultural activities like mobility patterns, site occupation, and resource use.

Central to human seasonality is the concept of traditional ecological knowledge (Kwiecien *et al.* 2022), or rather, local knowledge (LK).[1] LK is defined as the collective knowledge held by specific cultural groups, encompassing the accumulated wisdom and beliefs about interactions between human and non-human nature, and which is passed down through generations via cultural practices (Berkes & Berkes 2009). LK is typically linked to long-established communities that maintain a close connection to their natural surroundings (Orlove *et al.* 2010). The influence of LK on seasonal mobility and resource use has been observed in ethnographic accounts of diverse hunter-gatherer societies across the globe, including the southern African G/wi and !Kung (Ju/'hoansi) of the Kalahari (e.g. Lee 1979; Silberbauer 1981; Kelly 1983, 2013). Silberbauer's (1981) report on G/wi hunter-gatherers details how their rich LK of seasonality, including plant phenology, animal migrations, animal birthing seasons, and water availability, informs their mobility strategies.

The interconnection between hunter-gatherer LK and seasonality observed in the present is theorised to be similarly true for the archaeological past, given the substantial evidence suggesting that LSA hunter-gatherer communities are ancestral to recent and present San groups (Deacon & Deacon 1999; Mitchell 2002, 2005). It is widely accepted that annual seasonal changes in climate variables (such as rainfall and temperature) led to corresponding shifts in local ecosystems and thus critical resources available to foragers, including plants, animals, water, shelter, and raw materials (Prendergast *et al.* 2018; Pargeter & Faith 2020; Kwiecien *et al.* 2022). Guided by LK of these shifting resource availabilities, LSA hunter-gatherers likely developed certain adaptive strategies including mobility, site occupation, exploitation of resources, and social organisation on a seasonal basis.

Seasonal resource use, occupation, and mobility have become widely employed – albeit highly debated (e.g. Carter 1970, 1978; Parkington 1972, 2001; Sealy *et al.* 1986; Humphreys 1987, 2005, 2007; Wadley 1989; Mitchell 2005; Sealy 2006; Forssman 2019; Loftus *et al.* 2019) – frameworks for interpreting the LSA record.

[1] The term 'traditional' is laden with connotations of primitiveness, cultural stagnation, and a resistance to change (Antweiler 2019) – especially when invoked in the South African context (see Spiegel & Boonzaier 1988) – and so, like Antweiler (2019), alternative wording for the concept is preferred here: local knowledge.

While a detailed discussion of each criticism of these frameworks is beyond the current scope of this thesis, it is important to highlight that some analysts have taken issue with the use of ecological models to predict and describe forager behaviour. These models are regarded as reductive and disempowering interpretations that overestimate the role played by environmental context in influencing hunter-gatherer choices and activities (see Wadley 1989; Sealy 2006; Forssman 2019). Nevertheless, these models, I propose, are inherently human in that they seek to time human activities – the hunting of certain ungulates, the gathering of specific plant foods, shell fishing, bird exploitation, and so forth. Yet such studies do only time resource procurement or mobility in isolation because these facets are inextricably linked to every other facet of a society's existence. As Milner (1999: 52) explains, the social "lifeworld of a culture" is "tied intimately to seasonality and the availability of resources." Thus, archaeological seasonality is a human seasonality, a record of adaptations and responses, both economic and social, to fluctuations between one season and the next.

However, these supposedly fluctuating seasons are seldom defined, at least in a climatological sense, and are often difficult to study directly. Without a clear climatological definition, one is forced, at best, to rely on the uniformitarian assumption that 'summer' and 'winter' in the past were more or less as they exist in the present. At worst, these terms become empty labels – placeholders for periods of the year, stripped of the distinct ecological and climatological states they are presumed to represent. Climatological seasonality therefore has an important role to play in archaeological human seasonality discourse. As discussed in Section 3.5, however, reconstructing past seasonality is challenging – and making these reconstructions directly comparable and applicable to questions of human seasonality is arguably even more so. This difficulty is potentially rooted in the (limited) choice between on-site and off-site palaeorecords.

Off-site archives refer to those palaeoclimate records that are located away from the archaeological site under study, but which are analysed to offer a baseline understanding of regional climate dynamics that likely influenced local climate dynamics (Patalano & Roberts 2021). Conversely, on-site palaeoclimate archives include the stratigraphy of an archaeological site from which plant, animal, and geochemical proxy data can be analysed to offer a more local understanding of past climate, one that is arguably better positioned to address human-environment questions (Prendergast *et al.* 2018; Patalano & Roberts 2021).

Proxy data and interpretations drawn from off-site records are commonly, but often uncritically, funnelled into archaeological studies on human behaviour and environmental interactions. Lake,

wetland, and marine sediment cores, as well as hyrax middens and speleothems are examples of popular off-site archives that contribute to archaeological research in South Africa and elsewhere (Patalano & Roberts 2021). While such records may be invaluable for understanding regional palaeoclimate conditions (Patalano & Roberts 2021), they are fundamentally limited in an archaeological context due to spatial, temporal, and contextual detachment (Prendergast *et al.* 2018; Patalano & Roberts 2021). This issue is revisited in Chapter 6.

A noteworthy drawback of this approach, however, is that of anthropogenic bias. Macrobotanical (including charcoal) and macrofaunal remains form the foundation of archaeological assemblages. Yet as food and fuel waste, these materials are deposited as a direct consequence of human choice and activity and may in turn reflect but a filtered subgroup of the flora and fauna surrounding a site at a given time (see Cowling *et al.* 1999; Roberts *et al.* 2016; Stewart & Mitchell 2018; Patalano & Roberts 2021).

Ultimately, on-site archives and proxy data are preferred for reconstructing seasonality. These reconstructions can then contribute a climatological dimension to archaeological questions related to human seasonality, insofar as potential human bias is carefully considered and accounted for.

3.7. Rationale and aims of this project

It is against the backdrop of existing research into seasonality and tree growth rings studies in South Africa that this project emerges. Rainfall seasonality is an omnipresent phenomenon, closely encountered and experienced by human societies in the present and past. How present-day rainfall zones have shifted over glacial-interglacial cycles, however, remains a subject of debate, and existing palaeorecords are poorly positioned to address questions of climatological seasonality and, in turn, human seasonality.

To advance understanding, there is a need for alternative proxies that are:

- High-resolution (in both sampling and temporal scale);
- Located on-site;
- Less reliant on the qualitative inference of climate variables, and more reliant on observable, quantifiable relationships between climate and archive.

Schubert and Jahren's (2011) SPP applied to archaeological charcoal lends itself well to addressing all three of these requirements, while revisiting isotope dendroclimatology and isotope anthracology – both promising but underdeveloped avenues of palaeoclimate research in South Africa.

This project is organised into two parts, a modern calibration and an archaeological application, and seeks to address three questions:

1. **Does the SPP identify a seasonal signal in the serial $\delta^{13}C$ measurements of modern evergreen wood from South Africa?**
2. **Does the SPP identify a seasonal signal in the serial $\delta^{13}C$ measurements of modern evergreen charcoal from South Africa?**
3. **Does the SPP identify a seasonal signal in the serial $\delta^{13}C$ measurements of archaeological charcoal from the LGM and LGIT in South Africa?**

Questions 1 and 2 – the modern calibration – contribute to the need for proxies dependent on quantifiable relationships between record and climate variable, i.e. seasonal rainfall. February (1990, 1992, 1994, 2000) has long stressed the necessity of first ground-truthing a method using modern samples growing in known environmental conditions before any application to archaeological charcoal specimens. Modern samples can then be used "as a key" to better understand archaeological signals, and by extension, archaeological climates (February 1990: 1). Some of the applications of the SPP to fossil wood mentioned in Chapter 1 (e.g. Schubert *et al.* 2017; Vornlocher *et al.* 2021) did just this: they analysed modern wood samples obtained from the study site from which the fossil specimens derived. This allowed them to make comparisons between the modern and palaeo-seasonal signals identified by the proxy, thus strengthening their interpretations about fluctuations in rainfall seasonality over time. I therefore aim to use modern *Protea* and *Podocarpus* wood and charcoal samples against which I can compare the results of the archaeological Proteaceae and Podocarpaceae analyses.

More recently, Fitchett (2019: 51) has lamented the lack of contemporary testing to accompany and corroborate seasonality reconstructions from various proxies in South Africa. The ability to statistically differentiate between seasonal rainfall regimes should be a priority for any seasonality proxy (Fitchett & Bamford 2017). Consequently, I aim to determine whether the SPP is able to quantify from modern samples significant differences between contemporary seasonal rainfall regimes. In application to archaeological specimens, the terms 'summer' and 'winter' can be afforded meaningful, climatological definition which, in future, may pave the way to more informed seasonality studies in archaeology – studies that critically integrate human seasonality with climatological seasonality to contextualise the timing of activities (see Kwiecien *et al.* 2022).

CHAPTER 4

Methods and Materials

4.1. Introduction

This Chapter outlines the materials and methods used in the isotopic analysis of modern wood and charcoal, as well as the archaeological specimens. As the SPP had never before been applied to carbonised wood, this study required several methodological considerations to establish a laboratory protocol capable of reliably and repeatably generating high-resolution $\delta^{13}C$ results from a fragile material like charcoal. The methods and procedures presented in this Chapter are themselves the result of an iterative process, shaped by several tests and refinements, ultimately distilled into the most effective approach to meet the study's objectives. The research process is outlined here in its entirety, from field sampling, to sample preparation for isotope analysis, and finally to post-processing of the isotope results, for both the modern and archaeological samples.

4.2. Field Sampling

4.2.1. Species Selection

Trees from the *Protea* and *Podocarpus* genera were selected for analysis based on three key considerations:

1. Broad geographic distribution: the selected taxa needed to be well-represented across all of South Africa's rainfall zones: the SRZ in the east, the YRZ in the interior and along the south coast, and the WRZ in the west (Figure 4). This would ensure that the variability observed in their respective $\delta^{13}C$ profiles could be attributed to seasonal changes rather than differences in physiological responses between unrelated taxa.
2. Angiosperm and gymnosperm: meaningfully testing the SPP on carbonised wood requires that both of the major C3 groups are represented (Figure 5). By comparing the results obtained from an angiosperm and a gymnosperm, a more comprehensive conclusion about the applicability of the SPP to archaeological specimens can be reached. Expanding the modern calibration in this way broadens the number of archaeological specimens that can subsequently be tested.
3. Consistency with archaeological specimens: Proteaceae from Boomplaas Cave and Podocarpaceae from Waterfall Bluff, respectively, had previously been identified and made available for isotopic analysis. *Protea* and *Podocarpus* were therefore considered for the

modern calibration in order to maintain consistency between the modern and archaeological analyses.

4.2.2. Modern Site Selection

Modern wood samples were taken from one angiosperm genus (*Protea*) and one gymnosperm genus (*Podocarpus*) from the SRZ, YRZ, and WRZ (Figure 4&5). This was done so that the $\delta^{13}C$ profiles from known but variable seasonal rainfall environments could be represented and assessed. The locational and climate information for each sample is presented in Table 1. Within each rainfall zone, remote areas like parks and reserves are prioritised for sampling to reduce the likelihood of anthropogenic influence (e.g. scheduled watering) which would likely skew any seasonal signals identified in tree carbon isotope profiles (February 1996). Sampling in the WRZ and YRZ was conducted under permit from Cape Nature (CN-35-28-25863), and in the SRZ under permit from Ezemvelo KZN Wildlife (OP 2099/2023).

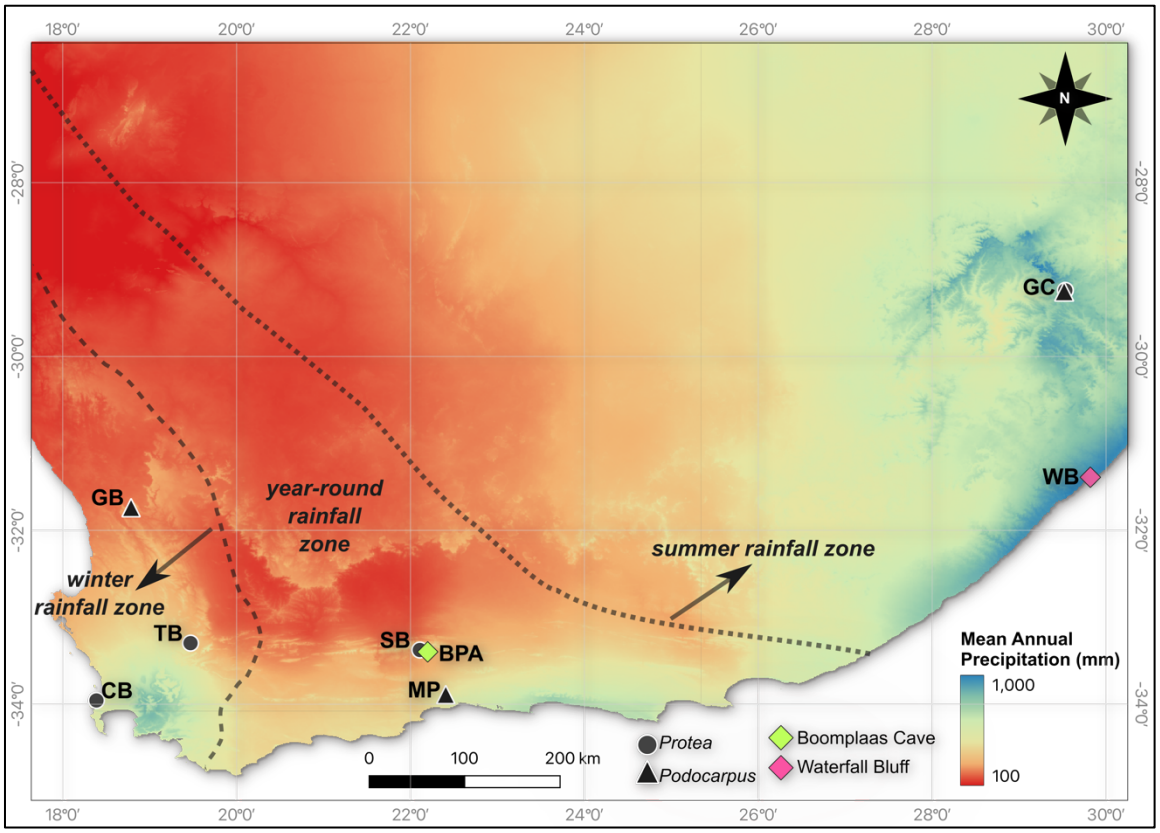

Figure 4. Map showing the modern sampling locations across the three rainfall zones. Summer Rainfall Zone sites: Giants Castle (GC) Game Reserve; Year-Round Rainfall Zone sites: Swartberg Pass (SB) and Montagu Pass (MP); Winter Rainfall Zone sites: Gifberg Pass (GB), Theronsberg Pass (TB) and Camps Bay (CB). Sites from which *Protea* samples were taken are represented with a black circle and sites from which *Podocarpus* samples were taken are represented with a black triangle (WorldClim2.1 precipitation data 1970-2000 (Fick & Hijmans 2017)).

Table 1. Locational and climate information for each modern site. Precipitation data taken from TerraClim at a ~4km resolution (Abatzoglou *et al.* 2018)*****

Sample ID	Location	Rainfall Zone	Species	Precipitation (mm)		
				Mean Annual (MAP)	Summer	Winter
GC4	Giant's Castle Game Reserve, Ukhahlamba-Drakensberg, KwaZulu-Natal 29°15'51'' S 29°31'15'' E	Summer	*Protea roupelliae*	991.40	838.63	152.77
GC2	Giant's Castle Game Reserve, Ukhahlamba-Drakensberg, KwaZulu-Natal 29°16'25'' S 29°31'19'' E	Summer	*Podocarpus latifolius*	991.40	838.63	152.77
SB	Swartberg Pass, Western Cape 33°21'54'' S 22°5'57'' E	Year-Round	*Protea nitida*	254.37	149.53	104.84
MP	Montagu Pass, Western Cape 33°54'23'' S 22°25'9''E	Year-Round	*Podocarpus latifoloius*	379.16	201.46	177.7
CB	Camps Bay, Western Cape 33°57'13'' S 18°22'45'' E	Winter	*Protea nitida*	438.58	98.3	340.26
TB2	Theronsberg Pass, Western Cape 33°17'7'' S 19°27'50'' E	Winter	*Protea nitida*	293.36	101.56	191.8
GB1	Gifberg Pass, Western Cape 31°44'56'' S 18°47'22'' E	Winter	*Podocarpus elongatus*	163.26	41.04	122.53

*****See Appendix 5 for more detailed, annual rainfall information.

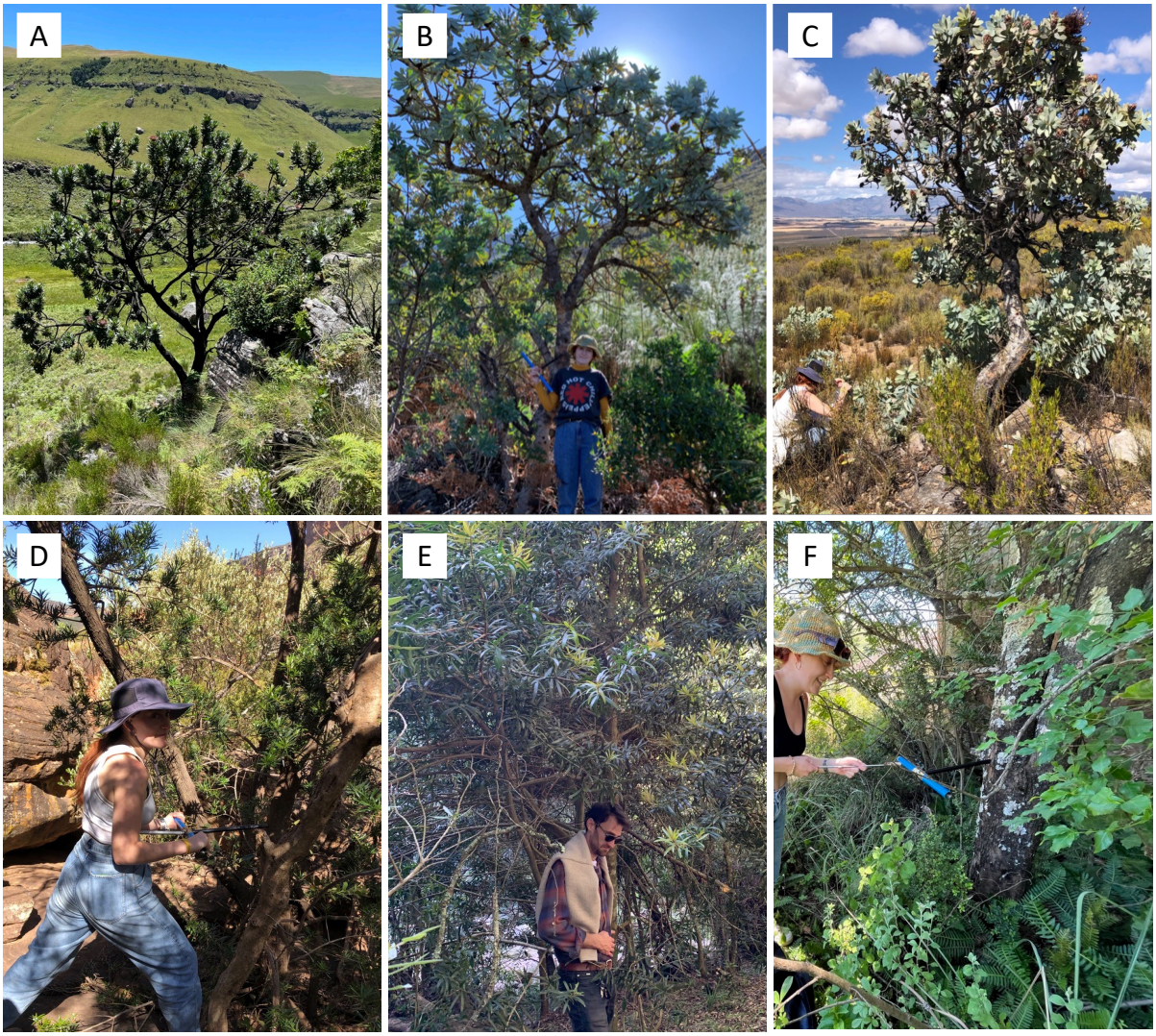

Figure 5. Photographs of *Protea* and *Podocarpus* trees and field sampling in each rainfall zone. **A:** *Protea roupelliae* in Giant's Castle, SRZ. **B:** *Protea nitida* in Swartberg Pass, YRZ. **C:** *Protea nitida* in Theronsberg Pass, WRZ. **D***: Podocarpus elongatus* in Gifberg Pass, WRZ. **E:** *Podocarpus latifolius* in Montagu Pass, YRZ. **F:** *Podocarpus latifolius* in Giant's Castle, SRZ.

4.2.3. Archaeological Site Selection

4.2.3.1. Waterfall Bluff

Two archaeological Podocarpaceae specimens were acquired from Waterfall Bluff, a coastal rockshelter in Mpondoland in eastern South Africa (Figure 4) (Fisher *et al.* 2020; Esteban *et al.* 2023a). The site is located in the Indian Ocean Coastal Belt (IOCB) biome and is predominantly surrounded by sour veld grasslands (Mucina *et al.* 2006). Although technically found in the SRZ, Waterfall Bluff receives more than a third of its annual rainfall in winter, resulting in more aseasonal rainfall patterns

(Fisher *et al.* 2020; Esteban *et al.* 2023a). Annual rainfall is approximately 984.42 mm (Fick & Hijmans 2017).[2]

Excavations at Waterfall Bluff commenced in 2015 and revealed well-stratified deposits containing faunal and floral remains, as well as lithic, shell, and ochre artefacts (Fisher *et al.* 2020; Esteban *et al.* 2023a). The analysis of these materials is integral to the Pondoland Paleoclimate, Paleoenvironment, Paleoecology, and Paleoanthropology Project (P5) which seeks to explore the relationship between hunter-gatherer behaviour and coastal environments (Fisher *et al.* 2020). Evidence indicates that the site was occupied during both glacial and interglacial phases of the Late Pleistocene and Holocene (Fisher *et al.* 2020). Waterfall Bluff is positioned close to a narrow part of the continental shelf which is thought to have constrained the extent of coastline transgression during glacial periods, enabling hunter-gatherers to exploit coastal resources even during the LGM (Fisher *et al.* 2020; Esteban *et al.* 2023a).

Podocarpaceae charcoal specimens WB_A and WB_B were obtained from the stratigraphic aggregate Light Brown Coarse Sands (LBCS) Chopi, which was dated between 18 080-17260 and 15 050-14 380 cal BP and therefore which covers the Late Pleistocene and, more specifically, the LGIT (Fisher *et al.* 2020). Important contextual information for the Waterfall Bluff specimens is summarised in Table 2. Proxy records suggest that the central and eastern regions of South Africa saw an increase in moisture availability and summer rainfall during the LGIT (e.g. synthesis by Chevalier & Chase 2015; Esteban *et al.* 2020).

4.2.3.2. Boomplaas Cave

Three archaeological Proteaceae charcoal specimens were obtained from Boomplaas Cave, a karstic cave in the Cango Valley which lies on the southern foothills of the Swartberg Mountain Range (Figure 4) (H. Deacon 1979). Today, Boomplaas Cave is located in the YRZ where it receives approximately 264.83 mm of rainfall each year (Fick & Hijmans 2017),[2] similar to the rainfall conditions experienced by the Swartberg modern sampling site (Table 1). The flora surrounding Boomplaas is a mosaic of fynbos and renosterveld vegetation controlled by slight changes in moisture availability, soil lithology, topography, and aspect (Vlok & Schutte-Vlok 2010).

Excavations led by Hilary Deacon between 1974 and 1979 revealed a rich, well-defined stratigraphy of material culture as well as floral and faunal remains spanning the Late Pleistocene and Holocene (H.

[2] Value for MAP obtained using WorldClim version 2.1 precipitation dataset covering 1970 to 2000.

Deacon 1979; J. Deacon 2023). These excavations formed part of a larger initiative to explore how climatic and environmental changes over the Quaternary influenced human behavioural variability in the southern Cape (H. Deacon 1979; J. Deacon 2023). Proteaceae charcoal specimens BPA4_21 and BPA4_24 were obtained from member LPC which has been radiocarbon dated between 26,100 and 24,300 cal BP, and BPA2_21 from member GWA dating between 21,920 and 21,410 cal BP (Pargeter *et al.* 2018). With these dates, LPC and GWA fall squarely in southern Africa's LGM (Chase & Meadows 2007; Stone 2014; Pargeter *et al.* 2018; Faith *et al.* 2024). The locational and stratigraphic information for these specimens is summarised in Table 2.

During the LGM, temperatures at Boomplaas Cave were approximately 6°C colder than today (Talma & Vogel 1992). Most palaoeclimate proxies suggest the dominance of westerly-driven winter rainfall during this period, yet the extent and nature of moisture availability remain a subject of debate (see review by Faith *et al.* 2024). Member LPC is associated with a peak in occupation intensity for the Late Pleistocene (Pargeter *et al.* 2018; Pargeter & Faith 2020). GWA, the height of the LGM, is associated with a slightly lower site occupation intensity relative to LPC (Pargeter & Faith 2020), showing short-term variability in site and landscape use, which may indicate seasonally-informed occupation (Pargeter *et al.* 2018).

Table 2. Locational and stratigraphic information for each archaeological charcoal specimen.

Sample ID	Site	Modern Rainfall Zone	Family	Layer and Age (cal BP)	Broad climate period
BPA4_21	Boomplaas Cave	Year-Round	Proteaceae	LPC (26,100 – 24,300)	LGM
BPA4_24					
BPA2_21				GWA (21,920 – 21,410)	
WB_A	Waterfall Bluff	Summer zone but technically year-round regime	Podocarpaceae	LBCS Chopi (18,080-17,260 to 15,050-14,380)	LGIT
WB_B					

4.2.4. Modern Sample Extraction

In contemporary dendrochronology, an increment borer (Figure 5b,d,f) is commonly used to extract a cylindrical increment core from the main stem or trunk of a tree (Grissino-Mayer 2003; Speer 2010; Belmecheri *et al.* 2022). However, the review of growth ring studies conducted in South Africa – presented in Chapter 2 – shows that the sampling of cross-sections (particularly stem discs) has historically been more popular in the region. The preference for stem discs is like due to the fact that a cross-sectional view is necessary in southern African trees where the secondary growth surface is

often anatomically complex and difficult to interpret (Lilly 1977; Curtis *et al.* 1978; McNaughton & Tyson 1979; Norström *et al.* 2008). Similarly, coring hardwoods is considered more difficult and requires additional effort to ensure the borer's auger does not break during coring (Grissino-Mayer 2003). The use of increment borers on indigenous hardwood (i.e. angiosperm) trees is therefore uncommon in South Africa (Steenkamp *et al.* 2008).

Although beneficial to studying South African trees, stem cross-sections are typically extracted using a chainsaw (Grissino-Mayer 2003), which can kill living trees. Thus, increment boring was chosen as a less harmful alternative. The emphasis here is on relative isotope changes, not absolute growth ring age determinations. The assumption is that the most recent portion of wood tissue (approx. 1-2 cm before the bark) reflects the average rainfall seasonality over the most recent growth period (approx. 5 years). A full disc cross-section is not required for this analysis, and so there is limited justification for the felling of a living tree.

The chosen borer was purchased from Haglöf, a popular manufacturer of increment borers. A 12-mm borer was selected as the larger size ensures that ample material can be obtained at a high, subannual resolution (i.e. multiple subsamples per growth increment) for isotope analysis. A single tree core of approximately 5 cm was extracted from the selected tree at each sample site. The increment borer was clean rinsed with ethanol to reduce the risk of contamination between samples and the possible spread of pathogens between trees (Grissino-Meyer 2003). Collected cores were placed into a carefully labelled sample bag and transported to the Stable Light Isotope Laboratory, Department of Archaeology at the University of Cape Town where they were left to air dry for at least eight weeks before laboratory processing commenced.

4.3. Laboratory Processing

4.3.1. Core Preparation

In the laboratory, the dried increment cores were processed to enhance the visibility of the transverse surface (cross-section) for microscopic analysis and subsampling. In the classical dendrochronological procedure, an adhesive is used to mount the core onto a grooved wooden block (Stokes and Smiley 1968; Asherin and Mata 2001; Speer 2010). Subsequently, a razor blade, surgical scalpel, microtome, or more commonly, a sanding machine is used to expose the cross-section (Asherin and Mata 2001; Speer 2010; Schollaen *et al.* 2017). However, such a method is unsuitable for this project for two reasons. Firstly, the water-soluble wood glues commonly used to mount cores were demonstrated to have a significant effect on both whole wood and cellulose $\delta^{13}C$ values and their use in

dendrochemistry is therefore not recommended (Braun-Wimmer *et al.* 2018). Secondly, this technique requires slicing or sanding away the unsecured top half of the core, resulting in its loss as waste material. This is incompatible with our requirements, as we need both core halves to remain intact so that one can be analysed as wood and the other charcoal.

Consequently, an alternative method of core bisection was chosen, wherein a Dremel® Moto-Saw Kit (MS20-1/5) was used to longitudinally bisect each core perpendicular to the primary growth axis. To reduce roughness and improve surface visibility, the cut transverse surface of each half was sanded by hand using progressively finer sandpaper (220-grit – 1200-grit). Speer (2010) recommends using a razor blade over sanding for preparing core surfaces for isotopic analysis, citing the potential risk of contamination from sanding swarf. Nonetheless, the laboratory protocol outlined here consists of a chemical pretreatment step, including an ultrasonic wash, and so the risk of swarf contamination affecting these results was deemed negligible.

Each core half was then measured and its length (mm) recorded (Table 3). This was crucial for enabling comparisons before and after carbonisation, in turn allowing for an evaluation of the shrinkage induced by this process.

4.3.2. Charcoalification

One prepared core half was made into charcoal in a reducing environment, following Hall *et al.* (2008). The wood sample was double wrapped in heavy duty aluminium foil and placed in a preheated muffle furnace (BWF-11/07, Being Technology, China) at 450°C for two hours. Afterwards, the sample was removed from the furnace and left to cool for at least one hour before the aluminium foil was unwrapped.

4.3.3. Digital Microscopy and Growth Interval Widths

Wood anatomy and growth interval boundaries of the modern samples were observed and measured using a stereomicroscope (Trinocular Tube Model SZ61TR, Olympus Corporation, Japan) and a DinoLite Digital Microscope (SalvisLab, Switzerland). Images of the transverse surface were taken at 10X, 20X, 40X, 60X, and 80X. The growth interval widths for each sample were recorded.

Once charcoalification was complete, the charcoal samples were assessed under a stereomicroscope and DinoLite, and the images compared to their wood counterparts. Growth interval boundaries in both *Protea* and *Podocarpus* charcoal were virtually invisible (Figure 10 & Appendix 1). Thus, a

shrinkage factor (%) was calculated for each increment core using the difference between core length before and after carbonisation. Shrinkage factors were applied to growth intervals measured in the wood samples to model and demarcate growth interval boundaries in the charcoals. This assumes that the degree of shrinkage that occurs during carbonisation propagates evenly and uniformly across the length of the wood. For this study, sample-specific shrinkage factors were used to analyse the charcoals. Each shrinkage factor and the details of their calculation are provided in Table 3. A critical oversight was made in not measuring the Swartberg charcoal (SB_ch) before and after carbonisation during initial analysis in 2021. Hence, the shrinkage factor calculated for CB (23.98 %) was applied to this sample, which contributes some uncertainty to high-resolution analysis of SB_ch.

Table 3. Calculation of sample specific shrinkage factors.

Sample	Rainfall Zone	Genus	Length before carbonisation (mm)	Length after carbonisation (mm)	Difference (mm)	Shrinkage (%)
GC4	Summer	*Protea*	46.39	37.13	9.26	19.96
TB2	Winter	*Protea*	47.88	42.05	5.83	12.18
GC2	Summer	*Podocarpus*	50.94	41.16	9.78	19.20
GB1	Winter	*Podocarpus*	57.03	43.59	13.46	23.60
MP1	Year-Round	*Podocarpus*	58.57	43.78	14.79	25.25
CB	Winter	Protea	49.95	37.97	11.98	23.98
SB	Year-Round	*Protea*	—	—	—	23.98

Archaeological charcoal samples were also analysed under a digital microscope and stereomicroscope to aid in the identification of the transverse surface that would serve as the site for subsampling. The small, irregular shapes, and fragile nature of the archaeological charcoals precluded the identification and measurement of growth intervals.

4.3.4. Chemical Pretreatment

Schubert and Jahren's (2011) SPP prioritises relative changes in $\delta^{13}C$ values across growth cycles as opposed to absolute $\delta^{13}C$ measurements. It is for this reason that the authors suggest chemical pretreatment and cellulose extraction are largely unnecessary in subsequent applications of the proxy. A mean observed offset of approximately 1 ‰ in $\delta^{13}C$ between whole wood and cellulose has contributed to cellulose becoming the preferred standard for the isotopic analysis of tree tissues (see Helle *et al.* 2022 and studies cited therein). Yet whole wood $\delta^{13}C$ has in some cases shown stronger

climate correlations than cellulose (e.g. Sidorova *et al.* 2008), and both materials are therefore regarded as viable options for climate reconstruction (McCarroll & Loader 2004). Moreover, the isotopic offset between whole wood and cellulose is less critical in this study which seeks to assess relative as opposed to absolute $\delta^{13}C$ values across growth increments. As a result, cellulose was not extracted from the modern wood samples. However, a chemical pretreatment step was conducted as it constitutes an essential step in the isotopic analysis of archaeological charcoals. Maintaining consistency between modern and archaeological analyses was deemed crucial.

To remove non-structural, mobile carbon, modern and archaeological samples were treated with successive acid-base-acid (ABA) washes, modified from the protocol outlined by Brock *et al.* (2010). Samples were placed into a clean beaker and covered in a 1M hydrochloric acid (HCl) solution. The beakers underwent a five-minute treatment in an ultrasonic bath (Bransonic® CPX3800H-E, Branson, USA) to ensure thorough immersion in the solution (Figure 6A&D). This process also served to remove swarf from the modern wood samples and sediment grains from the surfaces of the archaeological charcoals. Beakers were then transferred to an 80°C hot plate for fifteen minutes (Figure 6B). This was followed by a base wash in a 0.2M sodium hydroxide (NaOH) solution, including another round of ultrasonic treatment and fifteen minutes at 80°C. During the base wash of the modern *Protea* wood, the solution underwent significant discolouration, becoming a dark reddish-brown hue (Figure 6C). This was attributed to the leaching of tannins and other organic extractives from the wood. As a result, the NaOH wash was repeated once for the *Protea* woods to ensure thorough cleaning. Similarly, the NaOH solution became discoloured by humic substances during the pretreatment of the archaeological charcoals (Figure 6E), necessitating a second wash at 80°C followed by a third wash at room temperature. Samples were then treated to another acid wash, with the only adjustment being an extension of the hot plate time to 55 minutes. Following each wash, samples were rinsed three times with ultrapure Milli-Q® water.

Each sample was carefully transferred to a glass poly top vial, and wood samples were frozen at –18°C and then left in a freeze dryer (Scanvac CoolSafe 55-4, LaboGene, Denmark) overnight. Initial testing of this pretreatment protocol on two archaeological samples from Boomplaas Cave found that freeze drying of such a friable material led to cracking and breakage. To avoid this, modern and archaeological charcoals were instead oven-dried overnight at 70°C, following An *et al.* (2015).

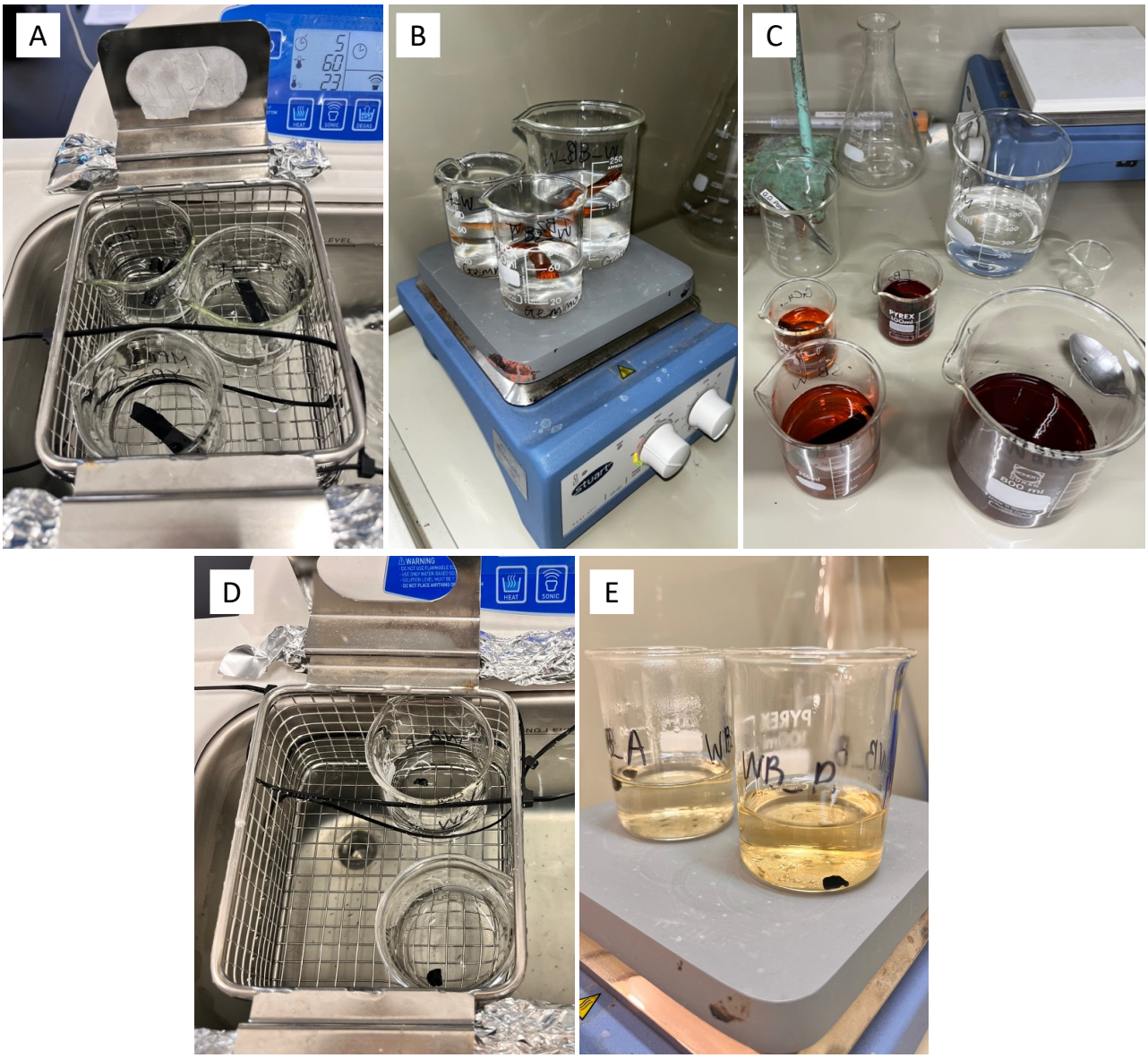

Figure 6. Chemical pretreatment of modern and archaeological wood and charcoal samples. **A:** *Podocarpus* charcoal in a 1M HCl solution placed into an ultrasonic bath. **B:** *Protea* wood samples in a 1M HCl solution on a hot plate. **C:** *Protea* wood after an initial wash in a 0.2M NaOH solution. The large beaker to the right contains the waste material. Note the significant discolouration of the solution. **D:** Archaeological Podocarpaceae specimens in a 1M HCl solution and placed in an ultrasonic bath. **E:** Second NaOH wash of the Podocarpaceae specimens. The solution is discoloured by humic substances.

4.3.5. Embedding

Once samples are prepared, and in this case pretreated, the next step in the protocol outlined by Schubert and Jahren (2011) is subsampling the 'rings' or growth intervals along the transverse section. For the authors, this step is completed "by hand using a razor blade" (Schubert & Jahren 2011: 7293). This was done on initial tests of the proxy on modern *Protea*, but here I identified that a major obstacle to precise subsampling was the lack of an effective mechanism to secure samples while slicing. This

was especially true for charcoal samples which could not be held with forceps nearly as firmly as their wood counterparts. Archaeological samples, it was observed, tend to be even more brittle and prone to breakage, and this, combined with their relatively small sizes (approx. 1 cm) and irregular shapes means that these samples are particularly difficult to subsample in the manner described by Schubert and Jahren.

The glues or resins commonly used to embed carbonates like shells for subsampling and isotopic analysis (e.g. Butler *et al.* 2009; Guo *et al.* 2023) could not be used in this study due to the increased risk of carbon contamination (see Branscombe *et al.* 2022). Thus, modern and archaeological samples were embedded in plaster of Paris which was prepared according to the ratio of one part distilled water to two parts plaster. Plaster of Paris was chosen because it is comprised of 100 % calcium sulphate hemihydrate which reduces the chance of carbon contamination of the samples. Just prior to hardening completely, the plaster was poured into a silicone loaf mould that was lined with tinfoil and samples were correctly oriented and gently pressed into the matrix. A hard plastic vial lid was pushed into the plaster at the 'bark end' of the sample; the area of most recent growth where subsampling would occur (Figure 7&8). This lid was removed once the plaster had hardened, leaving behind a depression in which a piece of weighing paper was placed to catch each sliced subsample. Once samples were embedded, the plaster of Paris was left to cure and dry for at least three days and up to one week before subsampling commenced.

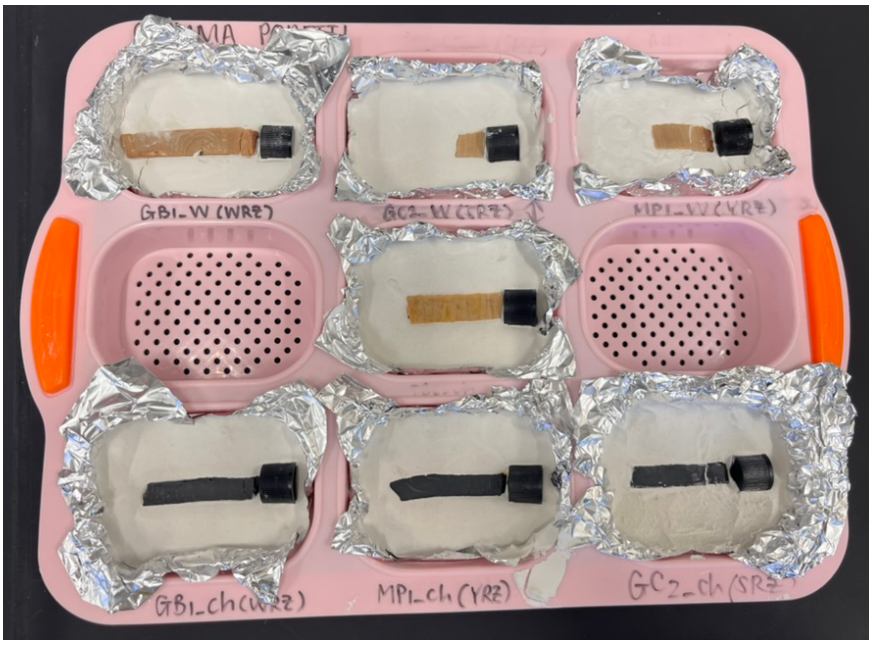

Figure 7. Photograph showing modern *Podocarpus* wood and charcoal embedded in plaster of Paris. The black object to the right of each sample is a hard plastic vial lid pressed into the plaster at the 'bark end.'

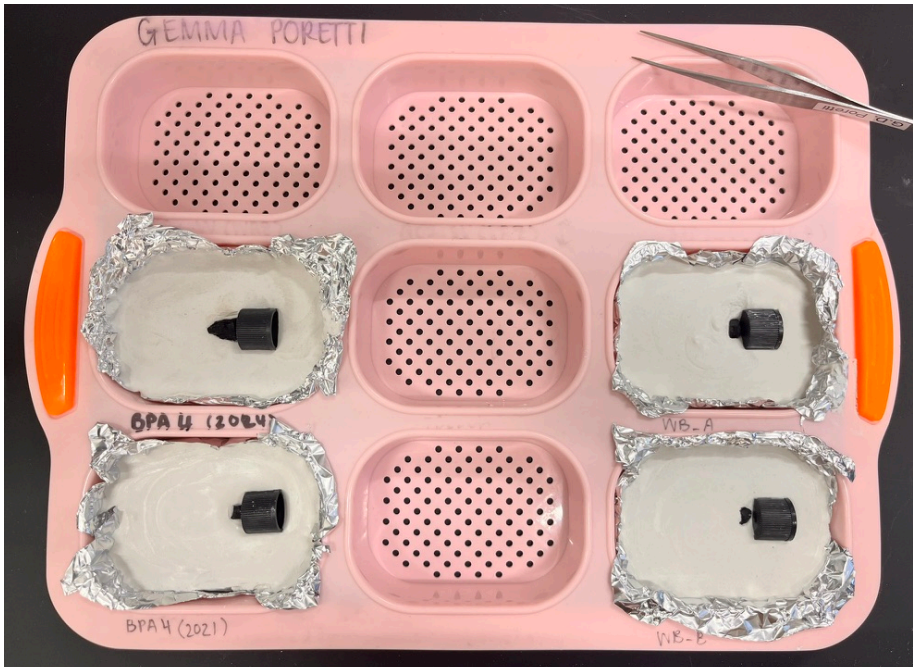

Figure 8. Photograph showing archaeological Proteaceae (left) and Podocarpaceae (right) charcoal embedded in plaster of Paris.

4.3.6. Subsampling

Multiple subsamples were obtained from across the transverse section of each modern and archaeological sample by hand using a scalpel to slice perpendicular to the axis of radial growth. This was aided by a stereomicroscope (Trinocular Tube Model SZ61TR, Olympus Corporation, Japan) and a lamp (TL2 Incandescent Illuminator, Olympus Corporation, Japan) to provide incident light. Subsampling in wood was guided by previously identified, visible growth increments of varying sizes (Appendix 1). In charcoal samples, where rings are less clearly defined, modelled growth ring boundaries – estimated using post-carbonisation shrinkage factors – were used as proxies to guide subsampling. Thus, subsampling was not based on equal-length arbitrary segments but rather on growth increment boundaries as much as possible.

Before the first subsample was taken, a scalpel was used to mark the plaster to note the location of the bark, or 'end' in the case of the archaeological samples. A calliper was then used to measure the distance from this mark for each subsample. A piece of weighing paper was cut into roughly 1.5 cm x 2 cm rectangles and placed into the depression or well left into the plaster by the now removed vial lid. A scalpel slice was taken and gathered in this well, and then transferred from the piece of weighing paper to a labelled centrifuge tube. This process was repeated until a desired length of the material had been subsampled. The weighing paper was replaced between each sample and all the used instruments were rinsed with ethanol to prevent cross contamination. SB_ch, CB_w, CB_ch, and

BPA2_21 were analysed in 2021 before the methods of embedding and measuring distance from bark were finalised, and so the total lengths subsampled are not known.

4.3.7. Stable Carbon Isotope Analysis

From the centrifuge tubes, each subsample was weighed into a tin capsule for isotopic analysis using a microbalance. Wood subsamples were weighed to approximately 2.00 mg, and charcoals to approximately 0.5 mg. This difference in desired weights accounted for the smaller size and mass of charcoals compared to wood, as well as the higher proportion of carbon in charcoals relative to wood.

Subsamples were combusted in a Flash 2000 organic elemental analyser and the gasses passed to a Delta V Plus isotope ratio mass spectrometer (IRMS) via a Conflo IV gas control unit. All three instruments are products of Thermo Scientific, Bremen, Germany.

The results were calibrated using the following in-house plant standards: Sucrose which was provided by Australian National University (ANU), Nasturtium (NAST) which was produced from dried nasturtium leaves collected from UCT campus, and Acacia which was made from *Acacia saligna* leaves from Glencairn, Cape Town. All in-house standards have been calibrated against International Atomic Energy Agency (IAEA) standards.

Results are expressed in delta notation (δ) in parts per thousand (‰) relative to the marine limestone standard Pee Dee Belemnite (PDB) according to the equation:

$$\delta^{13}C = [R_{sample}/R_{standard} - 1] \times 1000 \quad (2)$$

Where R_{sample} and $R_{standard}$ are the $^{13}C/^{12}C$ ratios of the sample and standard, respectively. The mean standard deviations for all three standards across the modern and archaeological isotopic analyses was 0.12 ‰ for $\delta^{13}C$.

4.4. Correcting for Bias in Subsampling Resolution

To quantify the effect of subsampling resolution on $\Delta\delta^{13}C_{meas}$, Schubert and Jahren (2011) modified their high-resolution dataset (averaging 27.9 subsamples per interval) obtained from eight growth intervals of a *Sophora* tree from Hawai'i into several lower resolution datasets using moving averages. From these, they recalculated $\Delta\delta^{13}C_{meas}$ and fit a hyperbolic curve through the data, which they then used to calculate the percentage for $\Delta\delta^{13}C_{max}$ represented by a given number of subsamples per

growth increment. The equation for the relationship between the percentage of maximum possible isotope change and subsampling resolution is given as:

$$\% \Delta\delta^{13}C_{max} = 3439(x - 1) / (100 + 34.39(x - 1)) ; R^2 = 0.999 \quad (3)$$

where *x* is the number of subsamples taken from a given growth increment. In the case of this *Sophora* sample, a resolution of 27.9 subsamples per growth interval yielded ~90% of $\Delta\delta^{13}C_{max}$, whereas only 4 subsamples per growth interval yielded ~50%. Thus, in scenarios characterised by low-resolution subsampling, the authors propose the application of specific correction equations such that $\Delta\delta^{13}C_{meas}$ can align more closely with $\Delta\delta^{13}C_{max}$.

Correction for resolution effects was hypothesised to be particularly critical for the modern and archaeological charcoal samples, which shrink in volume relative to the original wood (February 1996), and experience isotopic fractionation during the charcoaling process (Hall *et al.* 2008). These factors were expected to result in fewer subsamples on average from charcoal compared to wood, and a potential effect on the measured amplitudes. While this was not anticipated to push the seasonal amplitudes outside of the range expected for each rainfall zone, it was likely to produce a quantifiable offset that could be accounted for through correction. A threshold of an average of five and three subsamples per growth increment for wood and charcoal, respectively, was established: anything below this threshold would require correction for resolution effects.

4.5. Physical and Isotopic Growth Increment Boundaries

The central objective of this project is to determine the applicability of the SPP to archaeological charcoals, a material here observed to have largely indistinct growth increments. Unlike modern samples, where wood can be closely examined to aid in identifying charcoal growth increments, the wood from which archaeological charcoals originate cannot be studied. Isotopically identified boundaries – the rise and fall signal in sequential isotope measurements which does not necessarily adhere to prescriptive delineations – is thus all one has to work with when applying the SPP to archaeological samples. The effectiveness of these boundaries, in comparison to physically identified boundaries, must therefore be tested.

Although efforts were made to identify growth interval boundaries in both modern wood and charcoal samples, the precise relevance of these boundaries to applications of the proxy was assessed. This involved calculating two different values for $\Delta\delta^{13}C_{meas}$ for each sample: one based on identifying

maxima and minima within *physically identified boundaries* (PB), and another based on identifying maxima and minima within *isotopically identified boundaries* (IB). The relationship between the two different values for PB $\Delta\delta^{13}C_{meas}$ and IB $\Delta\delta^{13}C_{meas}$ and the value for $\Delta\delta^{13}C_{model}$ calculated for each site was assessed to see whether physically or isotopically identified boundaries are in closer alignment with climate data.

4.6. Modern and archaeological seasonality attributions: calculating $\Delta\delta^{13}C_{model}$, ΔP, and P_S/P_W

Testing the effectiveness of the proxy requires evaluating the average measured change in $\delta^{13}C$ across a given set of growth intervals ($\Delta\delta^{13}C_{meas}$) to the average change in $\delta^{13}C$ modelled ($\Delta\delta^{13}C_{model}$) from climatology data. This is because $\Delta\delta^{13}C_{meas}$ – the seasonal signal – is a function of both changes in the isotopic composition of atmospheric CO_2 ($\Delta\delta^{13}C_{CO2}$) and the ratio of summer to winter rainfall (P_S/P_W). With this information from climate data, the expected $\Delta\delta^{13}C_{meas}$ can be calculated for a given location using the following equation:

$$\Delta\delta^{13}C_{model} = \Delta\delta^{13}C_{CO2} - 0.82(\Delta P) + \Delta Y \quad (4)$$

where $\Delta\delta^{13}C_{CO2}$ is defined as a constant equalling 0.05 ‰ in the SH due to the negligible effect of seasonal CO_2 cycling in lower latitudes relative to the Northern Hemisphere, – 0.82 ‰ is a scalar, ΔP is the change in seasonal precipitation, and ΔY reflects seasonal changes in post-photosynthetic fraction to the value of 0.73 ‰ (Schubert & Jahren 2011: 7298). The variable ΔP is further defined as the difference between the ln-transformed values for the amount of summer precipitation (P_S) and winter precipitation (P_W):

$$\Delta P = \ln(P_S) - \ln(P_W) \quad (5)$$

Eq. (4) was used to calculate the modelled change for all modern sites (listed in Table 1) with the input of monthly precipitation data from TerraClim at a 4 km resolution (Appendix 5)(Abatzoglou *et al.* 2018). The results for $\Delta\delta^{13}C_{model}$ were compared to the values for $\Delta\delta^{13}C_{meas}$ derived from the $\delta^{13}C$ measurements by means of a regression analysis to ultimately evaluate whether this relationship is applicable to modern *Protea* and *Podocarpus* wood and charcoal from South Africa.

Should this relationship be established, Eq. (4) and Eq. (5) can be combined and rearranged to calculate seasonal changes in precipitation (ΔP) from $\delta^{13}C$ measurements:

$$\ln(P_S) - \ln(P_W) = (\Delta\delta^{13}C_{meas} - 0.05 - \Delta Y) / (-0.82) \quad (6)$$

Additionally, the SPP's equations can be further modified so that the ratio of summer to winter rainfall (P_S/P_W) may be calculated from $\delta^{13}C$ measurements:

$$P_S/P_W = e\text{^}[(\Delta\delta^{13}C_{meas} - 0.05 - \Delta Y) / (-0.82)] \quad (7)$$

The measured seasonal amplitudes of the modern *Protea* and *Podocarpus* samples, and the archaeological samples, were inputted into Eq. (6) and Eq. (7) to calculate ΔP and P_S/P_W, respectively. For the modern samples, the values obtained for these variables were checked against the values calculated using rainfall records and $\Delta\delta^{13}C_{model}$ (Eq. 4). The relationship between the measured and modelled values for ΔP and P_S/P_W were then assessed to determine whether isotope measurements can reliably be used to independently quantify these seasonal variables. The archaeological values for ΔP and P_S/P_W were compared to those calculated for the modern samples to evaluate changes in rainfall seasonality between the LGM and LGIT and the present.

CHAPTER 5

Results

5.1. Introduction

This Chapter presents the results of the high-resolution $\delta^{13}C$ analysis of modern *Protea* and *Podocarpus* wood and charcoal from all three rainfall zones, as well as archaeological Podocarpaceae and Proteaceae charcoals. Measured seasonal amplitudes are potentially influenced by five key factors: rainfall zone, material, genus, resolution, and growth increment demarcations. Table 4 summarises the expected effects of each factor, which constitute the five dimensions of analysis that this Chapter aims to address in the context of the modern calibration samples. Once these factors are understood in a modern context, the results of the archaeological specimens can be more meaningfully interpreted. The Summary presented at the end of this Chapter will revisit these factors to determine the applicability of the SPP to a South African context.

Table 4. Factors likely to affect measured seasonal amplitudes ($\Delta\delta^{13}C_{meas}$), and expectations for each.

Measured seasonal amplitude ($\Delta\delta^{13}C_{meas}$):				
Rainfall Zone	Material	Genus	Resolution	Growth Increment Demarcations
Highest measured amplitudes for WRZ, lowest for SRZ, intermediate for YRZ.	Offset between wood and charcoal due to shrinkage and $\delta^{13}C$ depletion with carbonisation.	No significant difference between *Protea* and *Podocarpus* from each rainfall zone.	Stronger climate correlations in samples with higher subsampling resolutions	Isotope boundaries correlate with climate just as strongly as physical boundaries do.

5.2. Modern Wood and Charcoal Analysis

Eleven modern samples were analysed from across South Africa's three rainfall zones: four *Protea* wood, three *Protea* charcoal, one *Podocarpus* wood, and three *Podocarpus* charcoal. Apart from TB2, GB1, and GC2, all modern samples were analysed as both wood and charcoal. The charcoal counterpart of the WRZ Protea TB2 (TB2_ch) was excluded due to instrumental error ($\sigma > 0.25$ ‰) in that particular run. The wood counterparts for the *Podocarpus* WRZ sample GB1 (GB1_w) and SRZ sample GC2 (GC2_w) were not processed or analysed. An initial comparison of results from the YRZ MP_w and MP_ch indicated that the SPP yields promising results when applied to *Podocarpus* wood and charcoal. Consequently, prioritising charcoal samples was considered more appropriate for the remainder of the project and therefore GB1_w and GC2_w were not analysed.

5.2.1. Microscopic analysis and growth increment widths

The transverse surface of *P. nitida* wood, such as TB2_w (Figure 9A&B), displays a diffuse porous structure with vessels evenly distributed across the growth increments. By comparison, *P. roupelliae* wood (Figure 9C&D) has smaller vessels and greater vessel uniformity and distribution, making its porosity more diffuse than *P. nitida*. Growth increments in this species are therefore almost entirely indistinct. Rays in this *P. nitida* are prominent, while those in *P. roupelliae* appear narrower and evenly spaced. The heterogenous structure and variability present in *Protea* wood complicated the identification and measurement of growth increments. Conversely, the transverse surface of MP_w, a *P. latifolius* sample (Figure 9E&F), exhibits clearly defined, uniform growth increments, with a consistent pattern of alternating earlywood and latewood. The number of identified growth increments and mean growth increment width for each modern wood sample are summarised in Table 5 (see Appendix 1 for detailed tables of growth increment widths).

The mean growth increment width calculated for the SRZ *P. roupelliae* sample GC4_w was 1.11 mm (Table 5). Yet this value cannot be said to represent the sample in its entirety. Only five of the outermost increments of GC4_w were measurable due to the diffuse-porous nature of the wood. Since the present study focuses on comparing high-resolution $\delta^{13}C$ measurements with local climate data averaged over the last five years, the youngest growth increments were prioritised. Although efforts were made to measure the widths as precisely as possible, certainty in these measurements cannot be guaranteed. This limitation applies to all *Protea* wood samples, where complex wood structure and appearance renders growth increment analysis less straightforward compared to *Podocarpus* wood.

Similarly, only 10 of the outermost increments of the *P. nitida* TB2_w were measured, with an average width of 1.83 mm (Table 5). The reddish-purple pigmentation observed in TB2_w sample (Figure 9B) is likely due to the high tannin content especially towards the pith of the core – the area forming part of the heartwood. Research on wood extracts has shown that heartwood tends to accumulate higher concentrations of tannins and other phenolic compounds (Hillis *et al.* 1987; Helle *et al.* 2022). The different compounds making up heartwood contain distinct isotopic signatures that could complicate seasonal $\delta^{13}C$ signals (see review by Helle *et al.* 2022). To avoid potential contamination, this portion of TB2_w was avoided during growth increment measurement and subsampling. After chemical pretreatment this pigmentation was drastically reduced. Nevertheless, it was deemed unnecessary to subsample from the heartwood as ample growth increments had already been subsampled.

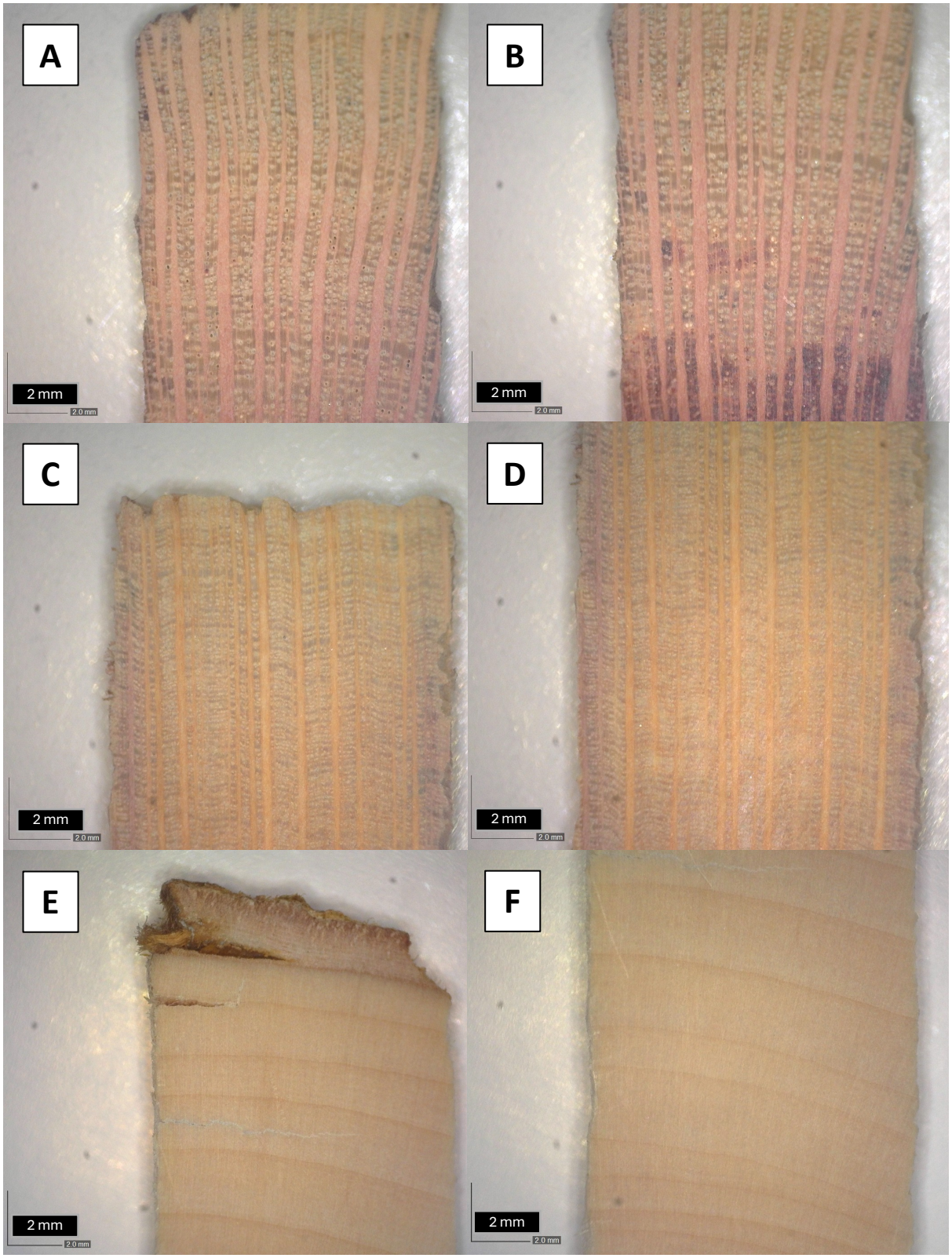

Figure 9. DinoLite digital images showing the transverse surfaces of three modern wood samples. **A-B:** Theronsberg (TB2, WRZ) *P. nitida* with diffuse porous structure and distinct rays. **C-D:** Giant's Castle (GC4, SRZ) *P. roupelliae* with smaller vessels and diffuse porous structure rendering growth increments indistinct. **E-F:** Montagu Pass (MP, YRZ) *P. latifolius* showing clear growth ring boundaries.

Table 5. Number of identified growth increments (GIs) and mean, maximum, and minimum GI width for each modern wood sample.

Sample ID	Site	Genus	No. of identified GIs	Mean Wood GI width: measured (mm)	Shrinkage Factor (%)	Mean Charcoal GI width: modelled (mm)
GC4	Giant's Castle	*Protea*	5[b]	1.11	19.96	0.89
GC2[a]		*Podocarpus*	32	1.50	19.20	1.21
SB	Swartberg	*Protea*	44	1.61	23.98[d]	1.23
MP	Montagu Pass	*Podocarpus*	32	1.29	25.25	0.97
CB	Camps Bay	*Protea*	24	2.08	23.98	1.58
TB2	Theronsberg	*Protea*	10[c]	1.83	12.18	1.61
GB1[a]	Gifberg	*Podocarpus*	49	0.44	23.60	0.34

[a] Wood samples that were analysed with the DinoLite but which were not isotopically tested. Only their charcoal counterparts were isotopically tested.
[b] Only the five outermost GIs of GC4_w were measured as extreme porosity made it a challenge precisely identify GI boundaries. The total number of physically identified GIs present in GC4_w is unknown.
[c] Only the ten outermost GIs of TB2_w were measured as this was the section unaffected by the reddish-purple tannin pigmentation.
[d] The charcoal counterpart of sample SB was neither analysed using the DinoLite nor measured for its length. Ultimately, a unique shrinkage factor could not be calculated for this sample and, as a result, the factor for CB was used to model SB charcoal GI widths.

Growth increments in the modern charcoal samples could not be directly measured due to the invisibility of distinct growth bands after carbonisation in both *Protea* and *Podocarpus* (Figure 10). Growth increments were slightly more visible in some cases, such as GB1_ch (Figure 10F), but boundaries could not be placed with certainty. For all charcoal samples, then, growth increment widths were modelled using shrinkage factors calculated according to the difference in sample length before and after carbonisation (Table 3). The mean growth increment widths for each charcoal sample are listed in Table 5 (see Appendix 1 for a more detailed listing of individual charcoal growth increment widths modelled using shrinkage factors).

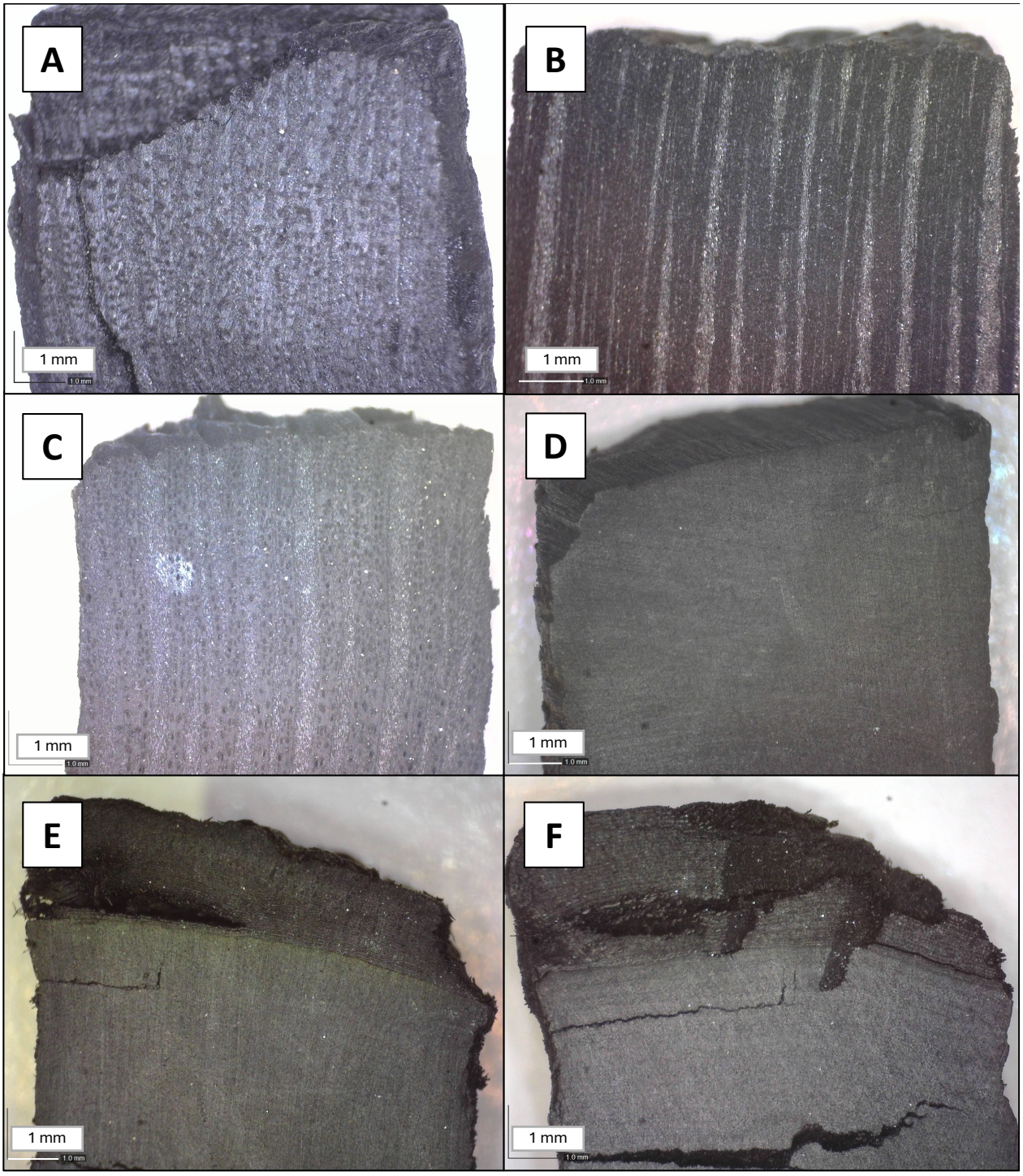

Figure 10. DinoLite digital images showing the transverse surfaces of six modern charcoal samples. **A:** Camps Bay (CB, WRZ) *P. nitida.* **B:** Giant's Castle (GC4, SRZ) *P. roupelliae*. **C:** Theronsberg (TB2, WRZ) *P. nitida.* **D:** Giant's Castle (GC2, SRZ) *P. latifolius.* **E:** Montagu Pass (MP, YRZ) *P. latifolius*. **F:** Gifberg (GB1, WRZ) *P. elongatus.*

5.2.2. General isotope results and subsampling resolution

A total of 506 $\delta^{13}C$ measurements were obtained from the eleven samples with the greatest number of subsamples taken from the GC4_w (n = 83), and the fewest from GB1_ch (n = 22) (Table 6). The average number of subsamples was 46 $\delta^{13}C$ measurements per wood or charcoal sample. Mean, maximum, and minimum $\delta^{13}C$ are also reported in Table 6 to provide an overview of the isotopic variability within and between samples. For wood samples, Table 6 shows that the least negative $\delta^{13}C$ value was recorded for CB_w (-25.43 ‰) and the most negative for MP_w (-26.30 ‰). GB1_w yielded the least negative $\delta^{13}C$ for the charcoals (-23.17 ‰), while MP_ch yielded the most negative (-27.26 ‰) (Table 6).

Table 6. Summary of MAP and general isotope results for each wood and charcoal sample.

Sample ID	Genus	Rainfall Zone	MAP (mm)	Material	Length subsampled (mm)	No. of $\delta^{13}C$ measurements	No. of $\delta^{13}C$ measurements per millimetre	Max. $\delta^{13}C$ (‰)	Min. $\delta^{13}C$ (‰)	Mean $\delta^{13}C$ (‰)	Range (Max - Min) (‰)
GC4_w	*Protea*	Summer	991.40	Wood	34.07	83	2.44	-24.81	-26.84	-26.02	2.03
GC4_ch				Charcoal	19.75	57	2.89	-26.34	-27.69	-27.15	1.35
GC2_ch	*Podocarpus*			Charcoal	8.06	30	3.77	-26.61	-27.66	-27.21	1.05
SB_w	*Protea*	Year-round	254.37	Wood	21.81	74	3.39	-25.13	-27.28	-26.13	2.15
SB_ch				Charcoal		50		-26.06	-28.47	-27.05	2.41
MP_w	*Podocarpus*	Year-Round	379.16	Wood	14.1	35	2.48	-25.29	-27.66	-26.3	2.37
MP_ch				Charcoal	8.95	27	3.02	-26.42	-28.34	-27.26	1.92
CB_w	*Protea*	Winter	438.58	Wood		37		-23.96	-26.63	-25.43	2.67
CB_ch				Charcoal		30		-25.27	-26.98	-26.1	1.71
TB2_w	*Protea*	Winter	293.36	Wood	10.81	61	5.64	-25.28	-27.45	-26.14	2.17
GB1_ch	*Podocarpus*	Winter	163.26	Charcoal	3.95	22	5.57	-22.61	-24.04	-23.17	1.43
				Mean	**15.19**	**46**	**3.65**				

Subsampling results indicate that GC4_w had the greatest length of its transverse surface subsampled (34.07 mm), and GB1_ch the shortest (3.95 mm) (Table 6). There appears to be no significant relationship between length subsampled and the number of subsamples or $\delta^{13}C$ measurements per millimetre ($R^2 = 0.384$, $p = 0.101$).

Table 7 compares the mean $\delta^{13}C$ results of *Protea* to *Podocarpus*. Whether the difference in mean $\delta^{13}C$ between *Protea* and *Podocarpus* wood is significant could not be determined only one *Podocarpus* wood value was available for comparison. However, a t-test found no statistically significant difference in mean $\delta^{13}C$ between *Protea* and *Podocarpus* charcoal (two-tailed: $t = -0.64$, $p = 0.584$). Current understanding of $\delta^{13}C$ variability between modern gymnosperms and angiosperms indicates that a significant difference is likely to occur between the two groups (Leavitt 2002; Sheldon *et al.* 2020; Hare & Lavergne 2021). This difference is not observed in the modern charcoal samples, and a greater number of *Podocarpus* wood samples are required to meaningfully determine whether the lack of difference holds true for wood. Likewise, MAP (Table 6) was also found to have no significant effect

on mean $\delta^{13}C$ in wood ($R^2 = 0.016$, $p = 0.837$), nor in charcoal ($R^2 = 0.308$, $p = 0.253$). Depletion in $\delta^{13}C$ is observed to occur in both *Protea* and *Podocarpus* during the charcoaling process.

Table 7. Difference in mean $\delta^{13}C$ between *Protea* and *Podocarpus* charcoal.

Sample ID	Rainfall Zone	Genus	Mean $\delta^{13}C$ Wood (‰)	Mean $\delta^{13}C$ Charcoal (‰)	Difference (‰)
GC2	Summer	*Podocarpus*		-27.21	
MP	Year-Round	*Podocarpus*	-26.3	-27.26	0.96
GB1	Winter	*Podocarpus*		-23.17	
		Mean	**-26.3**	**-25.88**	**0.96**
GC4	Summer	*Protea*	-26.02	-27.15	1.13
SB	Year-round	*Protea*	-26.13	-27.05	0.92
CB	Winter	*Protea*	-25.43	-26.1	0.67
TB2	Winter	*Protea*	-26.14		
		Mean	**-25.93**	**-26.77**	**0.91**

5.2.3. Isotope Results for the Modern Calibration of the SPP

5.2.3.1. Summer Rainfall Zone Protea – GC4

A total of 83 and 57 $\delta^{13}C$ measurements were taken across consecutive growth increments of GC4_w and GC4_ch, respectively (Table 6). The cyclical increase and decrease in $\delta^{13}C$ revealed by Schubert and Jahren (2011) in sequential evergreen growth increments was observed in GC4_w (Figure 11A). The SPP is concerned with relative changes in $\delta^{13}C$ identified across consecutive growth increments. While mean $\delta^{13}C$ in charcoal samples exhibits a more negative shift due to carbonisation, the assumption is that this depletion occurs uniformly across all $\delta^{13}C$ measurements. Although the absolute values differ between wood and charcoal, the relative fluctuations remain in-phase. Thus, despite depletion with carbonisation, a rise and fall pattern similar to that observed for GC4_w was identified for GC_ch (Figure 11A). The seasonal signal is therefore preserved in charcoal, despite being offset to lower values on the plot.

The amplitude of seasonality ($\delta^{13}C_{max}$ – preceding $\delta^{13}C_{min}$ = $\Delta\delta^{13}C_{meas}$) was calculated for all growth increments identified physically (i.e. based on growth increment microscopy and width measurements), and isotopically (i.e. based solely on cyclical trends observed in the plotted isotope series). The physical boundary (PB) and isotope boundary (IB) results for GC4 are summarised in Table 8 and Table 9, respectively. Averaging the $\delta^{13}C$ changes across the growth increments of GC4_w resulted in a value of 0.37 ‰ ± 0.17 ‰ for PB $\Delta\delta^{13}C_{meas}$ and 0.47 ‰ ± 0.25 ‰ for IB $\Delta\delta^{13}C_{meas}$. For GC4_ch, a $\Delta\delta^{13}C_{meas}$ of 0.51 ‰ ± 0.17 ‰ was calculated for PB, and 0.42 ‰ ± 0.17 ‰ for IB. GC4 is the

only example in this study in which charcoal $\Delta\delta^{13}C_{meas}$ exceeds wood $\Delta\delta^{13}C_{meas}$, at least in the case of physically identified boundaries.

Tables 8 and 9 also display the average number of $\delta^{13}C$ measurements per growth increment, here defined as subsampling resolution. Resolution is 7.20 for GC4_w PB, and 5.33 for IB. For GC4_ch, resolution is 5.50 measurements per growth increment for PB, and 7.29 for IB. For this sample, there does not appear to be a difference in subsampling resolution between wood and charcoal, nor between PB and IB $\Delta\delta^{13}C_{meas}$.

Not all growth increments were included in the analysis of $\Delta\delta^{13}C_{meas}$. For example, GC4 wood's PB growth increment 3 (Table A3.10 Appendix 3) only included two $\delta^{13}C$ measurements, which was considered too few subsamples to calculate a seasonal amplitude. The same issue of too few subsamples per growth increment occurred in growth increment 3 for GC4 charcoal's PB (Table A3.12 Appendix 3). In all samples thereafter where two or fewer subsamples represent a growth increment, that growth increment is excluded from both PB and IB $\Delta\delta^{13}C_{meas}$ calculations. Growth increment 1 was also excluded from the $\Delta\delta^{13}C_{meas}$ calculation of GC4_ch due to the resulting amplitude being less than 0.16 ‰ – the threshold corresponding to the analytical precision and repeatability limit established for all samples in this study.

5.2.3.2. Year-Round Rainfall Zone Protea – SB

A total of 74 $\delta^{13}C$ measurements were obtained from SB_w and 54 from SB_ch (Table 6). A seasonal isotope signal was identified in SB_w and was also preserved in SB_ch despite being offset to lower values on the plot due to carbonisation depletion (Figure 11B). For SB_w, eleven total growth increments were identified and subsampled. However, in calculating the sample's PB $\Delta\delta^{13}C_{meas}$, growth increments 2,3, 10, and 11 were excluded due to their $\Delta\delta^{13}C$ values being < 0.16 ‰ (Table A3.6 Appendix 3). Similarly, growth increments 1, 5, 6, and 7 either did not contain either a minimum or maximum value and so an intra-increment amplitude could not be calculated, resulting in the exclusion of these increments as well. Ultimately, only five of SB_w's growth increments were used to calculate PB $\Delta\delta^{13}C_{meas}$. SB_w's plotted measurements show six clearly identifiable $\delta^{13}C$ peaks and troughs (Figure 11B). Nevertheless, these cyclical increases and decreases did not align with physical growth boundaries. As a result, these maxima and minima were not included in the PB $\Delta\delta^{13}C_{meas}$ calculations, which came to 1.07 ‰ ± 0.79 ‰ for SB_w. They were, however, used to calculate IB $\Delta\delta^{13}C_{meas}$, which was found to be 1.29 ‰ ± 0.53 ‰. Only four clear peaks are evident in the plotted charcoal results (Figure 11B). Nevertheless, SB wood and charcoal are in-phase. Averaging SB_ch's

intra-increment amplitudes to calculate $\Delta\delta^{13}C_{meas}$ resulted in 0.44 ‰ ± 0.20 ‰ for PB and 0.91 ‰ ± 0.79 ‰ for IB. Seasonal amplitudes are therefore greater in the case of IB for both wood and charcoal.

Comparing PB $\Delta\delta^{13}C_{meas}$ values between wood and charcoal in the SB sample is somewhat complicated due to the fact that only five growth increments were modelled in the charcoal and therefore useable in the calculations. However, growth increment 4 in PB $\Delta\delta^{13}C_{meas}$ for SB_ch produced an intra-increment amplitude of 0.11 ‰ (Table A3.8 Appendix 3), below the 0.16 ‰ limit. While all physical growth increments were identified and measured in SB_w, the SB_ch subsamples were originally collected in 2021 prior to the standardising the measurement of distance from bark. Additionally, a critical oversight was made in not measuring the total length of SB_ch before subsampling commenced. Thus, when subsampling resumed in 2023, the exact distance from bark was unknown, and could not be determined for the new subsamples, which prevented their inclusion in the PB $\Delta\delta^{13}C_{meas}$ calculations. Conversely, a greater number of $\delta^{13}C$ measurements spanning the whole plotted series were included in the IB calculation for SB_ch (n = 50), as well as for both PB (n = 45) and IB (n = 74) $\Delta\delta^{13}C_{meas}$ for SB_w. Once again, minimal difference in subsampling resolution was found between PB and IB amplitudes for both wood and charcoal (Table 8 and Table 9).

5.2.3.3. Winter Rainfall Zone Proteas – CB and TB2

Two *Protea* samples from the WRZ were analysed, yet only CB was analysed as both wood and charcoal. In total, 37 $\delta^{13}C$ measurements were obtained from CB_w, 30 from CB_ch, and 61 from TB2_w (Table 6). A cyclical rise and fall pattern in $\delta^{13}C$ is present in both CB_w and CB_ch (Figure 11C). All CB_w $\delta^{13}C$ measurements and growth increments were included in calculating both PB and IB $\Delta\delta^{13}C_{meas}$, which were determined to be 0.83 ‰ ± 0.33 ‰ and 1.08 ‰ ± 0.61 ‰, respectively. Growth increment 6 was excluded from CB_ch's PB $\Delta\delta^{13}C_{meas}$ as its amplitude was < 0.16 ‰ (Table A3.3 Appendix 3). For CB_ch, PB $\Delta\delta^{13}C_{meas}$ was 0.40 ‰ ± 0.08 ‰ and IB $\Delta\delta^{13}C_{meas}$ was 0.84 ‰ ± 0.22 ‰. Notably, IB $\Delta\delta^{13}C_{meas}$ values are greater than PB values which is consistent with other samples assessed in this study. Subsampling resolution for both wood and charcoal is also higher in IB compared to PB (Table 8 and Table 9).

Five growth increments were used to calculate PB $\Delta\delta^{13}C_{meas}$ for TB2_w. A seasonal signal was identified in this sample (Figure 11D). In total, the subsampling resolution for PB $\Delta\delta^{13}C_{meas}$ TB2_w was averaged to be 12.20. Ultimately, PB $\Delta\delta^{13}C_{meas}$ for TB2_w was determined to be 0.48 ‰ ± 0.37 ‰. At 0.77 ‰ ± 0.21 ‰ the IB seasonal amplitude measured for TB2_w was relatively greater. Yet this remains

comparatively lower than the $\Delta\delta^{13}C_{meas}$ values recorded for the other WRZ *Protea* wood sample, CB_w, despite a significant subsampling resolution of 18.33.

5.2.3.4. Summer Rainfall Zone Podocarpus – GC2

Podocarpus sample GC2 from the SRZ was analysed only as charcoal, and a seasonal signal was identified (Figure 12A). Though 30 total $\delta^{13}C$ measurements were taken from along its transverse surface (Table 6), only 20 were used to calculate PB $\Delta\delta^{13}C_{meas}$ (Table 8). Eight growth increments were sampled, but increment 1 was excluded due to an intra-increment amplitude of < 0.16 ‰, and 2, 6, and 7 were excluded due to having either no minimum or maximum $\delta^{13}C$ value (Table A3.18 Appendix 3). PB $\Delta\delta^{13}C_{meas}$ was averaged to be 0.33 ‰ ± 0.14 ‰. For IB $\Delta\delta^{13}C_{meas}$, 20 $\delta^{13}C$ were included in the calculation. Growth increments 1 and 2, consisting of 4 and 3 subsamples, respectively, resulted in low amplitudes (< 0.16 ‰) and were ultimately excluded (Table A3.19 Appendix 3). The three remaining subsamples not included were located at either end of the series and were not incorporated into full isotope cycles. Four complete $\delta^{13}C$ cycles were used to calculate IB $\Delta\delta^{13}C_{meas}$ which was 0.39 ‰ ± 0.12 ‰. The resolution was 5 subsamples per growth increment for both PB and IB $\Delta\delta^{13}C_{meas}$ (Tables 8 & 9).

5.2.3.5. Year-Round Rainfall Zone Podocarpus – MP

For MP_w and MP_ch, 35 and 27 $\delta^{13}C$ measurements, respectively, were obtained during subsampling. In-phase, seasonal $\delta^{13}C$ cycles are evident in this sample (Figure 12B). Notably, MP_w PB $\Delta\delta^{13}C_{meas}$ and IB $\Delta\delta^{13}C_{meas}$ were identical as the isotope peaks and troughs were a near-perfect match with the physically identified growth increment boundaries (Tables 8 & 9). The value for MP_w $\Delta\delta^{13}C_{meas}$ was calculated to 1.20 ‰ ± 0.39 ‰, which represented 35 $\delta^{13}C$ measurements and seven growth increments with a resolution of 5 measurements per growth increment. As expected, the PB and IB $\Delta\delta^{13}C_{meas}$ values for MP_ch were relatively lower. Five growth increments and 20 $\delta^{13}C$ measurements were used to calculate PB $\Delta\delta^{13}C_{meas}$ which was averaged to 0.56 ‰ ± 0.28 ‰ (Table 8). Growth increment 1 was excluded due to low amplitude and growth increment 6 for having no minimum value (Table A3.16 Appendix 3). Four growth increments and all 27 $\delta^{13}C$ measurements were included in IB $\Delta\delta^{13}C_{meas}$ which, at 0.73 ‰ ± 0.44 ‰, was relatively higher than MP_ch PB $\Delta\delta^{13}C_{meas.}$ The subsampling resolution of MP_ch IB $\Delta\delta^{13}C_{meas}$ was also greater than that of PB $\Delta\delta^{13}C_{meas}$ (Tables 8 & 9).

5.2.3.6. Winter Rainfall Zone Podocarpus – GB1

GB1 had the greatest number of identified growth increments of all samples in this study, but these increments were relatively narrow (Table 5). When charcoaled, these already narrow growth increments experienced further reduction in width. As a result, only 22 subsamples were obtained from GB1_ch (Table 6). However, these measurements covered approximately 19 identified growth increments. A seasonal $\delta^{13}C$ signal is comparatively less clear, and likely not present, in GB1_ch (Figure 12C). A total of 15 growth increments were used to calculate PB $\Delta\delta^{13}C_{meas}$, yet thirteen were excluded due to having either no minimum or maximum $\delta^{13}C$ value, and another for having an intra-increment amplitude of only 0.04 ‰ (Table A3.20 Appendix 3). Ultimately, only one growth increment produced a useable intra-increment amplitude of 0.31 ‰. The SPP requires amplitudes from several consecutive growth increments which can be averaged to determine an average measured carbon isotope change which stands as a proxy for seasonality. With only one useable growth increment, a PB $\Delta\delta^{13}C_{meas}$ could not reliably be calculated for GB1_ch. The same issue occurred for IB $\Delta\delta^{13}C_{meas}$. Here, six isotopic growth increments were identified, but five were excluded for producing negligible intra-increment amplitudes (between 0.02 and 0.09 ‰) (Table A3.21 Appendix 3). The single useable growth increment produced an amplitude of 0.35 ‰ (Table 9), which alone could not be used as a value for IB $\Delta\delta^{13}C_{meas}$. Thus, GB1_ch was excluded from subsequent analysis as its results could not convincingly be compared to local climate data in order to validate the SPP. The reasons for the unexpected results of GB1_ch are discussed in Chapter 6.

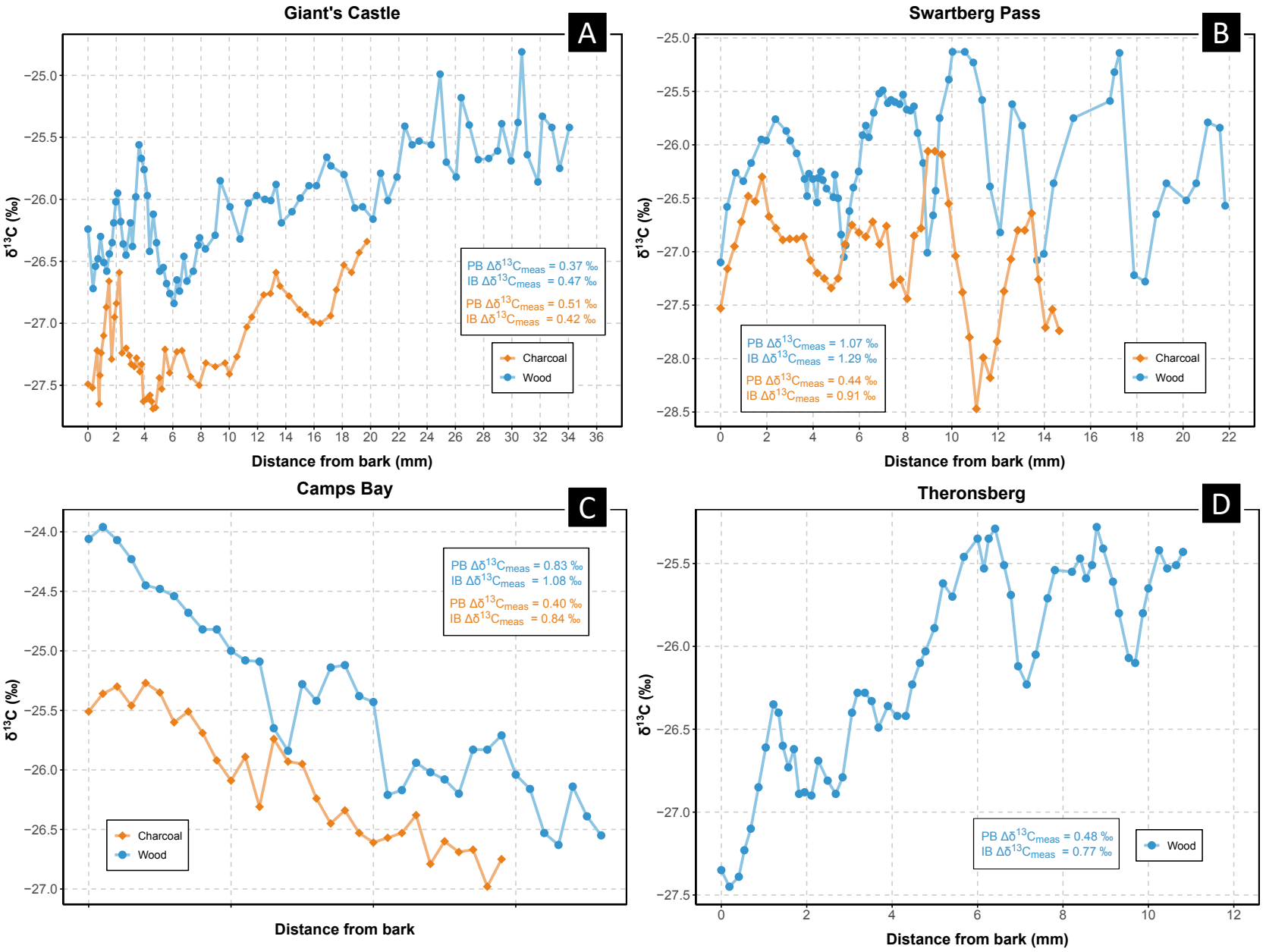

Figure 11. High-resolution $\delta^{13}C$ profiles of modern *Protea* wood and charcoal. **A:** SRZ (GC4); **B:** YRZ (SB); **C:** WRZ (CB); **D:** WRZ (TB2). Wood is in blue and charcoal in orange. Values for isotope boundary (IB) and physical boundary (PB) $\Delta\delta^{13}C_{meas}$ are presented on each plot. Note that the amplitude values for CB and TB2 are not corrected here.

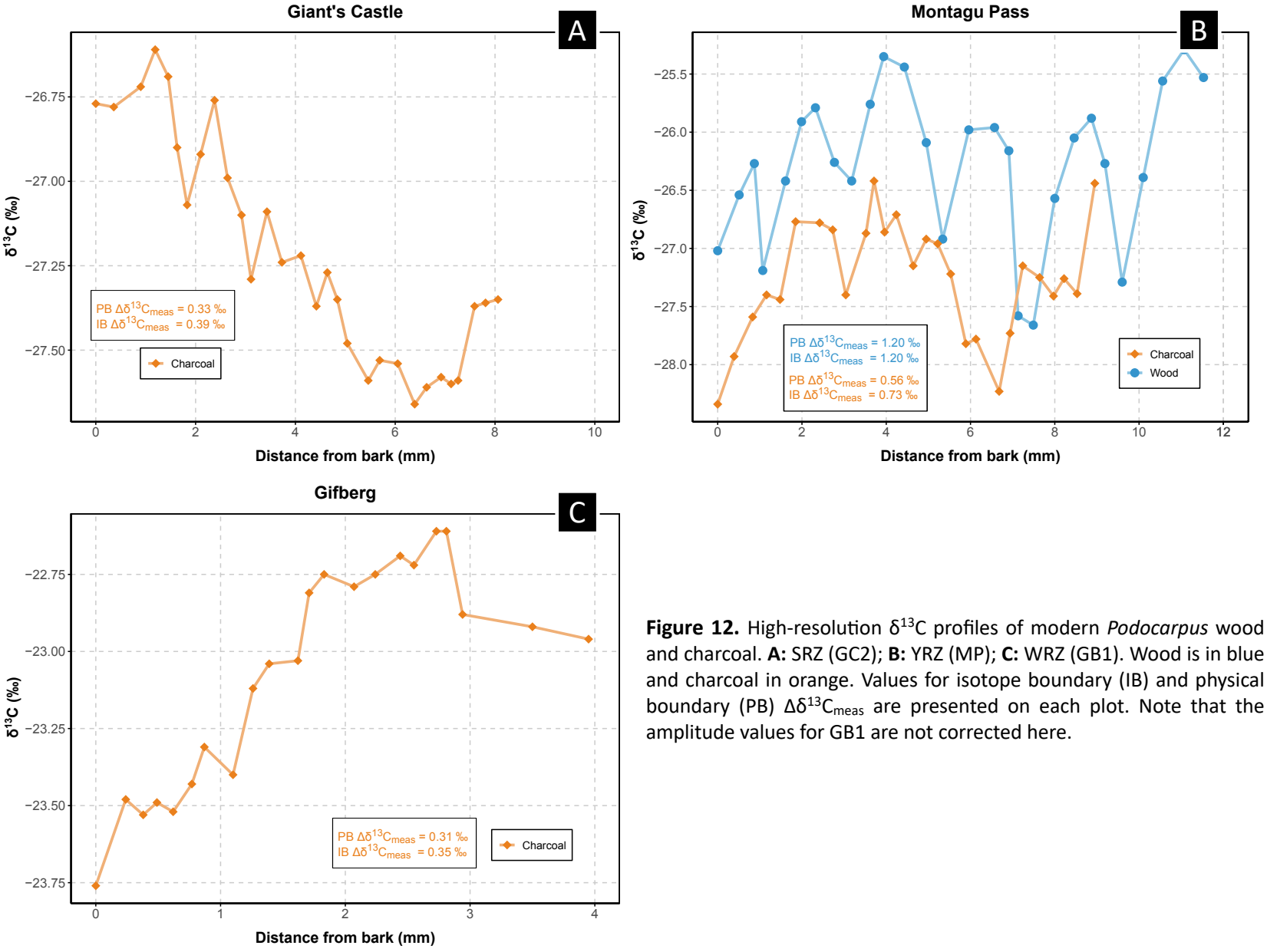

Figure 12. High-resolution $\delta^{13}C$ profiles of modern *Podocarpus* wood and charcoal. **A:** SRZ (GC2); **B:** YRZ (MP); **C:** WRZ (GB1). Wood is in blue and charcoal in orange. Values for isotope boundary (IB) and physical boundary (PB) $\Delta\delta^{13}C_{meas}$ are presented on each plot. Note that the amplitude values for GB1 are not corrected here.

Table 8. Summary of PB $\Delta\delta^{13}C_{meas}$ calculations for each modern wood and charcoal sample, and the applications of the correction equations (Eq. 8 to Eq. 19)

Sample ID	Rainfall Zone	Material	No. of GIs	No. of subsamples used in calculations	Resolution	$\Delta\delta^{13}C_{meas}$ (‰)	Schubert & Jahren Correction (% of $\Delta\delta^{13}C_{max}$)	Schubert & Jahren Correction $\Delta\delta^{13}C_{meas}$ (‰)	Grouped Correction (% of $\Delta\delta^{13}C_{max}$)	Grouped Correction $\Delta\delta^{13}C_{meas}$ (‰)	Sample Correction (% of $\Delta\delta^{13}C_{max}$)	Sample Correction $\Delta\delta^{13}C_{meas}$ (‰)	Genus Correction (% of $\Delta\delta^{13}C_{max}$)	Genus Correction $\Delta\delta^{13}C_{meas}$ (‰)	Winter Correction (% of $\Delta\delta^{13}C_{max}$)	Winter Correction $\Delta\delta^{13}C_{meas}$ (‰)
GC4_w	Summer	Wood	5	36	7.20	0.37	67.18	0.56	59.20	0.64	46.74	0.81	47.05	0.80		
GC4_ch	Summer	Charcoal	4	22	5.50	0.51	59.82	0.86	50.12	1.81	40.27	1.29	41.33	1.25		
GC2_ch	Summer	Charcoal	4	20	5.00	0.33	57.45	0.59	47.23	0.73	54.57	0.61	67.39	0.50		
SB_w	Year-Round	Wood	5	45	9.00	1.07	72.43	1.56	66.36	1.75	72.26	1.59	51.23	2.22		
SB_ch	Year-Round	Charcoal	4	25	6.25	0.44	63.96	0.68	54.96	0.79	46.01	0.94	44.50	0.98		
MP_w	Year-Round	Wood	7	35	5.00	1.20	57.22	2.10	47.02	2.57	80.75	1.49	67.14	1.79		
MP_ch	Year-Round	Charcoal	4	20	5.00	0.56	57.45	0.98	47.23	1.20	53.38	1.04	67.39	0.83		
CB_w	Winter	Wood	5	37	7.40	0.83	66.44	1.22	58.75	1.39	62.43	1.31	46.54	1.74	65.21	1.25
CB_ch	Winter	Charcoal	5	25	5.00	0.40	53.73	0.79	44.01	1.00	55.67	0.74	36.86	1.16	55.03	0.76
TB2_w	Winter	Wood	5	61	12.20	0.48	78.42	0.61	75.18	0.63	77.34	0.62	56.10	0.85	74.06	0.65
GB1_ch	Winter	Charcoal	1	3	3.00	0.31	40.75	0.76	29.99	1.03			49.61	0.62	44.16	0.70
		Mean	4.45	29.91	6.41											

Table 9. Summary of IB $\Delta\delta^{13}C_{meas}$ calculations for each modern wood and charcoal sample, and the applications of the correction equations (Eq. 8 to Eq. 19)

Sample ID	Rainfall Zone	Material	No. of GIs	No. of subsamples used in calculations	Resolution	$\Delta\delta^{13}C_{meas}$ (‰)	Schubert & Jahren Correction (% of $\Delta\delta^{13}C_{max}$)	Schubert & Jahren Correction $\Delta\delta^{13}C_{meas}$ (‰)	Grouped Correction (% of $\Delta\delta^{13}C_{max}$)	Grouped Correction $\Delta\delta^{13}C_{meas}$ (‰)	Sample Correction (% of $\Delta\delta^{13}C_{max}$)	Sample Correction $\Delta\delta^{13}C_{meas}$ (‰)	Genus Correction (% of $\Delta\delta^{13}C_{max}$)	Genus Correction $\Delta\delta^{13}C_{meas}$ (‰)	Winter Correction (% of $\Delta\delta^{13}C_{max}$)	Winter Correction $\Delta\delta^{13}C_{meas}$ (‰)
GC4_w	Summer	Wood	15	80	5.33	0.47	56.70	0.86	47.23	1.07	37.99	1.31	39.09	1.26		
GC4_ch	Summer	Charcoal	7	51	7.29	0.42	64.26	0.69	56.25	0.83	44.47	1.03	44.88	1.00		
GC2_ch	Summer	Charcoal	4	20	5.00	0.39	56.71	0.69	46.59	0.84	54.30	0.72	66.56	0.59		
SB_w	Year-Round	Wood	7	74	10.57	1.29	72.72	1.86	67.69	2.08	73.17	1.89	51.60	2.64		
SB_ch	Year-Round	Charcoal	6	50	8.33	0.91	68.35	1.27	61.87	1.40	48.00	1.82	48.16	1.80		
MP_w	Year-Round	Wood	7	35	5.00	1.20	57.22	2.10	47.02	2.57	80.75	1.49	67.14	1.79		
MP_ch	Year-Round	Charcoal	4	27	6.75	0.73	65.46	1.18	57.01	1.39	55.45	1.34	75.47	1.01		
CB_w	Winter	Wood	4	37	9.25	1.08	67.50	1.51	61.77	1.68	62.17	1.66	47.65	2.15	65.49	1.56
CB_ch	Winter	Charcoal	3	30	10.00	0.84	74.83	1.11	69.72	1.20	66.33	1.26	53.15	1.57	71.54	1.17
TB2_w	Winter	Wood	3	55	18.33	0.77	84.89	0.91	85.65	0.90	83.43	0.92	61.47	1.25	78.46	0.98
GB1_ch	Winter	Charcoal	1	5	5.00	0.35	57.91	0.61	47.59	0.74			67.90	0.52	58.82	0.60
		Mean	5.55	42.18	8.26											

5.2.4. Correcting for Resolution Effects

One hypothesis presented by Schubert and Jahren is that when fewer subsamples are collected within each growth increment, the seasonal amplitude measured within that increment tends to be smoothed, as it us unable to capture the full extent of a seasonal shift. For PB $\Delta\delta^{13}C_{meas,}$ the mean subsampling resolution was 8.16 for wood and 5.35 for charcoal. For IB $\Delta\delta^{13}C_{meas,}$ mean subsampling resolution increased slightly to 9.70 for wood and 7.47 for charcoal. Individually, no modern wood or charcoal samples qualified for correction for subsampling resolution (Tables 8 & 9).

However, resolution effects were still hypothesised to be pronounced in the analysis of the archaeological charcoals. To mitigate these effects, Schubert and Jahren's *Sophora* equation (Eq. 3) and several additional equations (Eq. 8-19) were tested on the modern samples (Tables 8 & 9) to determine and compare their ability to correct $\Delta\delta^{13}C_{meas}$ values. For the group of all modern wood and charcoal samples, each genus, individual samples, and the WRZ, Eq. (3) was refitted in MATLAB based on artificial averaging of the signal. This averaging was done by grouping two, three, and sometimes four successive $\delta^{13}C$ measurements and then evaluating the reduction in $\Delta\delta^{13}C_{meas}$. Each correction equation is presented below:

<u>Grouped Correction</u>

Created using the results from all modern *Protea* and *Podocarpus* samples.

$$\% \Delta\delta^{13}C_{max} = 2027(x - 1) / (100 + 17.59(x - 1)) \quad (8)$$

<u>Genus Correction</u>

Protea and *Podocarpus* results were separated, and a correction equation was created from and then applied back to each genus.

Protea:

$$\% \Delta\delta^{13}C_{max} = 2135(x - 1) / (100 + 28.62(x - 1)) \quad (9)$$

Podocarpus:

$$\% \Delta\delta^{13}C_{max} = 4603(x - 1) / (100 + 42.79(x - 1)) \quad (10)$$

<u>Sample Specific Correction</u>

A specific equation was created for individual samples:

SB_w (Protea):

$$\% \Delta\delta^{13}C_{max} = 2576(x - 1) / (100 + 22.64(x - 1)) \quad (11)$$

SB_ch (Protea):

$$\% \Delta\delta^{13}C_{max} = 3313(x - 1) / (100 + 52.58(x - 1)) \quad (12)$$

GC4_w and GC4_ch (Protea):

$$\% \Delta\delta^{13}C_{max} = 1815(x - 1) / (100 + 22.13(x - 1)) \quad (13)$$

CB_w and CB_ch (Protea):

$$\% \Delta\delta^{13}C_{max} = 6662(x - 1) / (100 + 88.79(x - 1)) \quad (14)$$

TB2_w (Podocarpus):

$$\% \Delta\delta^{13}C_{max} = 3538(x - 1) / (100 + 36.28(x - 1)) \quad (15)$$

MP_w (Podocarpus):

$$\% \Delta\delta^{13}C_{max} = 4391(x - 1) / (100 + 28.72(x - 1)) \quad (16)$$

MP_ch (Podocarpus):

$$\% \Delta\delta^{13}C_{max} = 10420(x - 1) / (100 + 169.5(x - 1)) \quad (17)$$

GC2_ch (Podocarpus):

$$\% \Delta\delta^{13}C_{max} = 12570(x - 1) / (100 + 204.6(x - 1)) \quad (18)$$

Winter Rainfall Correction

Created by grouping all WRZ results:

$$\% \Delta\delta^{13}C_{max} = 4430(x - 1) / (100 + 50.32(x - 1)) \quad (19)$$

In all equations, *x* is the number of subsamples per growth interval.

In addition to Schubert and Jahren's observed subsampling resolution effects, water stress was also considered a qualifier for correction in this study. It is well-documented that environmental stress, such as low water availability, limits tree growth and produces gaps in tree ring archives (e.g. Sarris *et al.* 2013; Vitali *et al.* 2024). It was hypothesised that since water stress affects both tree growth and carbon isotope fractionation, it would potentially affect the seasonal $\delta^{13}C$ signal by limiting stomatal behaviour and tissue production during dry periods. Thus, it was thought that water stress might

induce its own form of resolution effect, similar to the impact of low subsampling resolution, and this was ultimately corrected for.

Samples requiring correction for limited moisture availability were identified using mean $\delta^{13}C$ values. Wood samples with a mean $\delta^{13}C > -25.5$ ‰, and charcoals with a mean $\delta^{13}C > -27$ ‰ (to accommodate depletion in $\delta^{13}C$ with carbonisation) were selected for correction. With a mean $\delta^{13}C$ of -23.17 ‰, the charcoal sample GB1_ch certainly met the correction condition. However, GB1_ch was already excluded based on an insufficient number of growth increments available for calculating $\Delta\delta^{13}C_{meas}$, which is likely attributable to the level of water stress it experienced during its growth, as indicated by both MAP and mean $\delta^{13}C$ (Table 6). The only remaining samples requiring correction for water stress, then, were CB_w and CB_ch. These samples were corrected using five of the correction equations (Eq. 3, 8, 9, 14, and 19). The corrected values for PB and IB $\Delta\delta^{13}C_{meas}$ are shown in Table 8 and 9, respectively.

5.2.5. Comparison with modern climatology

5.2.5.1. Calculating $\Delta\delta^{13}C_{model}$ from rainfall data

For each site, the seasonal change in $\delta^{13}C$ ($\Delta\delta^{13}C_{meas}$) occurring in wood was modelled ($\Delta\delta^{13}C_{model}$) using rainfall data obtained from TerraClim at a ~4 km resolution (Abatzoglou *et al.* 2018) (Appendix 5). The Camps Bay and Swartberg samples were extracted and analysed in 2021, and so records for the years 2015 to 2021 were used. Montagu Pass was extracted in September 2022, Theronsberg and Gifberg in December 2022, and Giant's Castle in January 2023. Thus, rainfall data for the years 2016-2022 were used in these cases. Rainfall data are summarised in Table 10. These data were used to calculate $\Delta\delta^{13}C_{model}$ for each location over the 2015 to 2021 or 2016 to 2022 period.

Table 10. Climate data and data used to calculate $\Delta\delta^{13}$Cmodel, ΔP, and P_S/P_W for each site

Site	Sample ID	Rainfall Zone	MAP (mm)	Average P_S (mm)	Average P_W (mm)	ΔP	P_S/P_W	$\Delta\delta^{13}C_{model}$ (‰)
Giant's Castle	GC4_w GC4_ch GC2_ch	Summer	991.40	838.63	152.77	1.73 ± 0.33	5.92 ± 1.93	0.30 ± 0.27
Swartberg	SB_w SB_ch	Year-Round	254.37	149.53	104.84	0.38 ± 0.29	1.52 ± 0.42	1.40 ± 0.23
Montagu Pass	MP_w MP_ch	Year-Round	379.16	201.46	177.70	0.13 ± 0.14	1.15 ± 0.17	1.61 ± 0.12
Camps Bay	CB_w CB_ch	Winter	438.58	98.30	340.26	-1.24 ± 0.25	0.30 ± 0.08	2.74 ± 0.20
Theornsberg	TB2_w	Winter	293.36	101.56	191.80	-0.63 ± 0.30	0.55 ± 0.17	2.24 ± 0.25
Gifberg	GB1_ch	Winter	163.26	41.04	122.53	-1.10 ± 0.48	0.37 ± 0.18	2.62 ± 0.39

5.2.5.2. *Correlating $\Delta\delta^{13}C_{meas}$ with $\Delta\delta^{13}C_{model}$*

Both PB $\Delta\delta^{13}C_{meas}$ (Tables 11-13) and IB $\Delta\delta^{13}C_{meas}$ (Tables 14-16) were compared with $\Delta\delta^{13}C_{model}$ using a regression analysis to assess the strength of their correlation and whether high-resolution carbon isotopes from wood and charcoal can indeed stand as a proxy for seasonal rainfall averaged over several years. GB1_ch was excluded from the analysis, and only CB_w and CB_ch were corrected. This analysis also enabled the identification of the most suitable correction equation, and provided insight into whether $\Delta\delta^{13}C_{meas}$ calculated from PB or IB aligns more closely with climate data. The correlations for charcoal are stronger for both PB and IB (Table 13 for PB and Table 16 for IB), indicating that the presence of additional non-seasonal variability in the wood sample set, possibly in the form of an outlier. TB2_w is the only wood sample lacking a charcoal counterpart, suggesting this sample is to blame for the lower correlations yielded by the wood amplitudes. Alternative R^2 values for TB2_w corrected and excluded are shown in Table 12 for PB $\Delta\delta^{13}C_{meas}$ and Table 15 for IB $\Delta\delta^{13}C_{meas}$ The possible reason for TB2_w's divergence from rainfall data are discussed in Chapter 6.

Table 11. Physical Boundary (PB) regression analysis for wood and charcoal combined.

Sample ID	Rainfall Zone	Genus	Material	PB Uncorrected $\Delta\delta^{13}C_{meas}$ (‰)	PB Schubert & Jahren Corrected $\Delta\delta^{13}C_{meas}$ (‰)	PB Group Corrected $\Delta\delta^{13}C_{meas}$ (‰)	PB Sample Corrected $\Delta\delta^{13}C_{meas}$ (‰)	PB Genus Corrected $\Delta\delta^{13}C_{meas}$ (‰)	PB Winter Corrected $\Delta\delta^{13}C_{meas}$ (‰)	$\Delta\delta^{13}C_{model}$ (‰)
GC4_w	Summer	*Protea*	Wood	0.37	0.37	0.37	0.37	0.37	0.37	0.30
GC4_ch			Charcoal	0.51	0.51	0.51	0.51	0.51	0.51	0.30
GC2_ch		*Prodocarpus*	Charcoal	0.33	0.33	0.33	0.33	0.33	0.33	0.30
SB_w	Year-Round	*Protea*	Wood	1.07	1.07	1.07	1.07	1.07	1.07	1.40
SB_ch			Charcoal	0.44	0.44	0.44	0.44	0.44	0.44	1.40
MP_w	Year-Round	*Podocarpus*	Wood	1.20	1.20	1.20	1.20	1.20	1.20	1.61
MP_ch			Charcoal	0.56	0.56	0.56	0.56	0.56	0.56	1.61
CB_w	Winter	*Protea*	Wood	0.83	1.22	1.39	1.31	1.74	1.25	2.74
CB_ch			Charcoal	0.40	0.79	1.00	0.74	1.16	0.76	2.74
TB2_w	Winter	*Protea*	Wood	0.48	0.48	0.48	0.48	0.48	0.48	2.24
GB1_ch	Winter	*Podocarpus*	Charcoal	0.31	0.76	1.03		0.62	0.70	2.62
			RSQ	**0.073**	**0.330**	**0.436**	**0.322**	**0.494**	**0.322**	

Table 12. Physical Boundary (PB) regression analysis for wood only. Alternative R^2 values when TB2_w is corrected and excluded are also included

Sample ID	Rainfall Zone	Genus	PB Uncorrected $\Delta\delta^{13}C_{meas}$ (‰)	PB Schubert & Jahren Corrected $\Delta\delta^{13}C_{meas}$ (‰)	PB Group Corrected $\Delta\delta^{13}C_{meas}$ (‰)	PB Sample Corrected $\Delta\delta^{13}C_{meas}$ (‰)	PB Genus Corrected $\Delta\delta^{13}C_{meas}$ (‰)	PB Winter Corrected $\Delta\delta^{13}C_{meas}$ (‰)	$\Delta\delta^{13}C_{model}$ (‰)
GC4_w	Summer	*Protea*	0.37	0.37	0.37	0.37	0.37	0.37	0.30
SB_w	Year-Round	*Protea*	1.07	1.07	1.07	1.07	1.07	1.07	1.40
MP_w		*Podocarpus*	1.20	1.20	1.20	1.20	1.20	1.20	1.61
CB_w	Winter	*Protea*	0.83	1.22	1.39	1.31	1.74	1.25	2.74
TB2_w		*Protea*	0.48	0.48	0.48	0.48	0.48	0.48	2.24
		RSQ	**0.065**	**0.253**	**0.321**	**0.291**	**0.409**	**0.266**	
	TB2_w corrected		0.48	0.61	0.63	0.62	0.85	0.65	
		RSQ	**0.065**	**0.351**	**0.442**	**0.402**	**0.693**	**0.400**	
	TB2_w excluded	**RSQ**	**0.268**	**0.751**	**0.884**	**0.829**	**0.992**	**0.779**	

Table 13. Physical Boundary (PB) regression analysis for charcoal only

Sample ID	Rainfall Zone	Genus	PB Uncorrected $\Delta\delta^{13}C_{meas}$ (‰)	PB Schubert & Jahren Corrected $\Delta\delta^{13}C_{meas}$ (‰)	PB Group Corrected $\Delta\delta^{13}C_{meas}$ (‰)	PB Sample Corrected $\Delta\delta^{13}C_{meas}$ (‰)	PB Genus Corrected $\Delta\delta^{13}C_{meas}$ (‰)	PB Winter Corrected $\Delta\delta^{13}C_{meas}$ (‰)	$\Delta\delta^{13}C_{model}$ (‰)
GC4_ch	Summer	*Protea*	0.51	0.51	0.51	0.51	0.51	0.51	0.30
GC42_ch		*Podocarpus*	0.33	0.33	0.33	0.33	0.33	0.33	0.30
SB_ch	Year-Round	*Protea*	0.44	0.44	0.44	0.44	0.44	0.44	1.40
MP_ch		*Podocarpus*	0.56	0.56	0.56	0.56	0.56	0.56	1.61
CB_ch	Winter	*Protea*	0.40	0.79	1.00	0.74	1.16	0.76	2.74
		RSQ	**0.003**	**0.723**	**0.742**	**0.702**	**0.735**	**0.712**	

Table 14. Isotope Boundary (IB) regression analysis for wood and charcoal combined

Sample ID	Rainfall Zone	Genus	Material	IB Uncorrected $\Delta\delta^{13}C_{meas}$ (‰)	IB Schubert & Jahren Corrected $\Delta\delta^{13}C_{meas}$ (‰)	IB Group Corrected $\Delta\delta^{13}C_{meas}$ (‰)	IB Sample Corrected $\Delta\delta^{13}C_{meas}$ (‰)	IB Genus Corrected $\Delta\delta^{13}C_{meas}$ (‰)	IB Winter Corrected $\Delta\delta^{13}C_{meas}$ (‰)	$\Delta\delta^{13}C_{model}$ (‰)
GC4_w	Summer	*Protea*	Wood	0.47	0.47	0.47	0.47	0.47	0.47	0.30
GC4_ch			Charcoal	0.42	0.42	0.42	0.42	0.42	0.42	0.30
GC2_ch		*Prodocarpus*	Charcoal	0.39	0.39	0.39	0.39	0.39	0.39	0.30
SB_w	Year-Round	*Protea*	Wood	1.29	1.29	1.29	1.29	1.29	1.29	1.40
SB_ch			Charcoal	0.91	0.91	0.91	0.91	0.91	0.91	1.40
MP_w	Year-Round	*Podocarpus*	Wood	1.20	1.20	1.20	1.20	1.20	1.20	1.61
MP_ch			Charcoal	0.73	0.73	0.73	0.73	0.73	0.73	1.61
CB_w	Winter	*Protea*	Wood	1.08	1.51	1.68	1.66	2.15	1.56	2.74
CB_ch			Charcoal	0.84	1.11	1.20	1.26	1.57	1.17	2.74
TB2_w	Winter	*Protea*	Wood	0.77	0.77	0.77	0.77	0.77	0.77	2.24
GB1_ch	Winter	*Podocarpus*	Charcoal	0.35	0.61	0.74		0.52	0.60	2.62
			RSQ	**0.386**	**0.612**	**0.645**	**0.665**	**0.692**	**0.636**	

Table 15. Isotope Boundary (IB) regression analysis for wood only. Alternative R^2 values when TB2_w is corrected and excluded are also included

Sample ID	Rainfall Zone	Genus	PB Uncorrected $\Delta\delta^{13}C_{meas}$ (‰)	PB Schubert & Jahren Corrected $\Delta\delta^{13}C_{meas}$ (‰)	PB Group Corrected $\Delta\delta^{13}C_{meas}$ (‰)	PB Sample Corrected $\Delta\delta^{13}C_{meas}$ (‰)	PB Genus Corrected $\Delta\delta^{13}C_{meas}$ (‰)	PB Winter Corrected $\Delta\delta^{13}C_{meas}$ (‰)	$\Delta\delta^{13}C_{model}$ (‰)
GC4_w	Summer	*Protea*	0.47	0.47	0.47	0.47	0.47	0.47	0.30
SB_w	Year-Round	*Protea*	1.29	1.29	1.29	1.29	1.29	1.29	1.40
MP_w		*Podocarpus*	1.20	1.20	1.20	1.20	1.20	1.20	1.61
CB_w	Winter	*Protea*	1.08	1.51	1.68	1.66	2.15	1.56	2.74
TB2_w		*Protea*	0.77	0.77	0.77	0.77	0.77	0.77	2.24
		RSQ	**0.221**	**0.459**	**0.504**	**0.500**	**0.548**	**0.475**	
	TB2_w corrected			0.91	0.90	0.92	1.25	0.98	
		RSQ	**0.221**	**0.584**	**0.615**	**0.629**	**0.844**	**0.660**	
	TB2_w excluded	**RSQ**	**0.430**	**0.862**	**0.934**	**0.928**	**0.979**	**0.888**	

Table 16. Isotope Boundary (IB) regression analysis for charcoal only

Sample ID	Rainfall Zone	Genus	PB Uncorrected $\Delta\delta^{13}C_{meas}$ (‰)	PB Schubert & Jahren Corrected $\Delta\delta^{13}C_{meas}$ (‰)	PB Group Corrected $\Delta\delta^{13}C_{meas}$ (‰)	PB Sample Corrected $\Delta\delta^{13}C_{meas}$ (‰)	PB Genus Corrected $\Delta\delta^{13}C_{meas}$ (‰)	PB Winter Corrected $\Delta\delta^{13}C_{meas}$ (‰)	$\Delta\delta^{13}C_{model}$ (‰)
GC4_ch	Summer	*Protea*	0.42	0.42	0.42	0.42	0.42	0.42	0.30
GC42_ch		*Podocarpus*	0.39	0.39	0.39	0.39	0.39	0.39	0.30
SB_ch	Year-Round	*Protea*	0.91	0.91	0.91	0.91	0.91	0.91	1.40
MP_ch		*Podocarpus*	0.73	0.73	0.73	0.73	0.73	0.73	1.61
CB_ch	Winter	*Protea*	0.84	1.11	1.20	1.26	1.57	1.17	2.74
		RSQ	**0.692**	**0.910**	**0.932**	**0.938**	**0.926**	**0.926**	

5.2.5.3. Calculating ΔP and P_S/P_W from rainfall data

The rainfall data were further used to calculate seasonal changes in rainfall (ΔP) (Eq. 5) and the ratio of summer to winter rainfall (P_S/P_W) for each location over the 2015 to 2021 or 2016 to 2022 period (Table 10). These values are presented in Table 10. The SRZ site had the highest values for ΔP and P_S/P_W, the WRZ had lowest, and the YRZ yielded intermediate values.

5.2.5.4. Calculating ΔP and P_S/P_W from PB and IB $\Delta\delta^{13}C_{meas}$

Using Eq. (6) and Eq. (7), the seasonal changes in rainfall (ΔP) and the ratio of summer to winter rainfall (P_S/P_W) could be calculated from the $\delta^{13}C$ results obtained from the modern wood and charcoal samples. The Genus and Group Corrections were used for CB_w and CB_ch as these equations produced consistently strong correlations for wood and charcoal across PB and IB. These results are presented in Table 17. The implications of these values are discussed in Chapter 6.

Table 17. Values for ΔP and P_S/P_W calculated from PB and IB $\Delta\delta^{13}C_{meas}$.

Site	Sample ID	Rainfall Zone	PB $\Delta\delta^{13}C_{meas}$(‰)	PB ΔP	PB P_S/P_W	IB $\Delta\delta^{13}C_{meas}$(‰)	IB ΔP	IB P_S/P_W
Giant's Castle	GC4_w	Summer	0.37	1.65 ± 0.20	5.29 ± 1.08	0.47	1.52 ± 0.31	4.75 ± 1.24
	GC4_ch		0.51	1.48 ± 0.21	4.47 ± 0.94	0.42	1.58 ± 0.21	4.96 ± 1.00
	GC2_ch		0.33	1.69 ± 0.17	5.49 ± 0.84	0.39	1.62 ± 0.15	5.07 ± 0.74
Swartberg	SB_w	Year-Round	1.07	0.80 ± 0.97	3.09 ± 2.51	1.29	0.52 ± 0.64	1.99 ± 1.16
	SB_ch		0.44	1.57 ± 0.24	4.90 ± 1.15	0.91	0.98 ± 0.96	3.49 ± 2.06
Montagu Pass	MP_w	Year-Round	1.20	0.63 ± 0.47	2.06 ± 0.99	1.20	0.63 ± 0.47	2.06 ± 0.99
	MP_ch		0.56	1.42 ± 0.34	4.31 ± 1.38	0.73	1.20 ± 0.53	3.68 ± 1.77
Theornsberg	TB2_w	Winter	0.48	0.51 ± 0.45	4.88 ± 1.93	0.77	1.16 ± 0.25	3.26 ± 0.84
Grouped Correction								
Camps Bay	CB_w	Winter	1.39	0.41 ± 0.64	1.77 ± 1.16	1.68	0.05 ± 0.60	1.19 ± 0.62
	CB_ch		1.00	0.88 ± 0.49	2.62 ± 1.02	1.20	0.64 ± 0.32	1.96 ± 0.68
Genus Correction								
Camps Bay	CB_w	Winter	1.74	-0.03 ± 0.80	1.27 ± 1.14	2.15	-0.52 ± 0.92	0.77 ± 0.53
	CB_ch		1.16	0.69 ± 0.50	2.16 ± 0.83	1.57	0.19 ± 0.44	1.29 ± 0.61

5.3. Archaeological Charcoal Analysis

Five archaeological charcoal specimens were analysed: three Proteaceae (Figure 14) and two Podocarpaceae (Figure 13). Thus, the archaeological families analysed are consistent with those tested in the modern calibration. This meant that the modern results could be used as analogues to better understand the archaeological results, based on the uniformitarian assumption that the physiological behaviours of these taxa have remained unchanged over deep time.

5.3.1. Microscopic analysis of archaeological charcoals

The archaeological charcoal specimens were fragile and irregularly shaped (Figure 13 and 14). Special care was taken to assess the charcoals under a microscope in order to identify on each specimen the transverse surface which would serve as the site for subsampling. Transverse surfaces of Proteaceae were easier to identify compared to Podocarpaceae due to clear anatomical features such as xylem vessels and rays (Figure 14). Xylem tracheids and the earlywood/latewood boundaries that characterise gymnosperm growth surfaces were harder to identify, but were nonetheless identified in the Podocarpaceae specimens (Figure 13).

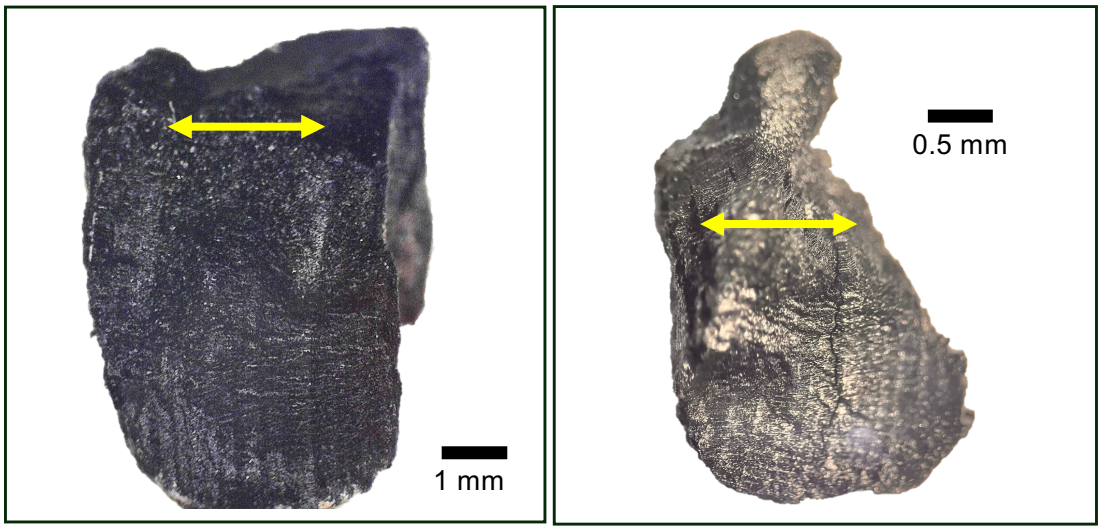

Figure 13. The transverse surfaces of the archaeological Podocarpaceae charcoal from Waterfall Bluff. **Right:** WB_A; **Left:** WB_B. Yellow arrow indicates direction of growth.

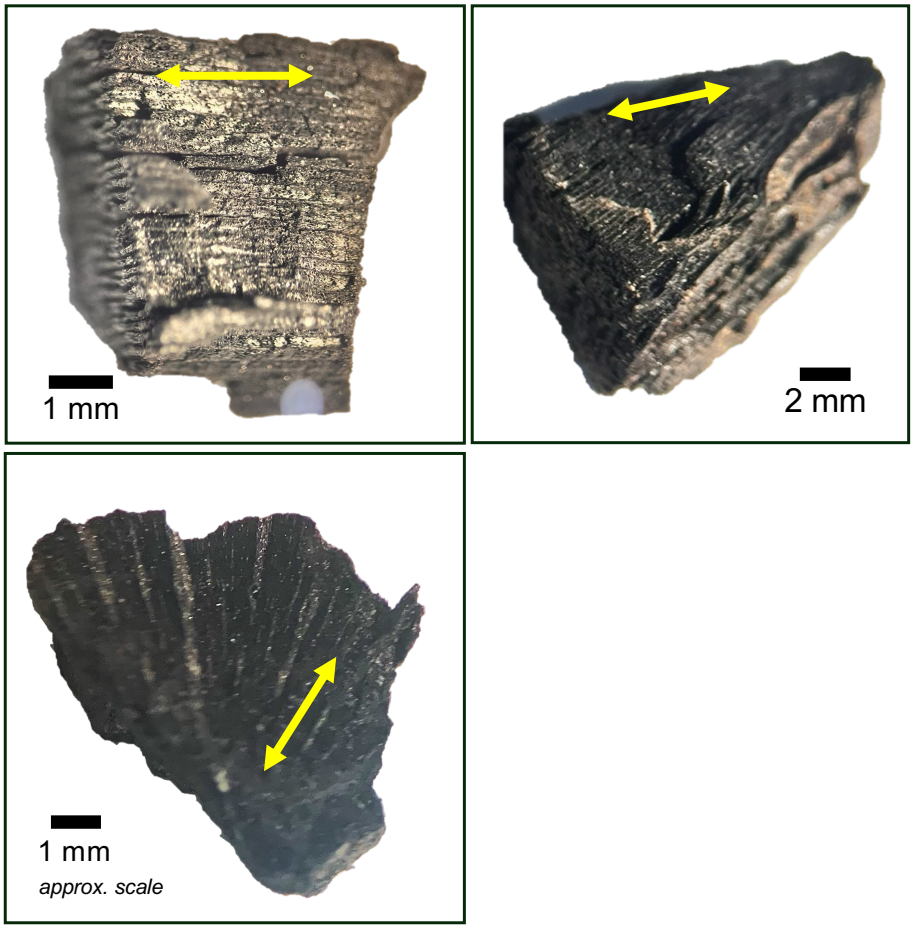

Figure 14. The transverse surfaces of the archaeological Proteaceae charcoal from Boomplaas Cave. Top left: BPA4.21; **Top right:** BPA4_24; **Bottom left:** BPA2.21. Yellow arrow indicates direction of growth.

5.3.2. General isotope results and subsampling resolution

A total of 78 $\delta^{13}C$ measurements were obtained from the five archaeological charcoal samples. The greatest number of subsamples was taken from the BPA4_21 (n = 29), and the fewest from WB_B (n = 8) (Table 18). The average number of subsamples was 15.60 $\delta^{13}C$ measurements per charcoal sample. Mean, maximum, and minimum $\delta^{13}C$ are also reported in Table 18 to provide an overview of the isotopic variability within and between archaeological samples.

Table 18. General isotope results for each archaeological sample

Sample ID	Site	Family	Layer and Age (cal. BP)	Transverse Length (mm)	No. of $\delta^{13}C$ measurements	No. of $\delta^{13}C$ measurements per millimetre	Max. $\delta^{13}C$ (‰)	Min. $\delta^{13}C$ (‰)	Mean $\delta^{13}C$ (‰)	Range (Max - Min) (‰)
BPA2_21	Boomplaas Cave	Proteaceae	GWA (21 920–21 410)	4.32	17	3.94	-24.18	-25.05	-24.64	0.87
BPA4_21			LPC (26 100–24 300)	3.82	10	2.62	-23.99	-24.39	-24.19	0.40
BPA4_24			LPC (26 100–24 300)	11.89	29	2.44	-23.84	-25.16	-24.55	1.32
WB_A	Waterfall Bluff	Podocarpaceae	LBCS Chopi (18 080-17 260 to 15 050-14 380)	4.74	14	2.95	-22.72	-23.24	-22.98	0.52
WB_B				2.26	8	3.54	-22.27	-23.18	-22.75	0.91
			Mean	5.41	15.60	3.10				

The mean $\delta^{13}C$ values recorded in the archaeological charcoals are evidently more positive than the modern charcoals. T-tests found statistically significant differences in mean $\delta^{13}C$ between modern *Protea* and archaeological Proteaceae charcoal (two-tailed: t = -7.92, p = 0.010), and between modern *Podocarpus* and archaeological Podocarpaceae charcoal (two-tailed: t = -20.33, p = 0.022). Additionally, a statistically significant difference in mean $\delta^{13}C$ was also observed between archaeological Proteaceae and Podocarpaceae specimens (two-tailed: t = -8.90, p = 0.003).

Assuming depletion with carbonisation similarly occurred in the past, it is likely that the original wood from which archaeological specimens derived had mean $\delta^{13}C$ values that were even more positive. This enrichment in woody plant $\delta^{13}C$ observed in archaeological materials can be attributed to the variations in $\delta^{13}C_{CO2}$ and the lower concentration of atmospheric CO_2 in the past compared to today. These changes altered carbon isotope discrimination ($\Delta^{13}C$), ultimately leading to more positive $\delta^{13}C$ values (Schubert & Jahren 2012; Hare *et al.* 2018). Determining the archaeological samples needing correction for water stress hinges on mean $\delta^{13}C$ values which cannot be evaluated and compared with modern values without adjustment for changing CO_2 concentrations. These adjustments are addressed below in Section 5.2.4 which discusses corrections for resolution effects.

A significant correlation was found between transverse length and the total number of $\delta^{13}C$ measurements obtained (R^2 = 0.928, p = 0.008). However, as with the modern samples, there appeared to be no significant relationship between transverse length and the number of $\delta^{13}C$ measurements per millimetre (R^2 = 0.368, p = 0.278) which is not surprising considering the material of analysis. Archaeological charcoal is fragile and prone to crumbling. This was especially true for the Proteaceae samples, each of which experienced some kind of breakage during the subsampling process. For example, at approximately 4 mm into subsampling BPA4_4, a large segment of the sample crumbled and could not be subsampled further due to significant mixing. This meant that approximately 3 mm of the transverse surface was lost. A similar issue occurred in subsampling BPA2_21, hence the presence of gaps in the plotted $\delta^{13}C$ series of these samples (Figure 15A&C). It also explains why these samples yielded such a low number of $\delta^{13}C$ measurements per millimetre (Table 18). Only 2.44 subsamples per millimetre – the lowest recorded among the archaeological samples – was calculated for BPA4_4, despite is being the largest fragment analysed.

5.3.3. SPP Archaeological Isotope Results

A rise and fall $\delta^{13}C$ pattern was observed across all five archaeological samples (Figure 15 & 16). Two elements of this analysis are essential to highlight. Firstly, growth increment boundaries could not be

physically identified with precision or certainty and were instead placed isotopically by locating maxima and minima along a given $\delta^{13}C$ series. Consequently, $\Delta\delta^{13}C_{meas}$ in this context refers only to the seasonal amplitude calculated according to isotopic growth increment boundaries (IB). Secondly, and most importantly, though the transverse surface and axis of growth were identifiable under a microscope, which end had derived from wood closer to the pith (older) or closer to the bark (younger) was unknown. This meant that there were essentially two ways to read the plots, each making different assumption about the relative age of each subsample: from left (older) to right (younger), or from right (older) to left (younger). For this analysis, $\Delta\delta^{13}C_{meas}$ was calculated as the average of both possible directions of growth. Table 19 presents the summarised results of the intra-increment analysis conducted on the archaeological charcoals to calculate $\Delta\delta^{13}C_{meas}$.

The greatest value for $\Delta\delta^{13}C_{meas}$ was calculated for BPA4_24 at 0.70 ‰ ± 0.28 ‰, which also achieved the highest subsampling resolution (4.78 subsamplers per growth increment). Both the lowest resolution (3.43 subsamples per growth increment) and seasonal amplitude (0.24 ‰ ± 0.09 ‰) were observed in WB_A. Across all five samples, the average number of subsamples per growth increment was 3.80 (Table 19).

Table 19. Archaeological charcoal $\Delta\delta^{13}C_{meas}$ and corrected $\Delta\delta^{13}C_{meas}$ (Group & Genus Corrections)

Sample ID	Site	Modern Rainfall Zone	No. of GIs	No. of subsamples used in calculations	Average no. of subsamples per GI	$\Delta\delta^{13}C_{meas}$ (‰)	Grouped Correction (% of $\Delta\delta^{13}C_{max}$)	Grouped Correction $\Delta\delta^{13}C_{meas}$ (‰)	Genus Correction (% of $\Delta\delta^{13}C_{max}$)	Genus Correction $\Delta\delta^{13}C_{meas}$ (‰)
BPA2_21	Boomplaas Cave	Year-Round	4.00	14.00	3.50	0.44	34.64	1.27	30.56	1.44
BPA4_21	Boomplaas Cave	Year-Round	2.50	9.00	3.60	0.27	35.88	0.77	31.54	0.87
BPA4_24	Boomplaas Cave	Year-Round	4.50	21.50	4.78	0.70	45.03	1.62	37.89	1.89
WB_A	Waterfall Bluff	Summer	3.50	12.00	3.43	0.24	33.91	0.74	53.77	0.46
WB_B	Waterfall Bluff	Summer	2.00	7.00	3.67	0.50	35.86	1.42	55.70	0.90
		Mean	3.30	12.70	3.80					

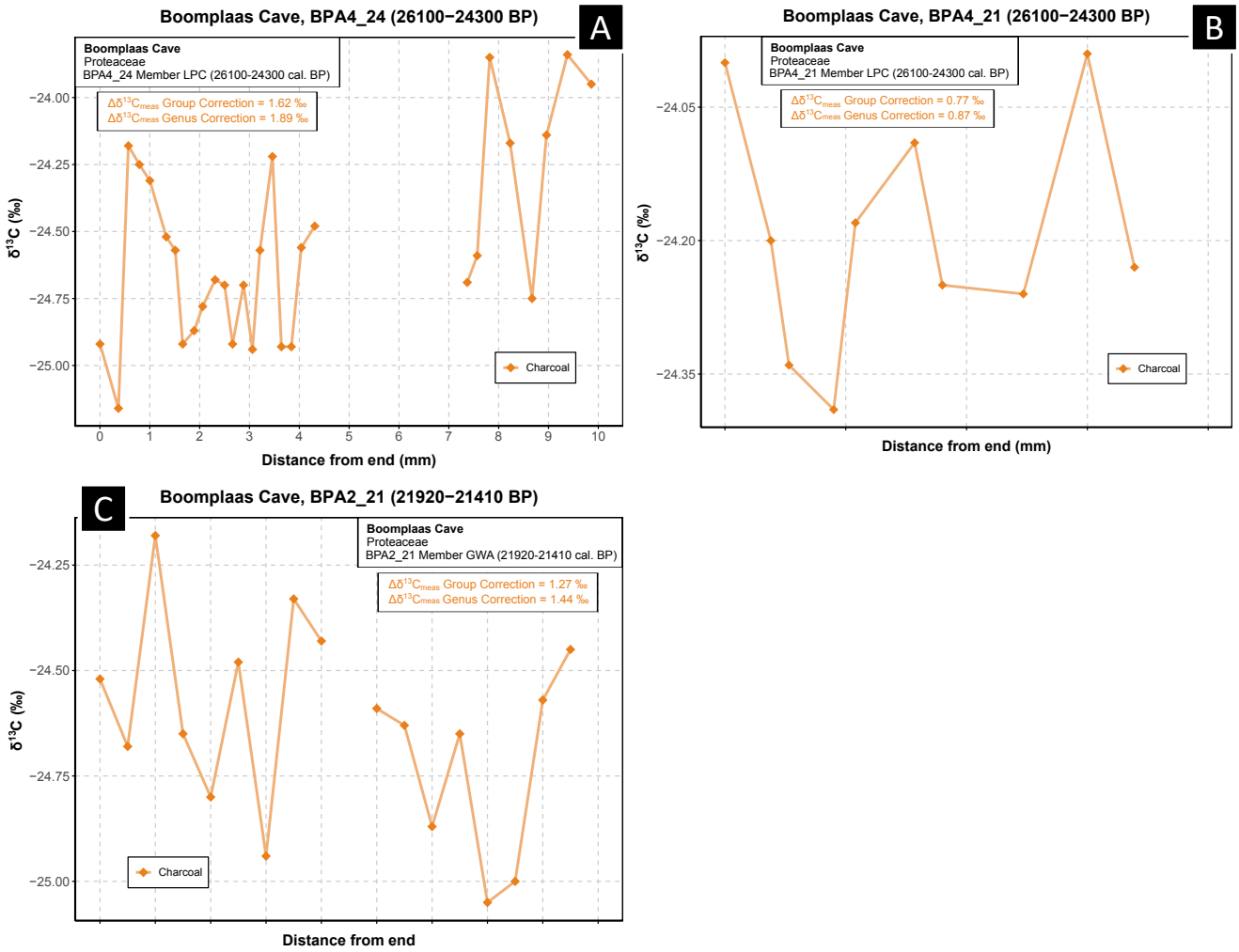

Figure 15. High-resolution $\delta^{13}C$ profiles of LGM archaeological Proteaceae specimens from Boomplaas Cave. **A:** BPA4_24 (Member LPC); **B:** BPA4_21 (Member LPC) **C:** BPA2_21 (Member GWA). Corrected $\Delta\delta^{13}C_{meas}$ values presented on each plot. These were corrected using the Group and Genus Corrections. Stratigraphic and age information is presented on each plot for each specimen.

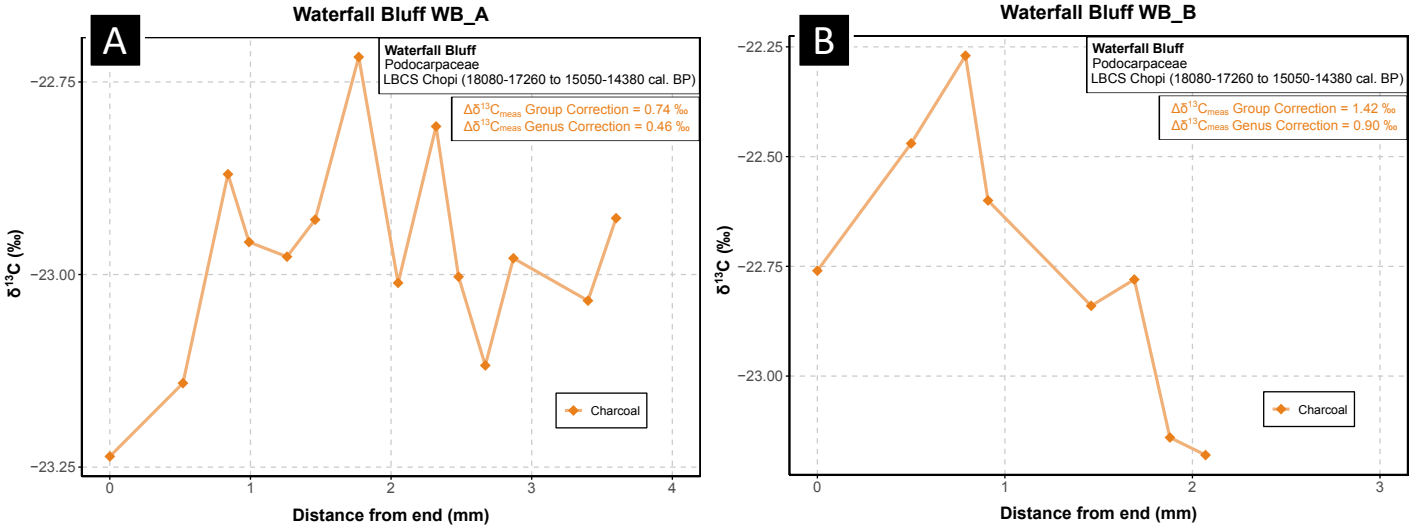

Figure 16. High-resolution $\delta^{13}C$ profiles of LGIT archaeological Podocarpaceae specimens from Waterfall Bluff. **A:** WB_A; **B:** WB_B. Both from LBCS Chopi. Corrected $\Delta\delta^{13}C_{meas}$ values presented on each plot. These were corrected using the Group and Genus Corrections. Stratigraphic and age information is presented on each plot for each specimen.

5.3.4. Correcting for Resolution Effects

With the highest subsampling resolution measured at just 4.78 subsamples per growth increment (Table 19), all five archaeological specimens met the condition for correction. $\Delta\delta^{13}C_{meas}$ was corrected using both the Grouped Correction (Eq. 8) and the Genus Correction (Eq. 9 and Eq. 10) (Table 19), which produced the most promising results in the modern wood and charcoal analysis. Corrected $\Delta\delta^{13}C_{meas}$ values increased proportionally, with BPA4_24 maintaining the highest seasonal amplitude (Grouped Correction = 1.62 ‰ ± 0.71 ‰; Genus Correction = 1.89 ‰ ± 0.81 ‰) and WB_A the lowest (Grouped Correction = 0.74 ‰ ± 0.30 ‰; Genus Correction = 0.46 ‰ ± 0.18 ‰).

The rise in atmospheric CO_2 between the Last Glacial and the onset of the Holocene is associated with a depletion in plant $\delta^{13}C$ of approximately -1.4 ‰ for gymnosperms, and approximately -0.5 ‰ for angiosperms (Hare *et al.* 2018). An additional -1 to -2 ‰ depletion has been linked to rising CO_2 as a consequence of anthropogenic activity and greenhouse gas emissions (Hare *et al.* 2018). However, it is important to note that adjusting archaeological results for changing CO_2 concentrations is unnecessary when hoping to calculate amplitudes of seasonality as these depend on relative carbon isotope changes during tree growth as opposed to absolute $\delta^{13}C$ values. This is arguably a key benefit of the SPP when applied to the archaeological and geological record. Nevertheless, determining the archaeological samples needing correction for water stress hinges on mean $\delta^{13}C$ values which cannot be evaluated and compared with modern values without adjustment for changing CO_2 concentrations.

Mean $\delta^{13}C$ for each sample was therefore adjusted for postglacial and anthropogenic post-industrial CO_2 increase. For the postglacial CO_2 rise, -1.4 ‰ was removed from mean $\delta^{13}C$ of the Podocarpaceae samples (gymnosperm), and -0.5 ‰ from the Proteaceae samples (angiosperm) (Hare *et al.* 2018). An additional -1.50 ‰ (as an intermediate value between -1 and -2 ‰) was subtracted to account for the anthropogenic CO_2 rise. Based upon this estimate, the Proteaceae samples are adjusted by -2.0 ‰, and the Podocarpaceae by -2.90 ‰. These adjusted values are listed in Table 20. All values are more positive than -27 ‰, meaning that each archaeological specimen required correction for water stress effects, as per the threshold established with the modern samples.

Table 20. Archaeological charcoal maximum, minimum, and mean $\delta^{13}C$ adjusted for rising CO_2 levels

Sample ID	Site	Family	Layer and Age (cal. BP)	CO_2 Adjustment Value (‰)	Adjusted Max. $\delta^{13}C$ (‰)	Adjusted Min. $\delta^{13}C$ (‰)	Adjusted Mean $\delta^{13}C$ (‰)	Range (Max - Min) (‰)
BPA2_21	Boomplaas Cave	Proteaceae	GWA (21 920–21 410)	-2.00	-26.18	-27.05	-26.64	0.87
BPA4_21			LPC (26 100–24 300)	-2.00	-25.99	-26.39	-26.19	0.40
BPA4_24			LPC (26 100–24 300)	-2.00	-25.84	-27.16	-26.55	1.32
WB_A	Waterfall Bluff	Podocarpaceae	LBCS Chopi (18 080-17	-2.90	-25.62	-26.14	-25.88	0.52
WB_B			260 to 15 050-14 380)	-2.90	-25.17	-26.08	-25.65	0.91

5.3.5. Calculating ΔP and P_S/P_W from archaeological $\Delta\delta^{13}C_{meas}$

Once corrected, Eq. (6) and Eq. (7) were used to calculate ΔP and P_S/P_W from the measured seasonal amplitudes of each sample (Table 21). This was done for both the $\Delta\delta^{13}C_{meas}$ values corrected using the Grouped Correction and the Genus Correction.

Table 21. Values for ΔP and P_S/P_W calculated from $\Delta\delta^{13}C_{meas}$ of the archaeological charcoals.

Sample ID	Family	Group Correction			Genus Correction		
		$\Delta\delta^{13}C_{meas}$ (‰)	ΔP	P_S/P_W	$\Delta\delta^{13}C_{meas}$ (‰)	ΔP	P_S/P_W
BPA2_21	Proteaceae	1.27	0.55	1.73	1.44	0.34	1.41
BPA4_21	Proteaceae	0.77	1.16	3.19	0.87	1.04	2.82
BPA4_24	Proteaceae	1.62	0.13	1.65	1.89	-0.21	0.81
WB_A	Podocarpaceae	0.74	1.20	3.30	0.46	1.54	4.65
WB_B	Podocarpaceae	1.42	0.37	1.44	0.90	1.00	2.72

5.4. Summary of results

This Chapter has reported the results of the high-resolution carbon isotope analysis of modern wood and charcoal samples from across South Africa's three rainfall zones, as well as the results of the archaeological analysis. Table 22 revisits the five key dimensions of analysis outlined in this Chapter's Introduction (Table 4 in Section 5.1) and summarises the key findings pertaining to the effect each dimension was found to have on measured seasonal amplitudes among the modern samples.

The findings of the modern calibration (Table 22) allow the archaeological seasonal amplitudes to be interpreted with greater confidence. A cyclical rise and fall $\delta^{13}C$ pattern was identified across all five archaeological samples. Subsampling resolution was lower in archaeological samples relative to modern samples, and so all archaeological charcoals qualified for correction for subsampling resolution effects. Additionally, the archaeological $\delta^{13}C$ results were adjusted to reflect the $\delta^{13}C$ depletion observed in C3 plants due to rising atmospheric CO_2 concentrations since the Last Glacial period, further accelerated by anthropogenic greenhouse gas emissions. This showed that all five specimens required correction for water stress effects. The $\Delta\delta^{13}C_{meas}$ values measured in the archaeological charcoals were used to calculate ΔP and P_S/P_W which, ultimately, help to determine whether the charcoals reflect a seasonal climate dominated by a greater proportion of either summer or winter rainfall. The implications of the ΔP and P_S/P_W values calculated from the archaeological, as well as modern, samples are explored more closely in Chapter 6.

Table 22. Key findings of the effect of each dimension of analysis on modern seasonal amplitudes

Factor	Expected Effect	Observed Effect
Rainfall Zone	Highest measured amplitudes for WRZ, lowest for SRZ, intermediate for YRZ.	When samples are considered in rainfall zone groups (Table 8 and 9): SRZ samples yielded the lowest amplitudes (W: 0.37-0.47 ‰; Ch: 0.33-0.51 ‰). With GB1_ch excluded due to low moisture availability, CB corrected, and TB2 a potential outlier, WRZ samples yielded the highest amplitudes (W: 1.39-2.15 ‰; Ch: 1.00-1.57 ‰). YRZ samples yielded amplitudes falling between the SRZ and WRZ (W: 1.07-1.29 ‰; Ch: 0.44-0.91 ‰).
Material	Offset between wood and charcoal due to shrinkage and $\delta^{13}C$ depletion with carbonisation.	During carbonisation, wood shrinks in length between approx. 12 and 25 % (Table 3 in Section 4.3.3.), and mean $\delta^{13}C$ is depleted by approx. 0.90 ‰ (Table 7). In all cases but PB $\Delta\delta^{13}C_{meas}$ of GC4_ch, wood amplitudes were greater than their charcoal counterparts by an average of 0.55 ‰ for PB Group, 0.62 ‰ for PB Genus, 0.33 ‰ for IB Group, and 0.37 ‰ for IB Genus. Despite this offset, charcoal amplitudes correlate strongly with rainfall data (Table 8 and 9).
Genus	No significant difference between *Protea* and *Podocarpus* from each rainfall zone.	No significant difference in mean $\delta^{13}C$ was observed between modern *Protea* and *Podocarpus* wood nor charcoal. Moreover, both *Protea* and *Podocarpus* amplitudes fall within range of what is expected for their respective rainfall zones, insofar as CB_w and CB_ch are corrected for water stress resolution effects, G1_ch excluded, and TB2_w is considered an outlier. Together, *Protea* and *Podocarpus* wood and charcoal amplitudes correlate with seasonal rainfall data (Table 13 and Table 16).
Resolution	Stronger climate correlations in samples with higher subsampling resolutions.	TB2_w achieved the highest subsampling resolution of all samples, yet yielded PB and IB amplitudes that diverge most substantially from what is expected for a WRZ (Table 8 & 9). This may not mean that higher amplitudes are not linked to greater climate correlations, but rather indicates that there are additional physiological factors at play in this sample. From the results, the true impact of subsampling resolution on $\Delta\delta^{13}C_{meas}$ cannot be confirmed yet, and this will be addressed in Chapter 6 and 7.
Growth Increment Demarcations	Isotope boundaries correlate with climate just as strongly as physical boundaries do.	Modern *Podocarpus* has clearly identifiable growth rings, while the diffuse-porous nature of modern *Protea* make it challenging to situate growth rings with certainty. Nevertheless, for both wood and charcoal, IB amplitudes actually demonstrate stronger correlations with rainfall data than do PB amplitudes (Tables 11-16). This indicates that both approaches are viable options when applying the SPP to South African taxa. IB $\Delta\delta^{13}C_{meas}$ can confidently be used as a reliable alternative to PB $\Delta\delta^{13}C_{meas}$ in situations where physical boundaries are absent.

CHAPTER 6

Discussion

6.1. Introduction

This Chapter presents a more detailed discussion and analysis of the modern and archaeological applications of the SPP. Analysing fifteen $\delta^{13}C$ profiles of evergreen wood from across diverse latitudes and environments, Schubert and Jahren (2011) determined that $\Delta\delta^{13}C_{meas}$ can be used as a proxy for seasonal rainfall. Additionally, they extrapolated that the SPP is likely applicable to all evergreen species, based fundamentally on their observation of no significant difference in the $\delta^{13}C$ profiles of both an angiosperm and a gymnosperm grown at the same site in west Pibiri, central Guyana (see Pons & Helle 2011). This conclusion, logically derived by Schubert and Jahren, is what this study has endeavoured to test as part of a broader effort to adapt the SPP for archaeological evergreen charcoals from South Africa.

Therefore, this Chapter explores the patterns identified in modern *Protea* (angiosperm) and *Podocarpus* (gymnosperm) wood and charcoal samples to assess the feasibility of applying the SPP to South African genera. The modern wood and charcoal $\delta^{13}C$ profiles serve as analogues for interpreting the profiles observed in archaeological charcoal from Boomplaas Cave and Waterfall Bluff, shedding light on rainfall seasonality during the LGM and LGIT. These seasonality reconstructions are compared with existing proxy records and reconstructions to evaluate their alignment, and to evaluate the strengths and benefits of the SPP as a high-resolution palaeoclimate proxy. Finally, implications of the proxy for local archaeology and palaeoscience are addressed, before the study's uncertainties and scope for future research are provided.

6.2. Seasonal amplitudes in Protea and Podocarpus wood

6.2.1. Does the SPP work in modern wood?

The results of this study demonstrate that the high-resolution $\delta^{13}C$ profiles measured from the wholewood of the indigenous genera *Protea* and *Podocarpus* indeed reflect the seasonal rainfall regimes of their growing environments. The seasonal amplitudes measured from the modern wood samples from the SRZ site of Giant's Castle, the YRZ sites of Swartberg Pass and Montagu Pass, and the WRZ site of Camps Bay are in agreement with the amplitudes predicted using local rainfall data. For physically identified growth increments (PB), there is a strong correlation between SRZ, YRZ, and

WRZ measured and modelled amplitudes when Camps Bay wood is corrected using either the Group (Eq. 9) or Genus Correction equations (Eq. 10)(Group Correction: R^2 = 0.884, p = 0.060; Genus Correction: R^2 = 0.992, p = 0.004) (Figure 17). It is important to note that the correlation is statistically significant for the Genus Correction, while the Group Correction just misses the threshold for statistical significance at the 95 % confidence level. For isotopically identified growth intervals (IB), the correlation between SRZ, YRZ, and WRZ measured and predicted seasonal amplitudes is both strong and statistically significant at the 95 % confidence level for both the Group and Genus Corrections applied to Camps Bay (Group Correction: R^2 = 0.934, p = 0.033; Genus Correction: R^2 = 0.979, p = 0.011). These results suggest that PB and IB $\Delta\delta^{13}C_{meas}$ values of *Protea* and *Podocarpus* wood are able to effectively capture rainfall patterns across three distinct rainfall zones. Both PB and IB seasonal amplitudes appear to serve equally well as reliable indicators of rainfall seasonality, insofar as the Genus Correction equation is used for those wood samples that likely experienced water stress during growth and/or were subsampled at a relatively coarser resolution.

6.2.2. Adjusting the modelled amplitude equation

Initially, Eq. (4) – originally presented by Schubert and Jahren (2011: 7298) to model $\delta^{13}C$ changes in evergreen wood from rainfall records – was used in this study to quantify $\Delta\delta^{13}C_{model}$. However, applying this equation resulted in negative $\Delta\delta^{13}C_{model}$ values for Giant's Castle. Obtaining negative seasonal amplitudes is not theoretically possible and were not observed in any of the measured results. This suggested that local factors, particularly those specific to the SH and summer-dominated rainfall regimes, may not be adequately accounted for by the original proxy – primarily developed using data for the Northern Hemisphere.

Two variables in Eq. (4) could potentially be adjusted to prevent negative values for $\Delta\delta^{13}C_{model}$: $\Delta\delta^{13}C_{CO2}$ or ΔY. Giant's Castle experiences both a pronounced summer rainfall regime and high MAP (Table 1). Of the sites examined by Schubert and Jahren in their original study, those in Thailand (see Poussart *et al.* 2004; Ohashi *et al.* 2009) offer the most comparable conditions to Giant's Castle. A major difference between the Thailand sites and Giant's Castle, however, is latitudinal position and therefore the seasonal cycling of the isotopic composition of CO_2 ($\Delta\delta^{13}C_{CO2}$). Compared to the Northern Hemisphere, $\Delta\delta^{13}C_{CO2}$ is thought to be minimal in the SH due to reduced land mass and vegetation cover, and the variable is therefore valued at only 0.05 ‰. Not enough is known about $\Delta\delta^{13}C_{CO2}$ in the SH to justify the adjustment of this variable in Eq. (4). However, it has been noted that $\Delta\delta^{13}C_{CO2}$ likely has a less pronounced control on intra-increment $\delta^{13}C$ compared to tree physiological response and physiological fractionation (Kagawa & Battipaglia 2022). Thus, the latter variable – ΔY – was selected

for adjustment. ΔY accounts for post-photosynthetic physiological processes and fractionation, which involves a complex array of plant processes such as carbohydrate transport, respiration, and the synthesis of different compounds which all occur after initial carbon fixation during photosynthesis (Badeck *et al.* 2005; Zhang *et al.* 2019). From the leaves, primary photosynthates (non-structural carbohydrates) are mobilised and transported to become reconstituted in wood cellulose during xylogenesis (Kagawa & Battipaglia 2022). These processes further alter the isotopic composition of wood relative to the primary photosynthates, but in a myriad of ways that are not well understood (Badeck et al. 2005; Gessler *et al.* 2014; Zhang et al. 2017; Kagawa & Battipaglia 2022). In their application of the SPP to fossil wood, Vornlocher *et al.* (2021) criticised the use of a constant 0.73 to account for post-photosynthetic fractionation in all evergreens over the geological record and suggested that more research be conducted to calculate more precise and contextual *values* for ΔY. With 0.73 being unusable, the value for ΔY was increased to 1.67 in Eq. (4), which was subsequently used to calculate $\Delta\delta^{13}C_{model}$ for all modern wood and charcoal samples.

6.2.3. Physical boundary and isotope boundary complexities

Identifying with precision the growth rings of the *Protea* wood samples was challenging and, as discussed in Chapter 5, a degree of analytical error likely influenced some of the identifications and measurements of PB $\Delta\delta^{13}C_{meas}$. This means that the comparison between PB and IB $\Delta\delta^{13}C_{meas}$ values in their alignment with rainfall data may be limited, as PB $\Delta\delta^{13}C_{meas}$ may not be a perfect representation of seasonality bracketed by actual anatomical growth increment boundaries. In trees growing outside of the temperate regions, where indistinct growth ring boundaries are common, this type of error in boundary positioning is inescapable (Verheyden *et al.* 2004).

The anatomical complexity present in the SRZ Giant's Castle wood may also be considered a potential limitation in the PB and IB $\Delta\delta^{13}C_{meas}$ comparison. Just six growth increments where physically measured in this wood sample due to complicated wood structure (Figure 11A and Table 5), and consequently, only the subsamples located within this range could be included in the calculation of PB $\Delta\delta^{13}C_{meas}$. Only 36 $\delta^{13}C$ measurements were used to calculate PB $\Delta\delta^{13}C_{meas}$, while 82 measurements and a longer length of the core including relatively older growth cycles were used to calculate IB $\Delta\delta^{13}C_{meas}$. This approach assumes that seasonal variability remains constant along the radial growth axis of a given wood sample such that different proportions yield comparable $\Delta\delta^{13}C_{meas}$ – provided no extreme shift in the normative seasonal rainfall regime occurred over the tree's lifetime. However, t-tests found no significant difference between PB and IB $\Delta\delta^{13}C_{meas}$ for Giant's Castle wood (two-tailed: $t = 1.07$, $p = 0.308$), nor between PB and IB $\Delta\delta^{13}C_{meas}$ calculated from only the first six growth

increments (two-tailed: t = 0.51, p = 0.620). Ultimately, the comparison between the abbreviated PB amplitude and the lengthier IB amplitude is reliable.

With this potential complication ruled out, the SPP does seem to work effectively in both *Protea* and *Podocarpus* wood. And considering the strong concordance of both PB and IB $\Delta\delta^{13}C_{meas}$ with local rainfall data, it can be concluded that the SPP is able to extract seasonal information from South African wood even in the absence of distinctive, measurable growth increments. This is especially relevant for many tree species in South Africa, notably angiosperms, which tend to have a complex wood anatomy that complicates the precise and accurate identification of growth rings and has historically contributed to their underrepresentation in classical dendrochronology (Chapter 2).

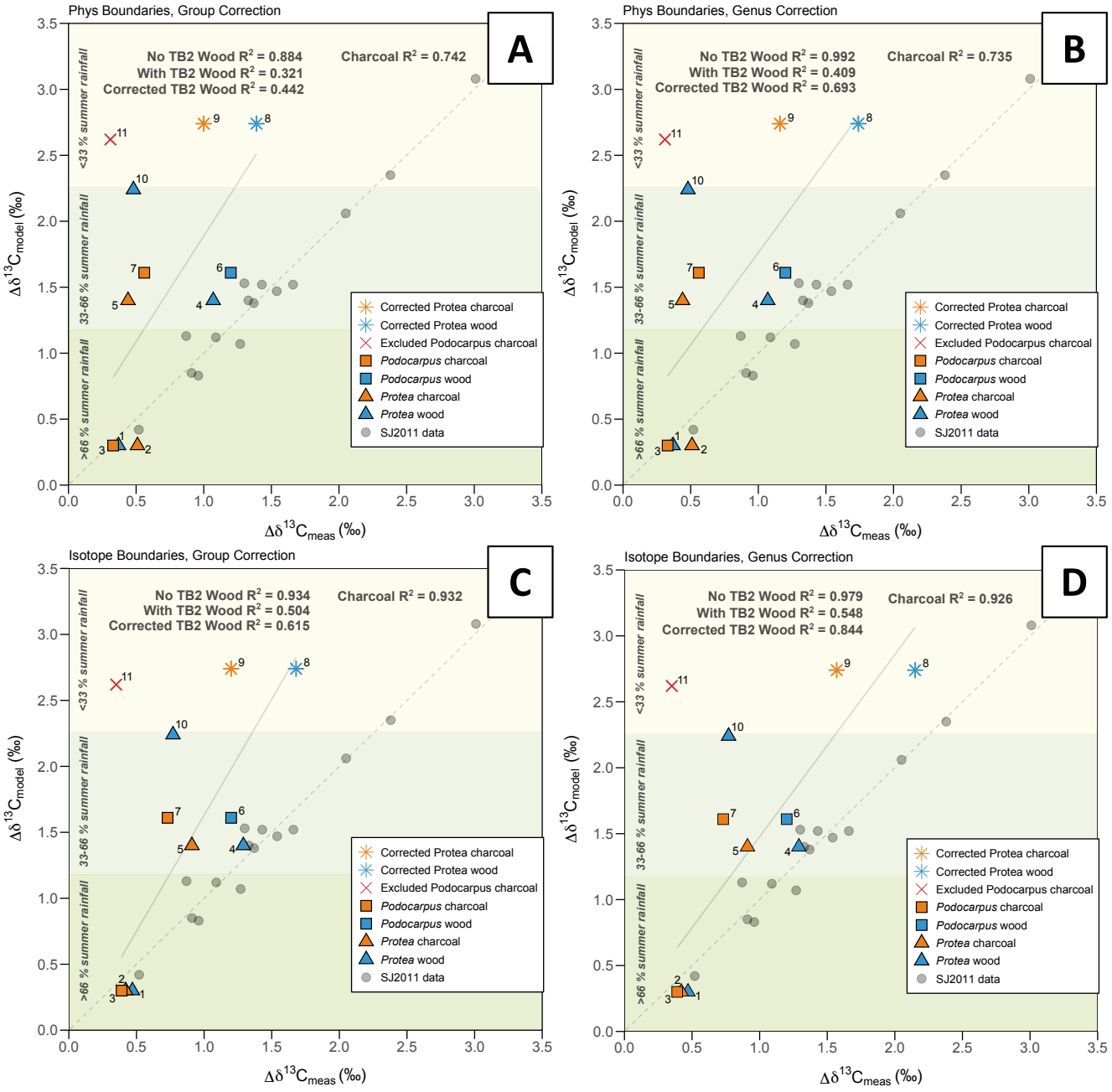

Figure 17. Measured versus modelled plots for the modern wood and charcoal results (**A:** PB Group Correction; **B:** PB Genus Correction; **C:** IB Group Correction; **D:** IB Genus Correction). 1 = Giant's Castle (GC4_w); 2 = Giant's Castle (GC4_ch); 3 = Giant's Castle (GC2_ch); 4 = Swartberg (SB_w); 5 = Swartberg (SB_ch); 6 = Montagu Pass (MP_w); 7 = Montagu Pass (MP_ch); 8 = Camps Bay (CB_w); 9 = Camps Bay (CB_ch); 10 = Theronsberg (TB2_w); 11 = Gifberg (GB1_ch)

6.2.4. Evergreen does not mean ever-growing: Water stress in the WRZ – Part I

Despite these promising results, it is observed that the WRZ wood samples in particular display noticeably weaker relationships with seasonal rainfall data. The Theronsberg wood sample has been excluded from the regression analysis described above. This is because there appears to be a

substantial discrepancy between the observed (PB $\Delta\delta^{13}C_{meas}$ = 0.48 ‰; IB $\Delta\delta^{13}C_{meas}$ = 0.77 ‰) and expected ($\Delta\delta^{13}C_{model}$ = 2.24 ‰) seasonal amplitudes (Table 11 & Table 14). With the addition of Theronsberg, the climate correlations for both PB and IB $\Delta\delta^{13}C_{meas}$ are deflated (PB $\Delta\delta^{13}C_{meas}$ Group Correction: R^2 = 0.321, p = 0.319; PB $\Delta\delta^{13}C_{meas}$ Genus Correction: R^2 = 0.409, p = 0.245; IB $\Delta\delta^{13}C_{meas}$ Group Correction: R^2 = 0.504, p = 0.179; IB $\Delta\delta^{13}C_{meas}$ Genus Correction: R^2 = 0.548, p = 0.153) (Figure 17). Given that the climate relationship persists for the other WRZ wood sample from Camps Bay, albeit somewhat tenuously, the indication is that additional factors may be contributing to Theronsberg's "isotopic divergence" (Savard & Daux 2020: 1223) from rainfall data.

One possible reason for this divergence is that the significant resolution at which Theronsberg was subsampled may have paradoxically contributed to its unexpectedly low measured amplitude. For the SPP to work effectively, it is thought that the highest subsampling resolution possible should be prioritised, so that the full extent seasonal $\delta^{13}C$ shifts can be recorded (Schubert & Jahren 2011). This relationship between subsampling resolution and the recovery of accurate seasonal isotope signals has been independently observed elsewhere (e.g. Leavitt & Szejner 2022), with some suggesting that four to six isotope measurements per growth ring at minimum are needed for reliable subannual climate analysis (Poussart *et al.* 2004). Yet it has also been observed that a subsampling resolution that is too high may be insufficient to capture large enough isotope variations between subsamples, ultimately leading to a general smoothing of the supposed seasonal signal (e.g. Verheyden *et al.* 2004). However, even though Theronsberg had the highest subsampling resolution achieved in this study, that achieved by Verheyden *et al.* (2004) was significantly higher on account of their use of a sliding microtome for the extremely close and precise subdivision of growth rings.

It is more likely that complex physiological processes occurring in response to microclimate conditions have resulted in this discrepancy. Theronsberg wood did not qualify for correction for resolution effects induced by water stress, based on its mean $\delta^{13}C$ value being more negative than -25.50 ‰. However, a closer look at its measured rainfall data indicates that the Theronsberg area is characterised by MAP and winter wet season rainfall amounts that are in fact lower than those recorded for Camps Bay (Table 1), a sample which was corrected for water stress. It appears that when a tree grows in an environment that is both highly seasonal and water stressed, such as Theronsberg, Camps Bay, and Gifberg (discussed in Section 6.3.), growth is limited to the wet season and may reduce drastically or even halt entirely as the dry season progresses. This would mean that the more positive $\delta^{13}C$ values typically expected at the height of the dry season are absent from the growth rings due to this seasonal growth cessation. Consequently, the $\delta^{13}C$ signal for the full wet-to-dry seasonal range is

truncated, as not all anticipated changes are recorded. This underscores the importance of contextualising tree growth and isotope signals within their specific growing environments. Such microclimate conditions can create circumstances wherein evergreen does not necessarily mean ever-growing.

This interpretation aligns with observations of growth cessation and altered carbon allocation dynamics occurring in trees growing under conditions of drought and water stress (Galiano *et al.* 2017; Guo *et al.* 2021; Solly *et al.* 2023). Growth cessation is also likely to occur during annual seasonal drying periods (Sarris *et al.* 2013; Pflug *et al.* 2015; Vincent-Barbaroux *et al.* 2019), including the summer droughts typical of Mediterranean-type climates, such as those in Camps Bay and Theronsberg. However, several studies indicate that while growth may cease in response to dry summer conditions, photosynthesis continues (Sarris *et al.* 2013; Pflug *et al.* 2015). Instead of being invested in tissue formation for secondary growth, the resulting photoassimilates, with more positive $\delta^{13}C$ values typically associated with drier conditions, are stored and later remobilised for tissue formation in autumn as moisture availability increases (Sarris *et al.* 2013; Pflug *et al.* 2015). These studies conclude that the extent of seasonality is recorded in growth ring isotope profiles but with a lag effect, and some of the seasonal signal will likely be lost. It is important to note that the study by Sarris *et al.* (2013) analysed *Pinus brutia*, an evergreen species, while Pflug *et al.* (2015) analysed *Quercus robur* and *Quercus petraea*, two deciduous species. Still, these studies appear to have reached the same conclusion about the impact of summer drought on subannual isotope profiles, tree phenology, and carbon dynamics.

This lag effect and subtle signal loss due to the remobilisation of stored summer drought carbon could potentially explain the dulled amplitude recorded in Theronsberg, as well as Camps Bay. However, the use of this older carbon to form growth ring tissues is doubtful for *Protea nitida*, an evergreen angiosperm. While both evergreen and deciduous trees do not seem to prioritise growth when moisture availability is limited, evidence indicates that evergreens are less likely to invest older, stored carbon into the formation of new tissues after rewatering (Galiano *et al.* 2017; Vincent-Barbaroux *et al.* 2019). When moisture availability increases, more recent photoassimilates are used in growth, while storage reserves are more likely to be directed below ground for metabolic processes and osmoregulation (Guo *et al.* 2021; Solly *et al.* 2023). Thus, Theronsberg likely did not incorporate older carbon reserves into its tissues at the onset of the productive period in autumn, suggesting that the issue here is less about a lag effect and more about a substantial loss of the seasonal signal. It appears that the dry summer conditions of Theronsberg were likely not captured in its wood tissue and

subsequent isotope profile due to seasonal growth cessation, leading in turn to a truncated seasonal amplitude that diverges from what is expected for a highly seasonal WRZ sample.

In addition to seasonal summer drying in a Mediterranean-type climate, the WRZ wood samples faced additional water stress in the form of the Cape Town Drought, characterised by both wet and dry season rainfall deficits (see Roffe *et al.* 2022). The deficits for the winter wet season in particular are evident in the rainfall data used in this study (Table A5.1 Appendix 5). The Camps Bay increment core was extracted in September 2021, shortly after drought conditions had started to improve. The $\delta^{13}C$ values of Camps Bay wood may therefore reflect a gradual recovery, which would explain the trend of increasingly positive $\delta^{13}C$ values – rehydration indicated by more negative $\delta^{13}C$ may not have been recorded yet (Figure 11C). The Theronsberg core, on the other hand, was extracted in December 2022 and therefore had more time to respond to improved rainfall conditions. It is possible that the negative $\delta^{13}C$ trend in Theronsberg wood reflects more recent and likely more stable post-drought conditions (Figure 11D), which agrees with C3 plant carbon isotope theory which states that greater water availability influences plant water use efficiency leading to more negative $\delta^{13}C$ values (Farquhar *et al.* 1989; McCarroll & Loader 2004; Diefendorf *et al.* 2010; Kohn 2010). That the Theronsberg $\delta^{13}C$ profile includes some degree of post-drought recovery while Camps Bay does not might offer an explanation for why the latter qualified for the water stress correction and the former did not. The mean $\delta^{13}C$ recorded for Camps Bay reflects the more positive $\delta^{13}C$ values incorporated into the sample's growth rings during the relatively drier wet seasons of the drought period, particularly those between 2015 and 2018 (Table A5.1 Appendix 5). By contrast, the mean $\delta^{13}C$ recorded for Theronsberg also reflects the more negative $\delta^{13}C$ values incorporated during the relatively wetter post-drought wet seasons such as 2020 and 2021 (Table A5.5 Appendix 5). When the Theronsberg series is separated into two segments, one with the older less negative $\delta^{13}C$ values, and the other containing only the more recent and more negative $\delta^{13}C$ values, mean $\delta^{13}C$ is recalculated at -25.74 ‰ and -26.76 ‰, respectively.

The water stress experienced by the Theronsberg sample (and the Camps Bay) is therefore twofold: on one hand, there is the broader meteorological drought signal (which is ultimately masked by more recent enhanced growth and more negative $\delta^{13}C$ values in the case of Theronsberg), and on the other there is the seasonal summer drying and growth cessation that typifies a Mediterranean-type climate. Taken together, these factors aptly underlie the reasons for the discrepancy between the measured and modelled $\Delta\delta^{13}C_{meas}$ for both WRZ wood samples, and especially for Theronsberg. This serves as an explanation as to why Theronsberg appears as an outlier in the scatter plots (Figure 17): there is theoretical backing for correcting Theronsberg for water stress effects, yet it was not initially corrected

due to its somewhat misleading mean $\delta^{13}C$ value. When corrected, Theronsberg's measured amplitudes increase (Group Correction: PB $\Delta\delta^{13}C_{meas}$ = 0.63 ‰, IB $\Delta\delta^{13}C_{meas}$ = 0.90 ‰; Genus Correction: PB $\Delta\delta^{13}C_{meas}$ = 0.85 ‰, IB $\Delta\delta^{13}C_{meas}$ = 1.25 ‰). And so do the correlations between measured and modelled seasonal amplitudes (Group Correction: PB R^2 = 0.442, p = 0.221; IB R^2 = 0.615, p = 0.116; Genus Correction: PB R^2 = 0.693, p = 0.080; IB R^2 = 0.844, p = 0.0275) (Figure 17). Once again, the correlations for IB amplitudes are stronger, yet only the Genus Corrected IB correlation is significant at the 95 % confidence level.

Despite the confounding effects of meteorological and seasonal water stress on the high-resolution $\delta^{13}C$ profiles and resulting seasonal amplitudes of the WRZ samples, the SPP successfully extracts climate information from across South Africa's seasonal rainfall gradient. A critical finding from the analysis of modern *Protea* and *Podocarpus* wood is that $\Delta\delta^{13}C_{meas}$ values calculated according to isotopically identified growth increment boundaries agree more closely with rainfall data than do physically identified boundaries. The greater reliability of isotopes over anatomical features in demarcating growth phases has been observed in regions like the tropics where physical identification and classical dendrochronology tend to be problematic (Poussart et al. 2004; Ohashi et al. 2009; Pons & Helle 2011). This outcome bodes well for subsequent testing of the SPP on both modern and archaeological charcoal.

6.3. Seasonal amplitudes in *Protea* and *Podocarpus* charcoal

Having confirmed the applicability of the SPP to modern *Protea* and *Podocarpus* wood, the next step is to assess whether seasonal $\delta^{13}C$ amplitudes are comparably preserved in their charcoal counterparts. This is, to my knowledge, the first experimental application of the SPP to evergreen charcoal. That the proxy works in both modern (Schubert & Jahren 2011; Schubert & Timmermann 2015) and fossil (Schubert *et al.* 2012; Schubert *et al.* 2017; Judd *et al.* 2019; Vornlocher *et al.* 2021) evergreen wood is reason enough to suggest that it can similarly be applied to carbonised evergreen wood. However, this assumes that little to no fractionation occurs during the charcoaling process (Turney *et al.* 2006).

6.3.1. Depletion with carbonisation

In all comparative cases between wood samples and their charcoal counterparts analysed in this study, a depletion in $\delta^{13}C$ with carbonisation was observed (Table 7). This observation aligns with findings from previous combustion experiments, which show more negative $\delta^{13}C$ values in charcoal relative to the original C3 wood (e.g. Czimczik *et al.* 2002; Ferrio *et al.* 2006; Turney *et al.* 2006; Hall *et al.* 2008).

Woody material is made up of a variety of isotopically unique and differentially thermolabile components (Loader *et al.* 2003; Turney *et al.* 2006; Hall *et al.* 2008; Audiard *et al.* 2018). At higher temperatures, cellulose is lost much more rapidly than lignin, with the former being ^{13}C-enriched and the latter ^{13}C-depleted (Czimczik *et al.* 2002; Loader *et al.* 2003; Turney *et al.* 2006; Bird & Ascough 2012; Mouraux *et al.* 2022). Thus, it is thought that the loss of cellulose at temperatures nearing, and especially exceeding, 500°C shifts bulk δ^{13}C values down to be closer to lignin values (see Baton *et al.* 2017; and the review by Mouraux *et al.* 2022). Moreover, in the present study, the mean offset between wood and charcoal was measured at -0.96 ‰ for *Podocarpus* and -0.91 ‰ for *Protea* (Table 7). The recorded depletion values are consistent with those previously documented for *Podocarpus* (Hall *et al.* 2008) and *Protea* (February 1996).

6.3.2. Does the SPP work in modern charcoal?

Despite the depletion commonly reported to occur with carbonisation at approximately 450 °C – the average temperature of a natural domestic wood-fuelled fire (Hall *et al.* 2008) – carbonised wood is concluded to preserve the isotopic climate signals present in the original wood and therefore act as a faithful source of palaeoclimate information (Hall *et al.* 2008; Fiorentino *et al.* 2015; Baton *et al.* 2017). This is evident here, where a cyclical rise and fall pattern is visible in all charcoal δ^{13}C profiles, and where these patterns indeed agree with rainfall data in terms of the SPP. With only the Camps Bay charcoal corrected for water stress effects, measured and predicted amplitudes are in close alignment (Group Correction: PB R^2 = 0.742, p = 0.061; IB R^2 = 0.932, p = 0.008; Genus Correction: PB R^2 = 0.735, p = 0.063; IB R^2 = 0.926, p = 0.009) (Figure 17). As is the case with the modern wood samples, IB $\Delta\delta^{13}C_{meas}$ shows a stronger correspondence with rainfall data than PB $\Delta\delta^{13}C_{meas}$, yet in the charcoal case both the Group and Genus corrections for Camps Bay appear to work equally well and are both statistically significant. These results suggest that the isotope boundaries identified in charcoal track with those identified in their wood counterparts to produce seasonal amplitudes in range with what is largely expected for each rainfall zone.

6.3.3. Shrinkage with carbonisation and materials-based resolution effects

However, there is something to be said about the ability of the charcoal δ^{13}C profiles to precisely capture the full extent of the seasonal changes observed in wood. Wood shrinks uniformly with carbonisation and so the reduction in total sample length is here thought to extend to individual growth increments and provides a reliable estimate for the changes occurring within growth increments during the charcoaling process. This notion of uniform shrinkage is supported by February (1990, 1992, 1994, 1996) who noted that the ratio between cell diameter and cell wall thickness does

not change after carbonisation, but that the number of vessels per unit area does. According to February (1992), the percentage shrinkage in radial vessel diameter in modern *Protea roupelliae* wood sourced from eastern South Africa (SRZ) ranges from 4 % to 23 %. The shrinkage described by February reflects changes to a specific anatomical feature during carbonisation. Conversely, a shrinkage factor derived from length measurements before and after carbonisation provides a broader perspective on how whole wood samples shrink during the charcoaling process. The *Protea* length-based shrinkage factors calculated in this study range from 12.18 % to 23.98 % (Table 3). These values appear to align with the range of vessel diameter shrinkage experienced by a species within the *Protea* genus reported by February. Thus, the observed shrinkage in overall dimensions seems consistent with more localised shrinkage observed in *Protea* radial vessels.

No such shrinkage tests have been conducted on modern *Podocarpus* wood, but the range calculated here is between 19.20 % and 25.25 % (Table 3) – falling towards the higher end of and then out of February's *P. roupelliae* range. Scholtz (1986) suggested that differential shrinkage is likely to occur between angiosperm and gymnosperm genera, and the effect of taxon on the degree of wood shrinkage with carbonisation has since been demonstrated (see Braadbaart & Poole 2008; Paradis-Grenouillet & Dufraisse *et al.* 2018). However, a t-test found no statistically significant difference in shrinkage factor between *Protea* and *Podocarpus* samples (two-tailed: $t = -1.02$, $p = 0.383$).[3]

Shrinkage with carbonisation may affect the resulting seasonal amplitudes calculated in charcoal. For instance, in the *Podocarpus* YRZ sample, Montagu Pass (Figure 12B), the overall rise and fall pattern is preserved in the charcoal, however the amplitude is less distinct at certain points as the valleys are not as sharply defined and do not reach a similar negative shift as observed in the wood. In these cases, where peaks and troughs are less pronounced in the charcoal, the resulting amplitudes are relatively lower than the wood amplitudes. This likely has something to do with the loss of subsampling and therefore temporal resolution that was hypothesised to occur in the analysis of a material like charcoal. That wood shrinks during carbonisation means the number of subsamples obtainable per unit area is unavoidably reduced. It was observed that for both PB $\Delta\delta^{13}C_{meas}$ and IB $\Delta\delta^{13}C_{meas}$, the subsampling resolution achieved for wood samples was on average greater than that achieved for charcoal samples (Table 8&9). This loss of resolution occurring in charcoal is ultimately associated with dulled amplitudes as fewer data points are unable to capture finer peaks and troughs – which is consistent with the relationship between resolution and $\Delta\delta^{13}C_{meas}$ discussed by Schubert and Jahren (2011).

[3] SB_ch was not measured pre- and post-carbonisation and was therefore excluded from the t-test.

Based on this observation, one could argue that it is essential to apply corrections to all charcoal samples, regardless of whether they meet the established correction criteria. However, it is important to recognise that the challenges associated with charcoal resolution are not merely a matter of too few subsamples per growth increment, *sensu* Schubert and Jahren (2011). Instead, they stem from the inherent limitations in measurable resolution due to the nature of the material. Lower resolution in wood necessitates correction to address insufficient subsampling. This is also true for charcoal, hence the establishment of charcoal-specific correction conditions. But in charcoal, a resolution that is low by wood standards may actually represent the optimal resolution for its material properties. The diminished amplitudes observed in charcoal may be close to the highest achievable for the material, which undergoes marked alteration in the form of structural and chemical changes during charcoalification. Therefore, this lower resolution may not necessarily indicate a need for correction; rather, it reflects the maximum (or near-maximum) level of detail that charcoal, as a proxy material, can provide. Consequently, while the amplitudes measured in charcoal may be comparatively lower, they likely represent the most accurate measurements achievable within the material's inherent limitations. Thus, in addition to the subsampling resolution effects outlined in the original proxy, this study identifies an additional resolution-related variable: material-based resolution effects. Whether this effect may similarly benefit from tailored correction is worth investigating and should be earmarked for future research seeking to enhance the effectiveness of the SPP in modern and archaeological charcoal. Correcting charcoal $\delta^{13}C$ results based on %C to strengthen consistency with wood $\delta^{13}C$ and, by extension, climate parameters has previously been suggested and applied (e.g. Ferrio *et al.* 2006; Turney *et al.* 2006; Aguilera *et al.* 2012; Audiard *et al.* 2018). Nevertheless, a consensus on the validity of these methods is yet to be reached, and the practice remains unstandardised in paleoclimate reconstruction using charcoals (Mouraux *et al.* 2022).

6.3.4. Evergreen does not mean ever-growing: Water stress in the WRZ – Part II

Notably, the Gifberg WRZ charcoal has been excluded from the charcoal regression analysis and discussion presented above. This is because its measured amplitudes exhibited a pronounced deviation from the expected amplitude (Figure 17). The water stress effects considered to affect Theronsberg and Camps Bay, the WRZ woods, are seemingly exacerbated in the case of Gifberg. The mean $\delta^{13}C$ for this charcoal sample was calculated at -23.17 ‰ (Table 6) which is much less negative when considered alongside the other wood samples, and especially the charcoal samples. If *Podocarpus* wood, as previously discussed, undergoes ^{13}C depletion by approximately -0.91 ‰ when carbonised at 450 °C, then the expectation is that the Gifberg wood counterpart would likely have a

mean $\delta^{13}C$ of approximately -22.98 ‰. Based on accepted carbon isotope theory, this would suggest that the Gifberg tree experienced an exceptional degree of water stress during growth, far surpassing the levels observed in the Theronsberg and Camps Bay trees which also experienced seasonal and meterological moisture scarcity. Gifberg is characterised by both general and seasonal aridity, manifest in the rainfall data used to calculate its modelled seasonal amplitude (Table A5.11 Appendix 5). The interpretation that the muted amplitudes measured in these WRZ wood samples result from summer growth cessation in a seasonally dry climate applies strongly to Gifberg. The growth increments in the Gifberg wood sample, though distinct, were incredibly narrow, with a mean width of 0.44 mm (Table 5). Though only four millimetres of this charcoal were subsampled, this equated to approximately 15 physical growth increments, yet evidently, there is little to no variability present in this charcoal's $\delta^{13}C$ profile (Figure 12C).

The indication is that year-round aridity leads to slowed growth, which halts entirely for an extended period of the calendar year during which extreme temperatures and low rainfall amounts cause the tree to deprioritise secondary growth. The isotopic hills and valleys typically expected for a tree growing under a seasonal rainfall regime are subsumed by baseline aridity, marked by truncated and highly irregular growth patterns. The Gifberg sample was therefore excluded from subsequent analysis, as this study aims to test the SPP which depends on $\delta^{13}C$ variability over a number of growth cycles. This variability may have been dampened in the case of Theronsberg and Camps Bay wood, but it was still both retrievable and redeemable. In the case of Gifberg, however, $\delta^{13}C$ variability is almost entirely absent, rendering the SPP inapplicable.

Though potentially disappointing, the Gifberg sample has highlighted a crucial limitation of the SPP: it appears to be heavily constrained by baseline aridity and may not be applicable for identifying seasonal signals in either wood or charcoal when MAP falls below a certain threshold. Nevertheless, in all other charcoal cases, the coherence between measured and modelled seasonal amplitudes indicates that $\delta^{13}C$ profiles and, by extension, climate signals are preserved in woody plant material after the charcoaling process – though with some slight offset and an unavoidable subtle loss in resolution culminating in relatively dulled signals. That a climate correlation was observed in *Protea* charcoal diverges from an existing study which found no significant relationship between *P. roupelliae* $\delta^{13}C$ and rainfall (February 1996). Conversely, the *Podocarpus* results presented here coincide with the findings of Hall *et al.* (2008) who identified that this genus produces charcoal that indeed records climate information in its $\delta^{13}C$ values.

The SPP works well in its ability to align measured amplitudes with modelled amplitudes – a critical first step in evaluating its potential to quantify rainfall seasonality. This quantification is achieved when the measured amplitudes are used to calculate the seasonal variation in rainfall and the ratio of summer to winter rainfall for each site, providing direct insight into seasonality without relying on inference.

6.4. Implications for ΔP and P_S/P_W from modern wood and charcoal amplitudes

The full capability of the SPP in terms of its ability quantify seasonal rainfall using ΔP and P_S/P_W is explored not in the original proxy paper, but in its subsequent palaeoclimate applications (Schubert *et al.* 2012; Schubert *et al.* 2017; Judd *et al.* 2019; Vornlocher *et al.* 2021). ΔP describes seasonal changes to rainfall amount between summer and winter, where positive values show that the bulk of the annual rains fall in summer while negative values show greater rainfall in winter. P_S/P_W is the ratio between summer and winter rainfall, where values greater than 1 indicate a summer rainfall regime, values less than 1 a winter rainfall regime, and values at or near 0 an almost perfect aseasonal rainfall regime.

6.4.1. Adding a rainfall zone to the SPP

In South Africa, this distinction between different rainfall regimes is rendered somewhat complicated by working definitions of the SRZ, YRZ, and WRZ. In recent palaeoclimate literature, a single description of contemporary seasonality dominates. That is the distinction between seasonal rainfall zones offered by Chase and Meadows (2007: 103-104): the SRZ includes those areas receiving >66 % of their mean annual precipitation in the summer months between October and March, while the WRZ covers areas receiving >66 % of their mean annual precipitation between April and September. The percentage range for the YRZ is only mentioned later in the paper: those regions receiving anywhere between 33-66 % of their mean annual precipitation in winter (Chase & Meadows 2007: 120). Chase and Meadows's popular delineation of rainfall zones has its roots in the work of Carr *et al.* (2006) who analysed rainfall data for the period 1951-1980 and sorted the country into a SRZ, YRZ, and WRZ based on this seemingly arbitrary two-thirds rule. Since its introduction, this rule has been widely deployed to become the standard framework for defining and identifying rainfall zones in palaeoclimate studies (e.g. Truc *et al.* 2013; Faith *et al.* 2019; Chase *et al.* 2019; Strobel *et al.* 2022; Quick *et al.* 2022; Chase *et al.* 2024; Faith *et al.* 2024).

No existing application of the SPP has sought to differentiate between three distinct rainfall zones. Previous applications worked only to quantify the difference in rainfall between one six-month period (summer) and the next (winter) using proportional terms that were numerical instead of qualitative or inferential. Thus, additional thresholds need to be placed on ΔP and P_S/P_W to account for the third zone – the YRZ. To define thresholds for a third zone – the year-round rainfall zone (YRZ) – a sensitivity test was conducted: I used a series of hypothetical values for P_S, P_W, and MAP to explore how the model responded under different assumed rainfall scenarios, helping to determine reasonable threshold values. ΔP between -0.66 and 0.66 demarcates the YRZ. Values more negative than -0.66 and more positive than 0.66 demarcate the WRZ and SRZ, respectively. For P_S/P_W, values between 0.52 and 1.94 distinguish the YRZ, while values less than 0.52 or greater than 1.94 distinguish the WRZ and SRZ, respectively. With the thresholds established, the modern wood and charcoal results can be interpreted and evaluated in terms of their alignment with rainfall data.

6.4.2. Seasonal rainfall regime attributions based on ΔP and P_S/P_W

For all modern wood and charcoal samples, values for ΔP are plotted against P_S/P_W in Figure 18. These values were calculated using IB $\Delta\delta^{13}C_{meas}$, with the Genus Correction applied to Camps Bay and Theronsberg, given that this sample set had the strongest correlation with seasonal rainfall data. Similarly, IB $\Delta\delta^{13}C_{meas}$ is the only amplitude that can possibly be calculated for the archaeological charcoal samples and so the same approach is used in the case of the modern samples to maintain consistency and allow for more reliable comparisons.

All rainfall data points, save for Theronsberg, fall within the expected ranges for their defined rainfall regime (Figure 18). Though technically situated within the WRZ geographic region, Theronsberg is a somewhat anomalous case wherein the proportions of seasonal rainfall between summer and winter fall just short of the thresholds established by Carr *et al.* (2006) and Chase and Meadows (2007). This may not historically be true for Theronsberg, but it is observed in the 2016 to 2022 rainfall data analysed in this study (Table 1), which shows 65.38 % of annual rainfall occurring in winter, and 34.62 % in summer. This explains why the Theronsberg rainfall data point lies within the YRZ sector, though just on the boundary with the WRZ in Figure 18. Its wood data point similarly reflects its more aseasonal rainfall regime, falling within the YRZ sector, however its wide distance from the climatological data point highlights the discrepancy between measured and modelled ΔP and P_S/P_W in this case.

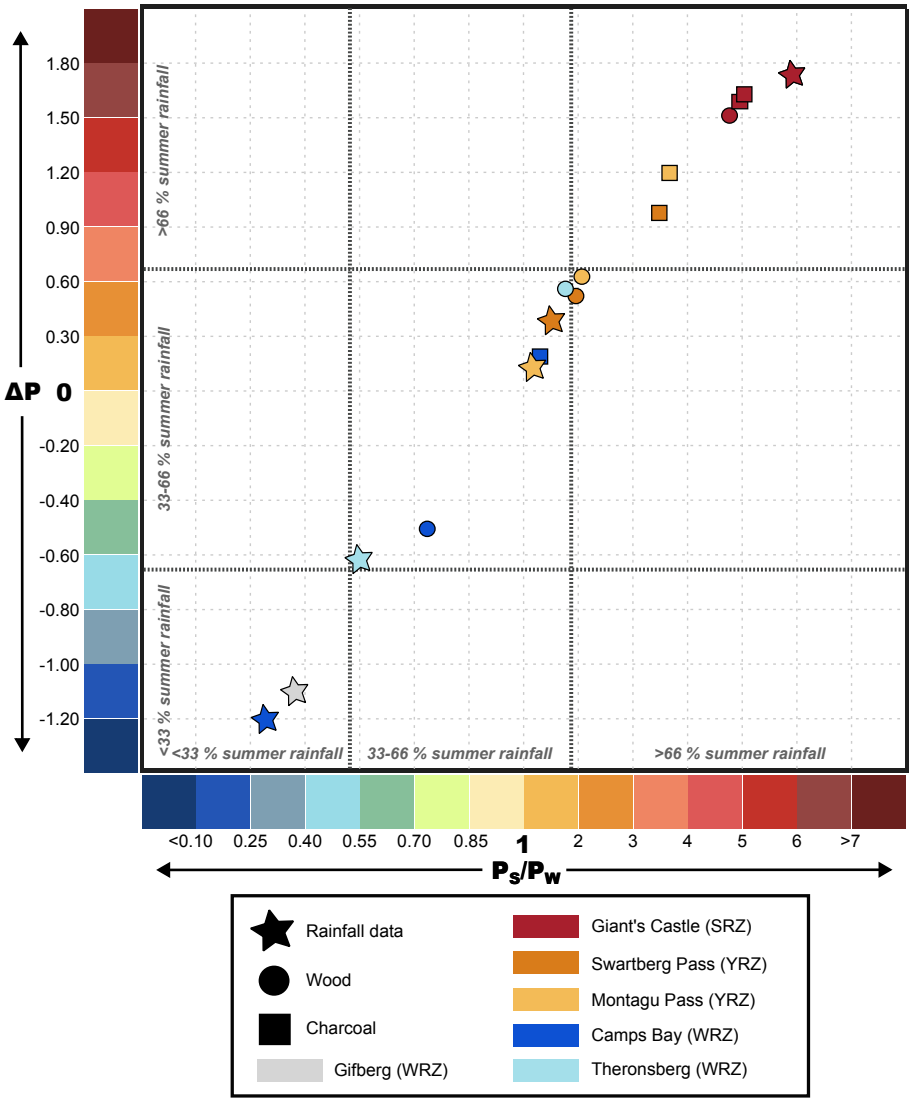

Figure 18. ΔP plotted against P_S/P_W for rainfall data, modern wood, and modern charcoal. Values calculated from IB $\Delta\delta^{13}C_{meas}$ Genus Correction.

In Figure 18, The Giant's Castle data points all fall within the bounds of the SRZ and are plotted closely together, implying a close correspondence between ΔP and P_S/P_W for rainfall data, wood, and charcoal. For all modern samples except Giant's Castle, wood and charcoal samples exhibit higher ΔP and P_S/P_W values than expected from climatology-based calculations. This discrepancy ultimately suggests that the proportion of summer rainfall is overestimated in these cases. Considering the wood samples, the degree of overestimation is notably more pronounced in the WRZ than in the YRZ, with WRZ wood showing a wider spread away from rainfall data, while YRZ wood displays a closer clustering. In both cases, however, the overestimated summer rainfall has displaced the WRZ and YRZ wood out of their anticipated seasonal rainfall zone ranges. Specifically, Camps Bay falls within the YRZ sector, while Swartberg and Montagu Pass wood appear on the boundary of the year-round and summer zones, just edging into the SRZ sector. Charcoal values for the YRZ and WRZ plot relatively

higher than their wood counterparts. The distance between wood and charcoal is greatest for the WRZ and smallest for the SRZ with the YRZ falling in between. This time, the overestimation is significant enough to push the charcoal datapoints well into the adjacent rainfall regime sector: Swartberg and Montagu Pass charcoals have shifted up into the SRZ sector, and Camps Bay into the YRZ sector.

It appears that the overestimation of summer rainfall occurring in the modern wood samples is exacerbated in the case of the modern charcoal samples. This phenomenon can be linked to the material-based resolution effects that accompany the application of the SPP to charcoal. Charcoal amplitudes are dulled relative to the original wood, and because lower amplitudes are associated with enhanced summer rainfall, the resulting charcoal ΔP and P_S/P_W values inevitably greatly inflate the proportion of summer rainfall received. Table 23 shows that this summer overestimation in charcoal, relative to wood, is minimal in the SRZ sample, and greatest amongst the YRZ samples, with charcoal on average reflecting a summer rainfall contribution that is approximately 0.96 times higher than what would be inferred from wood alone. This is a key characteristic of how the SPP functions in charcoal that will need to be considered in the subsequent analysis of the archaeological specimens.

Table 23. Difference between P_S/P_W calculated for charcoal and wood from the same site

Sample ID	Rainfall Zone	Charcoal P_S/P_W	Wood P_S/P_W	Difference
GC4	SRZ	4.96	4.75	0.21
SB	YRZ	3.49	1.99	1.50
MP	YRZ	3.68	2.06	1.62
CB	WRZ	1.29	0.77	0.52
			Mean	0.96

Based on these results, it would seem that the SPP can only be said to work reliably for *Protea* and *Podocarpus* wood and charcoal from the SRZ. While the precise attribution of the known rainfall regime to each sample shows varied and perhaps limited success in the modern testing of the SPP in a South African context – arguably due in part to the complexity introduced by the addition of a third rainfall zone – the numerical values for ΔP and P_S/P_W can still be compared across samples to closely evaluate their seasonality. Importantly, the comparison of rainfall regimes is limited not by the numerical model itself, but by the categorical classification into discrete zones. While the majority of my results indicate a summer or year-round rainfall signal (Table 24), a closer examination of the

actual calculated P_S/P_W values reveals additional detail and nuance that enhances the robustness of the seasonality reconstructions.

Table 24. Summary of ΔP and P_S/P_W information and seasonality attributions for each modern sample

Site	Sample ID	Rainfall Zone	IB $\Delta\delta^{13}C_{meas}$(‰	ΔP	standard deviation	Rainfall Zone based on ΔP	P_S/P_W	standard deviation	Rainfall Zone based on P_S/P_W	Conclusion about Summer vs. Winter Rain
Giant's Castle	GC4_w	Summer	0.47	1.52	0.31	Summer	4.75	1.24	Summer	summer 4.75 times rainier than winter
	GC4_ch		0.42	1.58	0.21	Summer	4.96	1.00	Summer	summer 4.96 times rainier than winter
	GC2_ch		0.39	1.62	0.51	Summer	5.07	0.74	Summer	summer 5.07 times rainier than winter
Swartberg	SB_w	Year-Round	1.29	0.52	0.64	Year-Round	1.99	1.16	Summer	summer 1.99 times arinier than winter
	SB_ch		0.91	0.98	0.96	Summer	3.49	2.06	Summer	summer 3.49 times rainier than winter
Montagu Pass	MP_w	Year-Round	1.20	0.63	0.47	Summer	2.06	0.99	Summer	summer 2.06 times rainier than winter
	MP_ch		0.73	1.20	0.53	Summer	3.68	1.77	Summer	summer 3.68 times rainier than winter
Theornsberg	TB2_w	Winter	1.25	0.57	0.40	Year-Round	1.87	0.80	Year-Round	summer 1.87 times rainier than winter
Camps Bay	CB_w	Winter	2.15	-0.52	0.92	Year-Round	0.77	0.53	Year-Round	winter 1.30 times rainier than summer
	CB_ch		1.57	0.19	0.44	Year-Round	1.29	0.61	Year-Round	summer 1.29 times rainier than winter

When considered across a spectrum of summer rainfall intensity, the modern *Protea* and *Podocarpus* wood and charcoal samples cluster with their respective rainfall zones (Figure 19). Specifically, the WRZ samples fall at one end of the spectrum, representing the lowest intensity of summer rain, while the SRZ samples sit at the opposite end, with the highest intensity. The YRZ samples fall in between, reflecting a relatively moderate level of summer rainfall intensity.

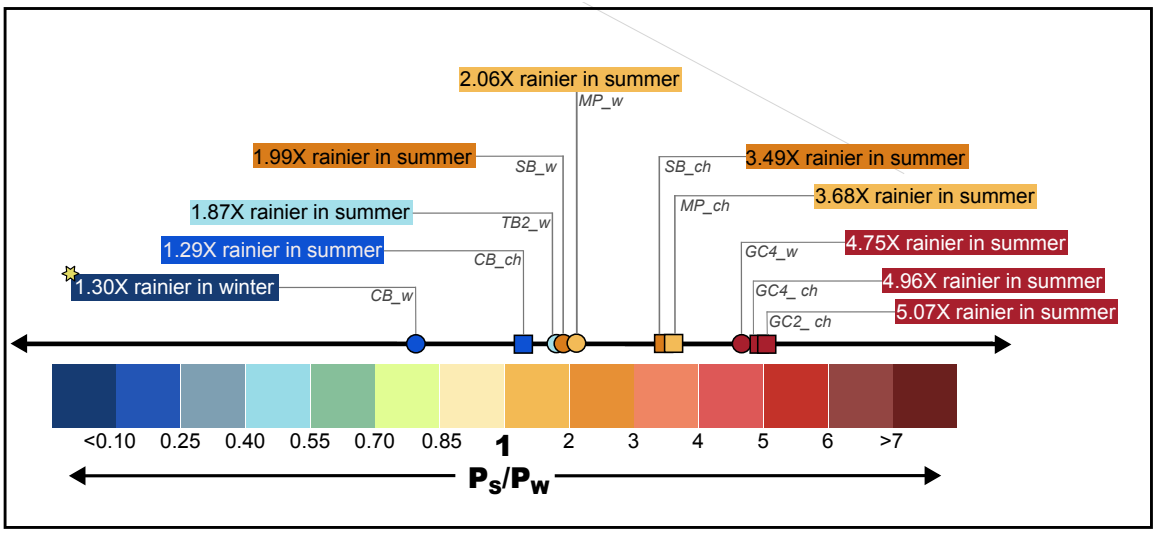

Figure 19. Spectrum of P_S/P_W values calculated from modern wood and charcoal seasonal amplitudes. SRZ sites yield the hightest ratios, WRZ the lowest ratios, and YRZ intermediate ratios.

Such a comparison is the true strength of the SPP. Like many existing seasonal rainfall proxies, it assesses the proportions of summer and winter rainfall at a specific location and time. However, unlike many existing proxies, the SPP is able to assign numerical values to its seasonality attributions, enabling for more textured and meaningful cross comparisons between values. This approach is grounded in quantitative data, rather than inference or assumption, and is less susceptible to

conflicting interpretations. Such a proxy is critically needed in palaeoclimate reconstruction in South Africa, and elsewhere, and the preliminary testing in archaeological charcoal specimens forms the focus of the following section.

6.5. Seasonal amplitudes, ΔP, and P_S/P_W in archaeological charcoal

The ability of the SPP to extract seasonal climate information from modern *Protea* and *Podocarpus* charcoal stands it in good stead to extract such information from archaeological Proteaceae and Podocarpaceae charcoal. While the bulk $\delta^{13}C$ analysis of archaeological charcoal fragments is relatively common, the examination of $\delta^{13}C$ at the "ring-scale" is less common but is thought to provide greater insight into the subannual hydroclimate dynamics of the archaeological past (Baton *et al.* 2017: 51). This section presents the results of a 'ring-scale' $\delta^{13}C$ analysis of Proteaceae and Podocarpaceae specimens from Boomplaas Cave and Waterfall Bluff, respectively, to ultimately evaluate whether the SPP is able to shed light on the nature of rainfall seasonality during the late Pleistocene in South Africa.

A rising/falling seasonal $\delta^{13}C$ pattern was observed in all archaeological specimens (Figure 15&16). Based on observations made in modern wood and charcoal, $\Delta\delta^{13}C_{meas}$ values that align with Chase and Meadows' (2007) rainfall zone definitions could be quantified to differentiate between the three rainfall zones. The upper $\Delta\delta^{13}C_{meas}$ limit for the SRZ is 1.18 ‰, and 2.26 ‰ for the WRZ. This means that $\Delta\delta^{13}C_{meas}$ values between 1.18 ‰ and 2.26 ‰ indicate a YRZ. Figure 20 shows the archaeological seasonal amplitudes plotted alongside the amplitudes calculated from modern wood and charcoal sampled from known seasonal rainfall conditions.

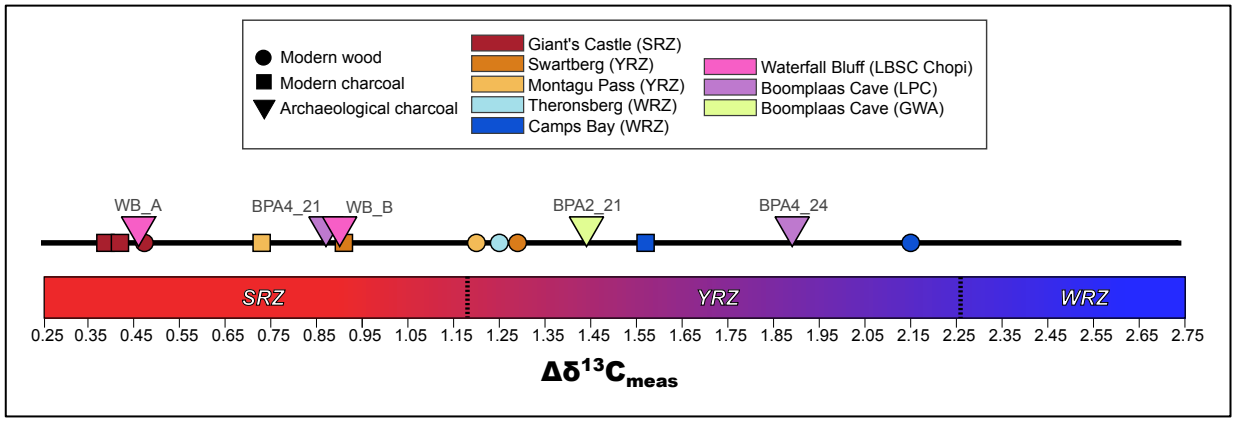

Figure 20. IB $\Delta\delta^{13}C_{meas}$ Genus Correction values for archaeological samples alongside modern wood and charcoal $\Delta\delta^{13}C_{meas}$.

6.5.1. Implications of carbonisation and materials-based resolution effects in archaeological charcoal

Before discussing the archaeological results in detail, a critical issue to consider is how carbonisation and resolution effects have influenced these measured seasonal amplitudes. The modern YRZ and WRZ charcoal samples showed a tendency towards an inflation of summer rainfall due to the complex interaction between depletion in $\delta^{13}C$ with carbonisation as well as resolution effects, ultimately resulting in a smoothing of the measured seasonal amplitudes. It is hypothesised that the SPP functions similarly in archaeological charcoal, and that the seasonal amplitudes calculated for the Boomplaas Cave and Waterfall Bluff samples are therefore dulled relative to the original wood from which they derived.

Resolution effects in archaeological charcoal are likely more pronounced compared to modern charcoal. Firstly, the small and fragile nature of archaeological charcoal limits the number of subsamples that can be extracted from each specimen. In contrast, modern charcoal, although fragile, are typically larger, more regularly shaped, and have a larger and more uniform surface area, allowing for more subsampling. As a result, fewer $\delta^{13}C$ measurements and seasonal cycles can be identified from archaeological charcoals, meaning that subsampling resolution effects are highly likely to occur. Secondly, materials-based resolution effects contribute to the issue. Charcoal, as a shrunken and isotopically depleted version of the original wood, produces $\delta^{13}C$ profiles characterised by diminished seasonal amplitudes, with cycles exhibiting less pronounced variability. While modern samples still display this inherent materials-based resolution effects, they do not necessarily and consistently coincide with low subsampling resolution. In archaeological samples, however, both factors are almost guaranteed to occur together, compounding the resolution limitations. This underscores the importance of correcting for these effects when applying the SPP to charcoal for palaeoclimate cases. It also means that the seasonal amplitudes for the archaeological specimens may overestimate summer rainfall at the LGM and/or LGIT.

6.5.2. Implications for rainfall seasonality at Waterfall Bluff during the LGIT

Testing the SPP on archaeological charcoal from the LGIT at Waterfall Bluff sheds light on climate dynamics and seasonality shifts along South Africa's east coast during glacial-interglacial cycles. This region has historically been underrepresented in seasonality reconstructions – especially in studies focused on the migrations of the SH westerlies – which have primarily concentrated on the WRZ in the west (Chase & Meadows 2007; Fitchett & Bamford 2017; Herbert & Fitchett 2022).

Waterfall Bluff A (WB_A) is tightly clustered with the modern SRZ wood and charcoal samples (Figure 20), indicating that a strong summer rainfall regime, similar to that of present-day Giant's Castle, likely prevailed at Waterfall Bluff during the deglaciation after the LGM. Waterfall Bluff B (WB_B) – a specimen from the same stratigraphic aggregate as WB_A – has a greater amplitude and is more closely associated with the charcoal sample from Swartberg, indicating a summer rainfall regime but one with a relatively greater influence of winter rainfall. The variance observed between these two samples is not entirely unexpected. The functioning of isotopes within trees and their growth rings is complex, with significant variability often occurring between even neighbouring trees of the same species (Leavitt & Szejner 2022). There is also the possibility that the two specimens were burnt at different temperatures in the domestic fires made by the inhabitants of Waterfall Bluff, as burning temperature has been shown to have a significant effect on the preservation of the climate signal within charcoal (e.g. Czimczik *et al.* 2002; Ferrio *et al.* 2006; Turney *et al.* 2006; Hall *et al.* 2008). In addition, there is the fact that LBCS Chopi, the stratigraphic aggregate from which the samples derive, spans approximately 4,000 years, making it highly likely that short-term fluctuations in rainfall seasonality occurred over this period. Furthermore, the seasonal amplitude for WB_A was calculated from a more highly resolved $\delta^{13}C$ series and includes a greater number of seasonal cycles. While this may suggest that WB_A offers a more accurate reflection of average seasonal rainfall over multiple growth seasons, it also explains why these results may differ from those of WB_B. Despite the ostensible discrepancy between WB_A and WB_B, the difference is not statistically significant (two-tailed t-test: $t = -1.17$, $p = 0.310$).

The ΔP values for both WB_A and WB_B are both greater than 1, indicating the dominance of summer rainfall (Table 21). The P_S/P_W ratios for WB_A and WB_B indicate that summer was rainier than winter by 4.77 ± 1.11 times for the former sample and 2.75 ± 0.38 times for the latter. When the $\Delta\delta^{13}C_{meas}$ values of both samples are averaged, as done by Schubert *et al.* (2017) for two fossil samples from the same site that lacked a significant difference, summer is shown to be 4.17 ± 1.35 times rainier than winter. Ultimately, these results indicate that Waterfall Bluff was predominantly characterised by wet summers during the LGIT.

This seasonality attribution agrees with existing interpretations for the time period. Available palaeoclimate evidence from the region suggests that the expansion of Antarctic sea ice during the last glacial resulted in the equatorward shift of the westerlies, leading to a significant northeast expansion of winter rainfall at the height of the LGM (Mills *et al.* 2012; Neumann *et al.* 2014; Chevalier & Chase 2015; Miller *et al.* 2019; Esteban *et al.* 2020; Herbert & Fitchett 2022). The presence of fynbos

type pollen in the Mahwaqa wetland, so far east of the Fynbos Biome, led Neumann *et al. (*2014) to suggest that the predominance of winter rains persisted after the LGM and into the Holocene. Yet pollen-based precipitation stacks constructed by Chevalier and Chase (2015) prompted them to conclude that high altitude and microclimate influences at Mahwaqa likely detracted from the seasonal precipitation signal. Alternative evidence indicates that the reduction in Antarctic sea ice following the LGM led to the concomitant southward retraction of the westerlies and, in turn, and increase in summer rainfall during the LGIT. This is the conclusion drawn from analyses of the carbon and hydrogen isotope compositions of plant leaf waxes preserved at the nearby Mfabeni peatland (Miller *et al.* 2019), as well as within the deposits of Waterfall Bluff itself (Esteban *et al.* 2020). A summer rainfall signal is therefore expected from the $\delta^{13}C$ profiles of the Podocarpaceae charcoals analysed here.

However, the significant degree to which the archaeological seasonality from WB_A aligns with the present-day seasonality of Giant's Castle is uncertain. This is because such pronounced seasonality does not exist at Waterfall Bluff even today – a coastal site that is less seasonal than inland Mpondoland and which currently receives approximately 36% of its annual rainfall in winter (Cawe 1994; Esteban *et al.* 2023a). While evidence points to increasing summer rain during the LGIT there is no evidence for such a rapid and pronounced shift from the winter-dominated LGM to such a summer-dominated LGIT. A critical point to consider is that charcoal $\delta^{13}C$ depletion and resolution effects are possibly exaggerating the proportion of summer rainfall by roughly 0.96 times (Table 23) compared to the values that would likely be inferred from their original wood counterparts.

Thus, the calculated P_S/P_W ratio for Waterfall Bluff may reflect a maximum potential value for summer rainfall seasonality. Future applications of the SPP to archaeological charcoal will need to account for this uncertainty. The modern calibration is crucial in this regard, as it enables the quantification of these effects. This does not imply that the SPP is inaccurate for archaeological charcoal, but rather less precise compared to its use on modern whole wood. The ability to quantify this imprecision demonstrates the SPP's promise in yielding high-resolution palaeoclimate data from archaeological charcoal. Nevertheless, given the presently unresolved uncertainties, and the limited sample size for Waterfall Bluff which precludes seasonality claims made with statistical certainty, the interpretations about past rainfall seasonality for the LGIT are not entirely conclusive and should be viewed with some degree of caution.

6.5.3. Implications for rainfall seasonality at Boomplaas Cave during the LGM

A greater number of studies seeking to understand shifts in rainfall seasonality during the LGM have been conducted in the present-day WRZ and YRZ (see reviews by Chase & Meadows 2007; Marean *et al.* 2014). Boomplaas Cave in particular has received significant attention and there is ongoing debate about the nature of LGM moisture availability implied by the various proxy records preserved at the Cango Valley site (Engelbrecht *et al.* 2019; Faith *et al.* 2024).

The Proteaceae specimens form Boomplaas Cave's early LGM member LPC are broadly distributed, with one sample (BPA4_24) closer to the WRZ Camps Bay wood amplitude and the other (BPA4_21) positioned beside the YRZ Swartberg charcoal sample (Figure 20). Though BPA4_24 is technically positioned in the YRZ sector, so too are the modern WRZ wood and charcoal samples from Camps Bay. BPA4_24 has a higher seasonal amplitude than that recorded for Camps Bay charcoal and, assuming depletion with carbonisation and that a general signal smoothing occurs in the archaeological specimens as it does in the modern, this indicates that a dominance of winter rainfall was present at Boomplaas Cave at the time. The position of BPA4_21, on the other hand, indicates that a more aseasonal rainfall regime with a stronger influence of summer rainfall characterised the area at the early LGM, comparable to the present-day seasonality experienced at the nearby Swartberg. The difference between the LPC Proteaceae specimens was found to be significant (two-tailed t-test: $t = -1.93$, $p = 0.005$). One sample indicates a marked shift, with increased winter rainfall compared to present conditions, while the other indicates little to no change from today. However, there is no indication of summer rainfall dominance in any amplitude measured from the LGM Boomplaas charcoals. Similar to Waterfall Bluff's variable results, however, BPA4_24's amplitude indicating enhanced winter rainfall is likely more reliable due to both its relatively higher subsampling resolution and greater number of representative growth cycles. The large discrepancy between these LPC samples indicates that the aforementioned factors possibly giving rise to within-stratigraphic unit variability have played less of a role than the more fundamental issue of resolution effects and analytical error.

The Proteaceae specimen from the later LGM member GWA (BPA2_21), which has no comparative specimen from the same unit, is positioned between the Camps Bay charcoal and Swartberg wood. This suggests that year-round rainfall conditions, *sensu* the Chase and Meadows (2007) two-thirds definition, dominated at the time, though with a greater input from winter rainfall compared to present-day seasonality in the Cango Valley. The difference between the seasonal amplitude calculated for this later LGM specimen and the earlier LGM specimen BPA4_24 is not statistically

significant (two-tailed t-test: t = -1.47, p = 0.165), emphasising the influence of winter rainfall at Boomplaas Cave over the course of the LGM. However, the difference between BPA2_21 and BPA4_21 is statistically significant (two-tailed t-test: t = 2.95, p = 0.013).

The ΔP values calculated for BPA4_24 and BPA2_21 are -0.21 and 0.35, respectively, indicating modern YRZ-like seasonality but with significant contribution from winter rainfall (Table 21). By contrast, BPA4_21 achieved a ΔP of 1.03, suggesting modern SRZ-like seasonality. The P_S/P_W ratio for LPC's BPA4_24 is 1.32 ± 1.52. A standard deviation of 1.52, which is greater than the mean ratio, indicates substantial growth-increment level $\Delta\delta^{13}C_{meas}$ variability for this sample, and possible outlier increments with very high P_S/P_W ratios. From this ratio, it appears that summers were 1.32 times rainier than winters which, although indicative of YRZ conditions, is similar to the ratio calculated for the modern Camps Bay wood (Table 24). The ratio calculated for GWA's BPA2_21 is 1.59, which again indicates YRZ conditions but is closer to the ratio calculated for Camps Bay charcoal than it is for either Swartberg or Montagu Pass, the modern YRZ samples (Table 24). BPA4_21, on the other hand, achieved a P_S/P_W ratio of 2.91, implying a relatively greater contribution of summer rain for LPC, similar to the ratios captured for the Swartberg and Camps Bay.

The trend suggested for BPA4_24 and BPA2_21 is that winter rainfall featured more prominently over the LGM, with its dominance decreasing between LPC and GWA with an added influence of summer rainfall at the peak of the LGM. BPA4_21 does not conform to this trend, suggesting it may be less reliable and may not accurately capture true LGM seasonality. Naturally, additional charcoal specimens will need to be analysed to verify the winter trend observed for BPA4_24 and BPA2_21. This will help to determine whether the variance observed between the two LPC charcoals is a recurring pattern – suggesting possible extreme short-term seasonal rainfall variability – or merely noise that distorts the seasonality trend, possibly indicating an outlier. Setting aside this uncertainty until more is known, the two more highly resolved Proteaceae charcoal results indicate that Boomplaas Cave was predominantly characterised by wet winters during the LGM. And considering that the proportion of summer rainfall is likely inflated in charcoal, the P_S/P_W ratios representing LPC and GWA are possibly the minimum potential values for LGM winter rainfall seasonality.

This aligns with various other proxy records. As with the Waterfall Bluff records, the established paradigm suggests that the expansion of Antarctic sea ice during the LGM caused a northward shift of the westerlies and storm tracks, leading to both the eastward expansion and increase in the frequency and intensity of winter frontal rains in the present-day YRZ (van Zinderen Bakker 1967; 1976;

Engelbrecht *et al.* 2019; Chase and Meadows 2007; Chase *et al.* 2017). Archaeological evidence from Boomplaas Cave, including macromammal remains (Klein 1978, 1983; Faith 2013a; 2013b), micromammal remains (Avery 1982; 2004; Thackeray & Fitchett 2016; Faith *et al.* 2019), macrobotanical assemblages (H. Deacon *et al.* 1983; Scholtz 1986), and stable isotope analyses of ungulate tooth enamel (Sealy *et al.* 2016), have all been interpreted as indicators of enhanced winter rainfall in the Cango Valley and Southern Cape during the LGM. Additional evidence supporting winter rainfall at this time includes fossil pollen and stable nitrogen and carbon isotope compositions from the Seweweekspoort hyrax middens (Chase *et al.* 2018).

These lines of evidence have led to the broad acceptance of the interpretation that winter rainfall increased in the Southern Cape during the LGM, with the debate now focusing on the volume of precipitation: whether the LGM was harsh and arid or relatively humid and productive. Early interpretations based on fauna (Klein 1978, 1983; Avery 1982) and charcoal (Scholtz 1986) linked the observed grassiness of the LGM to greater aridity. However, these two factors are not necessarily causally linked and could be explained by alternative mechanisms (Chase & Meadows 2007; Faith 2013b; Chase *et al.* 2018). Moreover, Faith *et al.* (2024) have recently suggested that such relationships have little to no observable ecological backing in the present-day. As a result, recent years have seen an increase in interpretations positing enhanced humidity and productivity during the LGM compared to the Holocene (Faith 2013a&b; Sealy *et al.* 2016; Chase *et al.* 2017; Chase et al. 2018; Pargeter *et al.* 2018; Faith *et al.* 2019; Pargeter & Faith 2020; Faith *et al.* 2024). Whether the SPP is able to contribute to these debates remains to be seen. Should additional, independent proxy data for rainfall volume and MAP arise, however, the SPP does have the potential to quantify in millimetres summer and winter rainfall (Schubert & Jahren 2011).

6.6. Implications for local archaeology and palaeoscience

The SPP applied to archaeological charcoal provides a quantitative, seasonally-resolved, on-site proxy that shows potential for expansion and integration with archaeological investigations. As mentioned in Chapter 3, regional-scale, off-site palaeorecords are limited by spatial, temporal, and contextual detachment from archaeological sites. For example, Chase *et al.* (2018) used hydroclimate reconstructions from the Seweweekspoort hyrax midden to interpret the lithic and faunal assemblages of Boomplaas Cave, 70 km east. While they found a strong alignment between the Seweweeks climate data and Boomplaas faunal record – indicating that the shift from the Late Pleistocene to Holocene prompted changes to hunter-gatherer technologies, subsistence strategies, and mobility patterns – the detachment between the two sites raises challenges. The 70 km distance

spans a landscape of variable microclimates, which complicates cross-site comparisons (see Prendergast *et al.* 2018), and while the Seweweeks chronology is well-constrained, the Boomplaas units at the time were less precisely dated, limiting the ability to directly correlate climate episodes with cultural episodes (updated dates are now available, see Pargeter *et al.* 2018). Furthermore, the hyrax midden is an independent environmental archive, beyond the immediate context of both the archaeological site and stratigraphic unit in which human behaviours are identified.

The SPP proposed here holds potential to overcome some of these detachment issues. By using archaeological charcoal – a material that is 1.) directly associated with human cultural behaviour, and 2.) found within the same sites being analysed archaeologically – this method may provide a seasonally-resolved climatological record that is temporally, spatially, and contextually aligned with archaeological evidence. This integration may offer a closer link between human seasonality and climatological seasonality, allowing for more nuanced insights into how humans engaged with their environmental conditions. After all, seasonal and annual climate patterns are the primary scales at which humans respond and adapt to their surroundings (Prendergast *et al.* 2018).

The $\delta^{13}C$ profiles of archaeological charcoal are less influenced by anthropogenic bias compared to the use of charcoal specimens in taxonomic and relative abundance analyses, or in comparison to faunal remains. The SPP is contingent only upon the presence of evergreen taxa, as their isotopic signature show the potential to reveal seasonality, regardless of whether these taxa were specifically selected by past populations. Similar approaches have been taken elsewhere in the search for high-resolution on-site proxies. Based on observed relationships between seasonality and rodent relative abundances, Thackeray and Fitchett (2016) and Faith *et al.* (2019) interpreted archaeological micromammal assemblages to examine the seasonal patterns of the Late Quaternary. The former study focused solely on Boomplaas Cave, while the latter tested its proxy at Nelson Bay Cave and Byneskranskop 1 in addition to Boomplaas. Micromammals are commonly deposited by raptors, so although found on-site, they are less susceptible to anthropogenic bias.

The proxies presented in these two quantitative micromammal studies share additional similarities with the SPP explored here. Both approaches rely on modern calibration and ground-truthing prior to testing on archaeological sites, both prioritise quantifying seasonality-ecology relationships rather than qualitatively inferring past climate conditions, and both aim to reconstruct climate to a seasonal resolution. Most notable, perhaps, is that they share a reconstruction of enhanced winter rainfall at Boomplaas Cave during the LGM. In this way, it may be posited that perhaps the SPP is not as novel

as initially proposed. Efforts have already been made to address the gap in reliable archaeological seasonality proxies. The gap may, therefore, lie more in expanding the application of existing proxies to a broader range of sites where human-environment and seasonality questions persist.

Regarding persistent questions, it is also important to consider persistent answers. There is a notable bias towards discussions of Boomplaas Cave in this study, and not just because charcoals from the site formed part of the analysis. When it comes to South African palaeorecords and investigations into the shifting position of the westerlies and movements of rainfall zone boundaries since the Late Pleistocene, much of the research has concentrated on WRZ and YRZ – the Western Cape – where Boomplaas remains a key site (see Chase & Meadows 2007). The far northern reach of the westerlies into the now-SRZ during the Late Pleistocene, however, remains a relatively less developed area of research (e.g. Fitchett & Bamford 2017). The recent resurgence in Boomplaas discourse can also be attributed to the ongoing *Cango Valley Archaeology and Paleoscape Project*, directed by Justin Pargeter, where a re-excavation of has uncovered new materials and provided impetus for testing additional research methods and approaches. As mentioned, existing (and emergent) lines of palaeoclimate evidence from the Cango Valley have all but confirmed the dominance of winter rainfall in the region during the Late Pleistocene. There is an argument to be made that perhaps the SPP is wasted on a site like Boomplaas – which has already formed the focus of so much research – where it is essentially rendered an expensive way to discover knowledge that is already known (e.g. Deetz 1977 discussing a common criticism of Historical Archaeology).

That is why testing on a site such as Waterfall Bluff is a critical contribution. On-site records used to infer seasonality do exist for the site (see Esteban *et al.* 2020), but no attempts have so far been made to quantify the proportions of summer and winter rainfall. Archaeologically, Fisher e*t al.* (2020) have posed questions about the nature of hunter-gatherer seasonal mobility and resource use at Waterfall Bluff. They suggest that hunter-gatherers undertook seasonal, logistical movements between the Lesotho highlands and the coastal lowlands, driven by the availability of resources like plant poisons. A high-resolution proxy for seasonality – such as the SPP – may help to climatically contextualise these movements.

Although existing records indicate winter rainfall dominance in the Cango Valley during the LGM, few have captured the variability of this regime across the full 7,000-year span of the period (ca. 24,000–18,000 cal BP; Chase & Meadows 2007). Based on their quantitative micromammal analysis, Faith *et al.* (2019) observed an increase in winter rainfall seasonality between LPC and GWA. Interestingly, the

charcoals analysed in this study revealed the opposite trend, with seasonality appearing to decrease between LPC and GWA. Both findings underscore that the LGM rainfall regime at Boomplaas was not consistently seasonal. The nature of this variability – whether shifting from more to less seasonal or *vice versa* – presents an intriguing discrepancy. This highlights the ongoing relevance of developing seasonality research at Boomplaas (see Faith *et al.* 2024). Only one GWA and two LPC were analysed in this study, emphasising the need to examine a larger dataset to resolve the discrepancy and confirm patterns of LGM seasonal variability more robustly. Especially given that Faith *et al.'s* (2019) observed seasonality increase between LPC and GWA was later used to interpret shifts in lithic technological organisation, site occupation intensity, and seasonal resource use (Pargeter & Faith 2020). Climatological reconstructions of seasonality implicate archaeology and human seasonality. Therefore, it is essential to ensure these reconstructions are not only precise but also as accurate as possible.

6.7. Additional uncertainties and scope for future research

The process of testing the applicability of the SPP on archaeological charcoal using modern analogues has shown there is considerable scope for future work. Some uncertainties and questions have already been mentioned in the above discussion, and this section aims to expand on these observations. The following list outlines outstanding questions, adjustments, and additions that could potentially enhance the SPP as a high-resolution palaeoclimate proxy.

- This study found no significant relationship between MAP and mean $\delta^{13}C$ among the modern wood (and charcoal) samples, despite their observed link in various parts of the world (Diefendorf *et al.* 2010; Kohn 2010). This raises doubts about its validity as an indicator of water stress in *Protea* and *Podocarpus* from South Africa. Plant responses to water availability may not directly correlate with MAP, highlighting uncertainty in the fundamental relationship between $\delta^{13}C$ and MAP, as well as summer and winter rainfall. Additionally, water-use efficiency is known to decrease under lower glacial pCO_2, potentially increasing water stress during dry periods; however, wetter conditions during the LGM in many regions complicate disentangling the effects of atmospheric CO_2 and rainfall on $\delta^{13}C$ values. While all archaeological samples qualified for correction for water stress based on mean $\delta^{13}C$, a clear seasonal signal was still observed. The tenuous link between MAP and mean $\delta^{13}C$ in modern samples suggests that the archaeological samples may not have experienced significant water stress and their positive $\delta^{13}C$ values may rather indicate shifting CO_2 dynamics. Further research is needed to clarify how MAP influences plant $\delta^{13}C$ variability.

- The equation used to calculate $\Delta\delta^{13}C_{model}$ (Eq. 4) warrants refinement for application to different contexts. This will require improved understanding of post-photosynthetic processes (Vornlocher *et al.* 2021) and seasonal CO_2 cycling in the SH (Judd *et al.* 2019).
- This study applied a uniform set of correction equations (Eq. 8 to Eq. 19) – based on Schubert and Jahren (2011) – for subsampling, water stress, and material effects. A closer examination of these correction methods is needed to determine if a single approach is universally applicable, or if each effect should receive its own tailored equation.
- Classical dendrology prioritises large sample sizes to achieve a site-level understanding of climate using growth ring data (McCarroll & Loader 2004; Speer 2010; Leavitt 2010). However, this study relied on one to two trees per rainfall zone. Rainfall zones are complex and heterogeneous (see Chapter 3), highlighting the limitation of using so few trees to represent these variable regions. The modern calibration would benefit from incorporating additional *Protea* and *Podocarpus* samples, as well as other evergreen species, from each rainfall zone. This expanded dataset would better account for within-zone variability and microclimate influences on $\delta^{13}C$ signatures, providing an improved understanding of the seasonal signals expected for each rainfall zone. Additionally, replicating the procedure on multiple individual trees from different sites and rainfall zones would help assess variability between trees and clarify how results from single trees relate to variability within each rainfall zone.
- To enhance the robustness of archaeological seasonality reconstructions, larger sample sizes from each site and stratigraphic unit – whether at Boomplaas, Waterfall Bluff, or other locations – are essential. While the seasonality attributions made in this study are promising, they are fundamentally preliminary results, constrained by limited sample sizes. Seasonal patterns cannot be confirmed for the LGM or LGIT until additional analyses are conducted. A more extensive dataset will not only improve reproducibility, but also help distinguish true seasonal signals from short-term climatic events, such as El Niño Southern Oscillation, thereby providing a clearer and more reliable understanding of past seasonality trends.
- An additional uncertainty not yet mentioned is whether the archaeological charcoals analysed in this study originate from the central stem (trunk) of the tree, or from other woody elements, such as branches. Comparing the $\delta^{13}C$ values of increment cores taken from trunks with archaeological charcoal that may have derived from a branch assumes there to be no significant isotopic difference between the two. This assumption is supported by experimental combustion testing and subsequent isotopic analysis, demonstrating that climate signals are preserved in both stems and branches of *Podocarpus* after carbonisation (Hall *et al.* 2008). Nevertheless, this assumption needs to be tested on additional evergreens, including *Protea*.

In southern Africa, a recent ethnobotanical study on the fuelwood preferences of the #Khomani San in the San resettlement farms of northern South Africa and southern Botswana found that most respondents (83 %) obtained fuelwood by collecting dead branches from the ground, while others (36 %) cut dead branches from trees, and only some (6%) cut live trees (Nott & Thondhlana 2017). Used with caution, these findings support the proposition that branches may have been valued as fuelwood by LSA hunter-gatherers. Consequently, there are grounds to include branches into the modern calibration of the SPP on charcoal, and this should be a focus of future research.

CHAPTER 7

Conclusion

High-resolution stable isotope measurements across tree growth increments offer valuable insight into the relationships between tree phenology, physiology, and isotope fractionation in response to the annual fluctuations in environmental and climatic variables. Given that regular, repetitive isotope cycles have been identified even in trees growing in regions like the tropics and subtropics – where the complexity of wood anatomy and growth patterns complicate applications of classical dendrochronology – the use of high-resolution analysis has gained increasing popularity in recent years. However, high-resolution analyses have received little to no traction in South Africa.

Schubert and Jahren's (2011) seasonal precipitation proxy couples the measured $\delta^{13}C$ across a series of growth intervals ($\Delta\delta^{13}C_{meas}$) and seasonal changes in precipitation. It has shown success in using such fine-scale $\delta^{13}C$ measurements across the radial growth of evergreen whole wood and fossil wood to quantify the ratio of past summer to winter seasonal rainfall (P_S/P_W). Fourteen of the fifteen datasets analysed by Schubert and Jahren (2011) in their development of the SPP came from the Northern Hemisphere. The only dataset representing Africa was that from Gazi Bay, Kenya (Verheyden *et al.* 2004), also in the Northern Hemisphere. Similarly, only one dataset derived from the SH, and that was from Harvey in southwestern Australia (Warren *et al.* 2001). Still, Schubert and Jahren concluded that the SPP is likely applicable to all evergreen species, based fundamentally on their observation of no significant difference in the $\delta^{13}C$ profiles of both an angiosperm and a gymnosperm grown at the same site in west Pibiri, central Guyana (De Micco *et al.* 2007). This assumption is what this study has endeavoured to empirically test as part of a broader effort to adapt the SPP for evergreen archaeological charcoal from South Africa. In doing so, this study has contributed an additional dataset comprising three evergreen species from five sites to the original calibration of the SPP, enabling it to better account for global evergreen variability and more accurately represent the SH and southern Africa.

The conspicuous lack of southern African representation in Schubert and Jahren's original 'global' dataset is hardly surprising. By 2011, the time of the SPP's publication, several $\delta^{13}C$ studies had been conducted on South African trees, including *W. wallichii* (February & Stock 1999), *B. salicina* (Norström *et al.* 2005), *A. digitata* (Robertson *et al.* 2006), *P. latifolius* (Hall *et al.* 2008), and *M. caffra* (Hall *et al.* 2009). Yet none of these were practically useable for Schubert and Jahren's purposes: the *A. digitata*

profile represented a deciduous tree, *B. salicina* was sampled at too low a resolution, *W. wallichii* was only sampled at an annual resolution, and although multiple $\delta^{13}C$ measurements were obtained from the growth rings of *P. latifolius* and *M. caffra*, the results were ultimately annualised. That so few $\delta^{13}C$ studies, and particularly those at a subannual resolution, have been conducted in South Africa relative to the Northern Hemisphere likely reflects the paucity of growth ring chronologies in the region, consistent with long-standing belief that southern African tree species are largely unsuitable for dendrochronology and dendroclimatology (Chapter 2). This perception has historically slowed the uptake and development of these fields in the region.

From the results presented in this dissertation, it appears possible to use high-resolution $\delta^{13}C$ analyses to extract seasonal rainfall information from South African evergreen angiosperm and gymnosperm whole and carbonised wood. Seasonal amplitudes measured from the modern samples are in close agreement with those modelled using rainfall data. Seasonal changes in rainfall (ΔP) and the ratio of summer to winter rainfall (P_S/P_W) allow proportions of summer and winter rainfall to be quantified from measured isotope results. As expected, WRZ sites yield the highest measured amplitudes and therefore lowest values for ΔP and P_S/P_W. SRZ yielded the lowest amplitudes and therefore greatest values for ΔP and P_S/P_W, and YRZ samples yielded intermediate amplitudes and ΔP and P_S/P_W values. Existing proxies for rainfall seasonality also represent past seasonality in proportional terms (e.g. Chase *et al.* 2015; Sealy *et al.* 2016), however, the SPP enables these proportions to receive numerical values which can be directly compared with a reduced reliance on assumption and qualitative inference.

This analysis marks a significant departure from the classical dendroclimatology, which relies primarily on measurements of growth ring widths. Additionally, no existing study on South African *Protea* or *Podocarpus* — wood or charcoal — has achieved such high sampling resolution, further distinguishing this study from the coarser resolutions typically used in isotope dendroclimatology in the region. Such resolutions led February (1996) to conclude there is no significant relationship between *P. roupelliae* and rainfall – a finding challenged by these results. What the findings of this study suggest for the state of growth ring research in South Africa is that problems and challenges may not lie inherently with local trees, but rather with a broader lack of theoretical and methodological imagination (along with the necessary resources to invest) in local growth ring studies (see Silva *et al.* 2019).

The modern calibration helps to establish expectations that aid in interpreting archaeological amplitudes, and values for ΔP and P_S/P_W:

- The strong correlations between isotope boundary amplitudes and seasonal rainfall data demonstrate that the SPP can prove effective without 1.) identifying and measuring growth increments, and 2.) assigning each growth increment an age using cross-dating or radiocarbon. *Protea* and *Podocarpus* growth ring boundaries are difficult to locate post carbonisation, so this result is promising for archaeological applications of the SPP to Proteaceae and Podocarpaceae charcoal. So long as the radial growth axis is identifiable, multiple $\delta^{13}C$ measurements can be successively taken along that surface.
- The complex interplay between $\delta^{13}C$ depletion and volume shrinkage that accompanies carbonisation leads to materials-based resolution effects, which results in charcoals achieving relatively lower amplitudes than their wood counterparts. This wood/charcoal offset is critical as lower amplitudes lead to an inflation of summer rainfall by approximately 0.96 times, as observed in the calibration samples.
- A major limitation of the SPP demonstrated by the analysis of the modern samples is that the proxy may not be applicable to evergreen trees growing in environments that are both highly seasonal and water stressed. In these cases, seasonal growth cessation truncates growth and, by extension, seasonal amplitudes. Interestingly, this water stress phenomenon affected only the WRZ wood and charcoal samples. Corrections are essential here to evaluate if a sample is redeemable for further testing. While Camps Bay and Theronsberg (initially considered an outlier due to measured/modelled discrepancy) qualified for correction, but Gifberg was ultimately excluded due to absent growth cycles. This underscores the need for effective, reliable correction conditions and indicators of water stress (other than MAP which showed no correlation with mean $\delta^{13}C$) that can also be applied to archaeological samples.
- Related to this issue, the modern calibration reveals that the resolution effects described by Schubert and Jahren (2011) may manifest differently in South African evergreens, where reduced resolution from water stress may introduce more complex challenges than subsampling resolution alone. Subsampling resolution effects occur when inadequate subsample numbers fail to capture the full isotope signal, and this limitation can be corrected with existing equations. On the other hand, water stress resolution effects arise when growth ceases intermittently due to low moisture availability, a phenomenon evidently prevalent in South African trees. This cessation disrupts the SPP's assumption of continuous growth in evergreens, leading to an array of isotopic errors linked to environmental variability. Subsampling effects are analytical errors, decoupled from climate factors, whereas water stress effects are inherently tied to climatic factors. Water stress effects may fundamentally

distort seasonal isotope signals, emphasising the need to account for regional growth dynamics when applying the SPP to possibly water-stressed environments.

Future work should prioritise increasing sample replication across all rainfall zones to better capture natural variability and improve the robustness of high-resolution $\delta^{13}C$ as a rainfall seasonality proxy. Expanding replication will also help validate the applicability of findings beyond individual trees and strengthen confidence in regional climate interpretations.

Nevertheless, these findings highlight the importance and necessity of ground-truthing a proxy using modern samples prior to archaeological testing, a point emphasised by February (1990, 1992, 1994, 2000) for decades. Furthermore, the SPP has empirically established ecological links between different rainfall regimes and growth ring $\delta^{13}C$ values. This addresses a growing concern in palaeoclimate seasonality studies regarding the need for robust methods to distinguish rainfall zones (Fitchett & Bamford 2017; Fitchett 2019; Faith *et al.* 2024).

This ability is showcased in the preliminary archaeological results, where statistically significant differences were observed in the seasonal amplitudes calculated for the Boomplaas LGM (enhanced winter rainfall; P_S/P_W between 0.81 and 1.41) and the Waterfall Bluff LGIT (enhanced summer rainfall; P_S/P_W between 2.72 and 4.65). These seasonality attributions support the established paradigm of the eastward expansion of the WRZ during the LGM, driven by the growth of polar ice and the northward shift of the SH westerlies. Deglaciation prompted the westerlies to retract, allowing for greater influence of tropical forcing and a corresponding increase in summer rainfall in the eastern part of the country during the LGIT. Though promising, these results should be interpreted with caution until additional samples are analysed to confirm the observed trends.

This project forms part of the ongoing and evolving effort to capture the nature of seasonal rainfall shifts over glacial-interglacial cycles, from the perspective that these shifts had a bearing on the cultural and behaviour variability of hunter-gatherers occupying the subcontinent during the Late Pleistocene. The seasonal rainfall history of South Africa remains a subject of debate, and understanding how climatological seasonality interfaced with human seasonality presents an even greater challenge. Critical barriers to this understanding have stemmed from the limited availability of precise, high-resolution paleoclimate proxies. In response, this study contributes a high-resolution, quantitative, on-site proxy for rainfall seasonality. The hope is that this proxy will find a place in future archaeological investigations. The successful application of the SPP applied to archaeological charcoal

from both gymnosperms and angiosperms in South Africa demonstrates its broad applicability, and there is little reason to suggest it cannot be applied globally to sites where evergreen charcoal has been identified. Ultimately, this research has shown the significant potential to quantitatively reconstruct rainfall seasonality from the high-resolution carbon isotope signatures of archaeological charcoal – a rich but underutilised material.

REFERENCES

Abatzoglou, J.T., Dobrowski, S.Z., Parks, S.A. and Hegewisch, K.C. 2018. TerraClimate, a high-resolution global dataset of monthly climate and climatic water balance from 1958–2015. *Scientific data* 5(1): 1-12.

Aguilera, M., Espinar, C., Ferrio, J.P., Pérez, G. and Voltas, J. 2009. A map of autumn precipitation for the third millennium BP in the Eastern Iberian Peninsula from charcoal carbon isotopes. *Journal of Geochemical Exploration* 102(3): 157-165.

Aguilera, M., Ferrio, J.P., Pérez, G., Araus, J.L. and Voltas, J. 2012. Holocene changes in precipitation seasonality in the western Mediterranean Basin: a multi-species approach using δ13C of archaeobotanical remains. *Journal of Quaternary Science*, *27*(2), pp.192-202.

Allott, L.F. 2006. Archaeological charcoal as a window on palaeovegetation and wood-use during the Middle Stone Age at Sibudu Cave. *Southern African Humanities* 18(1): 173-201.

An, C.B., Dong, W., Li, H., Zhang, P., Zhao, Y., Zhao, X. and Yu, S.Y. 2015. Variability of the stable carbon isotope ratio in modern and archaeological millets: evidence from northern China. *Journal of Archaeological Science* 53: 316-322.

Antweiler, C. 2019. Local knowledge theory and methods: An urban model from Indonesia. In *Investigating Local Knowledge: New Directions, New Approaches*. P. Sillitoe, Ed. London: Routledge: 1–34.

Asherin, L. A., and Mata, S.A. 2000. Basic tree-ring sample preparation techniques for aging aspen. In *Sustaining Aspen in Western Landscapes: Symposium Proceedings.* (Proceedings RMRS-P-18). W.D. Shepperd, D. Binkley, D.L. Bartos, T.J. Stohlgren, L.G. Eskew, Compilers. Fort Collins, Colorado, U.S: Department of Agriculture, Forest Service, Rocky Mountain Research Station. 347-354.

Audiard, B., Blasco, T., Brossier, B., Fiorentino, G., Battipaglia, G. and Théry-Parisot, I. 2018. δ13C referential in three Pinus species for a first archaeological application to Paleolithic contexts:“Between intra-and inter-individual variation and carbonization effect”. *Journal of Archaeological Science: Reports* 20: 775-783.

Avery, D.M. 1982. Micromammals as palaeoenvironmental indicators and an interpretation of the late Quaternary in the southern Cape Province, South Africa. *Annals of the South African Museum* 85(2): 183–374.

Avery, D.M. 2004. Size variation in the common molerat *Cryptomys hottentotus* from southern Africa and its potential for palaeoenvironmental reconstruction. *Journal of Archaeological Science* 31(3): 273–282

Avery, G. and Underhill, L.G. 1986. Seasonal exploitation of seabirds by late Holocene coastal foragers: analysis of modern and archaeological data from the Western Cape, South Africa. *Journal of Archaeological Science* 13(4): 339-360.

Badeck, F.W., Tcherkez, G., Nogués, S., Piel, C. and Ghashghaie, J. 2005. Post-photosynthetic fractionation of stable carbon isotopes between plant organs—a widespread phenomenon.

Rapid Communications in Mass Spectrometry: An International Journal Devoted to the Rapid Dissemination of Up-to-the-Minute Research in Mass Spectrometry 19(11): 1381-1391.

Bamford, M.K. 2015. Charcoal from pre-Holocene Stratum 5, Wonderwerk Cave, South Africa. *Palaeoecology of Africa* 33: 153-174.

Barbour, M.M., Walcroft, A.S. and Farquhar, G.D. 2002. Seasonal variation in δ13C and δ18O of cellulose from growth rings of Pinus radiata. *Plant, Cell & Environment* 25(11): 1483-1499.

Baton, F., Tu, T.T.N., Derenne, S., Delorme, A., Delarue, F. and Dufraisse, A. 2017. Tree-ring δ13C of archeological charcoals as indicator of past climatic seasonality. A case study from the Neolithic settlements of Lake Chalain (Jura, France). *Quaternary international* 457: 50-59.

Baverstock, J.D. 2021. *Revisiting the dendroclimatological potential of Afrocarpus falcatus, South Africa*. University of KwaZulu-Natal, MSc Thesis.

Belmecheri, S., Wright, W.E. and Szejner, P. 2022. Sample Collection and Preparation for Annual and Intra-annual Tree-Ring Isotope Chronologies. In *Stable Isotopes in Tree Rings: Inferring Physiological, Climatic and Environmental Responses*. R.T.W. Siegwolf, J.R. Brooks, J. Roden, M. Saurer, Eds. Cham: Springer International. 103-134.

Berkes, F. and Berkes, M. 2009. Ecological complexity, fuzzy logic and holism in indigenous knowledge. *Futures* 41: 6-12.

Bhugeloo, A. 2014. *Assessing the dendrochronological and dendroclimatological potential of Acacia nilotica (L.) in northern KwaZulu-Natal*. University of KwaZulu- Natal, MSc Thesis.

Bird, M.I. and Ascough, P.L. 2012. Isotopes in pyrogenic carbon: A review. *Organic Geochemistry* 42(12): 1529-1539.

Botai, C.M., Botai, J.O., De Wit, J.P., Ncongwane, K.P. and Adeola, A.M. 2017. Drought characteristics over the western cape province, South Africa. Water 9(11):876.

Braadbaart, F. and Poole, I. 2008. Morphological, chemical and physical changes during charcoalification of wood and its relevance to archaeological contexts. *Journal of archaeological science* 35(9): 2434-2445.

Bradley, R.S. 2011. High Resolution Paleocliamtology. In *Dendroclimatology. Developments in Paleoenvironmental Research.* M. Hughes, T. Swetnam, H. Diaz, Eds. Dordrecht: Springer. 3-15.

Branscombe, T., Lee-Thorp, J., Schulting, R. and Leng, M. 2022. Micromilling vs hand drilling in stable isotope analyses of incremental carbonates: The potential for δ13C contamination by embedding resin. *Rapid Communications in Mass Spectrometry* 36(14): e9318.

Braun-Wimmer, J., Oertel, A., Schneider, L., Kahle, H.P. and Treydte, K. 2018. Effects of sample preparation on stable isotope measurements of tree rings. *20th EGU General Assembly Conference Abstracts*: 10242.

Braun, K., Bar-Matthews, M., Matthews, A., Ayalon, A., Cowling, R.M., Karkanas, P., Fisher, E.C., Dyez, K., Zilberman, T. and Marean, C.W. 2019. Late Pleistocene records of speleothem stable isotopic compositions from Pinnacle Point on the South African south coast. *Quaternary Research* 91(1): 265-288.

Brock, F., Higham, T., Ditchfield, P. and Ramsey, C.B. 2010. Current pretreatment methods for AMS radiocarbon dating at the Oxford Radiocarbon Accelerator Unit (ORAU). *Radiocarbon* 52(1): 103-112.

Burls, N.J., Blamey, R.C., Cash, B.A., Swenson, E.T., Fahad, A.A., Bopape, M.J.M., Straus, D.M. and Reason, C.J., 2019. The Cape Town "day zero" drought and Hadley cell expansion. *Npj Climate and Atmospheric Science* 2:27.

Butler, P.G., Scourse, J.D., Richardson, C.A., Wanamaker Jr, A.D., Bryant, C.L. and Bennell, J.D. 2009. Continuous marine radiocarbon reservoir calibration and the 13C Suess effect in the Irish Sea: Results from the first multi-centennial shell-based marine master chronology. *Earth and Planetary Science Letters* 279(3-4): 230-241.

Carlquist, S. 1977a. Ecological factors in wood evolution: A floristic approach. *American Journal of Botany* 64: 887-896.

Carlquist, S. 1977b. Wood anatomy of Peneaceae (Myrtales): Comparative, phylogenetic and ecological implications. *Botanical Journal of the Linnaean Society* 75: 211-227.

Carr, A.S., Thomas, D.S., Bateman, M.D., Meadows, M.E. and Chase, B. 2006. Late Quaternary palaeoenvironments of the winter-rainfall zone of southern Africa: palynological and sedimentological evidence from the Agulhas Plain. *Palaeogeography, Palaeoclimatology, Palaeoecology* 239(1-2):147-165.

Carter, P.L. 1970. Late Stone Age exploitation patterns in southern Natal. *The South African Archaeological Bulletin* 25(98): 55-58.

Carter, P.L. 1978. *The prehistory of eastern Lesotho*. University of Cambridge, PhD Thesis.

Cartwright, C. and Parkington, J. 1997. The wood charcoal assemblages from Elands Bay Cave, southwestern Cape: principles, procedures and preliminary interpretation. *The South African Archaeological Bulletin* 52: 59-72.

Cawe, S.G. 1994. Rainfall and vegetation patterns in Transkei and environs. *South African Journal of Science* 90(2): 79-85.

Chase, B.M. and Meadows, M.E. 2007. Late Quaternary dynamics of southern Africa's winter rainfall zone. *Earth-Science Reviews* 84(3-4): 103-138.

Chase, B.M., Boom, A., Carr, A.S. and Reimer, P.J. 2024. Tropical forcing and ENSO dominate Holocene climates in South Africa's southern Cape. *Quaternary Science Reviews* 330: 108563.

Chase, B.M., Boom, A., Carr, A.S., Chevalier, M., Quick, L.J., Verboom, G.A. and Reimer, P.J. 2019. Extreme hydroclimate response gradients within the western Cape Floristic region of South Africa since the Last Glacial Maximum. *Quaternary Science Reviews* 219: 297e307.

Chase, B.M., Boom, A., Carr, A.S., Meadows, M.E. and Reimer, P.J. 2013. Holocene climate change in southernmost South Africa: rock hyrax middens record shifts in the southern westerlies. *Quaternary Science Reviews* 82: 199-205.

Chase, B.M., Carr, A.S., Boom, A., Tyrrell, G. and Reimer, P.J. 2023. Linking upwelling intensity and orbital-scale climate variability in South Africa's winter rainfall zone: Insights from a∼ 70,000-year hyrax midden record. *Quaternary Science Advances* 12: 100110.

Chase, B.M., Chevalier, M., Boom, A. and Carr, A.S. 2017. The dynamic relationship between temperate and tropical circulation systems across South Africa since the last glacial maximum. *Quaternary Science Reviews* 174: 54-62.

Chase, B.M., Faith, J.T., Mackay, A., Chevalier, M., Carr, A.S., Boom, A., Lim, S., Reimer, P.J. 2018. Climatic controls on Later Stone Age human adaptation in Africa's southern Cape. *Journal of Human Evolution* 114: 35–44.

Chase, B.M., Lim, S., Chevalier, M., Boom, A., Carr, A.S., Meadows, M.E. and Reimer, P.J. 2015. Influence of tropical easterlies in southern Africa's winter rainfall zone during the Holocene. *Quaternary Science Reviews* 107: 138-148.

Chase, B.M., Quick, L.J., Meadows, M.E., Scott, L., Thomas, D.S. and Reimer, P.J. 2011. Late glacial interhemispheric climate dynamics revealed in South African hyrax middens. *Geology* 39(1): 19-22.

Chase, B.M., Scott, L., Meadows, M.E., Gil-Romera, G., Boom, A., Carr, A.S., Reimer, P.J., Truc, L., Valsecchi, V. and Quick, L.J. 2012. Rock hyrax middens: a palaeoenvironmental archive for southern African drylands. *Quaternary Science Reviews* 56: 107-125.

Chevalier, M. and Chase, B.M. 2015. Southeast African records reveal a coherent shift from high-to low-latitude forcing mechanisms along the east African margin across last glacial–interglacial transition. *Quaternary Science Reviews* 125: 117-130.

Chevalier, M., Chase, B.M., Quick, L.J. and Scott, L. 2021. An atlas of southern African pollen types and their climatic affinities. In *Quaternary Vegetation Dynamics*: *The African Pollen Database*. J. Runge, W.D. Gosling, A. Lézine, L. Scott, Eds. Leiden: CRC Press. 239-257.

Chevalier, M., Cheddadi, R. and Chase, B.M. 2014. CREST (Climate REconstruction SofTware): a probability density function (PDF)-based quantitative climate reconstruction method. *Climate of the Past* 10(6): 2081-2098.

Chikumbirike, J. and Bamford, M.K. 2021. A Southern African Perspective on the Contribution of Charcoal Analyses to Archaeology. In *Oxford Research Encyclopedia of Anthropology*.

Cowling, R.M., Cartwright, C.R., Parkington, J.E. and Allsopp, J.C. 1999. Fossil wood charcoal assemblages from Elands Bay Cave, South Africa: implications for Late Quaternary vegetation and climates in the winter-rainfall fynbos biome. *Journal of Biogeography* 26(2): 367-378.

Curtis, B.A., Tyson, P.D., Dyer, T.G.J. 1978. Dendrochronological age determination of *Podocarpus falcatus. South African Journal of Science* 74: 92–95.

Czimczik, C.I., Preston, C.M., Schmidt, M.W., Werner, R.A. and Schulze, E.D. 2002. Effects of charring on mass, organic carbon, and stable carbon isotope composition of wood. *Organic Geochemistry 33*(11): 1207-1223.

De Mil, T., Meko, M., Belmecheri, S., February, E., Therrell, M., Van den Bulcke, J. and Trouet, V. 2021. A lonely dot on the map: Exploring the climate signal in tree-ring density and stable isotopes of clanwilliam cedar, South Africa. *Dendrochronologia* 69: 125879.

Deacon, H.J. 1979. Excavations at Boomplaas cave-a sequence through the upper Pleistocene and Holocene in South Africa. *World Archaeology* 10(3): 241-257.

Deacon, H.J. and Deacon, J. 1999. Environments of the past. In. Human Beginnings in South Africa: Uncovering the Secrets of the Stone Age. Cape Town: David Philip Publishers. 9-29.

Deacon, H.J., Scholtz, A., Daitz, L.D., 1983. Fossil charcoals as a source of palaeoecological information in the fynbos region. In Fynbos Palaeoecology: A Preliminary Synthesis, South African National Scientific Programmes Report No 75. H.J. Deacon, Q.B. Hendey, J.J.N Lambrechts, Eds. Cape Town: Mills Litho. 174-182.

Deacon, J. 2023. Boomplaas Cave, South Africa. In *Handbook of Pleistocene Archaeology of Africa: Hominin behavior, geography, and chronology*. A. Beyin, D.K. Wright, J. Wilkins, D.L. Olzsewski, Eds. Cham: Springer. 1285-1295.

Deacon, J. and Lancaster, N. 1988. *Late Quaternary Palaeoenvironments of Southern Africa.* New York: Oxford University Press.

Deetz, James. 1977. *In Small Things Forgotten: The Archaeology of Early American Life*. 1st ed. New York: Anchor Press.

Diefendorf, A.F., Mueller, K.E., Wing, S.L., Koch, P.L. and Freeman, K.H. 2010. Global patterns in leaf 13C discrimination and implications for studies of past and future climate. *Proceedings of the National Academy of Sciences* 107(13): 5738-5743.

Dunwiddie, P.W., LaMarche, V.C. 1980. A climatically responsive tree-ring record from *Widdringtonia cedarbergensis*, Cape Province, South Africa. *Nature* 286: 796–797.

Ehleringer, J.R. 2005. The influence of atmospheric CO_2, temperature, and water on the abundance of C3/C4 taxa. In *A History of Atmospheric CO_2 and Its Effects on Plants, Animals, and Ecosystems*. J.R. Ehleringer, T.E. Cerling, M.D. Dearing, Eds. New York: Springer. 185–213.

Engelbrecht, C.J., Landman, W.A., Engelbrecht, F.A. and Malherbe, J. 2015. A synoptic decomposition of rainfall over the Cape south coast of South Africa. *Climate Dynamics* 44(9-10): 2589-2607.

Engelbrecht, F.A., Marean, C.W., Cowling, R.M., Engelbrecht, C.J., Neumann, F.H., Scott, L., Nkoana, R., O'Neal, D., Fisher, E., Shook, E. and Franklin, J. 2019. Downscaling last glacial maximum climate over southern Africa. *Quaternary Science Reviews* 226(105879): 1-28.

Esteban, I., Bamford, M.K., House, A., Miller, C.S., Neumann, F.H., Schefuß, E., Pargeter, J., Cawthra, H.C. and Fisher, E.C. 2020. Coastal palaeoenvironments and hunter-gatherer plant-use at Waterfall Bluff rock shelter in Mpondoland (South Africa) from MIS 3 to the Early Holocene. *Quaternary Science Reviews* 250: 106664.

Esteban, I., Cawthra, H.C., Pargeter, J. and Fisher, E.C. 2023a. Waterfall Bluff, South Africa. In *Handbook of Pleistocene Archaeology of Africa: Hominin behavior, geography, and chronology*. A. Beyin, D.K. Wright, J. Wilkins, D.L. Olzsewski, Eds. Cham: Springer. 1737-1748.

Esteban, L.G., de Palacios, P., Gasson, P., García-Iruela, A., García-Fernández, F. and García-Esteban, L. 2024. Hardwoods: Anatomy and Functionality of Their Elements—A Short Review. *Forests* 15(7): 1162.

Esteban, L.G., de Palacios, P., Heinz, I., Gasson, P., García-Iruela, A. and García-Fernández, F. 2023b. Softwood anatomy: a review. *Forests* 14(2): 323.

Evans, M.N. and Schrag, D.P. 2004. A stable isotope-based approach to tropical dendroclimatology. *Geochimica et Cosmochimica Acta* 68(16): 3295-3305.

Faith, J.T. 2013a. Taphonomic and paleoecological change in the large mammal sequence from Boomplaas Cave, Western Cape, South Africa. *Journal of Human Evolution* 65(6): 715–730.

Faith, J.T. 2013b. Ungulate diversity and precipitation history since the Last Glacial Maximum in the Western Cape, South Africa. *Quaternary Science Reviews* 68: 191–199.

Faith, J.T., Chase, B.M. and Avery, D.M. 2019. Late Quaternary micromammals and the precipitation history of the southern Cape, South Africa. *Quaternary Research* 91(2): 848-860.

Faith, J.T., Chase, B.M. and Pargeter, J. 2024. The Last Glacial Maximum climate at Boomplaas Cave, South Africa. *Quaternary Science Reviews* 329: 108557.

Farquhar, G.D. and Sharkey, T.D. 1982. Stomatal conductance and photosynthesis. *Annual Review of Plant Physiology* 33(1): 317-345.

Farquhar, G.D., Ehleringer, J.R. and Hubick, K.T. 1989. Carbon isotope discrimination and photosynthesis. *Annual Review of Plant Physiology and Plant Molecular Biology* 40(1): 503-537.

Favre, A., Philippon, N., Pohl, B., Kalognomou, E.A., Lennard, C., Hewitson, B., Nikulin, G., Dosio, A., Panitz, H.J. and Cerezo-Mota, R. 2016. Spatial distribution of precipitation annual cycles over South Africa in 10 CORDEX regional climate model present-day simulations. *Climate Dynamics* 46(5-6): 1799-1818.

February, E., van der Merwe, N.J. 1992. Stable carbon isotope ratios of wood charcoal during the last 4000 years: anthropogenic and climatic influences. *South African Journal of Science* 88: 291–292.

February, E.C. 1990. *Climatic reconstruction using wood charcoal from archaeological sites.* University of Cape Town, M.A. thesis.

February, E.C. 1992. *The analysis of xylem anatomy of wood charcoal in archaeological deposits as a tool in climatic reconstruction.* Report to the Water Research Commission: The reconstruction of the climatic history of the last 2000 years in the summer rainfall area of South Africa. South African Museum, Cape Town.

February, E.C. 1994. Rainfall reconstruction using wood charcoal from two archaeological sites in South Africa. *Quaternary Research* 42(1): 100-107.

February, E.C. 1996. Plant xylem anatomy, dendrochronology and stable carbon isotopes as tools in rainfall reconstruction in Southern Africa. University of Cape Town, DPhil thesis.

February, E.C. 2000. Archaeological charcoal and dendrochronology to reconstruct past environments of southern Africa. *South African Journal of Science* 96(3): 111-115.

February, E.C. and Gagen, M. 2003. A dendrochronological assessment of two South African Widdringtonia species. *South African Journal of Botany* 69(3): 428-433.

February, E.C. and Stock, W.D. 1998a. The relationship between ring width measures and precipitation for Widdringtonia cedarbergensis. *South African Journal of Botany* 64(3): 213-216.

February, E.C. and Stock W.D., 1998b. An assessment of the dendrochronological potential of two *Podocarpus* species. *The Holocene* 8(6): 747-750.

February, E.C. and Stock, W.D. 1999. Declining trend in the 13C/12C ratio of atmospheric carbon dioxide from tree rings of South African Widdringtonia cedarbergensis. *Quaternary Research* 52(2): 229-236.

February, E.C., Mader, A.D. and Bond, W.J. 2006. Age determination of two South African Acacia species using ring counts and radiocarbon dating. *African Journal of Ecology* 44(3): 417-419.

Feng, X., Porporato, A. and Rodriguez-Iturbe, I. 2013. Changes in rainfall seasonality in the tropics. *Nature Climate Change* 3(9): 811-815.

Ferrio, J.P., Alonso, N., López, J.B., Araus, J.L. and Voltas, J. 2006. Carbon isotope composition of fossil charcoal reveals aridity changes in the NW Mediterranean Basin. *Global Change Biology* 12(7): 1253-1266.

Fick, S.E. and Hijmans, R.J. 2017. WorldClim 2: new 1-km spatial resolution climate surfaces for global land areas. *International Journal of Climatology* 37(12): 4302-4315.

Fiorentino, G., Ferrio, J.P., Bogaard, A., Araus, J.L. and Riehl, S. 2015. Stable isotopes in archaeobotanical research. *Vegetation History and Archaeobotany* 24(1): 215-227.

Fisher, E.C., Cawthra, H.C., Esteban, I., Jerardino, A., Neumann, F.H., Oertle, A., Pargeter, J., Saktura, R.B., Szabó, K., Winkler, S. and Zohar, I. 2020. Coastal occupation and foraging during the last glacial maximum and early Holocene at Waterfall Bluff, eastern Pondoland, South Africa. *Quaternary Research 97*: 1-41.

Fitchett, J.M. 2019. The Holocene Climates of South Africa. In *The Geography of South Africa: Contemporary Changes and New Directions*. J. Knight and C.M. Rogerson, Eds. Cham: Springer. 47-55.

Fitchett, J.M. and Bamford, M.K. 2017. The validity of the Asteraceae: Poaceae fossil pollen ratio in discrimination of the southern African summer-and winter-rainfall zones. *Quaternary Science Reviews* 160: 85-95.

Fitchett, J.M., Grab, S.W., Bamford, M.K. and Mackay, A.W. 2017. Late Quaternary research in southern Africa: progress, challenges and future trajectories. *Transactions of the Royal Society of South Africa* 72(3): 280-293.

Fonti, M.V., Vaganov, E.A., Wirth, C., Shashkin, A.V., Astrakhantseva, N.V. and Schulze, E.D. 2018. Age-effect on intra-annual δ13C-variability within Scots pine tree-rings from Central Siberia. *Forests* 9(6): 364.

Forbes, M.S., Raison, R.J., Skjemstad, J.O. 2006. Formation, transformation and transport of black carbon (charcoal) in terrestrial and aquatic ecosystems. *Science of the Total Environment* 370(1): 190–206.

Forssman, T. 2019. A review of hunter-gatherers in Later Stone Age research in southern Africa. *Goodwin Series* 12: 56-68.

Frank, D., Fang, K. and Fonti, P. 2022. Dendrochronology: Fundamentals and Innovations. In *Stable Isotopes in Tree Rings: Inferring Physiological, Climatic and Environmental Responses*. R.T.W. Siegwolf, J.R. Brooks, J. Roden, M. Saurer, Eds. Cham: Springer International. 21-59.

Fritts, H.C. 1976. Tree Rings and Climate. London: Academic Press.

Gagen, M., McCarroll, D., Loader, N.J., Robertson, I. 2011. Stable Isotopes in Dendroclimatology: Moving Beyond 'Potential'. In *Dendroclimatology: Developments in Paleoenvironmental Research*, vol 11. M. Hughes, T Swetnam, H. Diaz, Eds. Dordrecht: Springer. 147-172.

Galiano, L., Timofeeva, G., Saurer, M., Siegwolf, R., Martínez-Vilalta, J., Hommel, R. and Gessler, A. 2017. The fate of recently fixed carbon after drought release: towards unravelling C storage regulation in Tilia platyphyllos and Pinus sylvestris. *Plant, Cell & Environment* 40(9): 1711-1724.

Gebrekirstos, A., Bräuning, A., Sass-Klassen, U. and Mbow, C. 2014. Opportunities and applications of dendrochronology in Africa. *Current Opinion in Environmental Sustainability* 6: 48-53.

George, S.S. 2014. An overview of tree-ring width records across the Northern Hemisphere. *Quaternary Science Reviews 95:* 132-150.

Gessler, A., Ferrio, J.P., Hommel, R., Treydte, K., Werner, R.A. and Monson, R.K. 2014. Stable isotopes in tree rings: towards a mechanistic understanding of isotope fractionation and mixing processes from the leaves to the wood. *Tree Physiology* 34(8): 796-818.

Godwin, H. and Tansley, A.G. 1941. Prehistoric charcoals as evidence of former vegetation, soil and climate. *Journal of Ecology* 29(1): 117-126.

Gourlay, I.D. 1995a. The definition of seasonal growth zones in some African Acacia species-a review. *IAWA Journal* 16(4): 353-359.

Gourlay, I.D. 1995b. Growth ring characteristics of some African Acacia species. *Journal of tropical ecology* 11(1): 121-140.

Govaerts, R., Nic Lughadha, E., Black, N., Turner, R. and Paton, A. 2021. The World Checklist of Vascular Plants, a continuously updated resource for exploring global plant diversity. *Scientific Data* 8(1): 215.

Green, H., Pickering, R., Drysdale, R., Johnson, B.C., Hellstrom, J. and Wallace, M. 2015. Evidence for global teleconnections in a late Pleistocene speleothem record of water balance and vegetation change at Sudwala Cave, South Africa. *Quaternary Science Reviews* 110: 114-130.

Grissino-Mayer, H.D. 2003. A manual and tutorial for the proper use of an increment borer. *Tree-Ring Research* 59: 63–79

Groover, A., and Rosbischon, M. 2006. Developmental mechanisms regulating secondary growth in woody plants. *Current Opinion in Plant Biology* 9: 55–58.

Guo, J., Zong, X., de Winter, N.J., Goudsmit-Harzevoort, B., Peterse, F. and Ziegler, M. 2023. Assessing the effects of embedding resins on carbonate stable and clumped isotope analyses. *Rapid Communications in Mass Spectrometry* 37(17): e9597.

Guo, X., Peng, C., Li, T., Huang, J., Song, H., Zhu, Q. and Wang, M. 2021. The effects of drought and re-watering on non-structural carbohydrates of Pinus tabulaeformis seedlings. *Biology* 10(4): 281.

Hall, G., Woodborne, S. and Pienaar, M. 2009. Rainfall control of the δ13C ratios of Mimusops caffra from KwaZulu-Natal, South Africa. *The Holocene* 19(2): 251-260.

Hall, G., Woodborne, S. and Scholes, M. 2008. Stable carbon isotope ratios from archaeological charcoal as palaeoenvironmental indicators. *Chemical Geology* 247(3-4): 384-400.

Hall, M. 1976. Dendroclimatology, rainfall and human adaptation in the later Iron Age of Natal and Zululand. *Annals of the Natal Museum* 22: 693–703.

Hare, V.J. and Lavergne, A. 2021. Differences in carbon isotope discrimination between angiosperm and gymnosperm woody plants, and their geological significance. *Geochimica et Cosmochimica Acta 300:* 215-230.

Hare, V.J., Loftus, E., Jeffrey, A. and Ramsey, C.B. 2018. Atmospheric CO2 effect on stable carbon isotope composition of terrestrial fossil archives. *Nature Communications* 9(1): 252.

Heinrich, I. and Allen, K. 2013. Current Issues and Recent Advances in Australian Dendrochronology: Where to Next? *Geographical Research* 51(2): 180-191.

Helle, G. and Schleser, G.H. 2004. Beyond CO2-fixation by Rubisco–an interpretation of 13C/12C variations in tree rings from novel intra-seasonal studies on broad-leaf trees. *Plant, Cell & Environment* 27(3): 367-380.

Helle, G., Pauly, M., Heinrich, I., Schollän, K., Balanzategui, D. and Schürheck, L. 2022. Stable isotope Signatures of Wood, its Constituents and Methods of Cellulose Extraction. In *Stable Isotopes in Tree Rings: Inferring Physiological, Climatic and Environmental Responses*. R.T.W. Siegwolf, J.R. Brooks, J. Roden, M. Saurer, Eds. Cham: Springer International. 135-190..

Herbert, A.V. and Fitchett, J.M. 2021. Quantifying late Quaternary Australian rainfall seasonality changes using the Poaceae: Asteraceae pollen ratio. *Quaternary Research* 102: 24-38.

Herbert, A.V. and Fitchett, J.M. 2022. Palaeoclimate dynamics within the Summer Rainfall Zone of South Africa. *Palaeogeography, Palaeoclimatology, Palaeoecology* 601: 111134.

Hillis, W.E. 1987. *Heartwood and Tree Exudates*. Berlin: Springer Verlag.

Hirons, A. and Thomas, P.A. 2018. *Applied Tree Biology*. John Wiley & Sons.

Holmgren, K., Lee-Thorp, J.A., Cooper, G.R., Lundblad, K., Partridge, T.C., Scott, L., Sithaldeen, R., Talma, A.S. and Tyson, P.D. 2003. Persistent millennial-scale climatic variability over the past 25,000 years in Southern Africa. *Quaternary Science Reviews* 22(21-22): 2311-2326.

House, A., Bamford, M.K. and Chikumbirike, J. 2022. Charcoal from Holocene deposits at Wonderwerk Cave, South Africa: A source of palaeoclimate information. *Quaternary International* 614: 73-83.

Hughes, M.K., Kelly, P.M., Pilcher, J.R. and LaMarche, V.C., Eds. 1982. Climate From Tree Rings. Cambridge: Cambridge University Press.

Humphreys, A.J. 2005. De-! kunging'the Later Stone Age of the central interior of South Africa. *Southern African Field Archaeology* 13(14): 36-41.

Humphreys, A.J. 2007. Behavioural ecology and hunter-gatherers: from the Kalahari to the Later Stone Age. *South African Archaeological Bulletin* 62(186): 98-103.

Humphreys, A.J.B. 1987. Prehistoric seasonal mobility: what are we really achieving? *The South African Archaeological Bulletin* 4(145)*:* 34-38.

Jones, P.D., Briffa, K.R., Osborn, T.J., Lough, J.M., van Ommen, T.D., Vinther, B.M., Luterbacher, J., Wahl, E.R., Zwiers, F.W., Mann, M.E., Schmidt, G.A., Ammann, C.M., Buckley, B.M., Cobb, K.M., Esper, J., Goosse, H., Graham, N., Jansen, E., Kiefer, T., Kull, C., Küttel, M., Mosley-Thompson, E., Overpeck, J.T., Riedwyl, N., Schulz, M., Tudhope, A.W., Villalba, R., Wanner, H., Wolff, E., Xoplaki, E. 2009. High-resolution palaeoclimatology of the last millennium: a review of current status and future prospects. *The Holocene* 19: 3–49.

Judd, E.J., Ivany, L.C., DeConto, R.M., Halberstadt, A.R.W., Miklus, N.M., Junium, C.K. and Uveges, B.T. 2019. Seasonally resolved proxy data from the Antarctic Peninsula support a heterogeneous middle Eocene Southern Ocean. *Paleoceanography and Paleoclimatology* 34(5): 787-799.

Kabukcu, C. 2018. Wood charcoal analysis in archaeology. In *Environmental Archaeology*. E. Pişkin, A. Marciniak and M. Bartkowiak, Eds. Cham: Springer. 133-154.

Kagawa, A. and Battipaglia, G. 2022. Post-photosynthetic Carbon, Oxygen and Hydrogen Isotope Signal Transfer to Tree Rings—How Timing of Cell Formations and Turnover of Stored Carbohydrates Affect Intra-Annual Isotope Variations. In *Stable Isotopes in Tree Rings: Inferring Physiological, Climatic and Environmental Responses*. R.T.W. Siegwolf, J.R. Brooks, J. Roden, M. Saurer, Eds. Cham: Springer International. 429-462.

Kagawa, A., Sugimoto, A. and Maximov, T.C. 2006. Seasonal course of translocation, storage and remobilization of 13C pulse-labeled photoassimilate in naturally growing Larix gmelinii saplings. *New Phytologist* 171(4): 793-804.

Keeling, R.F. and Graven, H.D. 2021. Insights from time series of atmospheric carbon dioxide and related tracers. *Annual Review of Environment and Resources* 46(1): 85-110.

Kelly, R.L. 1983. Hunter-gatherer mobility strategies. Journal of Anthropological Research 39(3): 277-306.

Kelly, R.L. 2013. *The Lifeways of Hunter Gatherers: The Foraging Spectrum.* Cambridge University Press: Cambridge

Klein, R.G. 1978. A preliminary report on the larger mammals from the Boomplaas Stone Age cave site, Cango Valley, Oudtshoorn District, South Africa. *The South African Archaeological Bulletin* 33(127): 66-75.

Klein, R.G. 1983. Palaeoenvironmental implications of Quaternary large mammals in the fynbos region. In: *Fynbos Palaeoecology: A Preliminary Synthesis. South African National Scientific Programmes Report No. 75*. H.J. Deacon, Q.B. Hendey, J.J.N. Lambrechts, Eds. Cape Town: Mills Litho: 116–138.

Knight, J. and Fitchett, J.M. 2019. Climate change during the late quaternary in South Africa. In *The Geography of South Africa: Contemporary Changes and New Directions*. J. Knight and C.M. Rogerson, Eds. Cham: Springer. 37-45.

Kohn, M.J. 2010. Carbon isotope compositions of terrestrial C3 plants as indicators of (paleo) ecology and (paleo) climate. *Proceedings of the National Academy of Sciences* 107(46): 19691-19695.

Kruger, A.C. 2006. Observed trends in daily precipitation indices in South Africa: 1910–2004. *International Journal of Climatology: A Journal of the Royal Meteorological Society* 26(15): 2275-2285.

Kwiecien, O., Braun, T., Brunello, C.F., Faulkner, P., Hausmann, N., Helle, G., Hoggarth, J.A., Ionita, M., Jazwa, C.S., Kelmelis, S. and Marwan, N. 2022. What we talk about when we talk about seasonality–A transdisciplinary review. *Earth-Science Reviews* 225: 103843.

Landman, W.A., Malherbe, J., and Engelbrecht, F. 2017. South Africa's present-day climate. In *Understanding the Social and Environmental Implications of Global Change*. J. Mambo and K. Faccer, Eds. Stellenbosch: Africa Sun Media. 7–12.

Leavitt, S.W. 2002. Prospects for reconstruction of seasonal environment from tree-ring δ13C: baseline findings from the Great Lakes area, USA. *Chemical Geology* 192(1-2): 47-58.

Leavitt, S.W. 2010. Tree-ring C–H–O isotope variability and sampling. *Science of the Total Environment* 408(22): 5244-5253.

Leavitt, S.W. and Long, A. 1986. Stable-carbon isotope variability in tree foliage and wood. *Ecology* 67(4): 1002-1010.

Leavitt, S.W. and Long, A. 1991. Seasonal stable-carbon isotope variability in tree rings: possible palaeoenvironmental signals. *Chemical Geology* 87: 59–70.

Leavitt, S.W. and Szejner, P. 2022. Intra-annual tree-ring isotope variations: do they occur when environment remains constant?. *Trees*, *36*(3), pp.865-868.

Lee-Thorp, J.A. and Beaumont, P.B. 1995. Vegetation and seasonality shifts during the late Quaternary deduced from 13C/12C ratios of grazers at Equus Cave, South Africa. *Quaternary Research* 43(3): 426-432.

Lee, R. B. 1979. *The !Kung San: Man, Women and Work in a Foraging Society*. New York: Cambridge University Press.

Lennard, C. and Hegerl, G. 2015. Relating changes in synoptic circulation to the surface rainfall response using self-organising maps. *Climate Dynamics* 44: 861-879.

Lennox, S.J. and Wadley, L. 2019. A charcoal study from the Middle Stone Age, 77,000 to 65,000 years ago, at Sibudu, KwaZulu-Natal. *Transactions of the Royal Society of South Africa* 74(1): 38-54.

Lester, L.A. 2019. *Exploratory investigation of extending rainfall records in the Western Cape by means of dendroclimatology*. Stellenbosch University, M.Eng Thesis.

Li, G., Gao, L., Liu, F., Qiu, M. and Dong, G. 2022. Quantitative studies on charcoalification: Physical and chemical changes of charring wood. *Fundamental Research* 4(1): 113-122.

Lilly, M.A. 1977. *An assessment of the dendrochronological potential of indigenous tree species in South Africa*. Occasional Paper No. 18. Department of Geography and Environmental Studies, University of the Witwatersrand, Johannesburg.

Loader, N.J., Robertson, I. and McCarroll, D. 2003. Comparison of stable carbon isotope ratios in the whole wood, cellulose and lignin of oak tree-rings. *Palaeogeography, Palaeoclimatology, Palaeoecology* 196(3-4):395-407.

Loader, N.J., Switsur, V.R. and Field, E.M. 1995. High-resolution stable isotope analysis of tree rings: implications of'microdendroclimatology'for palaeoenvironmental research. *The Holocene* 5(4): 457-460.

Loftus, E., Lee-Thorp, J., Leng, M., Marean, C. and Sealy, J. 2019. Seasonal scheduling of shellfish collection in the Middle and Later Stone Ages of southern Africa. *Journal of Human Evolution* 128: 1-16.

Lukich, V. and Ecker, M. 2022. Pleistocene environments in the southern Kalahari of South Africa. *Quaternary International* 614: 50-58.

Mahlalela, P.T., Blamey, R.C. and Reason, C.J.C. 2019. Mechanisms behind early winter rainfall variability in the southwestern Cape, South Africa. Climate Dynamics, 53: 21-39.

Marean, C.W., Cawthra, H.C., Cowling, R.M., Esler, K.J., Fisher, E., Milewski, A., Potts, A.J., Singels, E. and De Vynck, J. 2014. Stone Age people in a changing South African Greater Cape Floristic Region. In *Fynbos: Ecology, Evolution, and Conservation of a Megadiverse Region.* N. Allsopp, J.F. Colville and G.A. Verboom, Eds. Oxford: Oxford University Press. 164-199.

McCarroll, D. and Loader, N.J. 2004. Stable isotopes in tree rings. *Quaternary Science Reviews* 23(7-8): 771-801.

McNaughton, J., Tyson, P.O. 1979. A Preliminary Assessment of *Podocarpus falcatus* in Dendrochronological and Dendroclimatological Studies in the Witelsbos Forest Reserve. *South African Forestry Journal* 11: 29–33.

Midgley, J.C. 2002. *A dendrochronological investigation of Pinus radiata from Silvermine Nature Reserve.* University of Cape Town, Hons Thesis.

Miller, C., Finch, J., Hill, T., Peterse, F., Humphries, M., Zabel, M. and Schefuß, E. 2019. Late Quaternary climate variability at Mfabeni peatland, eastern South Africa. *Climate of the Past* 15(3): 1153-1170.

Mills, S.C., Grab, S.W., Rea, B.R., Carr, S.J. and Farrow, A. 2012. Shifting westerlies and precipitation patterns during the Late Pleistocene in southern Africa determined using glacier reconstruction and mass balance modelling. *Quaternary Science Reviews* 55: 145-159.

Milner, N. 1999. Pitfalls and problems in analysing and interpreting the seasonality of faunal remains. *Archaeological Review from Cambridge* 16: 51-67.

Mitchell, P. 2002. *The Archaeology of Southern Africa*. Cambridge: Cambridge University Press.

Mitchell, P. J. 2005. Modelling Later Stone Age societies in southern Africa. In *African Archaeology: A Critical Introduction.* A. Stahl, Ed. Blackwell. 250-273

Mouraux, C., Delarue, F., Bardin, J., Nguyen Tu, T.T., Bellot-Gurlet, L., Paris, C., Coubray, S. and Dufraisse, A. 2022. Assessing the carbonisation temperatures recorded by ancient charcoals for δ13C-based palaeoclimate reconstruction. *Scientific Reports* 12(1): 14662.

Mucina, L., Scott-Shaw, C.R., Rutherford, M.C., Camp, K.G., Matthews, W.S., Powrie, L.W. and Hoare, D.B. 2006. Indian Ocean Coastal Belt. In *The Vegetation of South Africa, Lesotho and Swaziland.* L. Mucina, M.C. Rutherford, Eds. Pretoria: African National Biodiversity Institute. 568-583.

Ndebele, N.E., Grab, S. and Turasie, A. 2020. Characterizing rainfall in the south-western Cape, South Africa: 1841–2016. *International Journal of Climatology* 40(4): 1992-2014.

Neumann, F.H., Botha, G.A. and Scott, L. 2014. 18,000 years of grassland evolution in the summer rainfall region of South Africa: evidence from Mahwaqa Mountain, KwaZulu-Natal. *Vegetation History and Archaeobotany* 23: 665-681.

Norström, E., Holmgren, K. and Mörth, C.M. 2008. A 600-year-long δ18O record from cellulose of Breonadia salicina trees, South Africa. *Dendrochronologia* 26(1): 21-33.

Norström, E., Holmgren, K. and Morth, C.M., 2005. Rainfall-driven variations in δ13C composition and wood anatomy of Breonadia salicina trees from South Africa between AD 1375 and 1995. *South African Journal of Science* 101(3): 162-168.

Nott, M. and Thondhlana, G. 2017. Fuelwood preferences, use and availability in the# Khomani San resettlement farms, southern Kalahari, South Africa. *Forests, Trees and Livelihoods* 26(3): 156-169.
Ohashi, S., Okada, N., Nobuchi, T., Siripatanadilok, S. and Veenin, T. 2009. Detecting invisible growth rings of trees in seasonally dry forests in Thailand: isotopic and wood anatomical approaches. *Trees* 23(4): 813-822.

Ohashi, S., Okada, N., Nobuchi, T., Siripatanadilok, S. and Veenin, T. 2009. Detecting invisible growth rings of trees in seasonally dry forests in Thailand: isotopic and wood anatomical approaches. *Trees* 23(4): 813-822.

Orlove, B., Roncoli, C., Kabugo, M. and Majugu, A. 2010. Indigenous climate knowledge in southern Uganda: the multiple components of a dynamic regional system. *Climatic Change* 100: 243-265.

Otto, F.E., Wolski, P., Lehner, F., Tebaldi, C., Van Oldenborgh, G.J., Hogesteeger, S., Singh, R., Holden, P., Fučkar, N.S., Odoulami, R.C. and New, M. 2018. Anthropogenic influence on the drivers of the Western Cape drought 2015–2017. *Environmental Research Letters* 13(12): 124010.

Paradis-Grenouillet, S. and Dufraisse, A. 2018. Deciduous oak/chestnut: Differential shrinkage of wood during charcoalification? Preliminary experimental results and implications for wood diameter study in anthracology. *Quaternary International* 463: 258-267.

Pargeter, J. and Faith, J.T. 2020. Lithic miniaturization as adaptive strategy: a case study from Boomplaas Cave, South Africa. *Archaeological and Anthropological Sciences* 12(9): 225.

Pargeter, J., Loftus, E., Mackay, A., Mitchell, P. and Stewart, B. 2018. New ages from Boomplaas Cave, South Africa, provide increased resolution on late/terminal Pleistocene human behavioural variability. *Azania: Archaeological Research in Africa* 53(2): 156-184.

Parkington, J. 1972. Seasonal mobility in the late stone age. *African Studies* 31(4): 223-244.

Parkington, J. 2001. Presidential address: Mobility, seasonality and southern African hunter-gatherers. *The South African Archaeological Bulletin* 56(173/174): 1-7.

Pascale, S., Kapnick, S.B., Delworth, T.L. and Cooke, W.F. 2020. Increasing risk of another Cape Town "Day Zero" drought in the 21st century. Proceedings of the National Academy of Sciences 117(47): 29495-29503.

Patalano R, Roberts P. 2021. Climate Proxies. In *The Encyclopedia of Ancient History: Asia and Africa.* E. Harkness, R.J. McIntosh, J. Neelis, D.T. Potts, Eds. Hoboken: Wiley-Blackwell. 1-5.

Patrut, A., Woodborne, S., Von Reden, K.F., Hall, G., Hofmeyr, M., Lowy, D.A. and Patrut, R.T. 2015. African baobabs with false inner cavities: the radiocarbon investigation of the Lebombo Eco Trail baobab. *PLoS One* 10(1): e0117193.

Pearl, J.K., Keck, J.R., Tintor, W., Siekacz, L., Herrick, H.M., Meko, M.D. and Pearson, C.L. 2020. New frontiers in tree-ring research. *The Holocene* 30(6): 923-941.

Pflug, E.E., Siegwolf, R., Buchmann, N., Dobbertin, M., Kuster, T.M., Günthardt-Goerg, M.S. and Arend, M. 2015. Growth cessation uncouples isotopic signals in leaves and tree rings of drought-exposed oak trees. *Tree Physiology* 35(10): 1095-1105.

Pons, T.L. and Helle, G. 2011. Identification of anatomically non-distinct annual rings in tropical trees using stable isotopes. *Trees* 25(1): 83-93.

Poussart, P.F., Evans, M.N. and Schrag, D.P. 2004. Resolving seasonality in tropical trees: multi-decade, high-resolution oxygen and carbon isotope records from Indonesia and Thailand. *Earth and Planetary Science Letters* 218(3-4): 301-316.

Prendergast, A.L., Pryor, A.J., Reade, H. and Stevens, R.E. 2018. Seasonal records of palaeoenvironmental change and resource use from archaeological assemblages. *Journal of Archaeological Science: Reports* 21: 1191-1197.

Quick, L.J., Chase, B.M., Carr, A.S., Chevalier, M., Grobler, B.A. and Meadows, M.E. 2022. A 25,000 year record of climate and vegetation change from the southwestern Cape coast, South Africa. *Quaternary Research* 105: 82-99.

Rathgeber, C.B., Pérez-de-Lis, G., Fernández-de-Uña, L., Fonti, P., Rossi, S., Treydte, K., Gessler, A., Deslauriers, A., Fonti, M.V. and Ponton, S. 2022. Anatomical, Developmental and Physiological Bases of Tree-Ring Formation in Relation to Environmental Factors. In *Stable Isotopes in Tree Rings: Inferring Physiological, Climatic and Environmental Responses*. R.T.W. Siegwolf, J.R. Brooks, J. Roden, M. Saurer, Eds. Cham: Springer International. 61-99.

Reason, C.J.C., Rouault, M., Melice, J.L. and Jagadheesha, D. 2002. Interannual winter rainfall variability in SW South Africa and large scale ocean–atmosphere interactions. *Meteorology and Atmospheric Physics* 80: 19-29.

Roberts, P., Henshilwood, C.S., van Niekerk, K.L., Keene, P., Gledhill, A., Reynard, J., Badenhorst, S. and Lee-Thorp, J. 2016. Climate, environment and early human innovation: stable isotope and faunal proxy evidence from archaeological sites (98-59ka) in the southern Cape, South Africa. *PLoS One* 11(7): e0157408.

Robertson, I., Loader, N.J., Froyd, C.A., Zambatis, N., Whyte, I. and Woodborne, S. 2006. The potential of the baobab (Adansonia digitata L.) as a proxy climate archive. *Applied Geochemistry* 21(10): 1674-1680.

Roffe, S.J., Fitchett, J.M. and Curtis, C.J. 2019. Classifying and mapping rainfall seasonality in South Africa: A review. *South African Geographical Journal* 101(2): 158-174.

Roffe, S.J., Fitchett, J.M. and Curtis, C.J. 2020. Determining the utility of a percentile-based wet-season start-and end-date metrics across South Africa. *Theoretical and Applied Climatology* 140(3): 1331-1347.

Roffe, S.J., Fitchett, J.M. and Curtis, C.J. 2021a. Investigating changes in rainfall seasonality across South Africa: 1987–2016. *International Journal of Climatology* 41(S1): E2031-E2050.

Roffe, S.J., Fitchett, J.M. and Curtis, C.J. 2021b. Quantifying rainfall seasonality across South Africa on the basis of the relationship between rainfall and temperature. *Climate Dynamics* 56(7): 2431-2450.

Roffe, S.J., Steinkopf, J. and Fitchett, J.M. 2022. South African winter rainfall zone shifts: a comparison of seasonality metrics for Cape Town from 1841–1899 and 1933–2020. *Theoretical and Applied Climatology* 147(3): 1229-1247.

Saha, M.V., Scanlon, T.M. and D'Odorico, P. 2018. Climate seasonality as an essential predictor of global fire activity. *Global Ecology and Biogeography* 28(2): 198-210.

Salisbury, E.J. and Jane, F.W. 1940. Charcoals from Maiden Castle and their significance in relation to the vegetation and climatic conditions in prehistoric times*. The Journal of Ecology* 28(2): 310-325.

Sarris, D., Siegwolf, R. and Körner, C. 2013. Inter-and intra-annual stable carbon and oxygen isotope signals in response to drought in Mediterranean pines. *Agricultural and Forest Meteorology* 168: 59-68.

Savard, M.M. and Daux, V. 2020. An overview on isotopic divergences–causes for instability of tree-ring isotopes and climate correlations. *Climate of the Past* 16(4): 1223-1243.

Schollaen, K., Baschek, H., Heinrich, I., Slotta, F., Pauly, M. and Helle, G. 2017. A guideline for sample preparation in modern tree-ring stable isotope research. *Dendrochronologia* 44: 133-145.

Scholtz, A. 1986. *Palynological and palaeobotanical studies in the southern Cape.* University of Stellenbosch, M.A. thesis.

Schubert, B.A. and Jahren, A.H. 2011. Quantifying seasonal precipitation using high-resolution carbon isotope analyses in evergreen wood. *Geochimica et Cosmochimica Acta* 75(22): 7291-7303.

Schubert, B.A. and Jahren, A.H. 2012. The effect of atmospheric CO2 concentration on carbon isotope fractionation in C3 land plants. *Geochimica et Cosmochimica Acta 96:* 29-43.

Schubert, B.A. and Timmermann, A. 2015. Reconstruction of seasonal precipitation in Hawai'i using high-resolution carbon isotope measurements across tree rings. *Chemical Geology* 417: 273-278.

Schubert, B.A., Jahren, A.H., Davydov, S.P. and Warny, S. 2017. The transitional climate of the late Miocene Arctic: Winter-dominated precipitation with high seasonal variability. *Geology* 45(5): 447-450.

Schubert, B.A., Jahren, A.H., Eberle, J.J., Sternberg, L.S. and Eberth, D.A. 2012. A summertime rainy season in the Arctic forests of the Eocene. *Geology* 40(6): 523-526.

Schweingruber, F.H. 1988. *Tree Rings: Basics and Applications of Dendrochronology*. Dordrecht: Kluwer Academic Publishers.

Scott, A.C. and Damblon, F. 2010. Charcoal: Taphonomy and significance in geology, botany and archaeology. *Palaeogeography, Palaeoclimatology, Palaeoecology* 291(1-2): 1-10.

Scott, L. 2002. Grassland development under glacial and interglacial conditions in southern Africa: review of pollen, phytolith and isotope evidence. *Palaeogeography, Palaeoclimatology, Palaeoecology* 177(1-2): 47-57.

Scott, L., Sobol, M., Neumann, F.H., Romera, G.G., Fernández-Jalvo, Y., Bousman, C.B., Horwitz, L.K. and Van Aardt, A.C. 2022. Late Quaternary palaeoenvironments in the central semi-arid region of South Africa from pollen in cave, pan, spring, stream and dung deposits. *Quaternary International* 614: 84-97.

Sealy, J. 2006. Diet, mobility, and settlement pattern among Holocene hunter-gatherers in southernmost Africa. *Current Anthropology* 47(4): 569-595.

Sealy, J., Lee-Thorp, J., Loftus, E., Faith, J.T. and Marean, C.W. 2016. Late Quaternary environmental change in the Southern Cape, South Africa, from stable carbon and oxygen isotopes in faunal tooth enamel from Boomplaas Cave. *Journal of Quaternary Science* 31(8): 919-927.

Sealy, J.C., Van der Merwe, N.J., Hobson, K.A., Horton, D.R., Lewis, R.B., Parkington, J., Robertshaw, P. and Schwarcz, H.P. 1986. Isotope assessment and the seasonal-mobility hypothesis in the Southwestern Cape of South Africa [and comments and replies]. *Current Anthropology* 27(2): 135-150.

Sheldon, N.D., Smith, S.Y., Stein, R. and Ng, M. 2020. Carbon isotope ecology of gymnosperms and implications for paleoclimatic and paleoecological studies. *Global and Planetary Change* 184: 103060.

Sheppard, P.R. 2010. Dendroclimatology: extracting climate from trees. *Wiley Interdisciplinary Reviews: Climate Change* 1(3): 343-352.

Shestakova, T.A. and Martínez-Sancho, E. 2021. Stories hidden in tree rings: a review on the application of stable carbon isotopes to dendrosciences. *Dendrochronologia* 65: 125789.

Sidorova O., Lehmann M., Saurer M., Fonti M., Siegwolf R., Bigler C. 2018. Compound-specific carbon isotopes and concentrations of carbohydrates and organic acids as indicators of tree decline in Mountain pine. *Forests* 9:363

Silberbauer, G.B. 1981. *Hunter and Habitat in the Central Kalahari Desert.* Cambridge University Press: Cambridge.

Silva, M.D.S., Funch, L.S. and da Silva, L.B. 2019. The growth ring concept: seeking a broader and unambiguous approach covering tropical species. *Biological Reviews* 94(3): 1161-1178.

Smith, D. and Lewis, D. 2007. Dendrochronology. In *Encyclopedia of Quaternary Science*. S.A. Elias, Ed. Elsevier Scientific. 459-465.

Solly, E.F., Jaeger, A.C., Barthel, M., Werner, R.A., Zürcher, A., Hagedorn, F., Six, J. and Hartmann, M. 2023. Water limitation intensity shifts carbon allocation dynamics in Scots pine mesocosms. *Plant and Soil* 490(1): 499-519.

Sousa, P.M., Blamey, R.C., Reason, C.J., Ramos, A.M. and Trigo, R.M., 2018. The 'Day Zero'Cape Town drought and the poleward migration of moisture corridors. *Environmental Research Letters* 13(12): 124025.

Speer, J.H. 2010. *Fundamentals of Tree-Ring Research*. University of Arizona Press.

Spiegel, A. and Boonzaier, E. 1988. Promoting Tradition: Images of the South African Past. In *South African Keywords: The use and abuses of political concepts*. E. Boonzaier, J. Sharp, Eds. Cape Town: David Philip: 40–57.

Steenkamp, C.J., Vogel, J.C., Fuls, A., Van Rooyen, N. and Van Rooyen, M.W. 2008. Age determination of Acacia erioloba trees in the Kalahari. *Journal of Arid Environments* 72(4): 302-313.

Stepanova, A.V., Akinlabi, F.M., Sebiloane, K., Van Wyk, B.E. and Oskolski, A.A. 2021. Wood anatomy of the crown lineages in Proteoideae (Proteaceae): implications for evolution and adaptive value of bordered pits in imperforate tracheary elements. *Botanical Journal of the Linnean Society* 197*(*4): 439-477.

Stewart, B.A. and Mitchell, P.J. 2018. Late Quaternary palaeoclimates and human-environment dynamics of the Maloti-Drakensberg region, southern Africa. *Quaternary Science Reviews* 196: 1-20.

Stokes, M. A. and Smiley, T. L. 1968. *An Introduction to Tree-Ring Dating.* Chicago: The University of Chicago Press.

Stone, A.E. 2014. Last Glacial Maximum conditions in southern Africa: Are we any closer to understanding the climate of this time period?. *Progress in Physical Geography* 38(5): 519-542.

Stowe, M.J. and Sealy, J. 2016. Terminal Pleistocene and Holocene dynamics of southern Africa's winter rainfall zone based on carbon and oxygen isotope analysis of bovid tooth enamel from Elands Bay Cave. *Quaternary International* 404: 57-67.

Strobel, P., Bliedtner, M., Carr, A.S., Struck, J., Du Plessis, N., Glaser, B., Meadows, M.E., Quick, L.J., Zech, M., Zech, R. and Haberzettl, T. 2022. Reconstructing Late Quaternary precipitation and its source on the southern Cape coast of South Africa: A multi-proxy paleoenvironmental record from Vankervelsvlei. *Quaternary Science Reviews* 284: 107467.

Suresh, H.S. 2012. Do trees tell about the past? *Resonance* 17(1): 33-43.

Talma, A.S. and Vogel, J.C. 1992. Late Quaternary paleotemperatures derived from a speleothem from Cango caves, Cape province, South Africa. *Quaternary Research* 37(2): 203-213.

Thackeray, J.F. and Fitchett, J.M. 2016. Rainfall seasonality captured in micromammalian fauna in Late Quaternary contexts, South Africa. *Paleontologia africana* 51: 1-9.

Théry-Parisot, I., Chabal, L. and Chrzavzez, J., 2010. Anthracology and taphonomy, from wood gathering to charcoal analysis. A review of the taphonomic processes modifying charcoal assemblages, in archaeological contexts. *Palaeogeography, Palaeoclimatology, Palaeoecology* 291(1-2): 142-153.

Truc, L., Chevalier, M., Favier, C., Cheddadi, R., Meadows, M.E., Scott, L., Carr, A.S., Smith, G.F. and Chase, B.M. 2013. Quantification of climate change for the last 20,000 years from Wonderkrater, South Africa: Implications for the long-term dynamics of the Intertropical Convergence Zone. *Palaeogeography, Palaeoclimatology, Palaeoecology* 386: 575-587.

Turney, C.S.M., Wheeler, D. and Chivas, A.R. 2006. Carbon isotope fractionation in wood during carbonization. *Geochimica et Cosmochimica Acta* 70(4): 960-964.

Tyson, P.D. and Preston-Whyte, R.A. 2000. *The Weather and Climate of Southern Africa*. Cape Town: Oxford University Press.

van der Sleen, P., Zuidema, P.A. and Pons, T.L. 2017. Stable isotopes in tropical tree rings: theory, methods and applications. *Functional Ecology* 31(9): 1674-1689.

Van Zinderen Bakker, E.M. 1967. Upper Pleistocene stratigraphy and Holocene ecology on the basis of vegetation changes in Sub-Saharan Africa. In *Background to Evolution in Africa.* W.W. Bishop and J.D. Clark, Eds. Chicago: University of Chicago Press. 125–147.

Van Zinderen Bakker, E.M. 1976. The evolution of late Quaternary paleoclimates of Southern Africa. *Palaeoecology of Africa* 9: 160–202.

Verheyden, A., Helle, G., Schleser, G.H., Dehairs, F., Beeckman, H. and Koedam, N. 2004. Annual cyclicity in high-resolution stable carbon and oxygen isotope ratios in the wood of the mangrove tree Rhizophora mucronata. *Plant, Cell & Environment* 27(12): 1525-1536.

Vincent-Barbaroux, C., Berveiller, D., Lelarge-Trouverie, C., Maia, R., Máguas, C., Pereira, J., Chaves, M.M. and Damesin, C. 2019. Carbon-use strategies in stem radial growth of two oak species, one Temperate deciduous and one Mediterranean evergreen: what can be inferred from seasonal variations in the $\delta^{13}C$ of the current year ring? *Tree Physiology* 39(8): 1329-1341.

Vitali, V., Schuler, P., Holloway-Phillips, M., D'Odorico, P., Guidi, C., Klesse, S., Lehmann, M.M., Meusburger, K., Schaub, M., Zweifel, R. and Gessler, A. 2024. Finding balance: Tree-ring isotopes differentiate between acclimation and stress-induced imbalance in a long-term irrigation experiment. *Global Change Biology* 30(3): e17237.

Vlok J, Schutte-Vlok AL. 2010. *Plants of the Klein Karoo*. Hatfield: Umdaus Press.

Vogel, J.C. 1978. The geographical distribution of Kranz species in southern Africa. *South African Journal of Science* 75: 209-215.

Vogel, J.C., Fuls, A. and Visser, E. 2001. Radiocarbon adjustments to the dendrochronology of a yellowwood tree. *South African Journal of Science* 97(3): 164-166.

Vornlocher, J.R., Lukens, W.E., Schubert, B.A. and Quan, C. 2021. Late Oligocene Precipitation Seasonality in East Asia Based on δ13C Profiles in Fossil Wood. *Paleoceanography and Paleoclimatology* 36: 1-13.

Wadley, L. 1989. Legacies from the Later Stone Age. *Goodwin Series* 6: 42-53.

Warren, C.R., McGrath, J.F. and Adams, M.A. 2001. Water availability and carbon isotope discrimination in conifers. *Oecologia* 127: 476-486.

Wolski, P. 2018. How severe is Cape Town's “Day zero” drought?. *Significance* 15(2): 24-27.

Woodborne, S., Gandiwa, P., Hall, G., Patrut, A. and Finch, J. 2016. A regional stable carbon isotope dendro-climatology from the south African summer rainfall area. *PloS one* 11(7): e0159361.

Woodborne, S., Hall, G., Robertson, I., Patrut, A., Rouault, M., Loader, N.J. and Hofmeyr, M. 2015. A 1000-year carbon isotope rainfall proxy record from South African baobab trees (Adansonia digitata L.). *PLoS One* 10(5): e0124202.

Zacharias, M., Weijers, S. and Löffler, J. 2017. Growth rings in bush species of the South African savannah. *African Journal of Ecology* 56(2): 399-403.

Zhang, H.Y., Hartmann, H., Gleixner, G., Thoma, M. and Schwab, V.F. 2019. Carbon isotope fractionation including photosynthetic and post-photosynthetic processes in C3 plants: Low [CO2] matters. *Geochimica et Cosmochimica Acta*: 1-15.

Zhao, S., Pederson, N., D'Orangeville, L., HilleRisLambers, J., Boose, E., Penone, C., Bauer, B., Jiang, Y. and Manzanedo, R.D. 2019. The International Tree-Ring Data Bank (ITRDB) revisited: data availability and global ecological representativity. *Journal of Biogeography* 46(2): 355-368.

Zuntini, A.R., Carruthers, T., Maurin, O., Bailey, P.C., Leempoel, K., Brewer, G.E., Epitawalage, N., Françoso, E., Gallego-Paramo, B., McGinnie, C. and Negrão, R. 2024. Phylogenomics and the rise of the angiosperms. *Nature* 629: 843-850.

Zwane, B. and Bamford, M. 2021. A reconstruction of woody vegetation, environment and wood use at Sibudu Cave, South Africa, based on charcoal that is dated between 73 and 72 ka. *Quaternary International* 593: 95-103.

Zwane, B., Bamford, M., van Wijk, Y. and Wurz, S. 2023. An analysis and environmental interpretations of wood charcoal from the Later Stone Age deposit at Klasies River cave 1, Tsitsikamma Coast. *South African Journal of Botany* 160: 147-156.

APPENDIX 1

Growth Increment Widths & Microscope Images

Table A1.1: Camps Bay (CB) *Protea*

Shrinkage factor: 23.98%

GI	Measured Wood width (mm)	Modelled Charcoal width (mm)
1	1.34	1.34
2	1.44	1.44
3	1.86	1.86
4	1.65	1.65
5	2.04	2.04
6	1.65	1.65
7	1.95	1.95
8	3.43	3.43
9	1.85	1.85
10	1.00	1.00
11	4.78	4.78
12	2.55	2.55
13	3.12	3.12
14	2.42	2.42
15	1.86	1.86
16	1.64	1.64
17	1.95	1.95
18	1.73	1.73
19	2.08	2.08
20	2.38	2.38
21	2.21	2.21
22	1.56	1.56
23	1.38	1.38
24	2.08	2.08
Mean	2.08	2.08
Max.	4.78	4.78
Min.	1.00	1.00

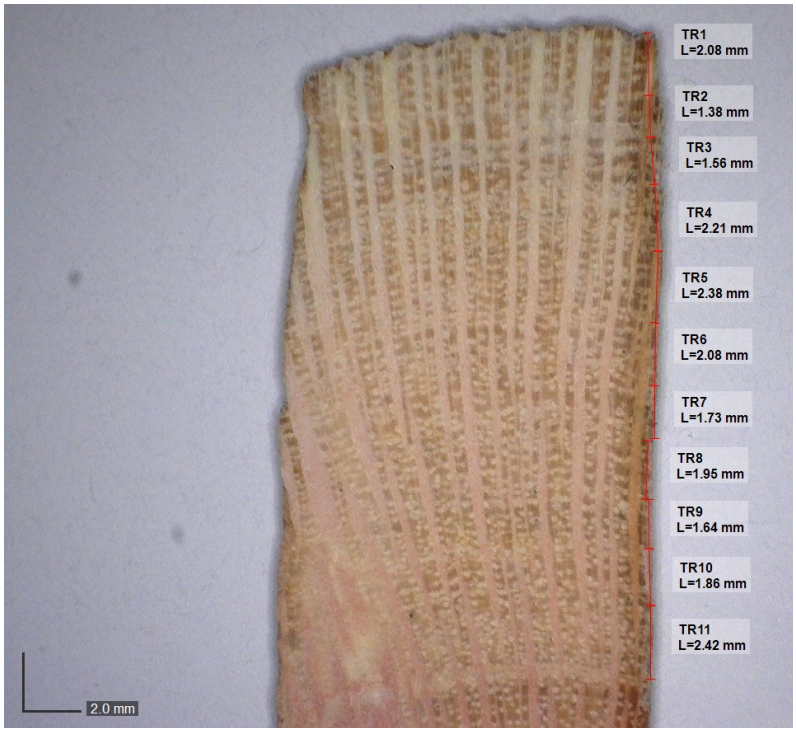

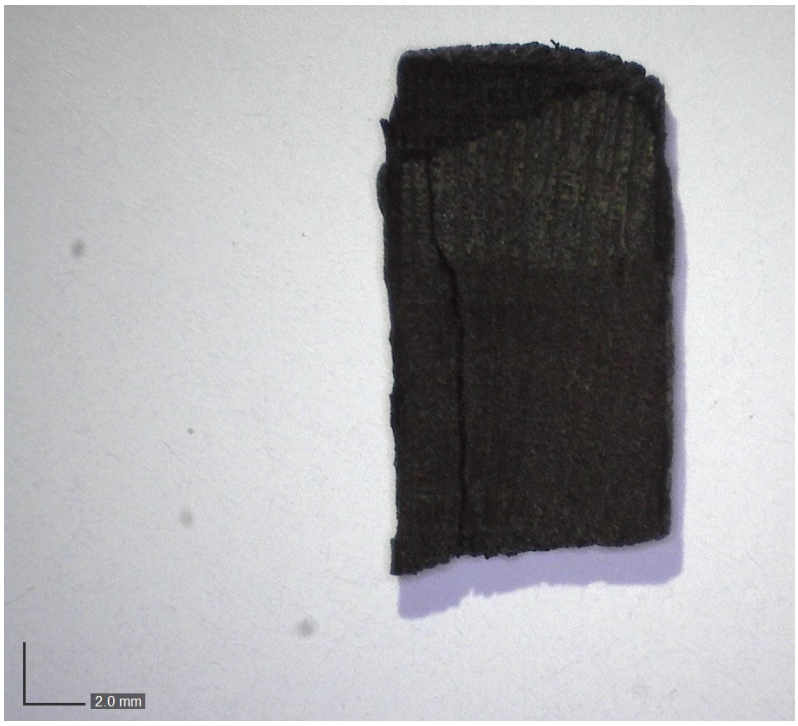

Figure A1.1. Digital images of CB_w and CB_ch (Wood and charcoal magnified at 20X).

Table A1.2: Swartberg (SB) *Protea*

Shrinkage factor: 23.98%

GI	Measured Wood width (mm)	Modelled Charcoal width (mm)
1	2.78	2.11
2	1.45	1.10
3	1.44	1.10
4	1.12	0.85
5	1.47	1.11
6	0.85	0.64
7	1.86	1.42
8	1.03	0.79
9	0.54	0.41
10	0.60	0.46
11	1.46	1.11
12	1.63	1.24
13	0.81	0.61
14	1.66	1.26
15	1.92	1.46
16	1.66	1.26
17	1.08	0.82
18	3.58	2.72
19	2.21	1.68
20	0.89	0.68
21	1.40	1.06
22	0.86	0.65
23	1.92	1.46
24	1.12	0.85
25	0.84	0.64
26	2.50	1.90
27	1.30	0.99
28	0.57	0.44
29	0.98	0.74
30	3.13	2.38
31	1.20	0.91
32	1.59	1.21
33	1.45	1.11
34	2.65	2.02
35	2.47	1.88
36	2.57	1.96
37	0.76	0.58
38	1.79	1.36
39	2.44	1.85
40	1.78	1.35
41	0.84	0.64
42	1.84	1.40
43	1.53	1.16
44	3.40	2.58
Mean	1.61	1.23
Max.	3.58	2.72
Min.	0.54	0.41

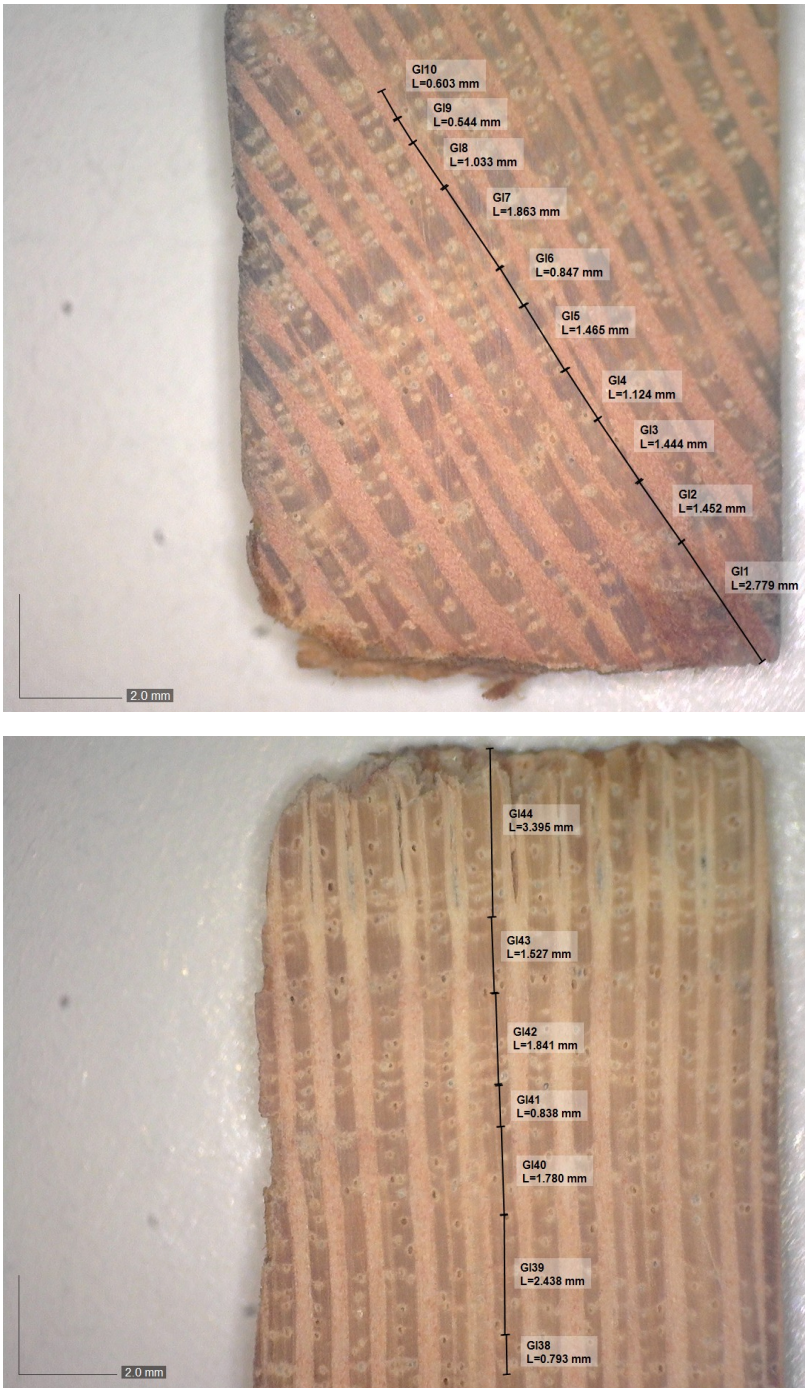

Figure A1.2. Digital images of SB_w showing several growth ring width measurements (Both magnified at 20X).

Table A1.3: Giant's Castle (GC4) *Protea*

Shrinkage Factor: 19.96%

GI	Measured Wood width (mm)	Modelled Charcoal Width (mm)
1	1.27	1.02
2	0.46	0.37
3	1.40	1.12
4	0.91	0.73
5	1.50	1.20
Mean	1.11	0.89
Max.	1.50	1.20
Min.	0.46	0.37

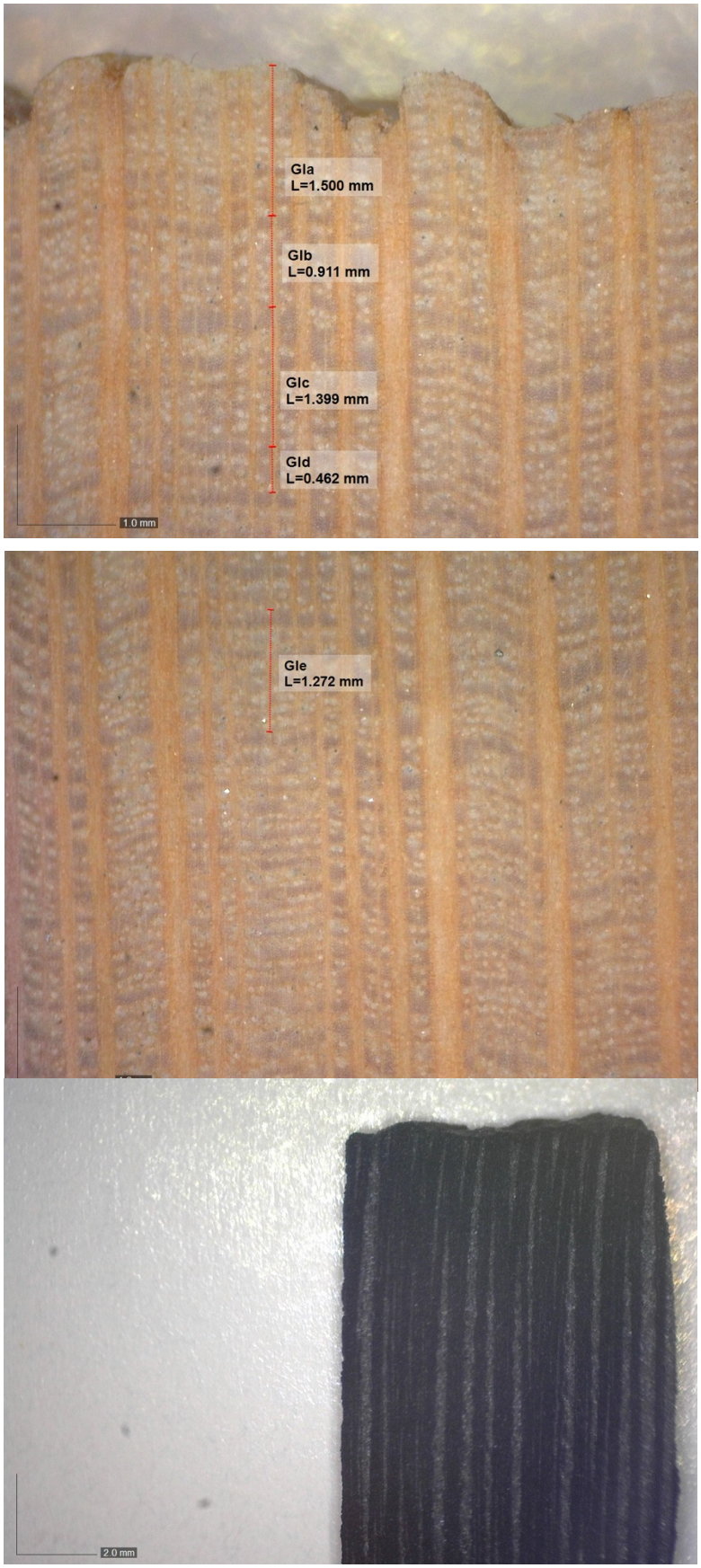

Figure A1.3. Digital images of GC4_w and GC4_ch showing several growth ring width measurements in wood (wood magnified at 50X and charcoal at

Table A1.4: Theronsberg (TB2) *Protea*

Shrinkage factor: 12.18%

GI	Measured Wood width (mm)	Modelled Charcoal Width (mm)
1	1.36	1.20
2	1.47	1.29
3	1.62	1.42
4	1.80	1.58
5	1.17	1.02
6	2.39	2.10
7	2.39	2.10
8	1.93	1.69
9	2.81	2.47
10	1.36	1.20
Mean	1.83	1.61
Max.	2.81	2.47
Min.	1.17	1.02

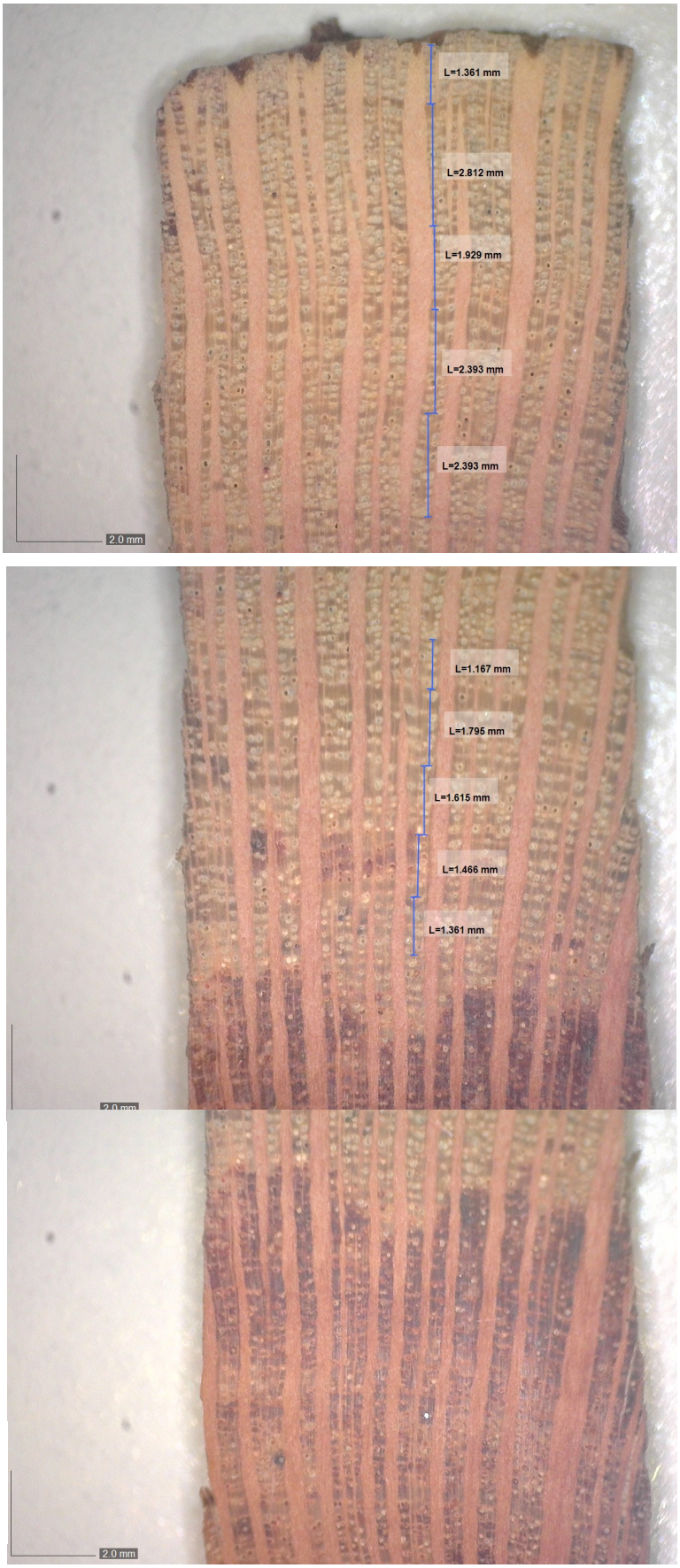

Figure A1.4. Digital images of TB2_w showing several growth ring width measurements (magnified at 20X).

Table A1.5: Giant's Castle (GC2) *Podocarpus*

Shrinkage factor: 19.20%

GI	Measured Wood width (mm)	Modelled Charcoal Width (mm)
1	1.47	1.19
2	1.29	1.04
3	1.63	1.32
4	3.45	2.79
5	3.23	2.61
6	2.93	2.36
7	2.80	2.26
8	3.26	2.63
9	3.60	2.91
10	4.93	3.99
11	0.36	0.29
12	0.61	0.50
13	0.69	0.56
14	0.87	0.70
15	0.18	0.15
16	0.46	0.37
17	0.14	0.12
18	1.25	1.01
19	0.76	0.61
20	1.01	0.81
21	0.64	0.51
22	1.89	1.52
23	1.83	1.48
24	0.34	0.28
25	0.74	0.60
26	1.74	1.41
27	1.61	1.30
28	1.57	1.27
29	0.20	0.16
30	0.37	0.30
31	1.24	1.00
32	0.83	0.67
Mean	1.50	1.21
Max.	4.93	3.99
Min.	0.14	0.12

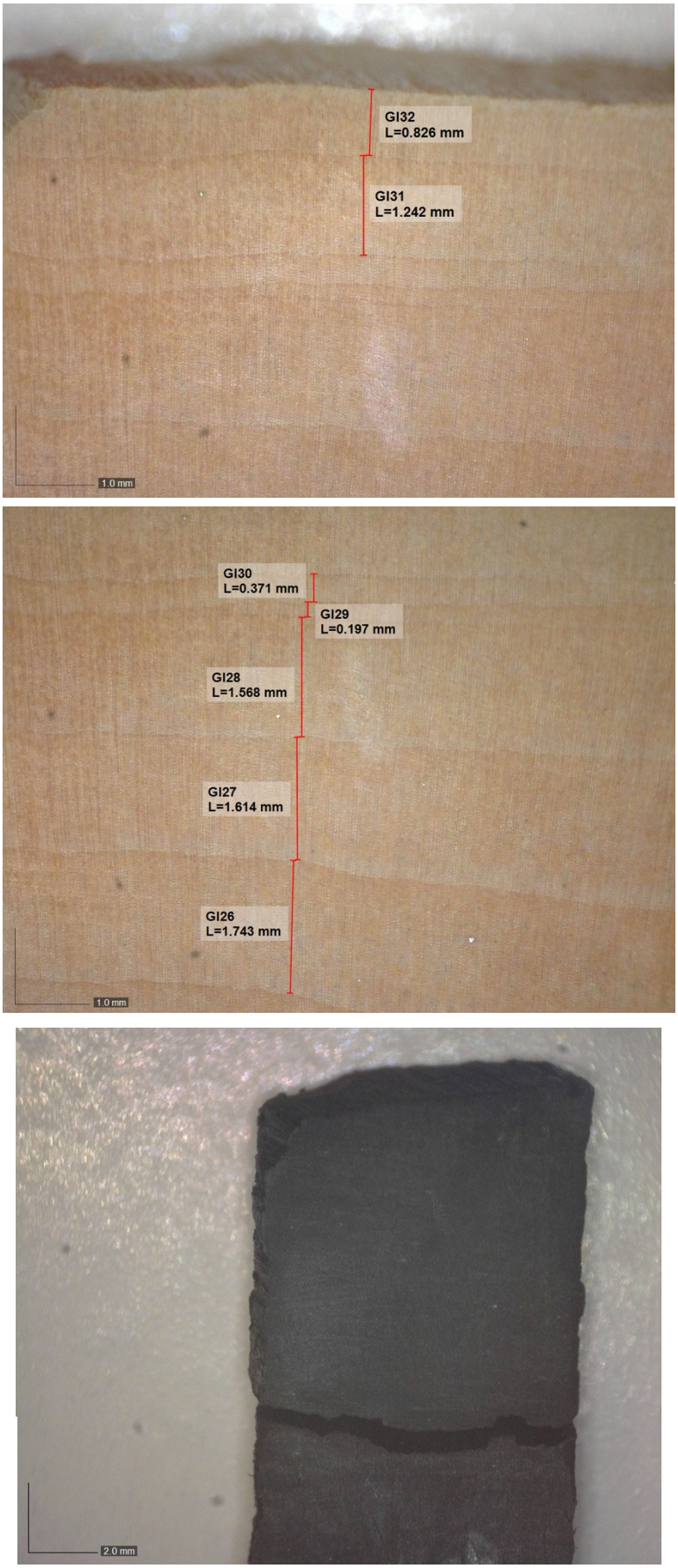

Figure A1.5. Digital images of GC2_w and GC2_ch showing several growth ring width measurements in wood (wood magnified at 40X and charcoal at

a

Table A1.6: Montagu Pass (MP) *Podocarpus*

Shrinkage factor: 25.25%

GI	Measured Wood width (mm)	Modelled Charcoal Width (mm)
1	0.45	0.34
2	0.88	0.66
3	0.67	0.50
4	0.24	0.18
5	0.78	0.58
6	1.42	1.06
7	1.91	1.43
8	0.93	0.69
9	1.24	0.93
10	1.51	1.13
11	1.24	0.93
12	1.45	1.08
13	0.99	0.74
14	1.66	1.24
15	0.95	0.71
16	0.93	0.70
17	0.87	0.65
18	1.09	0.81
19	0.90	0.67
20	0.84	0.63
21	1.00	0.74
22	0.80	0.60
23	1.05	0.79
24	1.01	0.76
25	2.56	1.92
26	1.43	1.07
27	2.44	1.82
28	2.61	1.95
29	2.30	1.72
30	1.69	1.26
31	1.97	1.47
32	1.52	1.14
Mean	1.29	0.97
Max.	2.61	1.95
Min.	0.24	0.18

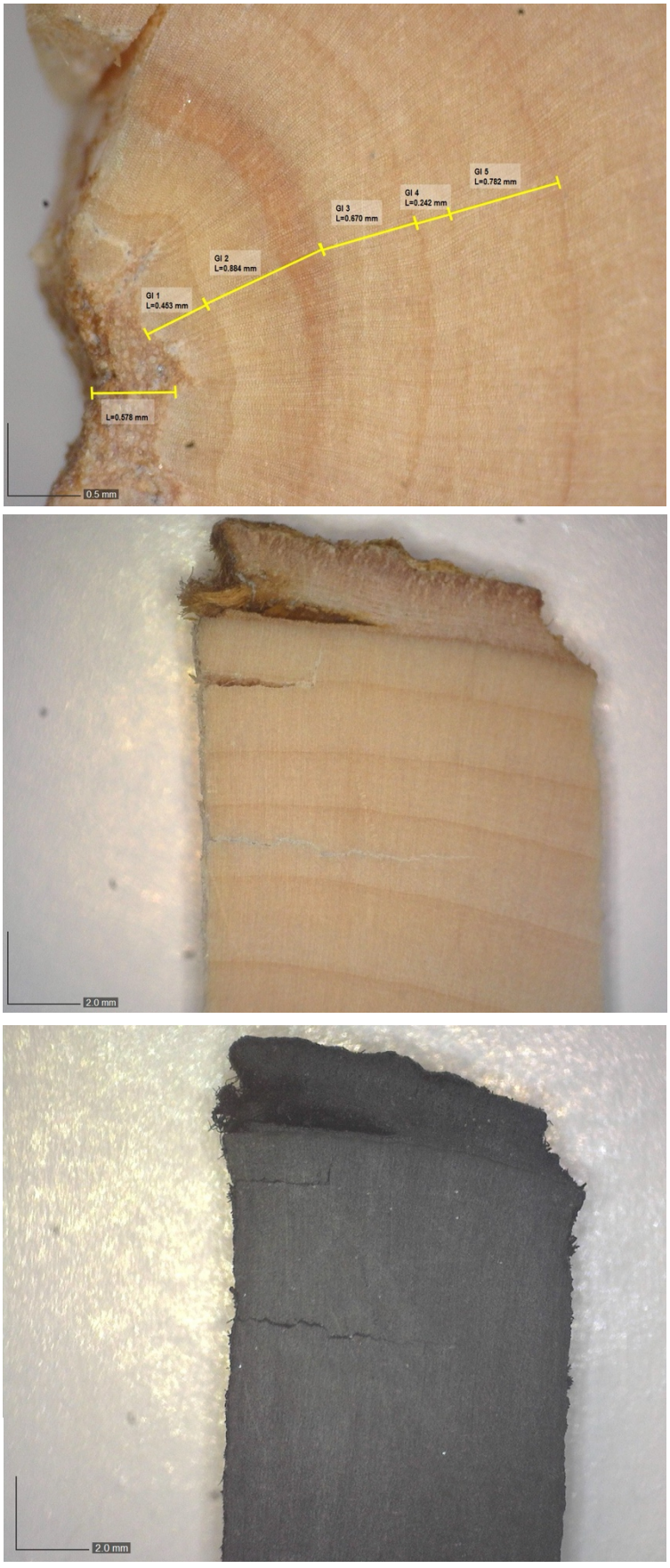

Figure A1.6. Digital images of MP_w and MP_ch showing several growth ring width measurements in wood (wood magnified at 80X and charcoal at 20X).

Ta

Shrinkage factor: 23.60%

GI	Measured Wood width (mm)	Modelled Charcoal Width (mm)
1	0.74	0.57
2	0.97	0.74
3	1.02	0.78
4	1.48	1.13
5	1.55	1.19
6	1.59	1.21
7	0.91	0.69
8	0.71	0.54
9	0.46	0.35
10	0.44	0.34
11	0.13	0.10
12	0.17	0.13
13	0.37	0.28
14	0.52	0.40
15	0.79	0.61
16	0.78	0.60
17	0.48	0.36
18	0.16	0.12
19	0.49	0.38
20	0.27	0.21
21	0.07	0.06
22	0.09	0.07
23	0.12	0.09
24	0.38	0.29
25	0.34	0.26
26	0.11	0.08
27	0.08	0.06
28	0.30	0.23
29	0.41	0.31
30	0.54	0.41
31	0.35	0.27
32	0.42	0.32
33	0.45	0.35
34	0.38	0.29
35	0.18	0.14
36	0.23	0.17
37	0.45	0.34
38	0.41	0.32
39	0.06	0.05
40	0.31	0.24
41	0.48	0.36
42	0.28	0.21
43	0.15	0.12
44	0.07	0.06
45	0.29	0.22
46	0.23	0.17
47	0.13	0.10
48	0.30	0.23
49	0.10	0.07
Mean	0.44	0.34
Max.	1.59	1.21
Min.	0.06	0.05

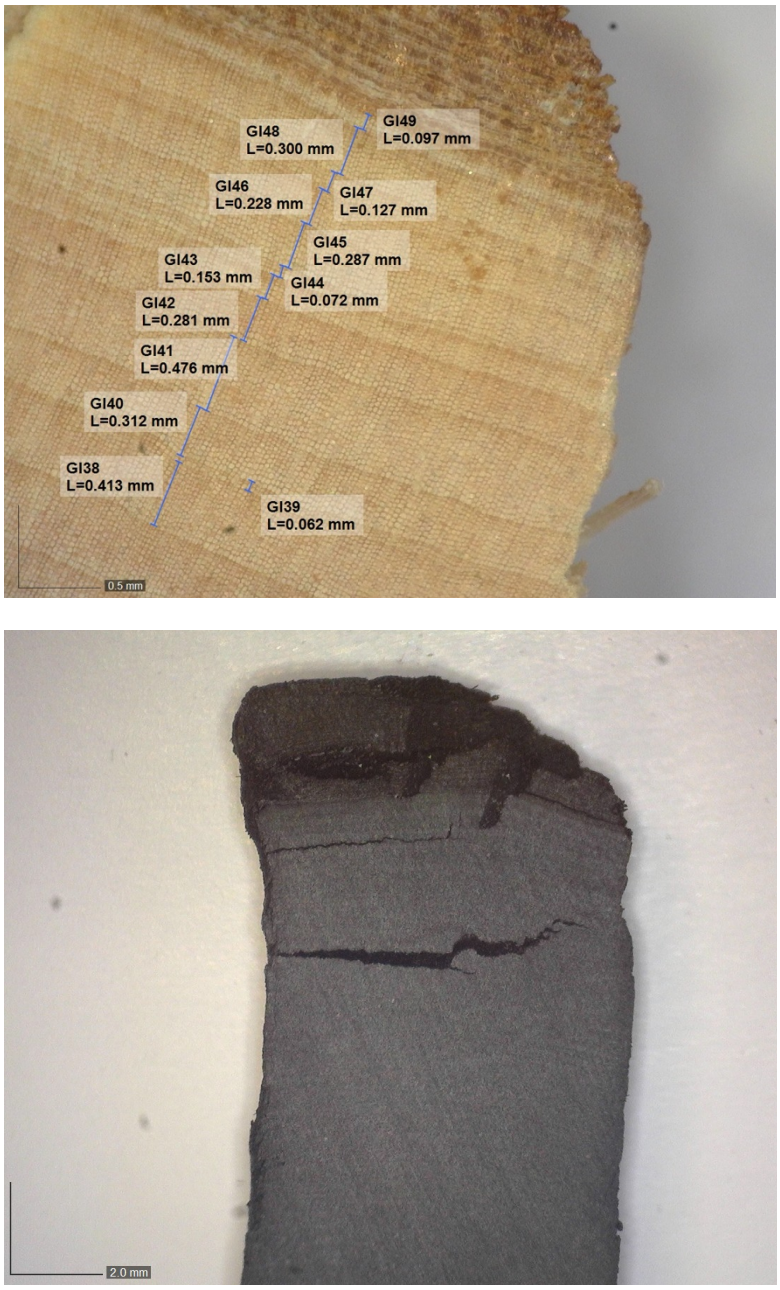

Figure A1.7. Digital images of GB1_w and GB1_ch showing several growth ring width measurements in wood (wood magnified at 80X and charcoal at 20X).

APPENDIX 2

Stable Carbon Isotope Results

Table A2.1. Camps Bay wood (CB_w)

Year	Sample ID	UCT No.	Subsample ID	Wt (mg)	Voltage (mv)	Area	%C	$\delta^{13}C$ (‰)	Std Corrected $\delta^{13}C$ (‰)
2021	CB_w	14205	CB1aW	1.959	2901	120.5	45.7	-24.52	-24.06
		14206	CB1bW	1.612	2388	96.8	44.6	-24.43	-23.96
		14207	CB1cW	2.004	3044	124.4	46.1	-24.54	-24.07
		14208	CB1dW	2.022	3057	124.7	45.8	-24.69	-24.23
		14209	CB1eW	2.022	3000	124.6	45.7	-24.91	-24.45
		14210	CB1fW	2.010	3014	122.9	45.4	-24.94	-24.48
		14211	CB1gW	2.029	2964	122.5	44.8	-25.01	-24.54
		14212	CB1hW	2.024	3102	127.8	46.9	-25.14	-24.68
		14213	CB1iW	2.011	2886	118.9	43.9	-25.28	-24.82
		14214	CB2aW	2.012	2975	124.3	45.8	-25.28	-24.82
		14215	CB2bW	2.022	3043	125.9	46.2	-25.47	-25.00
		14216	CB2cW	2.025	3038	125.2	45.9	-25.55	-25.08
		14217	CB2dW	2.029	3083	126.0	46.1	-25.55	-25.09
		14218	CB2eW	2.035	3058	126.7	46.2	-26.11	-25.65
		14219	CB2fW	2.016	3023	124.9	46.0	-26.30	-25.84
		14223	CB2gW	2.022	2986	125.1	45.9	-25.75	-25.28
		14224	CB3aW	2.029	2969	125.9	46.1	-25.88	-25.42
		14225	CB3bW	2.016	2978	124.3	45.8	-25.60	-25.14
		14226	CB3cW	2.041	3020	127.6	46.4	-25.59	-25.12
		14227	CB3dW	2.024	2969	125.7	46.1	-25.85	-25.38
		14228	CB3eW	2.037	3049	128.4	46.8	-25.90	-25.43
		14229	CB3fW	2.024	3037	127.5	46.8	-26.68	-26.21
		14230	CB4aW	2.039	3040	127.7	46.5	-26.63	-26.17
		14231	CB4bW	2.018	2935	124.1	45.7	-26.40	-25.94
		14232	CB4cW	2.039	3072	127.4	46.4	-26.48	-26.02
		14233	CB4dW	2.036	2941	125.8	45.9	-26.55	-26.08
		14234	CB5aW	2.022	3007	127.0	46.6	-26.66	-26.20
		14235	CB5bW	2.029	3039	127.9	46.8	-26.29	-25.83
		14236	CB5cW	2.010	2978	125.7	46.4	-26.29	-25.83
		14237	CB5dW	2.019	2959	125.0	46.0	-26.17	-25.71
		14241	CB5eW	2.023	3049	127.1	46.6	-26.51	-26.04
		14242	CB5fW	2.033	2927	126.9	46.3	-26.62	-26.16
		14243	CB5gW	2.028	2972	125.6	46.0	-26.99	-26.53
		14244	CB5hW	2.021	2950	127.1	46.7	-27.10	-26.63
		14245	CB5iW	2.035	3040	127.5	46.5	-26.60	-26.14
		14246	CB5jW	2.014	2884	124.5	45.9	-27.06	-26.39
		14247	CB5kW	2.025	2907	126.5	46.4	-27.01	-26.55

Table A2.2. Camps Bay charcoal (CB_ch)

Year	Sample ID	UCT No.	Subsample ID	Wt (mg)	Voltage (mv)	Area	%C	$\delta^{13}C$ (‰)	Std Corrected $\delta^{13}C$ (‰)
2021	CB_ch	14248	CB1aC	0.517	1250	53.8	77.3	-25.97	-25.51
		14249	CB1bC	0.522	1291	54.7	77.8	-25.83	-25.36
		14250	CB1cC	0.512	1300	54.2	78.6	-25.76	-25.30
		14251	CB1dC	0.525	1255	54.8	77.5	-25.92	-25.46
		14252	CB1eC	0.514	1259	54.7	79.0	-25.74	-25.27
		14256	CB2aC	0.512	1255	54.4	78.9	-25.82	-25.35
		14257	CB2bC	0.524	1267	55.9	79.2	-26.07	-25.60
		14258	CB2cC	0.518	1283	54.3	77.8	-25.97	-25.51
		14259	CB2dC	0.535	1327	57.3	79.5	-26.16	-25.69
		14260	CB3aC	0.520	1336	55.4	79.1	-26.38	-25.92
		14261	CB3bC	0.538	1389	56.9	78.5	-26.55	-26.09
		14262	CB3cC	0.514	1213	52.6	76.0	-26.35	-25.89
		14263	CB3dC	0.523	1285	56.0	79.5	-26.77	-26.31
		14264	CB4aC	0.534	1261	56.6	78.7	-26.20	-25.74
		14265	CB4bC	0.459	1187	49.3	79.8	-26.39	-25.93
		14266	CB4cC	0.520	1249	54.3	77.6	-26.41	-25.95
		14267	CB5aC	0.534	1068	52.2	72.6	-26.70	-26.24
		14268	CB5bC	0.533	1248	56.4	78.6	-26.91	-26.45
		14269	CB5cC	0.537	1335	56.9	78.7	-26.81	-26.34
		14270	CB5dC	0.496	1259	53.0	79.3	-26.99	-26.53
		14274	CB5eC	0.537	1366	57.7	79.8	-27.07	-26.61
		14275	CB5fC	0.510	1170	53.1	77.3	-27.03	-26.57
		14276	CB5gC	0.524	1326	56.2	79.6	-26.99	-26.53
		14277	CB5hC	0.513	1203	54.7	79.2	-26.84	-26.38
		14278	CB5iC	0.519	1289	55.7	79.7	-27.25	-26.79
		14279	CB5jC	0.524	1300	56.2	79.6	-27.06	-26.60

Table A2.3. Swartberg wood (SB_w)

Year	Sample ID	UCT No.	Subsample ID	Wt (mg)	Voltage (mv)	Area	%C	$\delta^{13}C$ (‰)	Std Corrected $\delta^{13}C$ (‰)	Distance from bark (mm)
2023	SB_w	21098	SB_W44A	2.015	1040	41.9	43.3	-30.85	-27.10	0.00
		21099	SB_W44B	1.949	1014	41.0	43.8	-30.32	-26.58	0.28
		21100	SB_W44C	2.020	1023	41.8	43.1	-29.99	-26.26	0.65
		21101	SB_W44D	2.021	1016	41.4	42.7	-30.07	-26.34	0.98
		21102	SB_W44E	2.008	1012	40.9	42.4	-29.90	-26.17	1.32
		21103	SB_W44F	2.016	1029	41.7	43.0	-29.68	-25.95	1.76
		21104	SB_W44G	2.006	1008	41.2	42.8	-29.69	-25.96	1.97
		21105	SB_W44H	2.029	1039	42.4	43.5	-29.48	-25.76	2.37
		21106	SB_W44I	2.018	1049	42.6	43.9	-29.59	-25.87	2.84
		21107	SB_W44J	2.000	1030	42.1	43.8	-29.68	-25.96	3.01
		21108	SB_W44K	2.027	1054	43.2	44.3	-29.81	-26.08	3.29
		21109	SB_W43A	2.022	1042	42.7	44.0	-30.06	-26.32	3.63
		21113	SB_W43B	2.031	1059	42.8	43.9	-30.21	-26.48	3.74
		21114	SB_W43C	2.014	1062	43.1	44.5	-30.00	-26.27	3.82
		21115	SB_W43D	1.984	1043	42.1	44.2	-30.05	-26.32	3.99
		21116	SB_W43E	2.024	1064	43.2	44.4	-30.28	-26.54	4.17
		21117	SB_W43F	2.008	1061	43.4	44.9	-30.04	-26.31	4.22
		21118	SB_W43G	2.011	1067	43.5	45.0	-29.98	-26.25	4.34
		21119	SB_W43H	2.005	1066	43.3	44.9	-30.07	-26.33	4.42
		21120	SB_W43I	2.020	1098	44.6	46.0	-30.14	-26.41	4.58

		21121	SB_W43J	1.925	1024	41.8	45.2	-30.23	-26.49	4.88
		21122	SB_W43K	1.830	981	39.7	45.1	-30.01	-26.28	4.94
		21123	SB_W42A	2.014	1066	43.5	44.9	-30.24	-26.50	5.08
		21124	SB_W42B	2.020	1081	44.1	45.5	-30.59	-26.84	5.21
		21128	SB_W42C	2.017	1061	43.1	44.5	-30.79	-27.05	5.33
		21129	SB_W42D	2.024	1044	42.7	43.9	-30.69	-26.94	5.41
		21130	SB_W42E	2.007	1060	43.0	44.6	-30.36	-26.62	5.57
		21131	SB_W42F	2.012	1058	43.1	44.5	-30.13	-26.40	5.74
		21132	SB_W42G	2.035	1083	44.0	45.0	-29.98	-26.25	5.97
		21133	SB_W42H	2.001	1069	43.6	45.3	-29.64	-25.91	6.14
		21134	SB_W42I	2.007	1067	43.5	45.1	-29.54	-25.82	6.28
		21135	SB_W42J	2.024	1063	43.5	44.7	-29.66	-25.93	6.41
		21136	SB_W42K	2.014	1055	43.1	44.5	-29.43	-25.70	6.62
		21137	SB_W41A	2.019	1066	43.3	44.6	-29.24	-25.52	6.86
		21138	SB_W41B	2.011	1031	42.5	44.0	-29.21	-25.49	7.01
		21139	SB_W41C	2.018	1075	43.9	45.2	-29.33	-25.61	7.23
		21143	SB_W41D	2.009	1070	43.5	45.0	-29.30	-25.58	7.37
		21144	SB_W41E	2.002	1059	43.1	44.8	-29.32	-25.60	7.54
		21145	SB_W40A	2.027	1076	43.7	44.9	-29.34	-25.62	7.74
		21146	SB_W40B	2.002	1061	43.3	45.0	-29.25	-25.53	7.89
		21147	SB_W40C	2.024	1084	44.3	45.6	-29.39	-25.67	8.05
		21148	SB_W40D	2.008	1060	43.3	44.8	-29.40	-25.68	8.21
		21149	SB_W40E	2.020	1075	43.8	45.1	-29.36	-25.64	8.36
		21150	SB_W40F	2.002	1080	44.3	46.0	-29.62	-25.89	8.52
		21151	SB_W40G	2.014	1063	43.8	45.2	-29.90	-26.17	8.76
		21152	SB_W40H	2.014	1071	43.7	45.2	-30.75	-27.01	8.94
		21153	SB_W40I	2.011	1065	43.5	45.0	-30.40	-26.66	9.19
		24395	SB-W1	2.150	3588	151.9	45.1	-28.97	-26.43	9.3
		24396	SB-W2	2.129	3535	149.6	44.9	-28.27	-25.75	9.47
		24397	SB-W3	2.056	3413	143.6	44.6	-27.90	-25.39	9.87
		24398	SB-W4	2.199	3637	154.3	44.8	-27.64	-25.13	10.03
		24399	SB-W5	2.127	3459	145.8	43.8	-27.63	-25.13	10.56
		24400	SB-W6	2.050	3462	146.3	45.6	-27.74	-25.23	10.93
		24401	SB-W7	2.126	3556	150.3	45.1	-28.10	-25.58	11.31
		24402	SB-W8	2.117	3571	151.1	45.6	-28.92	-26.39	11.65
		24403	SB-W9	2.049	3355	141.5	44.1	-29.37	-26.82	12.09
		24404	SB-W10	2.054	3392	143.3	44.5	-28.14	-25.62	12.61
		24405	SB-W11	2.096	3399	143.2	43.6	-28.35	-25.82	13.04
		24406	SB-W12	2.108	3547	150.6	45.6	-29.63	-27.08	13.68
		24410	SB-W13	2.020	3345	144.2	45.6	-29.58	-27.02	13.98
		24411	SB-W14	2.052	3414	145.4	45.2	-28.90	-26.36	14.4
		24412	SB-W15	2.008	3289	141.4	45.0	-28.27	-25.75	15.26
		24419	SB-W16	2.045	3380	143.4	44.8	-28.11	-25.59	16.84
		24428	SB-W17	2.052	3438	146.9	45.7	-27.83	-25.32	17.03
		24431	SB-W18	2.072	3301	141.1	43.5	-27.64	-25.14	17.25
		24421	SB-W19	2.125	3534	151.1	45.4	-29.78	-27.22	17.88
		24391	SB-W20	2.066	3855	164.4	50.8	-29.84	-27.28	18.36
		24418	SB-W21	2.030	3381	144.0	45.3	-29.20	-26.65	18.84
		24413	SB-W22	2.035	3382	143.7	45.1	-28.89	-26.36	19.28
		24420	SB-W23	2.011	3356	141.3	44.9	-29.06	-26.52	20.14
		24416	SB-W24	2.071	3496	148.9	45.9	-28.90	-26.36	20.57
		24432	SB-W25	2.050	3414	145.6	45.3	-28.31	-25.79	21.07
		24426	SB-W26	2.069	3471	148.5	45.8	-28.36	-25.84	21.59
		24417	SB-W27	2.043	3415	145.5	45.5	-29.12	-26.57	21.82

Table A2.4. Swartberg charcoal (SB_ch)

Year	Sample ID	UCT No.	Subsample ID	Wt (mg)	Voltage (mv)	Area	%C	$\delta^{13}C$ (‰)	Std Corrected $\delta^{13}C$ (‰)
2021	SB_ch	14424	SB1a	0.537	1345	58.6	81.6	-27.78	-27.53
		14425	SB1b	0.549	1375	60.6	82.4	-27.41	-27.16
		14426	SB1c	0.537	1310	58.7	81.7	-27.19	-26.95
		14427	SB1d	0.538	1302	58.2	80.8	-26.97	-26.72
		14428	SB1e	0.543	1399	59.4	81.8	-26.72	-26.48
		14429	SB1f	0.548	1401	60.6	82.7	-26.76	-26.53
		14430	SB1g	0.546	1339	59.4	81.3	-26.53	-26.30
		14431	SB2a	0.544	1417	60.3	82.8	-26.91	-26.67
		14432	SB2b	0.535	1168	53.9	75.3	-27.02	-26.78
		14433	SB2c	0.545	1322	58.9	80.8	-27.14	-26.89
		14437	SB2d	0.536	1403	58.5	81.5	-27.12	-26.88
		14438	SB2e	0.511	1296	55.8	81.6	-27.12	-26.88
		14439	SB3a	0.516	1285	56.7	82.1	-27.11	-26.86
		14440	SB3b	0.504	1261	54.5	80.8	-27.32	-27.08
		14441	SB3c	0.520	1263	54.7	78.6	-27.45	-27.20
		14442	SB3d	0.529	1317	57.4	81	-27.5	-27.25
		14443	SB3e	0.524	1268	57.5	79.4	-27.59	-27.34
		14370	SB4a	0.500	1238	54.5	80.2	-27.76	-27.25
		14371	SB4b	0.538	1361	58.7	80.2	-27.43	-26.93
		14372	SB4c	0.510	1197	55	79.4	-27.25	-26.75
		14373	SB4d	0.506	1149	52.3	76.1	-27.32	-26.82
		14374	SB4e	0.550	1384	60.2	80.6	-27.36	-26.86
		14375	SB4f	0.530	1301	57.7	80.1	-27.22	-26.72
		14376	SB5a	0.521	1326	56.6	79.9	-27.44	-26.93
		14377	SB5b	0.549	1193	54.4	72.9	-27.26	-26.76
		14378	SB5c	0.528	1268	56.5	78.8	-27.82	-27.31
		14379	SB5d	0.536	1276	58.3	80	-27.77	-27.26
		14380	SB5e	0.525	1278	57	79.8	-27.95	-27.44
		14381	SB5f	0.509	1114	53.2	77	-27.35	-26.85
		14382	SB5g	0.545	1085	54	72.8	-27.28	-26.78
2023	SB_ch	25041	SB-CH1	0.966	2645	111.8	75.3	-28.65	-26.06
		25042	SB-CH2	0.750	2073	87.2	75.7	-28.65	-26.06
		25043	SB-CH3	0.712	1991	82.7	75.6	-28.67	-26.09
		25044	SB-CH4	0.720	2025	83.9	75.9	-29.14	-26.55
		25045	SB-CH5	0.754	2093	87.6	75.6	-29.64	-27.04
		25046	SB-CH6	0.786	2148	89.3	73.9	-29.99	-27.38
		25047	SB-CH7	0.771	2091	87.6	73.9	-30.42	-27.80
		25108	SB-CH8	0.776	2096	86.5	72.3	-31.51	-28.47
		25109	SB-CH9	0.740	1916	78.9	69.1	-31.02	-27.99
		25110	SB-CH10	0.783	2136	88.6	73.3	-31.21	-28.18
		25111	SB-CH11	0.741	1950	80.3	70.2	-30.86	-27.84
		25112	SB-CH12	0.743	1888	77.7	67.8	-30.38	-27.37
		25113	SB-CH13	0.773	2037	84.4	70.8	-30.08	-27.07
		25114	SB-CH14	0.747	1950	80.5	69.9	-29.81	-26.80
		25115	SB-CH15	0.711	1898	78.3	71.4	-29.81	-26.80
		25116	SB-CH16	0.774	2136	90.1	75.5	-29.65	-26.64
		25117	SB-CH17	0.783	2125	88.2	73.0	-30.28	-27.26
		25118	SB-CH18	0.773	2149	89.0	74.7	-30.74	-27.71
		25119	SB-CH19	0.762	2081	87.3	74.2	-30.56	-27.54
		25120	SB-CH20	0.720	1992	82.1	73.9	-30.76	-27.74

Table A2.5. Giant's Castle wood (GC4_w)

Year	Sample ID	UCT No.	Subsample ID	Wt (mg)	Voltage (mv)	Area	%C	$\delta^{13}C$ (‰)	Std Corrected $\delta^{13}C$ (‰)	Distance from bark (mm)
2023	GC4_w	21531	GC4_Wa1	2.059	1116	44.9	39.7	-28.23	-26.24	0.00
		21532	GC4_Wa2	2.029	1188	47.9	43.0	-28.71	-26.72	0.36
		21533	GC4_Wa3	2.009	1167	47.1	42.7	-28.53	-26.54	0.53
		21534	GC4_Wa4	2.031	1202	48.4	43.4	-28.46	-26.48	0.71
		21535	GC4_Wa5	1.847	1096	44.0	43.3	-28.29	-26.30	0.89
		21536	GC4_Wa6	2.023	1220	49.1	44.1	-28.50	-26.51	1.12
		21537	GC4_Wa7	2.010	1213	48.9	44.2	-28.56	-26.58	1.33
		21538	GC4_Wa8	2.045	1214	49.0	43.6	-28.43	-26.44	1.51
		21539	GC4_Wb1	1.998	1180	47.6	43.3	-28.33	-26.35	1.71
		21540	GC4_Wb2	1.937	1169	47.1	44.2	-28.17	-26.19	1.82
		21541	GC4_Wb3	2.023	1217	49.1	44.2	-28.00	-26.02	1.97
		21542	GC4_Wb4	1.998	1218	49.0	44.6	-27.92	-25.95	2.10
		21543	GC4_Wb5	2.001	1225	49.3	44.9	-28.16	-26.18	2.32
		21547	GC4_Wb6	2.023	1233	49.3	44.4	-28.35	-26.36	2.49
		21548	GC4_Wc1	2.015	1220	49.0	44.3	-28.43	-26.45	2.69
		21549	GC4_Wc2	2.002	1212	48.7	44.3	-28.17	-26.19	3.00
		21550	GC4_Wc3	2.044	1255	50.6	45.0	-28.37	-26.38	3.15
		21551	GC4_Wc4	2.021	1225	49.2	44.3	-27.96	-25.98	3.38
		21552	GC4_Wc5	2.020	1222	49.2	44.3	-27.53	-25.56	3.61
		21553	GC4_Wc6	2.030	1251	50.2	45.0	-27.64	-25.67	3.78
		21554	GC4_Wd1	2.033	1251	50.4	45.1	-27.73	-25.76	3.97
		21555	GC4_Wd2	2.004	1218	49.2	44.6	-27.95	-25.97	4.20
		21556	GC4_We1	2.012	1225	49.3	44.5	-28.41	-26.42	4.36
		21557	GC4_We2	1.994	1233	49.6	45.2	-28.10	-26.12	4.62
		21558	GC4_We3	2.039	1251	50.2	44.8	-28.33	-26.35	4.85
		21559	GC4_We4	2.019	1235	49.5	44.6	-28.57	-26.58	5.08
		21563	GC4_We5	2.027	1226	49.3	44.2	-28.53	-26.55	5.33
		21564	GC4_We6	2.044	1260	50.7	45.1	-28.67	-26.68	5.56
		21565	GC4_Wf1	2.027	1255	50.4	45.3	-28.75	-26.76	5.79
		21566	GC4_Wf2	2.026	1243	49.9	44.8	-28.83	-26.84	6.09
		21567	GC4_Wf3	2.028	1249	50.0	44.9	-28.63	-26.65	6.29
		21568	GC4_Wf4	2.010	1224	49.1	44.4	-28.73	-26.74	6.48
		21569	GC4_Wf5	2.042	1254	50.3	44.8	-28.45	-26.46	6.79
		21570	GC4_Wf6	2.009	1217	48.8	44.2	-28.65	-26.66	7.00
		21571	GC4_Wf7	2.027	1236	49.8	44.7	-28.56	-26.58	7.45
		21572	GC4_Wf8	2.024	1243	50.0	44.9	-28.35	-26.37	7.78
		21573	GC4_Wf9	1.956	1203	48.2	44.8	-28.29	-26.31	7.90
		21574	GC4_Wf10	2.046	1245	50.1	44.5	-28.39	-26.40	8.31
		24414	GC4-W1	2.065	3315	140.2	43.3	-28.82	-26.29	9.00
		24436	GC4-W2	2.025	3326	140.7	44.3	-28.37	-25.85	9.36
		24430	GC4-W3	2.095	3485	147.6	45.0	-28.58	-26.06	10.05
		24415	GC4-W4	2.041	3376	142.6	44.6	-28.86	-26.32	10.76
		24425	GC4-W5	2.068	3441	144.8	44.7	-28.55	-26.03	11.34
		24435	GC4-W6	2.057	3405	144.7	44.9	-28.49	-25.97	11.93
		24434	GC4-W7	2.027	3315	142.2	44.8	-28.53	-26.00	12.52
		24433	GC4-W8	2.074	3387	144.0	44.3	-28.54	-26.01	12.94
		24429	GC4-W9	2.023	3365	142.8	45.0	-28.40	-25.88	13.31
		24991	GC4-W10	2.068	3392	144.0	45.3	-28.78	-26.19	13.69
		24992	GC4-W11	2.068	3414	145.0	45.6	-28.69	-26.10	14.44
		24993	GC4-W12	2.059	3403	144.7	45.7	-28.57	-25.99	15.02
		24994	GC4-W13	2.036	3339	141.5	45.2	-28.47	-25.89	15.64
		24995	GC4-W14	2.039	3335	141.5	45.2	-28.47	-25.89	16.17
		24996	GC4-W15	2.016	3333	141.3	45.6	-28.24	-25.66	16.90
		24997	GC4-W16	2.027	3311	140.2	45.0	-28.31	-25.73	17.19
		24998	GC4-W17	2.051	3386	143.8	45.6	-28.38	-25.80	18.12
		24999	GC4-W18	2.083	3458	147.0	45.9	-28.65	-26.07	18.88
		25000	GC4-W19	2.031	3363	143.1	45.9	-28.64	-26.06	19.43
		25001	GC4-W20	2.090	3368	143.4	44.7	-28.74	-26.16	20.17
		25002	GC4-W21	2.002	3323	141.1	45.9	-28.36	-25.79	20.71

		25006	GC4-W22	2.096	3437	146.5	45.5	-28.60	-26.01	21.22
		25007	GC4-W23	2.107	3471	147.8	45.6	-28.40	-25.82	21.87
		25008	GC4-W24	2.063	3386	144.0	45.4	-27.99	-25.41	22.42
		25009	GC4-W25	2.078	3439	146.4	45.9	-28.13	-25.56	22.94
		25010	GC4-W26	2.054	3372	143.3	45.4	-28.11	-25.53	23.43
		25011	GC4-W27	2.041	3359	142.9	45.6	-28.13	-25.56	24.29
		25012	GC4-W28	2.016	3344	142.0	45.9	-27.55	-24.99	24.92
		25013	GC4-W29	2.015	3319	140.8	45.5	-28.28	-25.70	25.36
		25014	GC4-W30	2.051	3393	144.2	45.7	-28.40	-25.82	26.06
		25015	GC4-W31	2.083	3446	146.5	45.8	-27.75	-25.18	26.41
		25016	GC4-W32	2.072	3422	145.5	45.7	-27.97	-25.40	26.98
		25017	GC4-W33	2.040	3355	142.4	45.4	-28.26	-25.68	27.62
		25021	GC4-W34	2.055	3399	144.4	45.7	-28.24	-25.67	28.36
		25022	GC4-W35	2.058	3410	145.3	45.9	-28.18	-25.61	28.99
		25023	GC4-W36	2.031	3337	141.9	45.5	-27.96	-25.39	29.28
		25024	GC4-W37	2.090	3458	146.9	45.7	-28.27	-25.69	29.94
		25025	GC4-W38	2.035	3352	142.9	45.7	-27.95	-25.38	30.43
		25026	GC4-W39	2.025	3309	140.5	45.1	-27.37	-24.81	30.70
		25027	GC4-W40	2.072	3398	144.6	45.4	-28.21	-25.64	31.09
		25028	GC4-W41	2.072	3393	144.3	45.3	-28.44	-25.86	31.84
		25029	GC4-W42	2.088	3458	147.3	45.9	-27.90	-25.33	32.16
		25030	GC4-W43	2.102	3432	146.4	45.3	-27.99	-25.42	32.83
		25031	GC4-W44	2.055	3377	143.8	45.6	-28.33	-25.75	33.38
		25032	GC4-W45	2.020	3338	141.9	45.7	-27.99	-25.42	34.07

Table A2.6. Giant's Castle charcoal (GC4_ch)

Year	Sample ID	UCT No.	Subsample ID	Wt (mg)	Voltage (mv)	Area	%C	$\delta^{13}C$ (‰)	Std Corrected $\delta^{13}C$ (‰)	Distance from bark (mm)
2023	GC4_ch	21575	GC4_CHa1	0.517	555	21.8	76.9	-29.50	-27.49	0.00
		21576	GC4_CHa2	0.541	564	22.2	74.6	-29.52	-27.52	0.32
		21580	GC4_CHa3	0.395	422	16.4	75.7	-29.22	-27.22	0.65
		21581	GC4_CHa4	0.537	578	22.8	77.1	-29.66	-27.65	0.79
		21582	GC4_CHa5	0.511	534	21.0	74.7	-29.43	-27.42	0.85
		21583	GC4_CHa6	0.527	537	21.2	73.0	-29.24	-27.24	0.94
		21584	GC4_CHa7	0.550	560	22.0	72.9	-29.09	-27.10	1.11
		21585	GC4_CHb1	0.546	564	22.3	74.4	-28.86	-26.87	1.30
		21586	GC4_CHb2	0.511	548	21.7	77.2	-28.65	-26.66	1.49
		21587	GC4_CHb3	0.529	557	22.0	75.7	-29.29	-27.29	1.67
		21588	GC4_CHb4	0.518	585	23.1	81.2	-28.95	-26.95	1.88
		21589	GC4_CHc1	0.552	591	23.3	76.7	-28.83	-26.84	2.01
		21590	GC4_CHc2	0.548	588	23.2	77.0	-28.57	-26.59	2.22
		21591	GC4_CHc3	0.553	588	23.3	76.7	-29.24	-27.24	2.41
		21592	GC4_CHc4	0.543	587	23.2	77.7	-29.20	-27.20	2.70
		21593	GC4_CHc5	0.540	568	22.8	76.8	-29.26	-27.26	2.93
		21597	GC4_CHc6	0.518	525	20.7	72.7	-29.33	-27.33	3.06
		21598	GC4_CHd1	0.507	535	21.3	76.4	-29.35	-27.35	3.28
		21599	GC4_CHd2	0.385	416	16.4	77.5	-29.28	-27.28	3.44
		21600	GC4_CHe1	0.487	536	21.2	79.2	-29.39	-27.39	3.67
		21601	GC4_CHe2	0.511	538	21.4	76.2	-29.33	-27.33	3.80
		21602	GC4_CHe3	0.532	560	22.5	77.1	-29.64	-27.63	3.92
		21603	GC4_CHe4	0.568	591	23.6	75.7	-29.62	-27.61	4.16
		21604	GC4_CHe5	0.456	474	18.8	74.8	-29.59	-27.58	4.39
		21605	GC4_CHf1	0.397	416	16.4	75.4	-29.64	-27.63	4.50
		21606	GC4_CHf2	0.556	591	23.4	76.7	-29.70	-27.69	4.60
		21607	GC4_CHf3	0.551	573	22.8	75.2	-29.69	-27.68	4.78
		21608	GC4_CHf4	0.546	564	22.5	74.9	-29.45	-27.44	5.05
		21609	GC4_CHf5	0.515	521	20.8	73.3	-29.54	-27.53	5.22
		21610	GC4_CHf6	0.540	569	22.8	76.7	-29.21	-27.21	5.45

		25121	GC4-CH1	0.726	1995	82.3	73.5	-30.42	-27.40	5.78
		25125	GC4-CH2	0.747	2071	85.9	74.6	-30.25	-27.23	6.29
		25126	GC4-CH3	0.732	2053	85.3	75.5	-30.24	-27.22	6.65
		25127	GC4-CH4	0.714	1961	81.0	73.5	-30.45	-27.43	7.26
		25128	GC4-CH5	0.786	2171	90.2	74.4	-30.52	-27.50	7.87
		25129	GC4-CH6	0.706	1946	80.4	73.8	-30.34	-27.32	8.34
		25130	GC4-CH7	0.704	1945	80.3	73.9	-30.37	-27.35	9.01
		25131	GC4-CH8	0.702	1951	80.7	74.6	-30.34	-27.32	9.70
		25132	GC4-CH9	0.749	2093	86.8	75.1	-30.43	-27.41	10.01
		25133	GC4-CH10	0.762	2134	88.2	75.1	-30.29	-27.27	10.54
		25134	GC4-CH11	0.757	2090	86.3	73.9	-30.04	-27.03	11.24
		25135	GC4-CH12	0.763	2111	87.7	74.5	-29.96	-26.95	11.59
		25136	GC4-CH13	0.719	1991	82.2	74.1	-29.78	-26.77	12.44
		25137	GC4-CH14	0.727	2018	83.3	74.3	-29.77	-26.76	12.91
		25138	GC4-CH15	0.753	2093	87.0	74.9	-29.60	-26.59	13.31
		25139	GC4-CH16	0.730	2020	83.7	74.3	-29.70	-26.70	13.59
		25143	GC4-CH17	0.792	2150	89.5	73.2	-29.79	-26.78	14.23
		25144	GC4-CH18	0.707	1938	80.4	73.7	-29.90	-26.89	14.98
		25145	GC4-CH19	0.733	2021	83.9	74.2	-29.94	-26.93	15.39
		25146	GC4-CH20	0.765	1856	76.8	65.1	-30.00	-26.99	15.95
		25147	GC4-CH21	0.750	2073	86.2	74.5	-30.01	-27.00	16.43
		25148	GC4-CH22	0.743	2026	83.6	73.0	-29.95	-26.94	17.17
		25149	GC4-CH23	0.764	2125	88.0	74.7	-29.74	-26.73	17.58
		25150	GC4-CH24	0.741	2052	84.9	74.3	-29.54	-26.53	18.11
		25151	GC4-CH25	0.736	2040	84.3	74.2	-29.60	-26.59	18.65
		25152	GC4-CH26	0.765	2099	87.3	74.0	-29.43	-26.43	19.19
		25153	GC4-CH27	0.741	2081	86.3	75.5	-29.34	-26.34	19.75

Table A2.7. Theronsberg wood (TB2_w)

Year	Sample ID	UCT No.	Subsample ID	Wt (mg)	Voltage (mv)	Area	%C	$\delta^{13}C$ (‰)	Std Corrected $\delta^{13}C$ (‰)	Distance from bark (mm)
2023	TB2_w	21635	TB2_Wa1	1.780	1047	42.1	42.1	-29.38	-27.35	0.00
		21636	TB2_Wa2	2.026	1176	47.8	42.0	-29.48	-27.45	0.19
		21637	TB2_Wa3	2.041	1229	49.8	43.4	-29.42	-27.39	0.41
		21638	TB2_Wa4	2.017	1217	49.5	43.6	-29.26	-27.23	0.54
		21639	TB2_Wa5	2.008	1233	49.9	44.2	-29.12	-27.10	0.69
		21640	TB2_Wa6	2.015	1224	49.7	43.9	-28.88	-26.85	0.87
		21641	TB2_Wa7	2.038	1230	50.5	44.0	-28.62	-26.61	1.04
		21642	TB2_Wa8	2.026	1238	50.4	44.3	-28.36	-26.35	1.22
		21643	TB2_Wa9	1.873	1139	46.1	43.8	-28.41	-26.40	1.34
		21644	TB2_Wb1	2.039	1217	49.6	43.3	-28.62	-26.60	1.44
		21645	TB2_Wb2	2.039	1241	50.5	44.1	-28.75	-26.73	1.57
		21646	TB2_Wb3	2.061	1208	50.1	43.2	-28.64	-26.62	1.70
		21650	TB2_Wb4	2.008	1216	50.1	44.4	-28.91	-26.89	1.82
		21651	TB2_Wb5	2.027	1244	50.7	44.5	-28.90	-26.88	1.95
		21652	TB2_Wb6	2.031	1217	50.0	43.8	-28.92	-26.90	2.11
		21653	TB2_Wb7	2.030	1243	50.9	44.6	-28.71	-26.69	2.27
		21654	TB2_Wb8	2.050	1247	51.0	44.3	-28.84	-26.81	2.49
		21655	TB2_Wb9	2.023	1221	50.8	44.6	-28.91	-26.89	2.68
		21656	TB2_Wb10	2.006	1233	50.2	44.5	-28.81	-26.79	2.84
		21657	TB2_Wb11	2.059	1242	51.3	44.4	-28.41	-26.40	3.06
		21658	TB2_Wb12	2.037	1242	50.7	44.3	-28.29	-26.28	3.19
		21659	TB2_Wb13	2.012	1216	50.3	44.5	-28.29	-26.28	3.36
		21660	TB2_Wb14	2.036	1237	50.8	44.4	-28.35	-26.33	3.52
		21661	TB2_Wb15	2.044	1243	50.9	44.3	-28.51	-26.49	3.68
		21665	TB2_Wb16	2.004	1220	49.4	43.9	-28.38	-26.36	3.90
		21666	TB2_Wb17	2.063	1268	51.7	44.6	-28.43	-26.42	4.12
		21667	TB2_Wc1	2.044	1249	51.1	44.4	-28.44	-26.42	4.32
		21668	TB2_Wc2	2.041	1245	50.9	44.3	-28.24	-26.23	4.47
		21669	TB2_Wc3	2.062	1273	51.9	44.8	-28.11	-26.10	4.65
		21670	TB2_Wc4	2.018	1230	50.1	44.2	-28.03	-26.03	4.78

		21671	TB2_Wc5	2.062	1254	51.8	44.7	-27.89	-25.89	4.99
		21672	TB2_Wc6	2.003	1225	50.3	44.6	-27.62	-25.62	5.19
		21673	TB2_Wc7	2.015	1252	50.9	44.9	-27.71	-25.70	5.41
		21674	TB2_Wc8	2.035	1257	51.3	44.8	-27.46	-25.46	5.68
		21675	TB2_Wc9	2.019	1244	50.8	44.8	-27.35	-25.35	6.00
		21676	TB2_Wd1	2.029	1243	50.6	44.4	-27.53	-25.53	6.15
		21680	TB2_Wd2	2.041	1271	51.6	45.0	-27.35	-25.35	6.26
		21681	TB2_Wd3	2.036	1258	51.2	44.7	-27.28	-25.29	6.41
		21682	TB2_Wd4	2.021	1243	51.0	44.9	-27.51	-25.51	6.62
		21683	TB2_Wd5	2.048	1258	51.3	44.6	-27.70	-25.69	6.78
		21684	TB2_Wd6	2.019	1249	51.0	44.9	-28.13	-26.12	6.95
		21685	TB2_Wd7	2.059	1270	52.0	44.9	-28.24	-26.23	7.15
		21686	TB2_Wd8	2.060	1269	51.7	44.6	-28.06	-26.05	7.36
		21687	TB2_Wd9	2.000	1244	50.5	45.0	-27.72	-25.71	7.64
		21688	TB2_Wd10	2.047	1280	52.1	45.2	-27.54	-25.54	7.81
		21689	TB2_Wd11	2.053	1271	51.5	44.6	-27.56	-25.55	8.21
		21690	TB2_Wd12	2.051	1271	51.8	45.0	-27.47	-25.47	8.40
		21691	TB2_We1	2.015	1243	50.4	44.5	-27.59	-25.59	8.54
		21695	TB2_We2	2.034	1259	50.9	44.5	-27.51	-25.51	8.68
		21696	TB2_We3	2.010	1251	50.6	44.7	-27.27	-25.28	8.79
		21697	TB2_We4	2.015	1268	51.2	45.2	-27.41	-25.41	8.94
		21698	TB2_We5	2.031	1263	51.2	44.9	-27.61	-25.61	9.17
		21699	TB2_We6	2.014	1262	51.2	45.2	-27.81	-25.80	9.31
		21700	TB2_We7	2.024	1273	51.5	45.3	-28.08	-26.07	9.54
		21701	TB2_We8	2.021	1267	51.6	45.4	-28.11	-26.10	9.69
		21702	TB2_We9	2.016	1265	51.1	45.1	-27.81	-25.80	9.87
		21703	TB2_We10	2.051	1278	51.8	44.9	-27.65	-25.65	10.00
		21704	TB2_We11	2.035	1279	51.8	45.3	-27.42	-25.42	10.25
		21705	TB2_We12	2.007	1258	51.2	45.4	-27.53	-25.53	10.44
		21706	TB2_We13	2.054	1280	51.8	44.8	-27.51	-25.51	10.65
		21707	TB2_We14	2.054	1283	52.4	45.4	-27.43	-25.43	10.81

Table A2.8. Montagu Pass wood (MP_w)

Year	Sample ID	UCT No.	Subsample ID	Wt (mg)	Voltage (mv)	Area	%C	$\delta^{13}C$ (‰)	Std Corrected $\delta^{13}C$ (‰)	Distance from bark (mm)
2024	MP_w	28110	MP_w1a	2.454	5063	211.2	46.7	-30.52	-27.02	0.00
		28111	MP_w1b	2.240	4631	193.2	46.8	-30.03	-26.54	0.51
		28112	MP_w1c	2.415	5005	209.2	47.0	-29.75	-26.27	0.87
		28113	MP_w1d	2.268	4686	194.0	46.5	-30.69	-27.19	1.07
		28114	MP_w2a	2.327	4822	200.4	46.8	-29.91	-26.42	1.61
		28115	MP_w2b	2.247	4694	193.1	46.7	-29.39	-25.91	1.99
		28116	MP_w2c	2.259	4732	195.2	46.9	-29.27	-25.79	2.32
		28117	MP_w2d	2.432	5045	210.0	46.9	-29.74	-26.26	2.77
		28118	MP_w2e	2.461	5087	212.5	46.9	-29.90	-26.42	3.18
		28119	MP_w3a	2.330	4788	201.0	46.8	-29.24	-25.76	3.62
		28120	MP_w3b	2.402	4983	207.5	46.9	-28.83	-25.35	3.94
		28124	MP_w3c	2.472	5127	212.7	46.7	-28.91	-25.44	4.43
		28125	MP_w3d	2.459	5083	211.6	46.7	-29.58	-26.09	4.95
		28126	MP_w4a	2.439	5015	209.0	46.6	-30.42	-26.92	5.34
		28127	MP_w4b1	2.392	4768	198.3	45.0	-29.46	-25.98	5.96
		28130	MP_w4c	2.509	5171	216.7	46.9	-29.45	-25.96	6.57
		28131	MP_w4d	2.373	4936	205.2	47.0	-29.65	-26.16	6.91
		28132	MP_w4e	2.401	5011	207.7	47.0	-31.09	-27.58	7.13
		28133	MP_w5a	2.310	4751	199.1	46.8	-31.17	-27.66	7.49
		28134	MP_w5b	2.346	4906	203.7	47.2	-30.06	-26.57	8.00
		28135	MP_w5c	2.480	5171	216.1	47.3	-29.53	-26.05	8.46
		28136	MP_w5d	2.395	4984	207.3	47.0	-29.36	-25.88	8.87
		28137	MP_w5e	2.515	5033	210.2	45.4	-29.75	-26.27	9.19
		28141	MP_w5f	2.422	5054	210.6	47.2	-30.79	-27.29	9.60
		28142	MP_w6a	2.389	4988	206.9	47.1	-29.87	-26.39	10.10
		28143	MP_w6b	2.397	5061	210.1	47.6	-29.04	-25.56	10.56

		28144	MP_w6c	2.441	5140	213.5	47.5	-28.76	-25.29	11.07
		28145	MP_w6d	2.473	5204	216.5	47.6	-29.01	-25.53	11.53
		28146	MP_w6e	2.473	4850	201.4	44.2	-29.51	-26.02	12.14
		28147	MP_w6f	2.446	5135	213.6	47.4	-29.63	-26.15	12.51
		28148	MP_w6g	2.339	4908	203.0	47.1	-30.02	-26.53	12.77
		28149	MP_w7a	2.507	5230	219.0	47.4	-29.52	-26.04	12.95
		28150	MP_w7b	2.323	4839	201.2	47.1	-29.86	-26.37	13.26
		28151	MP_w7c	2.410	5010	208.4	47.0	-30.49	-27.00	13.88
		28152	MP_w7d	2.314	4820	200.2	47.0	-30.33	-26.84	14.10

Table A2.9. Montagu Pass charcoal (MP_ch)

Year	Sample ID	UCT No.	Subsample ID	Wt (mg)	Voltage (mv)	Area	%C	$\delta^{13}C$ (‰)	Std Corrected $\delta^{13}C$ (‰)	Distance from bark (mm)
2024	MP_ch	28160	MP_ch1a	0.741	2425	99.4	72.9	-31.85	-28.34	0.00
		28161	MP_ch1b	0.696	2231	91.3	71.3	-31.44	-27.93	0.39
		28162	MP_ch1c	0.698	2328	95.9	74.6	-31.09	-27.59	0.83
		28163	MP_ch2a	0.704	2348	95.7	73.8	-30.90	-27.40	1.16
		28164	MP_ch2b	0.741	2191	91.3	67.0	-30.95	-27.44	1.48
		28165	MP_ch2c	0.771	1705	71.2	50.1	-30.27	-26.77	1.85
		28166	MP_ch2d	0.705	1762	72.7	56.1	-30.28	-26.78	2.42
		28167	MP_ch3a	0.705	2286	93.5	72.0	-30.33	-26.84	2.73
		28168	MP_ch3b	0.746	2376	97.7	71.1	-30.90	-27.40	3.04
		28169	MP_ch3c	0.721	2129	87.8	66.1	-30.36	-26.87	3.52
		28170	MP_ch3d	0.737	2488	101.5	74.8	-29.91	-26.42	3.71
		28171	MP_ch4a	0.843	2739	113.6	73.2	-30.35	-26.86	3.96
		28172	MP_ch4b	0.735	2364	96.4	71.3	-30.20	-26.71	4.24
		28177	MP_ch4c2	0.835	2664	112.7	73.3	-30.65	-27.15	4.64
		28178	MP_ch4d	0.792	2420	98.1	67.3	-30.41	-26.92	4.95
		28179	MP_ch4e	0.701	2366	96.0	74.4	-30.45	-26.96	5.22
		28180	MP_ch5a	0.818	2674	108.7	72.2	-30.72	-27.22	5.53
		28181	MP_ch5b	0.783	2526	102.6	71.1	-31.33	-27.82	5.89
		28182	MP_ch5c	0.752	2472	101.1	73.0	-31.29	-27.78	6.13
		28183	MP_ch5d	0.733	2415	100.3	74.3	-31.75	-28.23	6.68
		28184	MP_ch5e	0.838	2740	111.3	72.2	-31.24	-27.73	6.94
		28185	MP_ch5f	0.724	2382	97.3	73.0	-30.65	-27.15	7.24
		28186	MP_ch6a	0.743	2453	100.0	73.1	-30.75	-27.25	7.64
		28187	MP_ch6b	0.706	2340	94.9	73.0	-30.91	-27.41	7.97
		28188	MP_ch6c	0.743	2439	100.1	73.2	-30.76	-27.26	8.22
		28189	MP_ch6d	0.780	2568	104.5	72.8	-30.89	-27.39	8.53
		28190	MP_ch6e	0.701	2297	92.8	71.9	-29.92	-26.44	8.95

Table A2.10. Giant's Castle charcoal (GC2)

Year	Sample ID	UCT No.	Subsample ID	Wt (mg)	Voltage (mv)	Area	%C	$\delta^{13}C$ (‰)	Std Corrected $\delta^{13}C$ (‰)	Distance from bark (mm)
2024	GC2_ch	28214	GC_ch1a	0.768	2483	100.8	71.3	-29.58	-26.77	0.00
		28217	GC_ch1b	0.789	2585	105.1	72.3	-29.59	-26.78	0.36
		28220	GC_ch2a	0.708	2380	97.1	74.5	-29.53	-26.72	0.90
		28223	GC_ch2b	0.709	2321	93.8	71.8	-29.42	-26.61	1.19
		28226	GC_ch2c	0.710	2404	97.3	74.4	-29.50	-26.69	1.45
		28232	GC_ch3a	0.708	2366	95.1	72.9	-29.71	-26.90	1.63
		28235	GC_ch3b	0.779	2489	101.5	70.7	-29.88	-27.07	1.83
		28238	GC_ch4a	0.723	2425	98.2	73.7	-29.73	-26.92	2.10
		28241	GC_ch5a	0.777	2537	102.3	71.5	-29.57	-26.76	2.38
		28244	GC_ch5b	0.772	2629	106.2	74.7	-29.80	-26.99	2.64
		28250	GC_ch5c	0.736	2499	101.5	74.9	-29.91	-27.10	2.92
		28253	GC_ch5d	0.767	2531	102.1	72.3	-30.11	-27.29	3.11
		28256	GC_ch6a	0.702	2270	91.9	71.1	-29.91	-27.09	3.43
		28260	GC_ch6b	0.737	2444	98.7	72.7	-30.05	-27.24	3.73
		28265	GC_ch6c	0.776	2548	103.9	72.7	-30.04	-27.22	4.11

		28267	GC_ch6d	0.737	2370	95.7	70.5	-30.18	-27.37	4.42
		28269	GC_ch6e	0.768	2525	102.0	72.1	-30.08	-27.27	4.64
		28271	GC_ch7a	0.722	2341	94.3	70.9	-30.17	-27.35	4.84
		28273	GC_ch7b	0.768	2562	103.6	73.2	-30.30	-27.48	5.04
		28275	GC_ch7c	0.758	2548	103.3	74.0	-30.40	-27.59	5.46
		28277	GC_ch7d	0.703	2369	95.6	73.9	-30.35	-27.53	5.69
		28278	GC_ch7e	0.741	2296	93.3	68.4	-30.35	-27.54	6.05
		28276	GC_ch8a	0.726	2474	99.4	74.3	-30.48	-27.66	6.39
		28274	GC_ch8b	0.729	2408	97.5	72.6	-30.43	-27.61	6.63
		28272	GC_ch9a	0.709	2318	93.9	71.9	-30.40	-27.58	6.92
		28270	GC_ch9b	0.728	2417	97.7	72.9	-30.42	-27.60	7.12
		28268	GC_ch9c	0.711	2322	93.7	71.6	-30.41	-27.59	7.26
		28266	GC_ch9d	0.786	2436	98.5	68.0	-30.19	-27.37	7.59
		28261	GC_ch9e	0.705	2291	92.5	71.3	-30.18	-27.36	7.81
		28258	GC_ch9f	0.740	2209	89.4	65.6	-30.17	-27.35	8.06

Table A2.11. Gifberg charcoal (GB1_ch)

Year	Sample ID	UCT No.	Subsample ID	Wt (mg)	Voltage (mv)	Area	%C	$\delta^{13}C$ (‰)	Std Corrected $\delta^{13}C$ (‰)	Distance from bark (mm)
2024	GB1_ch	28222	GB_ch1a	0.735	2314	93.0	68.7	-26.53	-23.76	0.00
		28225	GB_ch2a	0.771	1856	74.9	52.7	-26.24	-23.48	0.24
		28231	GB_ch3a	0.740	2391	96.0	70.5	-26.30	-23.53	0.38
		28234	GB_ch4a	0.765	2494	100.5	71.3	-26.26	-23.49	0.49
		28237	GB_ch5a	0.764	2525	101.9	72.4	-26.28	-23.52	0.62
		28240	GB_ch5b+6	0.737	2417	97.5	71.8	-26.19	-23.43	0.77
		28243	GB_ch7a	0.715	2234	89.7	68.1	-26.08	-23.31	0.87
		28249	GB_ch8a	0.802	2602	104.8	71.0	-26.16	-23.40	1.10
		28252	GB_ch9a	0.640	2037	81.9	69.5	-25.88	-23.12	1.26
		28257	GB_ch9b	0.738	2324	94.1	69.2	-25.80	-23.04	1.39
		28255	GB_ch10a	0.710	2205	88.6	67.8	-25.79	-23.03	1.62
		28254	GB_ch10b	0.767	2393	96.4	68.2	-25.56	-22.81	1.71
		28251	GB_ch11a	0.757	2275	91.9	65.9	-25.51	-22.75	1.83
		28248	GB_ch11b	0.739	2300	92.3	67.8	-25.54	-22.79	2.07
		28242	GB_ch12a	0.779	2420	97.8	68.2	-25.50	-22.75	2.24
		28239	GB_ch12b	0.750	2294	92.2	66.8	-25.45	-22.69	2.44
		28236	GB_ch13a	0.759	2344	93.8	67.1	-25.48	-22.72	2.55
		28279	GB_ch13b	0.812	2405	97.0	64.9	-25.37	-22.61	2.73
		28233	GB_ch14a	0.775	2311	93.3	65.3	-25.36	-22.61	2.81
		28224	GB_ch15+16_2	0.904	2744	110.7	66.5	-25.64	-22.88	2.94
		28218	GB_ch17a	0.634	1903	76.6	65.6	-25.68	-22.92	3.50
		28215	GB_ch19a	0.673	1970	79.0	63.7	-25.72	-22.96	3.95

Table A2.12. Waterfall Bluff A (WB_A)

Year	Sample ID	UCT No.	Subsample ID	Wt (mg)	Voltage (mv)	Area	%C	$\delta^{13}C$ (‰)	Std Corrected $\delta^{13}C$ (‰)	Distance from bark (mm)
2024	WB_A	3011	WB_A_1	0.566	1115	18.2	53.7	-22.27	-23.24	0.00
		3022	WB_A_2	0.552	1170	19.4	58.9	-22.17	-23.14	0.52
		2998	WB_A_3	0.565	1199	20.2	59.7	-21.90	-22.87	0.84
		3012	WB_A_4	0.558	1229	20.4	61.2	-21.99	-22.96	0.99
		3016	WB_A_5	0.598	1224	20.5	57.3	-22.01	-22.98	1.26
		3021	WB_A_6	0.578	1225	20.4	58.9	-21.96	-22.93	1.46
		3004	WB_A_7	0.537	1119	18.3	57.0	-21.75	-22.72	1.77
		3030	WB_A_8	0.550	1198	19.9	60.5	-22.04	-23.01	2.05
		3003	WB_A_9	0.585	1235	20.5	58.7	-21.84	-22.81	2.32
		3032	WB_A_10	0.537	1187	19.6	61.0	-22.03	-23.00	2.48
		3020	WB_A_11	0.557	1242	20.9	62.6	-22.15	-23.12	2.67
		2999	WB_A_12	0.595	1322	22.4	62.9	-22.01	-22.98	2.87
		3014	WB_A_13	0.532	1193	19.9	62.5	-22.06	-23.03	3.40
		3017	WB_A_14	0.529	1158	19.1	60.4	-21.96	-22.93	3.60

Table A2.13. Waterfall Bluff B (WB_B)

Year	Sample ID	UCT No.	Subsample ID	Wt (mg)	Voltage (mv)	Area	%C	$\delta^{13}C$ (‰)	Std Corrected $\delta^{13}C$ (‰)	Distance from bark (mm)
2024	WB_B	3028	WB_B_1	0.522	995.0	15.9	51.0	-21.79	-22.76	0.00
		3006	WB_B_2	0.579	1232	20.6	59.4	-21.50	-22.47	0.50
		3002	WB_B_3	0.524	1140	18.6	59.3	-21.30	-22.27	0.79
		2996	WB_B_4	0.531	1122	18.2	57.4	-21.63	-22.60	0.91
		3026	WB_B_5	0.515	1118	18.3	59.3	-21.87	-22.84	1.46
		3033	WB_B_6	0.581	1257	21.3	61.2	-21.81	-22.78	1.69
		3031	WB_B_7	0.429	902	14.3	55.6	-22.17	-23.14	1.88
		3019	WB_B_8	0.565	1151	19.2	56.8	-22.21	-23.18	2.07

Table A2.14. Boomplaas 4_24 (BPA4_24)

Year	Sample ID	UCT No.	Subsample ID	Wt (mg)	Voltage (mv)	Area	%C	$\delta^{13}C$ (‰)	Std Corrected $\delta^{13}C$ (‰)	Distance from bark (mm)
2024	BPA4_24	2540	BPA4_24_1	0.583	1418.0	20.3	52.4	-23.34	-24.92	0.00
		2541	BPA4_24_2	0.504	1151	15.8	47.1	-23.59	-25.16	0.37
		2542	BPA4_24_3	0.583	1475	21.3	55.0	-22.61	-24.18	0.57
		2543	BPA4_24_4	0.521	1321	18.7	53.9	-22.68	-24.25	0.79
		2544	BPA4_24_5	0.559	1425	20.4	55.0	-22.74	-24.31	1.00
		2545	BPA4_24_6	0.543	1379	19.7	54.5	-22.95	-24.52	1.33
		2546	BPA4_24_7	0.578	1455	21.0	54.7	-23.00	-24.57	1.51
		2547	BPA4_24_8	0.595	1483	21.6	54.5	-23.34	-24.92	1.66
		2548	BPA4_24_9	0.545	1419	20.3	55.9	-23.29	-24.87	1.89
		2549	BPA4_24_10	0.566	1399	20.5	54.6	-23.21	-24.78	2.06
		2550	BPA4_24_11	0.509	1297	18.5	54.8	-23.11	-24.68	2.31
		2551	BPA4_24_12	0.554	1409	20.3	55.2	-23.13	-24.70	2.50
		2552	BPA4_24_13	0.537	1351	19.5	54.7	-23.34	-24.92	2.66
		2553	BPA4_24_14	0.521	1345	19.0	55.0	-23.13	-24.70	2.88
		2554	BPA4_24_15	0.524	1323	19.0	54.4	-23.36	-24.94	3.06
		2558	BPA4_24_16	0.556	1402	20.3	54.8	-23.00	-24.57	3.21
		2559	BPA4_24_17	0.529	1295	18.3	52.1	-22.65	-24.22	3.46
		2560	BPA4_24_18	0.525	1303	18.4	52.6	-23.36	-24.93	3.64
		2561	BPA4_24_19	0.471	1197	16.8	53.5	-23.36	-24.93	3.84
		2562	BPA4_24_20	0.517	1308	18.6	54.0	-22.99	-24.56	4.04
		2563	BPA4_24_21	0.557	1405	20.4	55.2	-22.91	-24.48	4.31
		2565	BPA4_24_23	0.559	1394	20.1	54.0	-23.12	-24.69	7.37
		2566	BPA4_24_24	0.583	1436	20.9	53.8	-23.02	-24.59	7.57
		2567	BPA4_24_25	0.552	1394	20.1	54.9	-22.29	-23.85	7.82
		2568	BPA4_24_26	0.570	1409	20.4	53.8	-22.60	-24.17	8.23
		2569	BPA4_24_27	0.520	1123	15.7	45.5	-23.18	-24.75	8.67
		2570	BPA4_24_28	0.540	1311	18.6	51.8	-22.58	-24.14	8.96
		2571	BPA4_24_29	0.550	1295	18.4	50.3	-22.28	-23.84	9.38
		2572	BPA4_24_30	0.535	1221	17.2	48.3	-22.38	-23.95	9.86

Table A2.15. Boomplaas 4_21 (BPA4_21)

Year	Sample ID	UCT No.	Subsample ID	Wt (mg)	Voltage (mv)	Area	%C	$\delta^{13}C$ (‰)	Std Corrected $\delta^{13}C$ (‰)	Distance from bark (mm)
2024	BPA4_21	3001	BPA_21_1	0.420	697.0	10.5	41.7	-23.03	-24.00	0.00
		3007	BPA4_21_2	0.555	1154	19.1	57.6	-23.23	-24.20	0.38
		3029	BPA4_21_3	0.431	954	15.1	58.4	-23.37	-24.34	0.53
		3027	BPA4_21_4	0.550	1187	19.6	59.5	-23.42	-24.39	0.90
		3000	BPA4_21_5	0.568	1193	19.8	58.3	-23.21	-24.18	1.08
		2997	BPA4_21_6	0.587	1258	21.2	60.3	-23.12	-24.09	1.57
		3015	BPA4_21_7	0.554	1202	20.0	60.4	-23.28	-24.25	1.80
		3018	BPA4_21_8	0.554	1225	20.4	61.5	-23.29	-24.26	2.47
		3013	BPA4_21_9	0.533	1162	19.2	60.3	-23.02	-23.99	3.00
		3005	BPA4_21_10	0.591	1240	20.7	58.6	-23.26	-24.23	3.39

Table A2.16. Boomplaas 2_21 (BPA2_21)

Year	Sample ID	UCT No.	Subsample ID	Wt (mg)	Voltage (mv)	Area	%C	$\delta^{13}C$ (‰)	Std Corrected $\delta^{13}C$ (‰)
2021	BPA2_21	14403	BPA 2.1	0.531	1151	47.2	66.4	-24.73	-24.52
		14404	BPA 2.2	0.507	1130	45.9	67.6	-24.89	-24.68
		14405	BPA 2.3	0.515	1128	46.8	67.9	-24.39	-24.18
		14406	BPA 2.4	0.514	1106	45.8	66.6	-24.86	-24.65
		14407	BPA 2.5	0.544	1153	47.4	65.2	-25.01	-24.80
		14408	BPA 2.6	0.461	1005	41.1	66.6	-24.69	-24.48
		14409	BPA 2.7	0.53	1155	47.1	66.5	-25.16	-24.94
		14410	BPA 2.8	0.524	1100	46.1	65.7	-24.54	-24.33
		14411	BPA 2.9	0.537	1166	47.2	65.6	-24.63	-24.43
		14412	BPA 2.10	0.539	1126	47.2	65.5	-24.80	-24.59
		14413	BPA 2.11	0.503	1071	43.7	64.9	-24.84	-24.63
		14414	BPA 2.12	0.543	1101	44.7	61.5	-25.09	-24.87
		14415	BPA 2.13	0.53	1089	44.1	62.2	-24.86	-24.65
		14383	BPA 2.14	0.542	1139	46.8	63.6	-25.53	-25.05
		14384	BPA 2.15	0.421	881	36.4	63.5	-25.48	-25.00
		14401	BPA 2.16	0.519	1097	45.5	65.5	-24.78	-24.57
		14402	BPA 2.17	0.539	1140	46.8	64.9	-24.66	-24.45

APPENDIX 3

Growth Increment Amplitudes: Calculating $\Delta\delta^{13}C_{meas}$

Grey rows indicate increments excluded because they lack either a minimum ($\delta^{13}C_{min}$) or maximum ($\delta^{13}C_{max}$) $\delta^{13}C$ value within the bounds of a given growth increment, as identified by physical ring structure or isotopic patterning. Red rows indicate increments excluded due to either an insufficient number of subsamples (<2) to represent seasonal change, and/or intra-increment amplitudes ($\Delta\delta^{13}C$) below the analytical precision and repeatability limit (0.16 ‰).

Table A3.1. Camps Bay wood PB

GI	No. of subsamples per GI	Max. ID	Min. ID	$\delta^{13}C$ Max. (‰)	$\delta^{13}C$ Min. (‰)	$\Delta\delta^{13}C_{meas}$ (‰)	Schubert & Jahren Correction (% of $\Delta\delta^{13}C_{max}$)	Schubert & Jahren Correction $\Delta\delta^{13}C_{meas}$ (‰)	Grouped Correction (% of $\Delta\delta^{13}C_{max}$)	Grouped Correction $\Delta\delta^{13}C_{meas}$ (‰)	Sample Correction (% of $\Delta\delta^{13}C_{max}$)	Sample Correction $\Delta\delta^{13}C_{meas}$ (‰)	Genus Correction (% of $\Delta\delta^{13}C_{max}$)	Genus Correction $\Delta\delta^{13}C_{meas}$ (‰)	Winter Correction (% of $\Delta\delta^{13}C_{max}$)	Winter Correction $\Delta\delta^{13}C_{meas}$ (‰)
1	11	cb5dw	cb5hw	-25.71	-26.63	0.92	77.47	1.19	73.47	1.25	67.44	1.36	55.28	1.66	73.44	1.25
2	4	cb4bw	cb5aw	-25.94	-26.20	0.26	50.78	0.51	39.80	0.65	54.55	0.48	34.46	0.75	52.96	0.49
3	6	cb3cw	cb3fw	-25.12	-26.21	1.09	63.23	1.72	53.92	2.02	61.24	1.78	43.91	2.48	63.00	1.73
4	7	cb2aw	cb2fw	-24.82	-25.84	1.02	67.36	1.51	59.17	1.72	63.17	1.61	47.14	2.16	66.13	1.54
5	9	cb1bw	cb1iw	-23.96	-24.82	0.86	73.34	1.17	67.36	1.28	65.77	1.31	51.92	1.66	70.52	1.22
Total	**37**		**Mean**	**-25.11**	**-25.94**	**0.83**	**66.44**	**1.22**	**58.75**	**1.39**	**62.43**	**1.31**	**46.54**	**1.74**	**65.21**	**1.25**
Mean	**7.40**		**st dev**	**0.78**	**0.69**	**0.33**		**0.46**		**0.52**		**0.50**		**0.65**		**0.47**

Table A3.2. Camps Bay wood IB

GI	No. of subsamples per GI	Max. ID	Min. ID	$\delta^{13}C$ Max. (‰)	$\delta^{13}C$ Min. (‰)	$\Delta\delta^{13}C_{meas}$ (‰)	Schubert & Jahren Correction (% of $\Delta\delta^{13}C_{max}$)	Schubert & Jahren Correction $\Delta\delta^{13}C_{meas}$ (‰)	Grouped Correction (% of $\Delta\delta^{13}C_{max}$)	Grouped Correction $\Delta\delta^{13}C_{meas}$ (‰)	Sample Correction (% of $\Delta\delta^{13}C_{max}$)	Sample Correction $\Delta\delta^{13}C_{meas}$ (‰)	Genus Correction (% of $\Delta\delta^{13}C_{max}$)	Genus Correction $\Delta\delta^{13}C_{meas}$ (‰)	Winter Correction (% of $\Delta\delta^{13}C_{max}$)	Winter Correction $\Delta\delta^{13}C_{meas}$ (‰)
1	3	cb5iw	cb5kw	-26.14	-26.55	0.41	40.75	1.01	29.99	1.37	48.00	0.85	27.16	1.51	44.16	0.93
2	12	cb5dw	cb5hw	-25.71	-26.63	0.92	79.09	1.16	75.97	1.21	68.06	1.35	56.61	1.63	74.57	1.23
3	7	cb3cw	cb3fw	-25.12	-26.21	1.09	67.36	1.62	59.17	1.84	63.17	1.73	47.14	2.31	66.13	1.65
4	15	cb1bw	cb2fw	-23.96	-25.84	1.88	82.80	2.27	81.96	2.29	69.44	2.71	59.70	3.15	77.09	2.44
Total	**37**		**Mean**	**-25.23**	**-26.31**	**1.08**	**67.50**	**1.51**	**61.77**	**1.68**	**62.17**	**1.66**	**47.65**	**2.15**	**65.49**	**1.56**
Mean	**9.25**		**st dev**	**0.95**	**0.36**	**0.61**		**0.57**		**0.49**		**0.78**		**0.75**		**0.65**

Table A3.3. Camps Bay charcoal PB

GI	No. of subsamples per GI	Max. ID	Min. ID	$\delta^{13}C$ Max. (‰)	$\delta^{13}C$ Min. (‰)	$\Delta\delta^{13}C_{meas}$ (‰)	Schubert & Jahren Correction (% of $\Delta\delta^{13}C_{max}$)	Schubert & Jahren Correction $\Delta\delta^{13}C_{meas}$ (‰)	Grouped Correction (% of $\Delta\delta^{13}C_{max}$)	Grouped Correction $\Delta\delta^{13}C_{meas}$ (‰)	Sample Correction (% of $\Delta\delta^{13}C_{max}$)	Sample Correction $\Delta\delta^{13}C_{meas}$ (‰)	Genus Correction (% of $\Delta\delta^{13}C_{max}$)	Genus Correction $\Delta\delta^{13}C_{meas}$ (‰)	Winter Correction (% of $\Delta\delta^{13}C_{max}$)	Winter Correction $\Delta\delta^{13}C_{meas}$ (‰)
1	4	cb6bc	cb6cc	-26.67	-26.98	0.31	50.78	0.61	39.80	0.78	54.55	0.57	34.46	0.90	52.96	0.59
2	10	cb5cc	cb5ic	-26.34	-26.79	0.45	75.58	0.60	70.62	0.64	66.69	0.67	53.74	0.84	72.11	0.62
3	3	cb4ac	cb5ac	-25.74	-26.24	0.50	40.75	1.23	29.99	1.67	48.00	1.04	27.16	1.84	44.16	1.13
4	4	cb3cc	cb3dc	-25.89	-26.31	0.42	50.78	0.83	39.80	1.06	54.55	0.77	34.46	1.22	52.96	0.79
5	4	cb2ac	cb2dc	-25.35	-25.69	0.34	50.78	0.67	39.80	0.85	54.55	0.62	34.46	0.99	52.96	0.64
6	5	cb1cc	cb1dc	-25.30	-25.46	0.16	57.91	0.28	47.59	0.34	58.55	0.27	39.82	0.40	58.82	0.27
Total	**25**		**Mean**	**-26.00**	**-26.40**	**0.40**	**53.73**	**0.79**	**44.01**	**1.00**	**55.67**	**0.74**	**36.86**	**1.16**	**55.03**	**0.76**
Mean	**5.00**		**st dev**	**0.52**	**0.51**	**0.08**		**0.26**		**0.40**		**0.19**		**0.41**		**0.22**

Table A3.4. Camps Bay charcoal IB

GI	No. of subsamples per GI	Max. ID	Min. ID	$\delta^{13}C$ Max. (‰)	$\delta^{13}C$ Min. (‰)	$\Delta\delta^{13}C_{meas}$ (‰)	Schubert & Jahren Correction (% of $\Delta\delta^{13}C_{max}$)	Schubert & Jahren Correction $\Delta\delta^{13}C_{meas}$ (‰)	Grouped Correction (% of $\Delta\delta^{13}C_{max}$)	Grouped Correction $\Delta\delta^{13}C_{meas}$ (‰)	Sample Correction (% of $\Delta\delta^{13}C_{max}$)	Sample Correction $\Delta\delta^{13}C_{meas}$ (‰)	Genus Correction (% of $\Delta\delta^{13}C_{max}$)	Genus Correction $\Delta\delta^{13}C_{meas}$ (‰)	Winter Correction (% of $\Delta\delta^{13}C_{max}$)	Winter Correction $\Delta\delta^{13}C_{meas}$ (‰)
1	9	cb5hc	cb6cc	-26.38	-26.98	0.60	73.34	0.82	67.36	0.89	65.77	0.91	51.92	1.16	70.52	0.85
2	8	cb4ac	cb5ec	-25.74	-26.61	0.87	70.65	1.23	63.59	1.37	64.63	1.35	49.76	1.75	68.57	1.27
3	13	cb1ec	cb3dc	-25.27	-26.31	1.04	80.49	1.29	78.19	1.33	68.59	1.52	57.78	1.80	75.53	1.38
Total	**30**		**Mean**	**-25.80**	**-26.63**	**0.84**	**74.83**	**1.11**	**69.72**	**1.20**	**66.33**	**1.26**	**53.15**	**1.57**	**71.54**	**1.17**
Mean	**10.00**		**st dev**	**0.56**	**0.34**	**0.22**		**0.26**		**0.27**		**0.31**		**0.36**		**0.28**

Table A3.5. Swartberg wood IB

GI	No. of subsamples per GI	Max. ID	Min. ID	$\delta^{13}C$ Max. (‰)	$\delta^{13}C$ Min. (‰)	$\Delta\delta^{13}C_{meas}$ (‰)	Schubert & Jahren Correction (% of $\Delta\delta^{13}C_{max}$)	Schubert & Jahren Correction $\Delta\delta^{13}C_{meas}$ (‰)	Grouped Correction (% of $\Delta\delta^{13}C_{max}$)	Grouped Correction $\Delta\delta^{13}C_{meas}$ (‰)	Sample Correction (% of $\Delta\delta^{13}C_{max}$)	Sample Correction $\Delta\delta^{13}C_{meas}$ (‰)	Genus Correction (% of $\Delta\delta^{13}C_{max}$)	Genus Correction $\Delta\delta^{13}C_{meas}$ (‰)
1	8	sb_w25	sb_w27	-25.79	-26.57	0.78	70.65	1.11	63.59	1.23	69.76	1.12	49.76	1.57
2	7	sb_w18	sb_w19	-25.14	-27.22	2.08	67.36	3.08	59.17	3.51	65.54	3.17	47.14	4.40
3	4	sb_w10	sb_w12	-25.62	-27.08	1.45	50.78	2.86	39.80	3.65	46.02	3.16	34.46	4.22
4	9	sb_w5	sb_w9	-25.13	-26.82	1.69	73.34	2.30	67.36	2.50	73.31	2.30	51.92	3.25
5	21	sb_w41b	sbw_40h	-25.49	-27.01	1.51	87.31	1.73	89.73	1.69	93.20	1.62	63.50	2.38
6	12	sb_w43g	sbw_42c	-26.25	-27.05	0.80	79.09	1.01	75.97	1.05	81.18	0.99	56.61	1.41
7	13	sbw_44h	sbw_43b	-25.76	-26.48	0.72	80.49	0.89	78.19	0.92	83.17	0.86	57.78	1.24
Total	**74**		**Mean**	**-25.60**	**-26.89**	**1.29**	**72.72**	**1.86**	**67.69**	**2.08**	**73.17**	**1.89**	**51.60**	**2.64**
Mean	**10.57**		**st dev**	**0.39**	**0.27**	**0.53**		**0.91**		**1.15**		**1.00**		**1.33**

Table A3.6. Swartberg wood PB

GI	No. of subsamples per GI	Max. ID	Min. ID	$\delta^{13}C$ Max. (‰)	$\delta^{13}C$ Min. (‰)	$\Delta\delta^{13}C_{meas}$ (‰)	Schubert & Jahren Correction (% of $\Delta\delta^{13}C_{max}$)	Schubert & Jahren Correction $\Delta\delta^{13}C_{meas}$ (‰)	Grouped Correction (% of $\Delta\delta^{13}C_{max}$)	Grouped Correction $\Delta\delta^{13}C_{meas}$ (‰)	Sample Correction (% of $\Delta\delta^{13}C_{max}$)	Sample Correction $\Delta\delta^{13}C_{meas}$ (‰)	Genus Correction (% of $\Delta\delta^{13}C_{max}$)	Genus Correction $\Delta\delta^{13}C_{meas}$ (‰)
1	1	sb_w27	n.m	-26.57										
2	3	sbw_25	sbw_26	-25.79	-25.84	0.04	40.75	0.11	29.99	0.15	35.46	0.12	27.16	0.16
3	2	sbw_22	sbw_23	-26.36	-26.52	0.16	25.59	0.64	17.24	0.94	21.00	0.77	16.60	0.98
4	6	sbw_18	sbw_20	-25.14	-27.28	2.14	63.23	3.38	53.92	3.97	60.41	3.54	43.91	4.87
5	4	sbw_15	n.m.	-25.75										
6	1	sbw_11	n.m.	-25.82										
7	2	sbw_10	n.m.	-25.62										
8	8	sbw_4	sbw_8	-25.13	-26.39	1.25	70.65	1.77	63.59	1.97	69.76	1.80	49.76	2.52
9	9	sb_w40a	sb_w40h	-25.62	-27.01	1.39	73.34	1.90	67.36	2.06	73.31	1.90	51.92	2.68
10	5	sb_w41a	sb_w41c	-25.52	-25.61	0.09	57.91	0.15	47.59	0.18	54.07	0.16	39.82	0.22
11	11	sb_w42i	sb_w42j	-25.82	-25.93	0.11	77.47	0.15	73.47	0.15	78.92	0.14	55.28	0.20
12	11	sb_w43g	sb_w43j	-26.25	-26.49	0.24	77.47	0.31	73.47	0.33	78.92	0.31	55.28	0.44
13	11	sb_w44h	sb_w44k	-25.76	-26.08	0.32	77.47	0.42	73.47	0.44	78.92	0.41	55.28	0.58
Total	**45**		**Mean**	**-25.58**	**-26.65**	**1.07**	**72.43**	**1.56**	**66.36**	**1.75**	**72.26**	**1.59**	**51.23**	**2.22**
Mean	**9.00**		**st dev**	**0.47**	**0.48**	**0.79**		**1.26**		**1.48**		**1.32**		**1.82**

Table A3.7. Swartberg charcoal IB

GI	No. of subsamples per GI	Max. ID	Min. ID	$\delta^{13}C$ Max. (‰)	$\delta^{13}C$ Min. (‰)	$\Delta\delta^{13}C_{meas}$ (‰)	Schubert & Jahren Correction (% of $\Delta\delta^{13}C_{max}$)	Schubert & Jahren Correction $\Delta\delta^{13}C_{meas}$ (‰)	Grouped Correction (% of $\Delta\delta^{13}C_{max}$)	Grouped Correction $\Delta\delta^{13}C_{meas}$ (‰)	Sample Correction (% of $\Delta\delta^{13}C_{max}$)	Sample Correction $\Delta\delta^{13}C_{meas}$ (‰)	Genus Correction (% of $\Delta\delta^{13}C_{max}$)	Genus Correction $\Delta\delta^{13}C_{meas}$ (‰)
1	10	sb_ch16	sb_ch20	-26.64	-27.74	1.09	75.58	1.45	70.62	1.55	52.02	2.10	53.74	2.04
2	3	sb_ch9	sb_ch10	-27.99	-28.18	0.19	40.75	0.47	29.99	0.63	32.30	0.59	27.16	0.70
3	9	sb_ch2	sb_ch8	-26.06	-28.47	2.41	73.34	3.28	67.36	3.57	50.91	4.73	51.92	4.63
4	11	sb_ch4f	sb_ch5e	-26.72	-27.44	0.72	77.47	0.93	73.47	0.98	52.94	1.36	55.28	1.30
5	7	sb_ch3a	sb_ch3e	-26.86	-27.34	0.48	67.36	0.71	59.17	0.81	47.84	1.00	47.14	1.02
6	10	sb_ch1g	sb_ch2c	-26.30	-26.89	0.59	75.58	0.78	70.62	0.84	52.02	1.13	53.74	1.10
Total	**50**		**Mean**	**-26.76**	**-27.68**	**0.91**	**68.35**	**1.27**	**61.87**	**1.40**	**48.00**	**1.82**	**48.16**	**1.80**
Mean	**8.33**		**st dev**	**0.67**	**0.58**	**0.79**		**1.04**		**1.11**		**1.51**		**1.46**

Table A3.8. Swartberg charcoal PB

GI	No. of subsamples per GI	Max. ID	Min. ID	$\delta^{13}C$ Max. (‰)	$\delta^{13}C$ Min. (‰)	$\Delta\delta^{13}C_{meas}$ (‰)	Schubert & Jahren Correction (% of $\Delta\delta^{13}C_{max}$)	Schubert & Jahren Correction $\Delta\delta^{13}C_{meas}$ (‰)	Grouped Correction (% of $\Delta\delta^{13}C_{max}$)	Grouped Correction $\Delta\delta^{13}C_{meas}$ (‰)	Sample Correction (% of $\Delta\delta^{13}C_{max}$)	Sample Correction $\Delta\delta^{13}C_{meas}$ (‰)	Genus Correction (% of $\Delta\delta^{13}C_{max}$)	Genus Correction $\Delta\delta^{13}C_{meas}$ (‰)
1	7	sb5b	sb5e	-26.76	-27.44	0.68	67.36	1.01	59.17	1.15	47.84	1.42	47.14	1.44
2	6	sb4f	sb5a	-26.72	-26.93	0.21	63.23	0.33	53.92	0.39	45.65	0.46	43.91	0.48
3	5	sb3a	sb3e	-26.86	-27.34	0.48	57.91	0.83	47.59	1.01	42.70	1.12	39.82	1.21
4	5	sb2b	sb2c	-26.78	-26.89	0.11	57.91	0.19	47.59	0.23	42.70	0.26	39.82	0.28
5	7	sb1g	sb2a	-26.30	-26.67	0.37	67.36	0.55	59.17	0.63	47.84	0.77	47.14	0.78
Total	**25**		**Mean**	**-26.66**	**-27.10**	**0.44**	**63.96**	**0.68**	**54.96**	**0.79**	**46.01**	**0.94**	**44.50**	**0.98**
Mean	**6.25**		**st dev**	**0.25**	**0.36**	**0.20**		**0.30**		**0.35**		**0.42**		**0.43**

Table A3.9. Giant's Castle (GC4 Protea) *wood* IB

GI	No. of subsamples per GI	Max. ID	Min. ID	$\delta^{13}C$ Max. (‰)	$\delta^{13}C$ Min. (‰)	$\Delta\delta^{13}C_{meas}$ (‰)	Schubert & Jahren Correction (% of $\Delta\delta^{13}C_{max}$)	Schubert & Jahren Correction $\Delta\delta^{13}C_{meas}$ (‰)	Grouped Correction (% of $\Delta\delta^{13}C_{max}$)	Grouped Correction $\Delta\delta^{13}C_{meas}$ (‰)	Sample Correction (% of $\Delta\delta^{13}C_{max}$)	Sample Correction $\Delta\delta^{13}C_{meas}$ (‰)	Genus Correction (% of $\Delta\delta^{13}C_{max}$)	Genus Correction $\Delta\delta^{13}C_{meas}$ (‰)
1	3	gc4_w42	gc4_w44	-25.33	-25.75	0.42	40.75	1.03	29.99	1.40	25.16	1.67	27.16	1.54
2	4	gc4_w39	gc4_w41	-24.81	-25.86	1.05	50.78	2.06	39.80	2.63	32.72	3.20	34.46	3.04
3	4	gc4_w36	gcw_w37	-25.39	-25.69	0.30	50.78	0.60	39.80	0.77	32.72	0.93	34.46	0.88
4	3	gc4_w31	gc4_w33	-25.18	-25.68	0.50	40.75	1.23	29.99	1.67	25.16	1.99	27.16	1.84
5	8	gc4_w28	gc4_w30	-24.99	-25.82	0.83	70.65	1.17	63.59	1.30	49.84	1.66	49.76	1.67
6	4	gc4_w21	gc4_w22	-25.79	-26.01	0.23	50.78	0.45	39.80	0.57	32.72	0.69	34.46	0.66
7	8	gc4_w15	gc4_w20	-25.66	-26.07	0.41	70.65	0.58	63.59	0.64	49.84	0.82	49.76	0.82
8	6	gc4_w9	gc4_w10	-25.88	-26.19	0.32	63.23	0.50	53.92	0.59	43.08	0.73	43.91	0.72
9	4	gc4_w2	gc4_w4	-25.85	-26.32	0.47	50.78	0.93	39.80	1.18	32.72	1.44	34.46	1.37
10	8	gc4_wf5	gc4_wf6	-26.46	-26.66	0.20	70.65	0.28	63.59	0.31	49.84	0.40	49.76	0.40
11	4	gc4_we5	gc4_wf2	-26.55	-26.84	0.29	50.78	0.57	39.80	0.73	32.72	0.89	34.46	0.85
12	3	gc4_we2	gc4_we4	-26.12	-26.58	0.46	40.75	1.13	29.99	1.54	25.16	1.83	27.16	1.70
13	8	gc4_wc5	gc4_we1	-25.56	-26.42	0.86	70.65	1.22	63.59	1.36	49.84	1.73	49.76	1.74
14	8	gc4_wb4	gc4_wc1	-25.95	-26.45	0.50	70.65	0.71	63.59	0.79	49.84	1.00	49.76	1.00
15	5	gc4_wa5	gc4_wa7	-26.30	-26.58	0.27	57.91	0.47	47.59	0.57	38.51	0.71	39.82	0.68
Total	**80**		**Mean**	**-25.72**	**-26.19**	**0.47**	**56.70**	**0.86**	**47.23**	**1.07**	**37.99**	**1.31**	**39.09**	**1.26**
Mean	**5.33**		**st dev**	**0.52**	**0.39**	**0.25**		**0.46**		**0.60**		**0.72**		**0.68**

Table A3.10. Giant's Castle (GC4 *Protea*) wood PB

GI	No. of subsamples per GI	Max. ID	Min. ID	$\delta^{13}C$ Max. (‰)	$\delta^{13}C$ Min. (‰)	$\Delta\delta^{13}C_{meas}$ (‰)	Schubert & Jahren Correction (% of $\Delta\delta^{13}C_{max}$)	Schubert & Jahren Correction $\Delta\delta^{13}C_{meas}$ (‰)	Grouped Correction (% of $\Delta\delta^{13}C_{max}$)	Grouped Correction $\Delta\delta^{13}C_{meas}$ (‰)	Sample Correction (% of $\Delta\delta^{13}C_{max}$)	Sample Correction $\Delta\delta^{13}C_{meas}$ (‰)	Genus Correction (% of $\Delta\delta^{13}C_{max}$)	Genus Correction $\Delta\delta^{13}C_{meas}$ (‰)
1	10	gc_wf5	gc_wf6	-26.46	-26.66	0.19	75.58	0.26	70.62	0.28	54.60	0.36	53.74	0.36
2	6	gc_we2	gc_we6	-26.12	-26.68	0.56	63.23	0.89	53.92	1.04	43.08	1.31	43.91	1.28
3	2	gc_wd1	gc_wd2	-25.76	-25.97	0.21	25.59	0.83	17.24	1.24	14.86	1.43	16.60	1.28
4	6	gc_wc2	gc_wc3	-26.19	-26.38	0.19	63.23	0.31	53.92	0.36	43.08	0.45	43.91	0.44
5	6	gc_wb4	gc_wb6	-25.95	-26.36	0.42	63.23	0.66	53.92	0.77	43.08	0.97	43.91	0.95
6	8	gc_wa1	gc_wa2	-26.24	-26.72	0.47	70.65	0.67	63.59	0.74	49.84	0.95	49.76	0.95
Total	**36**		**Mean**	**-26.19**	**-26.56**	**0.37**	**67.18**	**0.56**	**59.20**	**0.64**	**46.74**	**0.81**	**47.05**	**0.80**
Mean	**7.20**		**st dev**	**0.19**	**0.17**	**0.17**		**0.27**		**0.32**		**0.40**		**0.39**

Table A3.11. Giant's Castle (GC4 *Protea*) charcoal IB

GI	No. of subsamples per GI	Max. ID	Min. ID	$\delta^{13}C$ Max. (‰)	$\delta^{13}C$ Min. (‰)	$\Delta\delta^{13}C_{meas}$ (‰)	Schubert & Jahren Correction (% of $\Delta\delta^{13}C_{max}$)	Schubert & Jahren Correction $\Delta\delta^{13}C_{meas}$ (‰)	Grouped Correction (% of $\Delta\delta^{13}C_{max}$)	Grouped Correction $\Delta\delta^{13}C_{meas}$ (‰)	Sample Correction (% of $\Delta\delta^{13}C_{max}$)	Sample Correction $\Delta\delta^{13}C_{meas}$ (‰)	Genus Correction (% of $\Delta\delta^{13}C_{max}$)	Genus Correction $\Delta\delta^{13}C_{meas}$ (‰)
1	6	gc4_ch27	n.m.	-26.34										
2	16	gc4_ch15	gc4_ch21	-26.59	-27.00	0.41	83.76	0.48	83.56	0.49	63.03	0.64	60.50	0.67
3	8	gc4_chf6	gc4_ch5	-27.21	-27.50	0.29	70.65	0.41	63.59	0.45	49.84	0.58	49.76	0.58
4	7	gc4_chc2	gc4_chf2	-27.33	-27.69	0.36	67.36	0.53	59.17	0.61	46.78	0.77	47.14	0.76
5	6	gc4_chc4	gc4_che1	-27.20	-27.39	0.19	63.23	0.30	53.92	0.35	43.08	0.44	43.91	0.43
6	4	gc4_ch2	gc4_chc3	-26.59	-27.24	0.65	50.78	1.28	39.80	1.63	32.72	1.99	34.46	1.89
7	6	gc4_chb2	gc4_chb3	-26.66	-27.29	0.63	63.23	1.00	53.92	1.17	43.08	1.46	43.91	1.43
8	4	gc4_cha3	gc4_cha4	-27.22	-27.65	0.43	50.78	0.85	39.80	1.08	32.72	1.31	34.46	1.25
Total	**51**		**Mean**	**-26.97**	**-27.39**	**0.42**	**64.26**	**0.69**	**56.25**	**0.83**	**44.47**	**1.03**	**44.88**	**1.00**
Mean	**7.29**		**st dev**	**0.34**	**0.24**	**0.17**		**0.36**		**0.48**		**0.57**		**0.53**

Table A3.12. Giant's Castle (GC4 *Protea*) charcoal PB

GI	No. of subsamples per GI	Max. ID	Min. ID	$\delta^{13}C$ Max. (‰)	$\delta^{13}C$ Min. (‰)	$\Delta\delta^{13}C_{meas}$ (‰)	Schubert & Jahren Correction (% of $\Delta\delta^{13}C_{max}$)	Schubert & Jahren Correction $\Delta\delta^{13}C_{meas}$ (‰)	Grouped Correction (% of $\Delta\delta^{13}C_{max}$)	Grouped Correction $\Delta\delta^{13}C_{meas}$ (‰)	Sample Correction (% of $\Delta\delta^{13}C_{max}$)	Sample Correction $\Delta\delta^{13}C_{meas}$ (‰)	Genus Correction (% of $\Delta\delta^{13}C_{max}$)	Genus Correction $\Delta\delta^{13}C_{meas}$ (‰)
1	6	gc4_chf4	gc4_chf5	-27.44	-27.53	0.09	63.23	0.14	53.92	0.16	43.08	0.21	43.91	0.20
2	5	gc4_che2	gc4_che3	-27.33	-27.63	0.30	57.91	0.53	47.59	1.10	38.51	0.79	39.82	0.76
3	2	gc4_chd2	gc4_che1	-27.28	-27.39	0.11	25.59	0.43	17.24	2.47	14.86	0.73	16.60	0.66
4	6	gc4_chc2	gc4_chc3	-26.59	-27.24	0.65	63.23	1.03	53.92	1.92	43.08	1.52	43.91	1.49
5	4	gc4_chb2	gc4_chb3	-26.66	-27.29	0.64	50.78	1.26	39.80	3.15	32.72	1.95	34.46	1.85
6	7	gc4_cha3	gc4_cha4	-27.22	-27.65	0.43	67.36	0.64	59.17	1.08	46.78	0.92	47.14	0.91
Total	**22**		**Mean**	**-26.95**	**-27.45**	**0.51**	**59.82**	**0.86**	**50.12**	**1.81**	**40.27**	**1.29**	**41.33**	**1.25**
Mean	**5.50**		**st dev**	**0.38**	**0.22**	**0.17**		**0.34**		**0.97**		**0.54**		**0.51**

Table A3.13. Theronsberg wood IB

GI	No. of subsamples per GI	Max. ID	Min. ID	$\delta^{13}C$ Max. (‰)	$\delta^{13}C$ Min. (‰)	$\Delta\delta^{13}C_{meas}$ (‰)	Schubert & Jahren Correction (% of $\Delta\delta^{13}C_{max}$)	Schubert & Jahren Correction $\Delta\delta^{13}C_{meas}$ (‰)	Grouped Correction (% of $\Delta\delta^{13}C_{max}$)	Grouped Correction $\Delta\delta^{13}C_{meas}$ (‰)	Sample Correction (% of $\Delta\delta^{13}C_{max}$)	Sample Correction $\Delta\delta^{13}C_{meas}$ (‰)	Genus Correction (% of $\Delta\delta^{13}C_{max}$)	Genus Correction $\Delta\delta^{13}C_{meas}$ (‰)	Winter Correction (% of $\Delta\delta^{13}C_{max}$)	Winter Correction $\Delta\delta^{13}C_{meas}$ (‰)
1	13	tb2_we3	tb2_we8	-25.28	-26.10	0.83	80.49	1.03	78.19	1.06	79.30	1.04	57.78	1.43	75.53	1.09
2	24	tb2_wd3	tb2_wd7	-25.29	-26.23	0.94	88.78	1.06	92.40	1.02	87.08	1.08	64.76	1.45	81.03	1.16
3	18	tb2_wa8	tb2_wb9	-26.35	-26.89	0.54	85.39	0.63	86.36	0.63	83.91	0.65	61.88	0.88	78.82	0.69
Total	**55**		**Mean**	**-25.64**	**-26.41**	**0.77**	**84.89**	**0.91**	**85.65**	**0.90**	**83.43**	**0.92**	**61.47**	**1.25**	**78.46**	**0.98**
Mean	**18.33**		**st dev**	**0.62**	**0.42**	**0.21**		**0.24**		**0.24**		**0.24**		**0.33**		**0.26**

Table A3.14. Theronsberg wood PB

GI	No. of subsamples per GI	Max. ID	Min. ID	$\delta^{13}C$ Max. (‰)	$\delta^{13}C$ Min. (‰)	$\Delta\delta^{13}C_{meas}$ (‰)	Schubert & Jahren Correction (% of $\Delta\delta^{13}C_{max}$)	Schubert & Jahren Correction $\Delta\delta^{13}C_{meas}$ (‰)	Grouped Correction (% of $\Delta\delta^{13}C_{max}$)	Grouped Correction $\Delta\delta^{13}C_{meas}$ (‰)	Sample Correction (% of $\Delta\delta^{13}C_{max}$)	Sample Correction $\Delta\delta^{13}C_{meas}$ (‰)	Genus Correction (% of $\Delta\delta^{13}C_{max}$)	Genus Correction $\Delta\delta^{13}C_{meas}$ (‰)	Winter Correction (% of $\Delta\delta^{13}C_{max}$)	Winter Correction $\Delta\delta^{13}C_{meas}$ (‰)
1	14	tb2_we3	tb2_we8	-25.28	-26.10	0.83	81.72	1.01	80.17	1.03	80.46	1.03	58.80	1.40	76.36	1.08
2	12	tb2_wd3	tb2_wd7	-25.29	-26.23	0.94	79.09	1.19	75.97	1.24	77.98	1.21	56.61	1.66	74.57	1.26
3	9	tb2_wc9	tb2_wd1	-25.35	-25.53	0.18	73.34	0.25	67.36	0.27	72.53	0.25	51.92	0.35	70.52	0.26
4	17	tb2_wb12	tb2_wb15	-26.28	-26.49	0.21	84.62	0.25	85.03	0.25	83.19	0.25	61.23	0.34	78.31	0.27
5	9	tb2_wa8	tb2_wb1	-26.35	-26.60	0.25	73.34	0.35	67.36	0.38	72.53	0.35	51.92	0.49	70.52	0.36
Total	**61**		**Mean**	**-25.71**	**-26.19**	**0.48**	**78.42**	**0.61**	**75.18**	**0.63**	**77.34**	**0.62**	**56.10**	**0.85**	**74.06**	**0.65**
Mean	**12.20**		**st dev**	**0.55**	**0.42**	**0.37**		**0.45**		**0.47**		**0.46**		**0.63**		**0.49**

Table A3.15. Montagu Pass wood PB and IB

GI	No. of subsamples per GI	Max. ID	Min. ID	$\delta^{13}C$ Max. (‰)	$\delta^{13}C$ Min. (‰)	$\Delta\delta^{13}C_{meas}$ (‰)	Schubert & Jahren Correction (% of $\Delta\delta^{13}C_{max}$)	Schubert & Jahren Correction $\Delta\delta^{13}C_{meas}$ (‰)	Grouped Correction (% of $\Delta\delta^{13}C_{max}$)	Grouped Correction $\Delta\delta^{13}C_{meas}$ (‰)	Sample Correction (% of $\Delta\delta^{13}C_{max}$)	Sample Correction $\Delta\delta^{13}C_{meas}$ (‰)	Genus Correction (% of $\Delta\delta^{13}C_{max}$)	Genus Correction $\Delta\delta^{13}C_{meas}$ (‰)
1	4	mp_w7a	mp_w7c	-26.04	-27.00	0.96	50.78	1.89	39.80	2.42	70.76	1.36	60.47	1.59
2	7	mp_w6c	mp_w6g	-25.29	-26.53	1.24	67.36	1.84	59.17	2.09	96.75	1.28	77.42	1.60
3	5	mp_w5d	mp_w5f	-25.88	-27.29	1.42	57.91	2.45	47.59	2.98	81.74	1.73	67.90	2.09
4	5	mp_w4c	mp_w5a	-25.96	-27.66	1.70	57.91	2.93	47.59	3.57	81.74	2.08	67.90	2.50
5	5	mp_w3b	mp_w4a	-25.35	-26.92	1.57	57.91	2.71	47.59	3.30	81.74	1.92	67.90	2.31
6	5	mp_w2c	mp_w2e	-25.79	-26.42	0.63	57.91	1.08	47.59	1.31	81.74	0.77	67.90	0.92
7	4	mp_w1c	mp_w1d	-26.27	-27.19	0.92	50.78	1.81	39.80	2.31	70.76	1.30	60.47	1.52
Total	**35**		**Mean**	**-25.80**	**-27.00**	**1.20**	**57.22**	**2.10**	**47.02**	**2.57**	**80.75**	**1.49**	**67.14**	**1.79**
Mean	**5.00**		**st dev**	**0.36**	**0.43**	**0.39**		**0.64**		**0.77**		**0.45**		**0.54**

Table A3.16. Montagu Pass charcoal PB

GI	No. of subsamples per GI	Max. ID	Min. ID	$\delta^{13}C$ Max. (‰)	$\delta^{13}C$ Min. (‰)	$\Delta\delta^{13}C_{meas}$ (‰)	Schubert & Jahren Correction (% of $\Delta\delta^{13}C_{max}$)	Schubert & Jahren Correction $\Delta\delta^{13}C_{meas}$ (‰)	Grouped Correction (% of $\Delta\delta^{13}C_{max}$)	Grouped Correction $\Delta\delta^{13}C_{meas}$ (‰)	Sample Correction (% of $\Delta\delta^{13}C_{max}$)	Sample Correction $\Delta\delta^{13}C_{meas}$ (‰)	Genus Correction (% of $\Delta\delta^{13}C_{max}$)	Genus Correction $\Delta\delta^{13}C_{meas}$ (‰)
1	3	mp_ch6c	mp_ch6d	-27.26	-27.39	0.13	40.75	0.31	29.99	0.43	47.47	0.27	27.16	0.47
2	6	mp_ch5f	mp_ch6b	-27.15	-27.41	0.26	63.23	0.41	53.92	0.48	54.99	0.47	73.31	0.35
3	5	mp_ch4d	mp_ch5b	-26.92	-27.82	0.91	57.91	1.56	47.59	1.90	53.57	1.69	67.90	1.33
4	4	mp_ch3d	mp_ch4a	-26.42	-26.86	0.44	50.78	0.86	39.80	1.10	51.37	0.85	60.47	0.72
5	5	mp_ch2c	mp_ch3b	-26.77	-27.40	0.62	57.91	1.08	47.59	1.31	53.57	1.16	67.90	0.92
6	4	mp_ch1c	n.m.	-27.59										
Total	**20**		**Mean**	**-26.82**	**-27.37**	**0.56**	**57.45**	**0.98**	**47.23**	**1.20**	**53.38**	**1.04**	**67.39**	**0.83**
Mean	**5.00**		**st dev**	**0.31**	**0.40**	**0.28**		**0.48**		**0.59**		**0.52**		**0.41**

Table A3.17. Montagu Pass charcoal IB

GI	No. of subsamples per GI	Max. ID	Min. ID	$\delta^{13}C$ Max. (‰)	$\delta^{13}C$ Min. (‰)	$\Delta\delta^{13}C_{meas}$ (‰)	Schubert & Jahren Correction (% of $\Delta\delta^{13}C_{max}$)	Schubert & Jahren Correction $\Delta\delta^{13}C_{meas}$ (‰)	Grouped Correction (% of $\Delta\delta^{13}C_{max}$)	Grouped Correction $\Delta\delta^{13}C_{meas}$ (‰)	Sample Correction (% of $\Delta\delta^{13}C_{max}$)	Sample Correction $\Delta\delta^{13}C_{meas}$ (‰)	Genus Correction (% of $\Delta\delta^{13}C_{max}$)	Genus Correction $\Delta\delta^{13}C_{meas}$ (‰)
1	9	mp_ch5f	mp_ch6b	-27.15	-27.41	0.26	73.34	0.35	67.36	0.38	57.25	0.45	83.25	0.31
2	5	mp_ch4d	mp_ch5d	-26.92	-28.23	1.31	57.91	2.27	47.59	2.76	53.57	2.45	67.90	1.94
3	6	mp_ch3d	mp_ch4c2	-26.42	-27.15	0.73	63.23	1.16	53.92	1.36	54.99	1.34	73.31	1.00
4	7	mp_ch2c	mp_ch3b	-26.77	-27.40	0.62	67.36	0.92	59.17	1.05	55.97	1.11	77.42	0.80
Total	**27**		**Mean**	**-26.82**	**-27.55**	**0.73**	**65.46**	**1.18**	**57.01**	**1.39**	**55.45**	**1.34**	**75.47**	**1.01**
Mean	**6.75**		**st dev**	**0.31**	**0.47**	**0.44**		**0.80**		**1.00**		**0.83**		**0.68**

Table A3.18. Giant's Castle (GC2 *Podocarpus*) charcoal PB

GI	No. of subsamples per GI	Max. ID	Min. ID	$\delta^{13}C$ Max. (‰)	$\delta^{13}C$ Min. (‰)	$\Delta\delta^{13}C_{meas}$ (‰)	Schubert & Jahren Correction (% of $\Delta\delta^{13}C_{max}$)	Schubert & Jahren Correction $\Delta\delta^{13}C_{meas}$ (‰)	Grouped Correction (% of $\Delta\delta^{13}C_{max}$)	Grouped Correction $\Delta\delta^{13}C_{meas}$ (‰)	Sample Correction (% of $\Delta\delta^{13}C_{max}$)	Sample Correction $\Delta\delta^{13}C_{meas}$ (‰)	Genus Correction (% of $\Delta\delta^{13}C_{max}$)	Genus Correction $\Delta\delta^{13}C_{meas}$ (‰)
1	6	gc_ch9a	gc_ch9c	-27.58	-27.59	0.01	63.23	0.01	53.92	0.01	55.97	0.01	73.31	0.01
2	2	gc_ch8b	n.m.	-27.61										
3	5	gc_ch7a	gc_ch7c	-27.35	-27.59	0.23	57.91	0.41	47.59	0.49	54.75	0.43	67.90	0.35
4	5	gc_ch6a	gc_ch6d	-27.09	-27.37	0.27	57.91	0.47	47.59	0.57	54.75	0.50	67.90	0.40
5	4	gc_ch5a	gc_ch5d	-26.76	-27.29	0.53	50.78	1.05	39.80	1.34	52.83	1.01	60.47	0.88
6	1	gc_ch4a	n.m.	-26.92										
7	1	n.m.	gc_ch3b		-27.07									
8	6	gc_ch2b	gc_ch3a	-26.61	-26.90	0.28	63.23	0.45	53.92	0.53	55.97	0.51	73.31	0.39
Total	**20**		**Mean**	**-26.96**	**-27.29**	**0.33**	**57.45**	**0.59**	**47.23**	**0.73**	**54.57**	**0.61**	**67.39**	**0.50**
Mean	**5.00**		**st dev**	**0.33**	**0.29**	**0.14**		**0.31**		**0.41**		**0.27**		**0.25**

Table A3.19. Giant's Castle (GC2 *Podocarpus*) charcoal IB

GI	No. of subsamples per GI	Max. ID	Min. ID	$\delta^{13}C$ Max. (‰)	$\delta^{13}C$ Min. (‰)	$\Delta\delta^{13}C_{meas}$ (‰)	Schubert & Jahren Correction (% of $\Delta\delta^{13}C_{max}$)	Schubert & Jahren Correction $\Delta\delta^{13}C_{meas}$ (‰)	Grouped Correction (% of $\Delta\delta^{13}C_{max}$)	Grouped Correction $\Delta\delta^{13}C_{meas}$ (‰)	Sample Correction (% of $\Delta\delta^{13}C_{max}$)	Sample Correction $\Delta\delta^{13}C_{meas}$ (‰)	Genus Correction (% of $\Delta\delta^{13}C_{max}$)	Genus Correction $\Delta\delta^{13}C_{meas}$ (‰)
1	4	gc_ch9a	gc_ch9b	-27.58	-27.60	0.02	50.78	0.05	39.80	0.06	52.83	0.04	60.47	0.04
2	3	gc_ch7e	gc_ch8a	-27.54	-27.66	0.12	40.75	0.31	29.99	0.41	49.37	0.25	49.61	0.25
3	4	gc_ch6e	gc_ch7c	-27.27	-27.59	0.32	50.78	0.62	39.80	0.79	52.83	0.60	60.47	0.52
4	4	gc_ch6a	gc_ch6d	-27.09	-27.37	0.27	50.78	0.54	39.80	0.68	52.83	0.52	60.47	0.45
5	5	gc_ch5a	gc_ch5d	-26.76	-27.29	0.53	57.91	0.92	47.59	1.12	54.75	0.98	67.90	0.79
6	7	gc_ch2b	gc_ch3b	-26.61	-27.07	0.46	67.36	0.68	59.17	0.77	56.81	0.80	77.42	0.59
Total	**20**		**Mean**	**-26.93**	**-27.33**	**0.39**	**56.71**	**0.69**	**46.59**	**0.84**	**54.30**	**0.72**	**66.56**	**0.59**
Mean	**5.00**		**st dev**	**0.30**	**0.21**	**0.12**		**0.17**		**0.19**		**0.21**		**0.14**

Table A3.20. Gifberg charcoal PB

GI	No. of subsamples per GI	Max. ID	Min. ID	$\delta^{13}C$ Max. (‰)	$\delta^{13}C$ Min. (‰)	$\Delta\delta^{13}C_{meas}$ (‰)	Schubert & Jahren Correction (% of $\Delta\delta^{13}C_{max}$)	Schubert & Jahren Correction $\Delta\delta^{13}C_{meas}$ (‰)	Grouped Correction (% of $\Delta\delta^{13}C_{max}$)	Grouped Correction $\Delta\delta^{13}C_{meas}$ (‰)	Sample Correction (% of $\Delta\delta^{13}C_{max}$)	Sample Correction $\Delta\delta^{13}C_{meas}$ (‰)	Genus Correction (% of $\Delta\delta^{13}C_{max}$)	Genus Correction $\Delta\delta^{13}C_{meas}$ (‰)	Winter Correction (% of $\Delta\delta^{13}C_{max}$)	Winter Correction $\Delta\delta^{13}C_{meas}$ (‰)
1	1	n.m.	gb_ch19a													
2	3	gb_ch14a	gb_ch17a	-22.61	-22.92	0.31	40.75	0.76	29.99	1.03			49.61	0.62	44.16	0.70
3	1	gb_ch13b	n.m.	-22.61												
4	1	n.m.	gb_ch13a													
5	2	gb_ch12a	n.m.	-22.75												
6	2	gb_ch11a	gb_ch11b	-22.75	-22.79	0.04	25.59	0.14	17.24	0.21			32.24	0.11	29.47	0.12
7	2	gb_ch10b	n.m.	-22.81												
8	2	gb_ch9b	n.m.	-23.04												
9	1	gb_ch8a	n.m.	-23.40												
10	1	gb_ch7a	n.m.	-23.31												
11	2	gb_ch5b+6	n.m.	-23.43												
12	1	gb_ch4a	n.m.	-23.49												
13	1	gb_ch3a	n.m.	-23.53												
14	1	gb_ch2a	n.m.	-23.48												
15	1	gb_ch1a	n.m.	-23.76												
Total	**3**		**Mean**	**-22.61**	**-22.92**	**0.31**	**40.75**	**0.76**	**29.99**	**1.03**			**49.61**	**0.62**	**44.16**	**0.70**
Mean	**3.00**		**st dev**													

Table A3.21. Gifberg charcoal IB

GI	No. of subsamples per GI	Max. ID	Min. ID	$\delta^{13}C$ Max. (‰)	$\delta^{13}C$ Min. (‰)	$\Delta\delta^{13}C_{meas}$ (‰)	Schubert & Jahren Correction (% of $\Delta\delta^{13}C_{max}$)	Schubert & Jahren Correction $\Delta\delta^{13}C_{meas}$ (‰)	Grouped Correction (% of $\Delta\delta^{13}C_{max}$)	Grouped Correction $\Delta\delta^{13}C_{meas}$ (‰)	Sample Correction (% of $\Delta\delta^{13}C_{max}$)	Sample Correction $\Delta\delta^{13}C_{meas}$ (‰)	Genus Correction (% of $\Delta\delta^{13}C_{max}$)	Genus Correction $\Delta\delta^{13}C_{meas}$ (‰)	Winter Correction (% of $\Delta\delta^{13}C_{max}$)	Winter Correction $\Delta\delta^{13}C_{meas}$ (‰)
1	5	gb_ch14a	gb_ch19a	-22.61	-22.96	0.35	57.91	0.61	47.59	0.74			67.90	0.52	58.82	0.60
2	3	gb_ch12b	gb_ch13a	-22.69	-22.72	0.03	40.75	0.08	29.99	0.10			49.61	0.06	44.16	0.07
3	3	gb_ch11a	gb_ch11b	-22.75	-22.79	0.04	40.75	0.09	29.99	0.12			49.61	0.07	44.16	0.08
4	5	gb_ch7a	gb_ch8a	-23.31	-23.40	0.09	57.91	0.15	47.59	0.18			67.90	0.13	58.82	0.15
5	3	gb_ch4a	gb_ch5a	-23.49	-23.52	0.02	40.75	0.05	29.99	0.07			49.61	0.04	44.16	0.05
6	3	gb_ch2a	gb_ch3a	-23.48	-23.53	0.06	40.75	0.14	29.99	0.19			49.61	0.12	44.16	0.13
Total	**5**		**Mean**	**-22.61**	**-22.96**	**0.35**	**57.91**	**0.61**	**47.59**	**0.74**			**67.90**	**0.52**	**58.82**	**0.60**
Mean	**5.00**		**st dev**													

Table A3.22. Waterfall Bluff (WB_A)

Isotopic GI	Subsample range	No. of subsamples per GI	Max. ID	Min. ID	$\delta^{13}C$ Max. (‰)	$\delta^{13}C$ Min. (‰)	$\Delta\delta^{13}C_{meas}$ (‰)	Grouped Correction (% of $\Delta\delta^{13}C_{max}$)	Grouped Correction $\Delta\delta^{13}C_{meas}$ (‰)	Genus Correction (% of $\Delta\delta^{13}C_{max}$)	Genus Correction $\Delta\delta^{13}C_{meas}$ (‰)
	Growing right to left (right older than left)										
1	12 to 13	2	wb_a_12	wb_a_13	-22.98	-23.03	0.06	17.24	0.32	32.24	0.17
2	9 to 11	3	wb_a_9	wb_a_11	-22.81	-23.12	0.31	29.99	1.03	49.61	0.63
3	6 to 8	3	wb_a_7	wb_a_8	-22.72	-23.01	0.29	29.99	0.98	49.61	0.59
4	1 to 5	5	wb_a_3	wb_a_5	-22.87	-22.98	0.11	47.59	0.23	67.90	0.16
	Mean	3.33			-22.80	-23.04	0.24	35.86	0.75	55.70	0.46
	st dev	1.53			0.08	0.07	0.11		0.45		0.26
WB_A	**Growing left to right (left older than right)**										
1	1 to 4	4	wb_a_3	wb_a_1	-22.87	-23.24	0.37	39.80	0.92	60.47	0.61
2	5 to 7	3	wb_a_7	wb_a_5	-22.72	-22.98	0.26	29.99	0.86	49.61	0.52
3	8 to 10	3	wb_a_9	wb_a_8	-22.81	-23.01	0.20	29.99	0.68	49.61	0.41
4	11 to 13	3	wb_a_12	wb_a_11	-22.98	-23.12	0.14	29.99	0.46	49.61	0.28
	Mean	3.25			-22.84	-23.09	0.24	32.44	0.73	52.32	0.45
	st dev	0.50			0.11	0.12	0.10		0.21		0.14
	Combined mean	**3.43**			**-22.82**	**-23.06**	**0.24**	**33.91**	**0.74**	**53.77**	**0.46**
	st dev	**0.79**			**0.09**	**0.10**	**0.09**		**0.30**		**0.18**

Table A3.23. Waterfall Bluff (WB_B)

	Growing right to left (right older than left)										
Isotopic GI	Subsample range	No. of subsamples per GI	Max. ID	Min. ID	$\delta^{13}C$ Max. (‰)	$\delta^{13}C$ Min. (‰)	$\Delta\delta^{13}C_{meas}$ (‰)	Grouped Correction (% of $\Delta\delta^{13}C_{max}$)	Grouped Correction $\Delta\delta^{13}C_{meas}$ (‰)	Genus Correction (% of $\Delta\delta^{13}C_{max}$)	Genus Correction $\Delta\delta^{13}C_{meas}$ (‰)
1	6 to 8	3	wb_b_6	wb_b_8	-22.78	-23.18	0.40	29.99	1.35	49.61	0.82
2	1 to 5	5	wb_b_3	wb_b_5	-22.27	-22.84	0.57	47.59	1.20	67.90	0.84
	Mean	4			-22.52	-23.01	0.49	38.79	1.28	58.75	0.83
	st dev	1.41			0.36	0.24	0.12		0.10		0.02
WB_B	**Growing left to right (left older than right)**										
1	1 to 4	3	wb_b_3	wb_b_1	-22.27	-22.78	0.51	29.99	1.71	49.61	1.03
2	5 to 7	3	wb_b_6	wb_b_5	-22.78	-22.84	0.06	29.99	0.20	49.61	0.12
	Mean	3.00			-22.27	-22.78	0.51	29.99	1.71	49.61	1.03
	st dev										
	Combined mean	**3.67**			**-22.44**	**-22.93**	**0.50**	**35.86**	**1.42**	**55.70**	**0.90**
	st dev	**1.15**			**0.30**	**0.22**	**0.09**		**0.26**		**0.12**

Table A3.24. Boomplaas Cave (BPA2_21)

	Growing right to left (right older than left)										
Isotopic GI	Subsample range	No. of subsamples per GI	Max. ID	Min. ID	$\delta^{13}C$ Max. (‰)	$\delta^{13}C$ Min. (‰)	$\Delta\delta^{13}C_{meas}$ (‰)	Grouped Correction (% of $\Delta\delta^{13}C_{max}$)	Grouped Correction $\Delta\delta^{13}C_{meas}$ (‰)	Genus Correction (% of $\Delta\delta^{13}C_{max}$)	Genus Correction $\Delta\delta^{13}C_{meas}$ (‰)
1	13 to 15	3	bpa2_13	bpa2_14	-24.65	-25.05	0.40	29.99	1.33	27.16	1.47
2	10 to 12	3	bpa2_10	bpa2_12	-24.59	-24.87	0.28	29.99	0.93	27.16	1.03
3	6 to 7	2	bpa2_6	bpa2_7	-24.48	-24.94	0.46	17.24	2.67	16.60	2.77
4	1 to 5	5	bpa2_3	bpa2_5	-24.18	-24.80	0.62	47.59	1.30	39.82	1.56
	Mean	3.67			-24.47	-24.91	0.43	35.86	1.19	31.38	1.35
	st dev	1.15			0.26	0.13	0.17		0.22		0.28
BPA2_21	**Growing left to right (left older than right)**										
1	1 to 4	4	bpa2_3	bpa2_2	-24.18	-24.68	0.50	39.80	1.26	34.46	1.45
2	5 to 7	3	bpa2_6	bpa2_5	-24.48	-24.80	0.32	29.99	1.07	27.16	1.18
3	7 to 9	3	bpa2_8	bpa2_7	-24.33	-24.94	0.61	29.99	2.03	27.16	2.25
4	11 to 13	3	bpa2_13	bpa2_12	-24.65	-24.87	0.22	29.99	0.73	27.16	0.81
5	14 to 17	4	bpa2_17	bpa2_14	-24.45	-25.05	0.60	39.80	1.51	34.46	1.74
	Mean	3.40			-24.42	-24.87	0.45	33.92	1.32	30.08	1.49
	st dev	0.58			0.18	0.14	0.17	5.38	0.49	4.00	0.55
	Combined mean	**3.50**			**-24.44**	**-24.88**	**0.44**	**34.64**	**1.27**	**30.56**	**1.44**
	st dev	**0.76**			**0.19**	**0.13**	**0.16**		**0.39**		**0.45**

Table A3.25. Boomplaas Cave (BPA4_21)

	Growing right to left (right older than left)										
Isotopic GI	Subsample range	No. of subsamples per GI	Max. ID	Min. ID	$\delta^{13}C$ Max. (‰)	$\delta^{13}C$ Min. (‰)	$\Delta\delta^{13}C_{meas}$ (‰)	Grouped Correction (% of $\Delta\delta^{13}C_{max}$)	Grouped Correction $\Delta\delta^{13}C_{meas}$ (‰)	Genus Correction (% of $\Delta\delta^{13}C_{max}$)	Genus Correction $\Delta\delta^{13}C_{meas}$ (‰)
1	8 to 10	3	bpa4_21_9	bpa4_21_10	-23.99	-24.23	0.25	29.99	0.82	27.16	0.90
2	5 to 8	4	bpa4_21_6	bpa4_21_8	-24.09	-24.26	0.17	39.80	0.42	34.46	0.48
3	1 to 4	4	bpa4_21_1	bpa4_21_4	-24.00	-24.39	0.39	39.80	0.98	34.46	1.13
	Mean	3.50			-23.99	-24.31	0.27	36.53	0.74	32.03	0.84
	st dev	0.71			0.01	0.11	0.10		0.11		0.16
BPA4_21	**Growing left to right (left older than right)**										
1	4 to 7	4	bpa4_21_6	bpa4_21_4	-24.09	-24.39	0.30	39.80	0.74	34.46	0.86
2	8 to 10	3	bpa4_21_9	bpa4_21_8	-23.99	-24.26	0.27	29.99	0.90	27.16	1.00
	Mean	3.50			-24.04	-24.32	0.28	34.90	0.82	30.81	0.93
	st dev	0.71			0.07	0.09	0.02		0.11		0.10
	Combined mean	**3.60**			**-24.03**	**-24.31**	**0.27**	**35.88**	**0.77**	**31.54**	**0.87**
	st dev	**0.55**			**0.06**	**0.08**	**0.08**		**0.22**		**0.24**

Table A3.26. Boomplaas Cave (BPA4_24)

	Growing right to left (right older than left)										
Isotopic GI	**Subsample range**	**No. of subsamples per GI**	**Max. ID**	**Min. ID**	**$\delta^{13}C$ Max. (‰)**	**$\delta^{13}C$ Min. (‰)**	**$\Delta\delta^{13}C_{meas}$ (‰)**	**Grouped Correction (% of $\Delta\delta^{13}C_{max}$)**	**Grouped Correction $\Delta\delta^{13}C_{meas}$ (‰)**	**Genus Correction (% of $\Delta\delta^{13}C_{max}$)**	**Genus Correction $\Delta\delta^{13}C_{meas}$ (‰)**
1	2 to 8	7	bpa4_24_3	bpa4_24_8	-24.18	-24.92	0.74	59.17	1.25	47.14	1.57
2	9 to 13	5	bpa4_24_11	bpa4_24_13	-24.68	-24.92	0.23	47.59	0.49	39.82	0.59
3	14 to 15	2	bpa4_24_14	bpa4_24_15	-24.70	-24.94	0.24	17.24	1.38	16.60	1.43
4	16 to 18	3	bpa4_24_17	bpa4_24_18	-24.22	-24.93	0.71	29.99	2.38	27.16	2.63
5	23 to 27	5	bpa4_24_25	bpa4_24_27	-23.85	-24.75	0.90	47.59	1.89	39.82	2.25
	Mean	5			-24.23	-24.88	0.65	46.09	1.50	38.48	1.76
	st dev	1.63			0.34	0.09	0.29		0.82		0.90
BPA4_24	**Growing left to right (left older than right)**										
1	27 to 30	4	bpa4_24_29	bpa4_24_27	-23.84	-24.75	0.91	39.80	2.28	34.46	2.64
2	23 to 26	4	bpa4_24_25	bpa4_24_23	-23.85	-24.69	0.84	39.80	2.12	34.46	2.45
3	15 to 18	4	bpa4_24_17	bpa4_24_15	-24.22	-24.94	0.72	39.80	1.80	34.46	2.08
4	13 to 14	2	bpa4_24_14	bpa4_24_13	-24.70	-24.92	0.22	17.24	1.25	16.60	1.30
5	8 to 12	5	bpa4_24_11	bpa4_24_8	-24.68	-24.92	0.24	47.59	0.50	39.82	0.59
6	2 to 7	6	bpa4_24_3	bpa4_24_2	-24.18	-25.16	0.99	53.92	1.83	43.91	2.24
	Mean	4.60			-24.15	-24.89	0.74	44.19	1.71	37.42	2.00
	st dev	0.89			0.34	0.18	0.30		0.71		0.81
	Combined mean	**4.78**			**-24.19**	**-24.89**	**0.70**	**45.03**	**1.62**	**37.89**	**1.89**
	st dev	**0.28**			**0.32**	**0.14**	**0.28**		**0.71**		**0.81**

APPENDIX 4
Calculating ΔP and P_S/P_W

Table A4.1. Camps Bay wood (IB)

Uncorrected			
GI	**$\Delta\delta^{13}C_{meas}$ (‰)**	**ΔP**	**P_S/P_W**
1	0.41	1.60	4.94
2	0.92	0.98	2.65
3	1.09	0.77	2.16
4	1.88	-0.20	0.82
mean	1.08	0.79	2.64
sd	0.61	0.74	1.72
Group Corrected			
GI	**$\Delta\delta^{13}C_{meas}$ (‰)**	**ΔP**	**P_S/P_W**
1	1.37	0.43	1.54
2	1.21	0.62	1.86
3	1.84	-0.15	0.86
4	2.29	-0.70	0.50
mean	1.68	0.05	1.19
sd	0.49	0.60	0.62
Genus Corrected			
GI	**$\Delta\delta^{13}C_{meas}$ (‰)**	**ΔP**	**P_S/P_W**
1	1.51	0.26	1.29
2	1.63	0.12	1.12
3	2.31	-0.72	0.49
4	3.15	-1.74	0.18
mean	2.15	-0.52	0.77
sd	0.75	0.92	0.53

Table A4.2. Camps Bay wood (PB)

Uncorrected			
GI	**$\Delta\delta^{13}C_{meas}$ (‰)**	**ΔP**	**P_S/P_W**
1	0.92	0.98	2.65
2	0.26	1.78	5.93
3	1.09	0.77	2.16
4	1.02	0.85	2.35
5	0.86	1.05	2.85
mean	0.83	1.09	3.19
sd	0.33	0.40	1.56
Group Corrected			
GI	**$\Delta\delta^{13}C_{meas}$ (‰)**	**ΔP**	**P_S/P_W**
1	1.25	0.57	1.77
2	0.65	1.30	3.67
3	2.02	-0.37	0.69
4	1.72	0.00	1.00
5	1.28	0.54	1.72
mean	1.39	0.41	1.77
sd	0.52	0.64	1.16
Genus Corrected			
GI	**$\Delta\delta^{13}C_{meas}$ (‰)**	**ΔP**	**P_S/P_W**
1	1.66	0.07	1.07
2	0.75	1.18	3.25
3	2.48	-0.93	0.39
4	2.16	-0.54	0.58
5	1.66	0.08	1.08
mean	1.74	-0.03	1.27
sd	0.65	0.80	1.14

Table A4.3. Camps Bay charcoal (IB)

Uncorrected			
GI	**$\Delta\delta^{13}C_{meas}$ (‰)**	**ΔP**	**P_S/P_W**
1	0.60	1.37	3.92
2	0.87	1.04	2.82
3	1.04	0.83	2.29
mean	0.84	1.08	3.01
sd	0.22	0.27	0.83
Group Correction			
GI	**$\Delta\delta^{13}C_{meas}$ (‰)**	**ΔP**	**P_S/P_W**
1	0.89	1.01	2.75
2	1.37	0.43	1.54
3	1.33	0.48	1.61
mean	1.20	0.64	1.96
sd	0.27	0.32	0.68
Genus Correction			
GI	**$\Delta\delta^{13}C_{meas}$ (‰)**	**ΔP**	**P_S/P_W**
1	1.16	0.69	1.99
2	1.75	-0.03	0.97
3	1.80	-0.10	0.91
mean	1.57	0.19	1.29
sd	0.36	0.44	0.61

Table A4.4. Camps Bay charcoal (PB)

Uncorrected			
GI	**$\Delta\delta^{13}C_{meas}$ (‰)**	**ΔP**	**P_S/P_W**
1	0.31	1.72	5.58
2	0.45	1.55	4.71
3	0.50	1.49	4.43
4	0.42	1.59	4.88
5	0.34	1.68	5.38
mean	0.40	1.60	5.00
sd	0.08	0.10	0.48
Group Corrected			
GI	**$\Delta\delta^{13}C_{meas}$ (‰)**	**ΔP**	**P_S/P_W**
1	0.78	1.15	3.15
2	0.64	1.32	3.75
3	1.67	0.06	1.07
4	1.06	0.81	2.25
5	0.85	1.06	2.87
mean	1.00	0.88	2.62
sd	0.40	0.49	1.02
Genus Corrected			
GI	**$\Delta\delta^{13}C_{meas}$ (‰)**	**ΔP**	**P_S/P_W**
1	0.90	1.00	2.72
2	0.84	1.08	2.93
3	1.84	-0.15	0.86
4	1.22	0.61	1.84
5	0.99	0.89	2.45
mean	1.16	0.69	2.16
sd	0.41	0.50	0.83

Table A4.5. Swartberg wood (IB)

GI	$\Delta\delta^{13}C_{meas}$ (‰)	ΔP	P_S/P_W
1	0.78	1.14	3.14
2	2.08	-0.43	0.65
3	1.45	0.32	1.38
4	1.69	0.04	1.04
5	1.51	0.25	1.29
6	0.80	1.12	3.07
7	0.72	1.22	3.39
mean	1.29	0.52	1.99
sd	0.53	0.64	1.16

Table A4.6. Swartberg wood (PB)

GI	$\Delta\delta^{13}C_{meas}$ (‰)	ΔP	P_S/P_W
4	2.14	-0.51	0.60
8	1.25	0.57	1.77
9	1.39	0.40	1.50
12	0.24	1.80	6.08
13	0.32	1.71	5.51
mean	1.07	0.80	3.09
sd	0.80	0.97	2.51

Table A4.7. Swartberg charcoal (IB)

GI	$\Delta\delta^{13}C_{meas}$ (‰)	ΔP	P_S/P_W
1	1.09	0.76	2.14
2	0.19	1.87	6.46
3	2.41	-0.84	0.43
4	0.72	1.22	3.39
5	0.48	1.51	4.54
6	0.59	1.38	3.97
mean	0.91	0.98	3.49
sd	0.79	0.96	2.06

Table A4.8. Swartberg charcoal (PB)

GI	$\Delta\delta^{13}C_{meas}$ (‰)	ΔP	P_S/P_W
1	0.68	1.27	3.55
2	0.21	1.84	6.31
3	0.48	1.51	4.54
5	0.37	1.65	5.19
mean	0.44	1.57	4.90
sd	0.20	0.24	1.15

Table A4.9. Giant's Castle (GC4) wood (IB)

GI	$\Delta\delta^{13}C_{meas}$ (‰)	ΔP	P_S/P_W
1	0.42	1.59	4.88
2	1.05	0.82	2.27
3	0.30	1.73	5.62
4	0.50	1.49	4.43
5	0.83	1.09	2.96
6	0.23	1.82	6.18
7	0.41	1.60	4.96
8	0.32	1.71	5.54
9	0.47	1.52	4.59
10	0.20	1.85	6.38
11	0.29	1.74	5.71
12	0.46	1.53	4.64
13	0.86	1.04	2.84
14	0.50	1.49	4.43
15	0.27	1.77	5.85
mean	0.47	1.52	4.75
sd	0.25	0.31	1.24

Table A4.10. Giant's Castle (GC4) wood (PB)

GI	$\Delta\delta^{13}C_{meas}$ (‰)	ΔP	P_S/P_W
1	0.19	1.86	6.43
2	0.56	1.41	4.10
4	0.19	1.86	6.43
5	0.42	1.59	4.90
6	0.47	1.52	4.58
mean	0.37	1.65	5.29
sd	0.17	0.20	1.08

Table A4.11. Giant's Castle (GC4) charcoal (IB)

GI	$\Delta\delta^{13}C_{meas}$ (‰)	ΔP	P_S/P_W
2	0.41	1.60	4.96
3	0.29	1.75	5.74
4	0.36	1.66	5.25
5	0.19	1.87	6.46
6	0.65	1.30	3.69
7	0.63	1.33	3.78
8	0.43	1.57	4.82
mean	0.42	1.58	4.96
sd	0.17	0.21	1.00

Table A4.12. Giant's Castle (GC4) charcoal (PB)

GI	$\Delta\delta^{13}C_{meas}$ (‰)	ΔP	P_S/P_W
2	0.30	1.73	5.65
4	0.65	1.30	3.69
5	0.64	1.32	3.73
6	0.43	1.57	4.82
mean	0.51	1.48	4.47
sd	0.17	0.21	0.94

Table A4.13. Theronsberg wood (IB)

Uncorrected			
GI	$\Delta\delta^{13}C_{meas}$ (‰)	ΔP	P_S/P_W
1	0.83	1.09	2.98
2	0.94	0.95	2.59
3	0.54	1.44	4.21
mean	0.77	1.16	3.26
sd	0.21	0.25	0.84
Group Corrected			
GI	$\Delta\delta^{13}C_{meas}$ (‰)	ΔP	P_S/P_W
1	1.06	0.81	2.25
2	1.02	0.86	2.35
3	0.63	1.33	3.79
mean	0.90	1.00	2.80
sd	0.24	0.29	0.86
Genus Corrected			
GI	$\Delta\delta^{13}C_{meas}$ (‰)	ΔP	P_S/P_W
1	1.43	0.36	1.43
2	1.45	0.33	1.39
3	0.88	1.03	2.80
mean	1.25	0.57	1.87
sd	0.33	0.40	0.80

Table A4.14. Theronsberg wood (PB)

Uncorrected			
GI	$\Delta\delta^{13}C_{meas}$ (‰)	ΔP	P_S/P_W
1	0.83	1.09	2.98
2	0.94	0.95	2.59
3	0.18	1.88	6.53
4	0.21	1.84	6.31
5	0.25	1.79	5.98
mean	0.48	1.51	4.88
sd	0.37	0.45	1.93
Group Corrected			
GI	$\Delta\delta^{13}C_{meas}$ (‰)	ΔP	P_S/P_W
1	1.03	0.84	2.32
2	1.24	0.59	1.80
3	0.27	1.77	5.86
4	0.25	1.80	6.03
5	0.38	1.64	5.15
mean	0.63	1.33	4.23
sd	0.47	0.57	2.02
Genus Corrected			
GI	$\Delta\delta^{13}C_{meas}$ (‰)	ΔP	P_S/P_W
1	1.40	0.39	1.47
2	1.66	0.07	1.07
3	0.35	1.67	5.31
4	0.34	1.68	5.37
5	0.49	1.50	4.49
mean	0.85	1.06	3.54
sd	0.63	0.77	2.11

Table A4.15. Montagu Pass wood (IB & PB)

GI	$\Delta\delta^{13}C_{meas}$ (‰)	ΔP	P_S/P_W
1	0.96	0.92	2.52
2	1.24	0.59	1.80
3	1.42	0.37	1.45
4	1.70	0.03	1.03
5	1.57	0.18	1.20
6	0.63	1.33	3.80
7	0.92	0.98	2.65
mean	1.20	0.63	2.06
sd	0.39	0.47	0.99

Table A4.16. Montagu Pass charcoal (IB)

GI	$\Delta\delta^{13}C_{meas}$ (‰)	ΔP	P_S/P_W
1	0.26	1.78	5.94
2	1.31	0.49	1.64
3	0.73	1.20	3.32
4	0.62	1.34	3.81
mean	0.73	1.20	3.68
sd	0.44	0.53	1.77

Table A4.17. Montagu Pass charcoal (PB)

GI	$\Delta\delta^{13}C_{meas}$ (‰)	ΔP	P_S/P_W
2	0.26	1.78	5.94
3	0.91	0.99	2.70
4	0.44	1.56	4.78
5	0.62	1.34	3.81
mean	0.56	1.42	4.31
sd	0.28	0.34	1.38

Table A4.18. Giant's Castle (GC2) charcoal (IB)

GI	$\Delta\delta^{13}C_{meas}$ (‰)	ΔP	P_S/P_W
3	0.32	1.71	5.54
4	0.27	1.77	5.84
5	0.53	1.45	4.25
6	0.46	1.54	4.67
mean	0.39	1.62	5.07
sd	0.12	0.15	0.74

Table A4.19. Giant's Castle (GC2) charcoal (PB)

GI	$\Delta\delta^{13}C_{meas}$ (‰)	ΔP	P_S/P_W
3	0.23	1.81	6.12
4	0.27	1.77	5.84
5	0.53	1.45	4.25
8	0.28	1.75	5.76
mean	0.33	1.69	5.49
sd	0.14	0.17	0.84

Table A4.20. Waterfall Bluff (WB_A)

Uncorrected

GI	$\Delta\delta^{13}C_{meas}$ (‰)	ΔP	P_S/P_W
2	0.31	1.72	5.58
3	0.29	1.74	5.70
4	0.11	1.97	7.15
1	0.37	1.65	5.21
2	0.26	1.78	5.94
3	0.20	1.85	6.36
4	0.14	1.93	6.87
mean	0.24	1.81	6.12
sd	0.09	0.11	0.71

Genus Corrected

GI	$\Delta\delta^{13}C_{meas}$ (‰)	ΔP	P_S/P_W
2	0.63	1.33	3.80
3	0.59	1.38	3.96
4	0.16	1.91	6.72
1	0.61	1.36	3.89
2	0.52	1.46	4.31
3	0.41	1.60	4.94
4	0.28	1.76	5.79
mean	0.46	1.54	4.77
sd	0.18	0.22	1.11

Table A4.21. Waterfall Bluff (WB_B)

Uncorected

GI	$\Delta\delta^{13}C_{meas}$ (‰)	ΔP	P_S/P_W
1	0.40	1.60	4.97
2	0.57	1.40	4.05
1	0.51	1.47	4.37
mean	0.50	1.49	4.46
sd	0.09	0.10	0.47

Genus Corrected

GI	$\Delta\delta^{13}C_{meas}$ (‰)	ΔP	P_S/P_W
1	0.82	1.10	3.01
2	0.84	1.07	2.91
1	1.03	0.84	2.32
mean	0.90	1.00	2.75
sd	0.12	0.14	0.38

Table A4.22. Boomplaas Cave (BPA4_21)

Uncorrected

GI	$\Delta\delta^{13}C_{meas}$ (‰)	ΔP	P_S/P_W
1	0.25	1.80	6.04
2	0.17	1.89	6.65
3	0.39	1.62	5.07
1	0.30	1.74	5.68
2	0.27	1.77	5.86
mean	0.27	1.76	5.86
sd	0.08	0.10	0.57

Genus Corrected

GI	$\Delta\delta^{13}C_{meas}$ (‰)	ΔP	P_S/P_W
1	0.90	1.00	2.71
2	0.48	1.51	4.52
3	1.13	0.72	2.06
1	0.86	1.05	2.85
2	1.00	0.88	2.42
mean	0.87	1.03	2.91
sd	0.24	0.29	0.95

Table A4.23. Boomplaas Cave (BPA4_24)

Uncorrected

GI	$\Delta\delta^{13}C_{meas}$ (‰)	ΔP	P_S/P_W
1	0.74	1.20	3.30
2	0.23	1.82	6.15
4	0.71	1.23	3.43
5	0.90	1.00	2.72
1	0.91	0.99	2.69
2	0.84	1.07	2.92
3	0.72	1.22	3.39
4	0.24	1.80	6.08
5	0.99	0.89	2.44
mean	0.70	1.25	3.68
sd	0.28	0.34	1.42

Genus Corrected

GI	$\Delta\delta^{13}C_{meas}$ (‰)	ΔP	P_S/P_W
1	1.57	0.18	1.19
2	0.59	1.38	3.98
4	2.63	-1.11	0.33
5	2.25	-0.65	0.52
1	2.64	-1.12	0.33
2	2.45	-0.89	0.41
3	2.08	-0.44	0.64
4	0.59	1.37	3.95
5	2.24	-0.64	0.53
mean	1.89	-0.21	1.32
sd	0.81	0.98	1.52

Table A4.24. Boomplaas Cave (BPA2_21)

Uncorrected

GI	$\Delta\delta^{13}C_{meas}$ (‰)	ΔP	P_S/P_W
1	0.40	1.61	5.00
2	0.28	1.76	5.79
4	0.62	1.34	3.82
1	0.50	1.49	4.43
2	0.32	1.71	5.51
3	0.61	1.35	3.87
4	0.22	1.83	6.23
5	0.60	1.37	3.92
mean	0.44	1.56	4.82
sd	0.16	0.20	0.95

Genus Corrected

GI	$\Delta\delta^{13}C_{meas}$ (‰)	ΔP	P_S/P_W
1	1.47	0.30	1.35
2	1.03	0.84	2.32
4	1.56	0.20	1.22
1	1.45	0.33	1.39
2	1.18	0.66	1.94
3	2.25	-0.64	0.53
4	0.81	1.11	3.03
5	1.74	-0.03	0.97
mean	1.44	0.35	1.59
sd	0.45	0.54	0.80

APPENDIX 5
Climatology Data

Table A5.1. Camps Bay rainfall data (2015-2021)

year	month	rainfall (mm)	MJJASO	NDJFMA	annual rainfall (mm)
2015	1	15.7	305.7	65.5	371.2
2015	2	2.9			
2015	3	2.7			
2015	4	4.4			
2015	5	28.4			
2015	6	122.8			
2015	7	88.9			
2015	8	33.5			
2015	9	26.5			
2015	10	5.6			
2015	11	25.9			
2015	12	13.9			
2016	1	33.9	273.7	118.8	392.5
2016	2	2.7			
2016	3	27.7			
2016	4	37.9			
2016	5	45.1			
2016	6	54			
2016	7	76.7			
2016	8	50.6			
2016	9	40.3			
2016	10	7			
2016	11	5.2			
2016	12	11.4			
2017	1	5.5	227.2	86	313.2
2017	2	3.6			
2017	3	8.5			
2017	4	38			
2017	5	6.1			
2017	6	100.7			
2017	7	30.3			
2017	8	46.8			
2017	9	18.6			
2017	10	24.7			
2017	11	24.5			
2017	12	5.9			
2018	1	5.8	347.4	91.7	439.1
2018	2	16.8			
2018	3	11.6			
2018	4	39.9			
2018	5	86.7			
2018	6	68.9			
2018	7	55.9			
2018	8	56.9			
2018	9	68.8			
2018	10	10.2			
2018	11	8.9			
2018	12	8.7			

2019	1	11	381.4	100.6	482
2019	2	7.3			
2019	3	25.8			
2019	4	23.4			
2019	5	51.7			
2019	6	79			
2019	7	118.5			
2019	8	34.3			
2019	9	26.3			
2019	10	71.6			
2019	11	9.3			
2019	12	23.8			
2020	1	22.4	384.5	98	482.5
2020	2	5.4			
2020	3	3			
2020	4	29.1			
2020	5	49.6			
2020	6	74.8			
2020	7	97.1			
2020	8	99.9			
2020	9	45.2			
2020	10	17.9			
2020	11	32.3			
2020	12	5.8			
2021	1	6.8	461.9	127.5	589.4
2021	2	3.3			
2021	3	57.6			
2021	4	3.8			
2021	5	119.3			
2021	6	112.5			
2021	7	88.1			
2021	8	87.7			
2021	9	15.8			
2021	10	38.5			
2021	11	27			
2021	12	29			
			MAP	438.5571429	
			Ps	98.3	
			Pw	340.2571429	

Table A5.2. Camps Bay calculating ΔP, P_S/P_W, and $\Delta\delta^{13}C_{model}$ from rainfall data

	MJJASO	NDJFMA	ΔP	Ps/Pw	model
2015	305.70	65.50	-1.54	0.21	2.98
2016	273.70	118.80	-0.83	0.43	2.40
2017	227.20	86.00	-0.97	0.38	2.52
2018	347.40	91.70	-1.33	0.26	2.81
2019	381.40	100.60	-1.33	0.26	2.81
2020	384.50	98.00	-1.37	0.25	2.84
2021	461.90	127.50	-1.29	0.28	2.78
mean	340.26	98.30	-1.24	0.30	2.74
sd	78.43	20.61	0.25	0.08	0.20

Table A5.3. Swartberg rainfall data (2015-2021)

year	month	rainfall (mm)	MJJASO	NDJFMA	annual rainfall (mm)
2015	1	16.3	155	141.6	296.6
2015	2	15.6			
2015	3	26.8			
2015	4	30.2			
2015	5	14			
2015	6	34.3			
2015	7	32.8			
2015	8	21.8			
2015	9	41.1			
2015	10	11			
2015	11	42.3			
2015	12	10.4			
2016	1	55.4	89.1	141.5	230.6
2016	2	12.6			
2016	3	31.1			
2016	4	22.6			
2016	5	15.8			
2016	6	12			
2016	7	17.3			
2016	8	11.3			
2016	9	28.1			
2016	10	4.6			
2016	11	10.2			
2016	12	9.6			
2017	1	22.2	85.4	128.3	213.7
2017	2	20.2			
2017	3	17.2			
2017	4	26.5			
2017	5	8.1			
2017	6	11.7			

2017	7	7			
2017	8	19.7			
2017	9	17.2			
2017	10	21.7			
2017	11	30.5			
2017	12	11.7			
2018	1	15.8	109.5	133.9	243.4
2018	2	28.1			
2018	3	32.7			
2018	4	20.3			
2018	5	22.6			
2018	6	9.1			
2018	7	9.7			
2018	8	17.5			
2018	9	34.5			
2018	10	16.1			
2018	11	27			
2018	12	10			
2019	1	9.9	71.9	149.2	221.1
2019	2	45.1			
2019	3	27.3			
2019	4	21			
2019	5	14.6			
2019	6	9.2			
2019	7	13.8			
2019	8	1.3			
2019	9	18.5			
2019	10	14.5			
2019	11	27.9			
2019	12	18			
2020	1	71.3	81.6	163.6	245.2
2020	2	23.1			
2020	3	17.1			
2020	4	12.8			
2020	5	10.7			
2020	6	6.2			
2020	7	6.6			
2020	8	20.2			
2020	9	18.5			
2020	10	19.4			
2020	11	25.6			
2020	12	13.7			
2021	1	20.8	141.4	188.6	330
2021	2	19.2			
2021	3	33			
2021	4	10.9			
2021	5	29.4			
2021	6	11.6			
2021	7	21			

2021	8	25.9			
2021	9	7.3			
2021	10	46.2			
2021	11	37.6			
2021	12	67.1			
			MAP	254.371429	
			Ps	149.528571	
			Pw	104.842857	

Table A5.4. Swartberg calculating ΔP, P_S/P_W, and $\Delta\delta^{13}C_{model}$ from rainfall data

	MJJASO	NDJFMA	ΔP	Ps/Pw	model
2015	155.00	141.60	-0.09	0.91	1.79
2016	89.10	141.50	0.46	1.59	1.34
2017	85.40	128.30	0.41	1.50	1.39
2018	109.50	133.90	0.20	1.22	1.56
2019	71.90	149.20	0.73	2.08	1.12
2020	81.60	163.60	0.70	2.00	1.15
2021	141.40	188.60	0.29	1.33	1.48
mean	104.84	149.53	0.38	1.52	1.40
sd	31.95	20.60	0.29	0.42	0.23

Table A5.5. Theronsberg rainfall data (2016-2022)

year	month	rainfall (mm)	MJJASO	NDJFMA	annual rainfall (mm)
2016	1	44.8	155.5	108.4	263.9
2016	2	3.7			
2016	3	21.8			
2016	4	23.1			
2016	5	31.1			
2016	6	29.7			
2016	7	35.6			
2016	8	27.8			
2016	9	27.1			
2016	10	4.2			
2016	11	6.2			
2016	12	8.8			
2017	1	7.6	131.6	79.9	211.5
2017	2	6.5			
2017	3	9.1			
2017	4	30.4			

2017	5	5.7			
2017	6	50			
2017	7	14.6			
2017	8	31.3			
2017	9	12.8			
2017	10	17.2			
2017	11	20.2			
2017	12	6.1			
2018	1	6.3	193.1	82.4	275.5
2018	2	22.2			
2018	3	14.6			
2018	4	21			
2018	5	48.8			
2018	6	34.1			
2018	7	28.8			
2018	8	36.9			
2018	9	37.7			
2018	10	6.8			
2018	11	10.4			
2018	12	7.9			
2019	1	6.5	205.7	81.8	287.5
2019	2	15.2			
2019	3	17			
2019	4	9.2			
2019	5	33.1			
2019	6	47.6			
2019	7	70.1			
2019	8	18			
2019	9	15.1			
2019	10	21.8			
2019	11	14.4			
2019	12	19.5			
2020	1	33	235.3	87	322.3
2020	2	2.3			
2020	3	9.5			
2020	4	15.1			
2020	5	23.8			
2020	6	52.9			
2020	7	64.4			
2020	8	61.7			
2020	9	21.9			
2020	10	10.6			
2020	11	23.8			
2020	12	3.3			
2021	1	14.6	268.8	146.1	414.9
2021	2	3.4			
2021	3	42.1			
2021	4	7.3			
2021	5	61.9			

2021	6	69.5			
2021	7	54.5			
2021	8	51.8			
2021	9	6.1			
2021	10	25			
2021	11	38.3			
2021	12	40.4			
2022	1	19.4	152.6	125.3	277.9
2022	2	15.7			
2022	3	19.3			
2022	4	6.9			
2022	5	21.3			
2022	6	44.9			
2022	7	12.8			
2022	8	46			
2022	9	15.7			
2022	10	11.9			
2022	11	20.6			
2022	12	43.4			
			MAP	293.357143	
			Ps	101.557143	
			Pw	191.8	

Table A5.6. Theronsberg calculating ΔP, P_S/P_W, and $\Delta\delta^{13}C_{model}$ from rainfall data

	MJJASO	NDJFMA	ΔP	Ps/Pw	model
2016	155.50	108.40	-0.36	0.70	2.02
2017	131.60	79.90	-0.50	0.61	2.13
2018	193.10	82.40	-0.85	0.43	2.42
2019	205.70	81.80	-0.92	0.40	2.48
2020	235.30	87.00	-0.99	0.37	2.54
2021	268.80	146.10	-0.61	0.54	2.22
2022	152.60	125.30	-0.20	0.82	1.88
mean	191.80	101.56	-0.63	0.55	2.24
sd	49.15	25.93	0.30	0.17	0.25

Table A5.7. Giant's Castle rainfall data (2016-2022)

year	month	rainfall (mm)	MJJASO	NDJFMA	annual rainfall (mm)
2016	1	174.7	194.6	705.8	900.4
2016	2	111			
2016	3	112.8			
2016	4	58.2			
2016	5	47.7			
2016	6	12.9			
2016	7	19.5			
2016	8	22.2			
2016	9	25.3			
2016	10	67			
2016	11	130.7			
2016	12	118.4			
2017	1	214	143.6	797.4	941
2017	2	172.1			
2017	3	122.3			
2017	4	44.3			
2017	5	19.4			
2017	6	6.8			
2017	7	5.9			
2017	8	16.7			
2017	9	25.3			
2017	10	69.5			
2017	11	90.8			
2017	12	153.9			
2018	1	146.5	155.9	728.5	884.4
2018	2	148.4			
2018	3	169.9			
2018	4	70.3			
2018	5	23.7			
2018	6	6.8			
2018	7	7.4			
2018	8	30.6			
2018	9	30.7			
2018	10	56.7			
2018	11	87.3			
2018	12	106.1			
2019	1	124.7	85.7	807.2	892.9
2019	2	202.4			
2019	3	140.2			
2019	4	89.3			
2019	5	15			
2019	6	3.6			
2019	7	2.5			
2019	8	9.6			
2019	9	18.5			
2019	10	36.5			
2019	11	109.5			
2019	12	141.1			

2020	1	181.1	114.2	906.9	1021.1
2020	2	188.6			
2020	3	87.7			
2020	4	92.3			
2020	5	4.9			
2020	6	1.5			
2020	7	1.4			
2020	8	13.2			
2020	9	25			
2020	10	68.2			
2020	11	134.9			
2020	12	222.3			
2021	1	215.8	181.1	865.4	1046.5
2021	2	135.3			
2021	3	126.5			
2021	4	51.6			
2021	5	22.4			
2021	6	7.9			
2021	7	3.5			
2021	8	28.8			
2021	9	58.2			
2021	10	60.3			
2021	11	116			
2021	12	220.2			
2022	1	189.3	194.3	1059.2	1253.5
2022	2	169.5			
2022	3	194.5			
2022	4	134			
2022	5	44.5			
2022	6	6.3			
2022	7	6.1			
2022	8	11.5			
2022	9	36.6			
2022	10	89.3			
2022	11	121.2			
2022	12	250.7			
			MAP	991.4	
			Ps mean	838.628571	
			Pw mean	152.771429	

Table A5.8. Giant's Castle calculating ΔP, P_S/P_W, and $\Delta\delta^{13}C_{model}$ from rainfall data

	MJJASO	NDJFMA	ΔP	Ps/Pw	model
2016	194.60	705.80	1.29	3.63	0.66
2017	143.60	797.40	1.71	5.55	0.31
2018	155.90	728.50	1.54	4.67	0.46
2019	85.70	807.20	2.24	9.42	-0.12
2020	114.20	906.90	2.07	7.94	0.02
2021	181.10	865.40	1.56	4.78	0.44
2022	194.30	1059.20	1.70	5.45	0.33
mean	152.77	838.63	1.73	5.92	0.30
sd	41.55	120.06	0.33	1.93	0.27

Table A5.9. Montagu Pass rainfall data (2016-2022)

year	month	ainfall (mm)	MJJASO	NDJFMA	annual rainfall (mm)
2016	1	52.1	154.2	175.1	329.3
2016	2	18.4			
2016	3	41.8			
2016	4	31.8			
2016	5	15.6			
2016	6	21.7			
2016	7	32.5			
2016	8	17.8			
2016	9	55.2			
2016	10	11.4			
2016	11	15.8			
2016	12	15.2			
2017	1	30.5	166.4	176.1	342.5
2017	2	20.7			
2017	3	22.6			
2017	4	26.1			
2017	5	14.8			
2017	6	13.6			
2017	7	15.1			
2017	8	43.4			
2017	9	36			
2017	10	43.5			
2017	11	57.4			
2017	12	18.8			
2018	1	20.7	181.9	176.6	358.5
2018	2	26.5			
2018	3	42.9			
2018	4	19.4			

2018	5	22.7			
2018	6	14.4			
2018	7	16.2			
2018	8	35.8			
2018	9	65.4			
2018	10	27.4			
2018	11	49.5			
2018	12	17.6			
2019	1	20.7	154.4	214.9	369.3
2019	2	49.3			
2019	3	44.8			
2019	4	27			
2019	5	33.5			
2019	6	13			
2019	7	29.2			
2019	8	4.9			
2019	9	42.5			
2019	10	31.3			
2019	11	37.3			
2019	12	35.8			
2020	1	74	168.3	219.9	388.2
2020	2	27.3			
2020	3	21.6			
2020	4	17.5			
2020	5	30.9			
2020	6	16.7			
2020	7	15.7			
2020	8	37.9			
2020	9	20.7			
2020	10	46.4			
2020	11	53.8			
2020	12	25.7			
2021	1	32	265.5	257.1	522.6
2021	2	27.3			
2021	3	54.5			
2021	4	21.8			
2021	5	59.2			
2021	6	15.5			
2021	7	34.9			
2021	8	53			
2021	9	20.9			
2021	10	82			
2021	11	47.4			
2021	12	74.1			

2022	1	13.4	153.2	190.5	343.7
2022	2	47.1			
2022	3	31.6			
2022	4	24.4			
2022	5	25.5			
2022	6	28.9			
2022	7	25.6			
2022	8	30.1			
2022	9	25			
2022	10	18.1			
2022	11	12			
2022	12	62			
			MAP	379.157143	
			Ps	201.457143	
			Pw	177.7	

Table A5.10. Montagu Pass calculating ΔP, P_S/P_W, and $\Delta\delta^{13}C_{model}$ from rainfall data

	MJJASO	NDJFMA	ΔP	Ps/Pw	model
2016	154.20	175.10	0.13	1.14	1.62
2017	166.40	176.10	0.06	1.06	1.67
2018	181.90	176.60	-0.03	0.97	1.74
2019	154.40	214.90	0.33	1.39	1.45
2020	168.30	219.90	0.27	1.31	1.50
2021	265.50	257.10	-0.03	0.97	1.75
2022	153.20	190.50	0.22	1.24	1.54
mean	177.70	201.46	0.13	1.15	1.61
sd	40.08	30.80	0.14	0.17	0.12

Table A5.11. Gifberg rainfall data (2016-2022)

year	month	rainfall (mm)	MJJASO	NDJFMA	annual rainfall (mm)
2016	1	17.9	125.4	49.2	172.4
2016	2	0.3			
2016	3	6.7			
2016	4	17.3			
2016	5	25.1			
2016	6	16.9			

2016	7	37.6			
2016	8	16.1			
2016	9	28.3			
2016	10	1.4			
2016	11	4.8			
2016	12	2.2			
2017	1	1.8	71.9	44.6	116.5
2017	2	1.3			
2017	3	2			
2017	4	20.8			
2017	5	1.1			
2017	6	41.7			
2017	7	8.8			
2017	8	10.7			
2017	9	3.1			
2017	10	6.5			
2017	11	17.6			
2017	12	1.1			
2018	1	0.6	128.8	33	161.8
2018	2	5.7			
2018	3	9.4			
2018	4	12.1			
2018	5	32.9			
2018	6	25.6			
2018	7	26.1			
2018	8	21.1			
2018	9	21.5			
2018	10	1.6			
2018	11	2.7			
2018	12	2.5			
2019	1	6.6	123.6	32.3	155.9
2019	2	6.5			
2019	3	7.3			
2019	4	4.9			
2019	5	18.9			
2019	6	24.5			
2019	7	51			
2019	8	7.6			
2019	9	10.7			
2019	10	10.9			
2019	11	1.1			
2019	12	5.9			
2020	1	4.3	159.3	26.8	186.1
2020	2	0.6			
2020	3	0.3			
2020	4	14.8			
2020	5	8.5			
2020	6	46.3			
2020	7	47.1			
2020	8	36.4			
2020	9	9.4			
2020	10	11.6			

2020	11	5.2			
2020	12	1.6			
2021	1	1.7	150.8	42.4	193.2
2021	2	1.2			
2021	3	8.2			
2021	4	4.3			
2021	5	34.2			
2021	6	36.8			
2021	7	32.3			
2021	8	32.9			
2021	9	2.7			
2021	10	11.9			
2021	11	11.8			
2021	12	15.2			
2022	1	1.8	97.9	59	156.9
2022	2	2.1			
2022	3	5.8			
2022	4	8			
2022	5	14.9			
2022	6	46.3			
2022	7	8.8			
2022	8	19			
2022	9	7.5			
2022	10	1.4			
2022	11	4.8			
2022	12	36.5			
			MAP	163.2571429	
			Ps	41.04285714	
			Pw	122.5285714	

Table A5.12. Gifberg calculating ΔP, P_S/P_W, and $\Delta\delta^{13}C_{model}$ from rainfall data

	MJJASO	NDJFMA	ΔP	Ps/Pw	model
2016	125.40	49.20	-0.94	0.39	2.49
2017	71.90	44.60	-0.48	0.62	2.11
2018	128.80	33.00	-1.36	0.26	2.84
2019	123.60	32.30	-1.34	0.26	2.82
2020	159.30	26.80	-1.78	0.17	3.18
2021	150.80	42.40	-1.27	0.28	2.76
2022	97.90	59.00	-0.51	0.60	2.14
mean	122.53	41.04	-1.10	0.37	2.62
sd	29.92	11.16	0.48	0.18	0.39